Ab-initio Statistical Mechanics for Ordering and Segregation at the (110) Surface of Ni90%-Al

Ralf Drautz

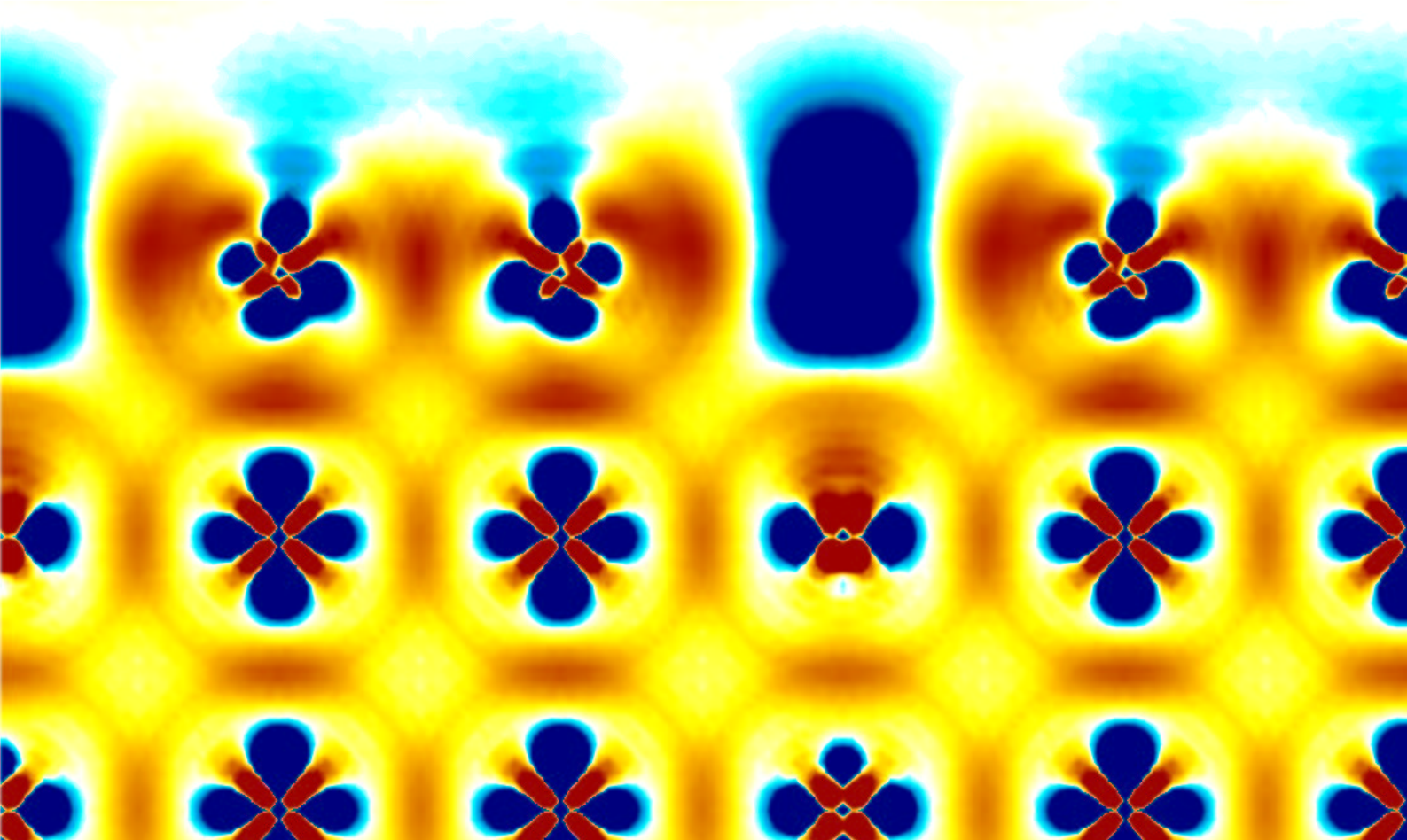

Ab-initio Statistical Mechanics for Ordering and Segregation at the (110) Surface of Ni90%-Al

Von der Fakultät Physik der Universität Stuttgart zur
Erlangung der Würde eines Doktors der Naturwissenschaften
(Dr. rer. nat.) genehmigte Abhandlung

vorgelegt von

Ralf Drautz

geboren in Bad Cannstatt

Hauptberichter:	Prof. Dr. M. Fähnle
Mitberichter:	Prof. Dr. G. Wunner
Tag der Einreichung:	27. Februar 2003
Tag der mündlichen Prüfung:	2. Mai 2003

Max-Planck-Institut für Metallforschung
Stuttgart
2003

Contents

Chapter 1

Introduction

Unlike one century ago, when quantum mechanics and statistical mechanics were developed, nowadays materials science has nothing to do with finding laws of nature. Laws of nature in materials science are known and accepted. At the beginning of the 21st century materials science is devoted to understanding, predicting and engineering the consequences of the laws found one hundred years ago. The advent of powerful computer systems in the past years allowed first-principles theories to be developed. First-principles theories that can be built on the laws of nature aiming to describe real materials as opposed to model systems. In order to implement first-principles theories, it is crucial to find transformations, enumerations and coarse graining algorithms that allow to systematically deal with the "most relevant states" from the vast amount of possibilities that result if only few particles are brought together without having to handle all possibilities explicitly. This purely numerical difficulty requires a "physical understanding" of the system investigated. In this context "physical understanding" means that the general behavior of a system can be understood by simple quantities. Hence, phenomenological models and their terminology are also necessary.

In this work the (110) surface of Ni90%-Al is approached using a first-principles theory. Chapters 3 to 8 introduce the building blocks of the theory for the examination of the Ni90%-Al surface. Only few surface calculations are necessary to show that simple phenomenological "broken bond" models completely fail to describe experimental facts. The (110) surface indeed behaves differently from the bulk. Although the energetics of the surface turns out to be not completely different from the bulk, surface modifications together with frustration effects present in the bulk but not in the surface, provide the understanding of ordering and segregation at the surface. A deeper insight to the surface energetics from further calculations then raises the question whether the (110) surface of Ni90%-Al behaves more like a 1, 2 or 3-dimensional system.

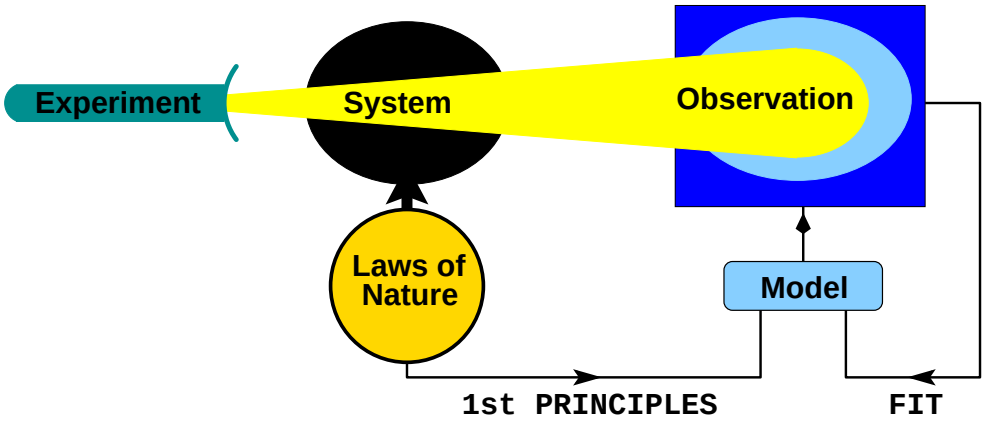

Figure 1.1: "Material scientists in Platos Cave". An experiment is looked at as a projection. The experimental observations are compared to a shadow on the wall. Hitherto materials scientists had to explain and understand the results of their experiments within self-contained models, parameters had to be fitted to the experimental result so that the model reproduced the experimental result. First-principles theories directly relate the parameters required in a model to the laws of nature.

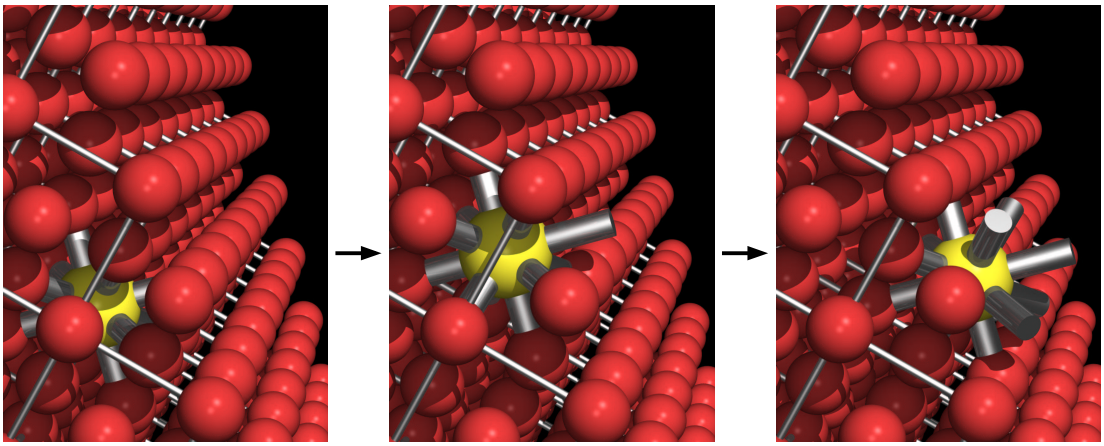

Figure 1.2: Segregation of Al to the (110) surface of Ni (chapter 9).

The fact that the surface behaves different from the bulk is of interest also from a materials science and engineering point of view: The surface behavior is of great importance because any bulk material makes contact to the surroundings via its surface, such as chemical reactions, adsorption phenomena, heat transfer, etc. Thus a first-principles theory provides valuable information for the understanding and engineering of materials and their surface properties.

Chapter 2

Experimental findings

This work was initiated by experiments carried out by Dr. H. Reichert from the department of Prof. Dosch at the Max-Planck-Institut for Metals Research in Stuttgart. In the experiments for the (110) surface of Ni90%-Al segregation of Al to the surface and order in the surface was observed. A short introduction to x-ray diffraction will be given before the experiments are explained.

2.1 Introduction to x-ray diffraction

We follow [1,2,3] for a brief introduction to the mechanisms and principles of x-ray diffraction.

We assume that when a x-ray plane wave with wave vector $\boldsymbol{k}_i$ is scattered at a single electron that is located at $\boldsymbol{r}$, the amplitude of the outgoing spherical wave A_1 with wave vector $\boldsymbol{k}_f$ is proportional to the amplitude A_0 of the ingoing wave (Thompson formula [4, 5]),

$$A_1\left(\boldsymbol{k}_f\right)\exp\left(-i\boldsymbol{k}_f\boldsymbol{r}\right) = A_0\frac{e^2}{mc^2}\frac{1}{R_0}\exp\left(-i\boldsymbol{k}_i\boldsymbol{r}\right)\,, \tag{2.1}$$

where e is the electron charge, m its mass, R_0 is the distance to the observer, and the factor $\frac{1}{R_0}$ takes into account that a spherical wave results from the scattering process. The value of the constant $\frac{e^2}{mc^2}$ is very small (3×10^{-15}m). Thus, the total scattering cross section is small even for a crystal possessing many electrons. Therefore it is assumed that the kinematical approximation, where the total scattered amplitude is calculated as the sum of contributions of single electrons, is valid.

For elastic scattering the energy and thus the wavelength λ of the ingoing and the outgoing wave is the same,

$$\|\boldsymbol{k}_i\| = \|\boldsymbol{k}_f\| = \|\boldsymbol{k}\| = \frac{2\pi}{\lambda}\,. \tag{2.2}$$

The variable of interest is the momentum transfer,

$$\boldsymbol{q} = \boldsymbol{k}_f - \boldsymbol{k}_i\,. \tag{2.3}$$

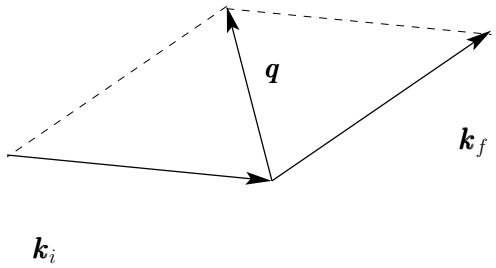

Figure 2.1: Definition of the momentum transfer $\boldsymbol{q} = \boldsymbol{k}_f - \boldsymbol{k}_i$.

The result of a scattering experiment can be interpreted as a map in momentum space,

$$A_1(\boldsymbol{q}) = A_0 \frac{e^2}{mc^2} \frac{1}{R_0} \exp(i\boldsymbol{q}\boldsymbol{r}) \ . \tag{2.4}$$

In order to calculate the total scattered amplitude A of a crystal it is necessary to sum up the contributions from all electrons. In quantum mechanics the electron density $\rho(\boldsymbol{r})$ is a continuous variable, the summation becomes an integration,

$$A = A_0 \frac{e^2}{mc^2} \frac{1}{R_0} \int dV \rho(\boldsymbol{r}) \exp(i\boldsymbol{q}\boldsymbol{r}) \ . \tag{2.5}$$

This shows that an x-ray scattering experiment is a mere Fourier transformation of the charge density.

In x-ray experiments the largest portion of photons is scattered at core electrons that do not change when the chemical surroundings of the atoms change. Hence, it is assumed that the charge density can be modeled as superposition of atomic charge densities in order to calculate the scattering amplitude,

$$\rho(\boldsymbol{r}) = \sum_n \rho_n(\boldsymbol{r} - \boldsymbol{r}_n) \ , \tag{2.6}$$

where the position of atom n is specified by the vector $\boldsymbol{r}_n$. We find

$$\begin{aligned} A &= A_0 \frac{e^2}{mc^2} \frac{1}{R_0} \sum_n \int dV \rho_n(\boldsymbol{r} - \boldsymbol{r}_n) \exp(i\boldsymbol{q}\boldsymbol{r}) \\ &= A_0 \frac{e^2}{mc^2} \frac{1}{R_0} \sum_n \int dV \rho_n(\boldsymbol{r}) \exp(i\boldsymbol{q}(\boldsymbol{r} + \boldsymbol{r}_n)) \\ &= A_0 \frac{e^2}{mc^2} \frac{1}{R_0} \sum_n f_n(\boldsymbol{q}) \exp(i\boldsymbol{q}\boldsymbol{r}_n) \ , \end{aligned} \tag{2.7}$$

with the atomic form factors,

$$f_n(\boldsymbol{q}) = \int dV \rho_n(\boldsymbol{r}) \exp(i\boldsymbol{q}\boldsymbol{r}) \ . \tag{2.8}$$

The assumptions made in Eq. (2.7) confine the information available from a single x-ray experiment to pair-correlations (Section 8.5.1).

If the atomic positions $\boldsymbol{r}_n$ form the array of a crystal, *e.g.*, $\boldsymbol{r}_n = n_1\boldsymbol{a}_1 + n_2\boldsymbol{a}_2 + n_3\boldsymbol{a}_3 + \boldsymbol{r}_{n_0}$, where $\boldsymbol{r}_{n_0}$ is the position of atom n in the unit cell at the origin, the equations can further be simplified,

$$\begin{aligned} A &= A_0 \frac{e^2}{mc^2} \frac{1}{R_0} \sum_{n_0} f_{n_0}(\boldsymbol{q}) \exp(i\boldsymbol{q}\boldsymbol{r}_{n_0}) \sum_{n_1 n_2 n_3} \exp\left(i\boldsymbol{q}\left(n_1\boldsymbol{a}_1 + n_2\boldsymbol{a}_2 + n_3\boldsymbol{a}_3\right)\right) \\ &= A_0 \frac{e^2}{mc^2} \frac{1}{R_0} F(\boldsymbol{q}) \sum_{n_1 n_2 n_3} \exp\left(i\boldsymbol{q}\left(n_1\boldsymbol{a}_1 + n_2\boldsymbol{a}_2 + n_3\boldsymbol{a}_3\right)\right) \\ &= A_0 \frac{e^2}{mc^2} \frac{1}{R_0} F(\boldsymbol{q}) S_{N_1}(\boldsymbol{q}\boldsymbol{a_1}) S_{N_2}(\boldsymbol{q}\boldsymbol{a_2}) S_{N_3}(\boldsymbol{q}\boldsymbol{a_3}) \,, \end{aligned} \tag{2.9}$$

whereby the structure factor of the unit cell,

$$F(\boldsymbol{q}) = \sum_{n_0} f_{n_0}(\boldsymbol{q}) \exp(i\boldsymbol{q}\boldsymbol{r}_{n_0}) \,, \tag{2.10}$$

and the function,

$$S_N(x) = \sum_{n=0}^{N-1} \exp(ixn) = \frac{1 - \exp(ixN)}{1 - \exp(ix)} \,, \tag{2.11}$$

are introduced. The diffracted intensity $I = \|A\|^2$ is proportional to the so-called slit function,

$$\|S_N(x)\|^2 = \frac{\sin^2(Nx/2)}{\sin^2(x/2)} \,, \tag{2.12}$$

which is sharply peaked at $x = 2\pi m$ (m is an integer number) for large N. In the limit $N \to \infty$ scattering intensity is only found for $\boldsymbol{q}$ vectors that meet the Laue conditions (with h, k, l integer numbers),

$$\boldsymbol{q}\,\boldsymbol{a}_1 = 2\pi h \,, \qquad \boldsymbol{q}\,\boldsymbol{a}_2 = 2\pi k \,, \qquad \boldsymbol{q}\,\boldsymbol{a}_3 = 2\pi l \,. \tag{2.13}$$

These three equations are solved simultaneously if the momentum transfer $\boldsymbol{q}$ can be generated as,

$$\boldsymbol{q} = h\boldsymbol{b}_1 + k\boldsymbol{b}_2 + l\boldsymbol{b}_3 \,, \tag{2.14}$$

with the reciprocal space unit cell vectors,

$$\boldsymbol{b}_1 = 2\pi \frac{\boldsymbol{a}_2 \times \boldsymbol{a}_3}{\boldsymbol{a}_1(\boldsymbol{a}_2 \times \boldsymbol{a}_3)} \,, \qquad \boldsymbol{b}_2 = 2\pi \frac{\boldsymbol{a}_3 \times \boldsymbol{a}_1}{\boldsymbol{a}_1(\boldsymbol{a}_2 \times \boldsymbol{a}_3)} \,, \qquad \boldsymbol{b}_3 = 2\pi \frac{\boldsymbol{a}_1 \times \boldsymbol{a}_2}{\boldsymbol{a}_1(\boldsymbol{a}_2 \times \boldsymbol{a}_3)} \,. \tag{2.15}$$

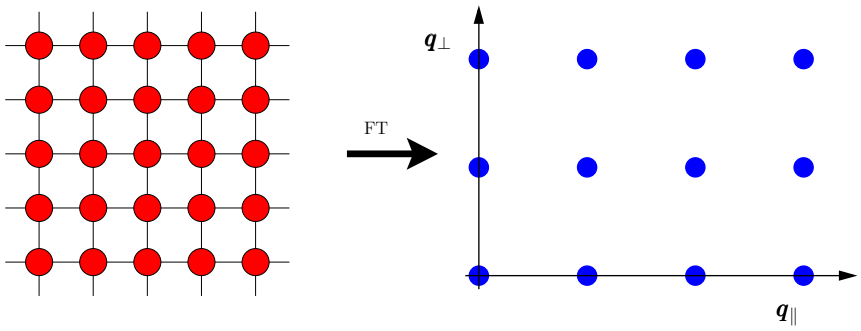

Figure 2.2: Scattered intensity from bulk material gives rise to Bragg peaks in momentum transfer space.

2.2 Surface x-ray diffraction

2.2.1 Geometrical considerations

As was shown in the previous section, scattering from an infinite $3d$ crystal results in a regular mesh in reciprocal space, Fig. 2.2. For an infinite $2d$ monolayer exhibiting basis vectors $\boldsymbol{a}_1$ and $\boldsymbol{a}_2$, the scattering amplitude from Eq. (2.9) becomes,

$$A = A_0 \frac{e^2}{mc^2} \frac{1}{R_0} F(\boldsymbol{q}) \sum_{n_1 n_2} \exp\left(i\boldsymbol{q}\left(n_1\boldsymbol{a}_1 + n_2\boldsymbol{a}_2\right)\right) . \tag{2.16}$$

Thus only the first two Laue conditions have to be met. The momentum transfer $\boldsymbol{q} = \boldsymbol{q}_\parallel + \boldsymbol{q}_\perp$ can then be split in two orthogonal parts, $\boldsymbol{q}_\parallel \boldsymbol{q}_\perp = 0$. $\boldsymbol{q}_\perp$ is orthogonal to $\boldsymbol{a}_1$ and $\boldsymbol{a}_2$,

$$\boldsymbol{a}_1\boldsymbol{q}_\perp = \boldsymbol{a}_2\boldsymbol{q}_\perp = 0\,, \tag{2.17}$$

whereas $\boldsymbol{q}_\parallel$ is constructed to fulfill the two Laue conditions,

$$\boldsymbol{q}_\parallel \boldsymbol{a}_1 = 2\pi h\,, \qquad \boldsymbol{q}_\parallel \boldsymbol{a}_2 = 2\pi k\,. \tag{2.18}$$

The Laue conditions are met for all vectors $\boldsymbol{q}_\perp$, but only for certain vectors $\boldsymbol{q}_\parallel$. Therefore the scattered intensity from a $2d$ monolayer appears as sketched in Fig. 2.3. The continuous intensity for a given value $\boldsymbol{q}_\parallel$ for scans along $\boldsymbol{q}_\perp$ are called Bragg or crystal truncation rods.

The scattering intensity that is expected from a semi-infinity surface can be constructed as a superposition of bulk scattering, giving rise to Bragg peaks, and monolayer scattering from the topmost surface layers, giving rise to intensity along rods, see Fig. 2.4. The detailed scattering intensity must be calculated from Eq. (2.5). Generally for surface experiments one is mostly interested in intensity scattered from electrons close to the surface. Photons from real x-ray sources exhibit a finite coherence length, the x-ray beam has a finite diameter and the penetration depth of the x-ray beam in the material is also

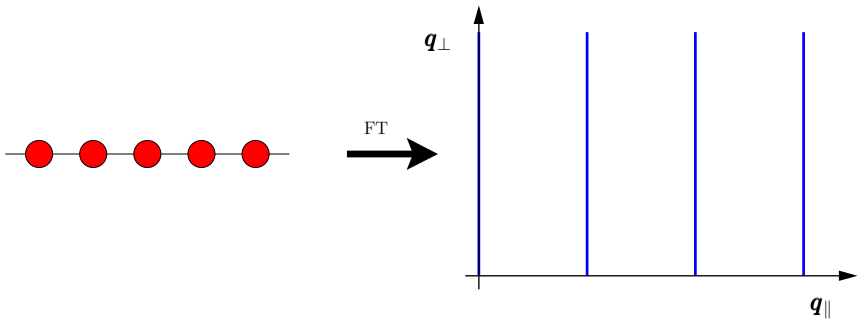

Figure 2.3: Sketch of the scattered intensity from a monolayer.

finite. These effects were not taken into account in the derivation of Eq. (2.5). In order to increase the portion of photons coherently scattered at surface electrons, surface x-ray experiments are usually carried out with a grazing beam that has a small angle between surface layer and x-ray beam.

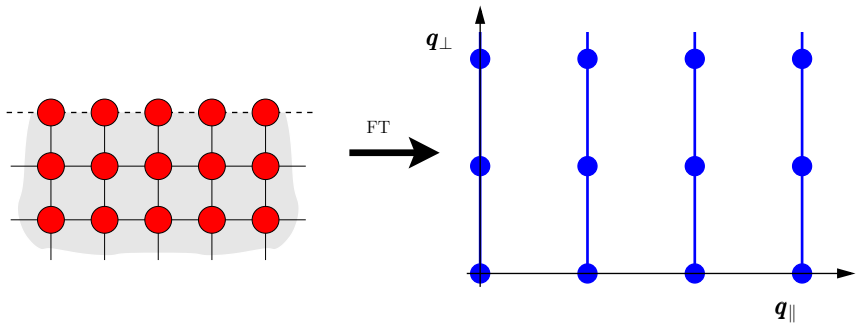

Figure 2.4: Sketch of the scattered intensity from a surface.

Sometimes the size or shape of the unit cell of the surface is different from the bulk unit cell, *e.g.*, because the atoms reconstruct at the surface, Fig. 2.5, or the surface is ordered while the bulk material beneath is disordered, Fig. 2.6. For simplicity, it is assumed that the unit cell vectors within the surface are elongated by factors of n_1, n_2 with respect to the unreconstructed/disordered surface, $\boldsymbol{A}_1 = n_1\boldsymbol{a_1}$, $\boldsymbol{A}_2 = n_2\boldsymbol{a_2}$. Hence the new Laue conditions for $\boldsymbol{q}_\parallel$ are,

$$\boldsymbol{q}_\parallel \boldsymbol{a}_1 = \frac{2\pi h}{n_1}, \qquad \boldsymbol{q}_\parallel \boldsymbol{a}_2 = \frac{2\pi k}{n_2}. \tag{2.19}$$

For scans where $\boldsymbol{q}_\parallel \boldsymbol{a}_2$ is kept constant therefore $n_1 - 1$ new rods appear between two rods from the unreconstructed/disordered surface. These new rods are referred to as superstructure rods while the scattering intensities from the unreconstructed/disordered surface are called fundamental rods.

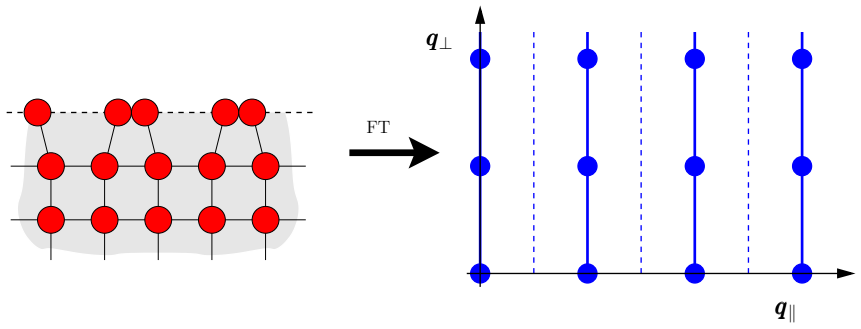

Figure 2.5: Additional rods appear within the surface scattered intensity if the surface layer reconstructs.

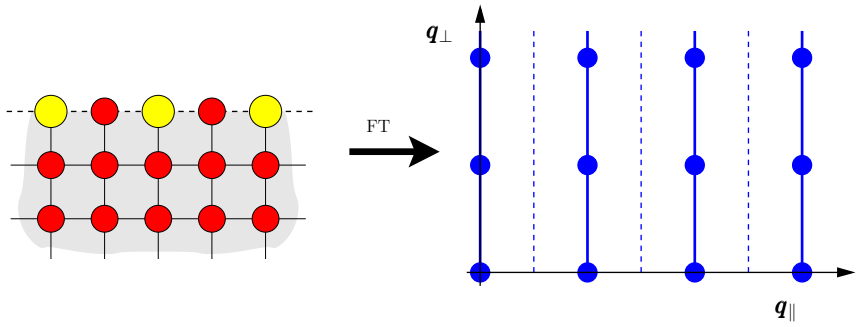

Figure 2.6: Additional rods from an ordered surface are superimposed with fundamental rods.

2.2.2 Information on the rods

The expected intensity along the rods can be calculated from detailed models for the charge density $\rho(\boldsymbol{r})$ at the surface, using Eq. (2.5) (The simple assumptions made in the derivation of Eq. (2.5) are not always justified, and for a detailed quantitative analysis the theory needs to be extended to take into account the finite coherence length of the x-ray, the finite diameter of the x-ray beam and the finite penetration depth into the material. To a certain extent, also the scattering cross section depends on the energy of the x-rays). The calculated intensity then can be compared with the measured intensity in order to verify or falsify surface models.

From model calculations, some general behavior can be extracted, see Fig. 2.7.

a. Relaxations of the interlayer distances at the surface or roughness of the surface generally give rise to an asymmetric intensity along the rods between two bulk Bragg peaks.

b. Characteristic modulations of the intensity along rods can reveal whether a surface is ordered or disordered and how many layers of the surface are ordered.

c. The line width of the rods, *e.g.*, the intensity distribution orthogonal to the rods, carries information about the "quality" of the surface, such as the degree of order within the surface or the surface morphology.

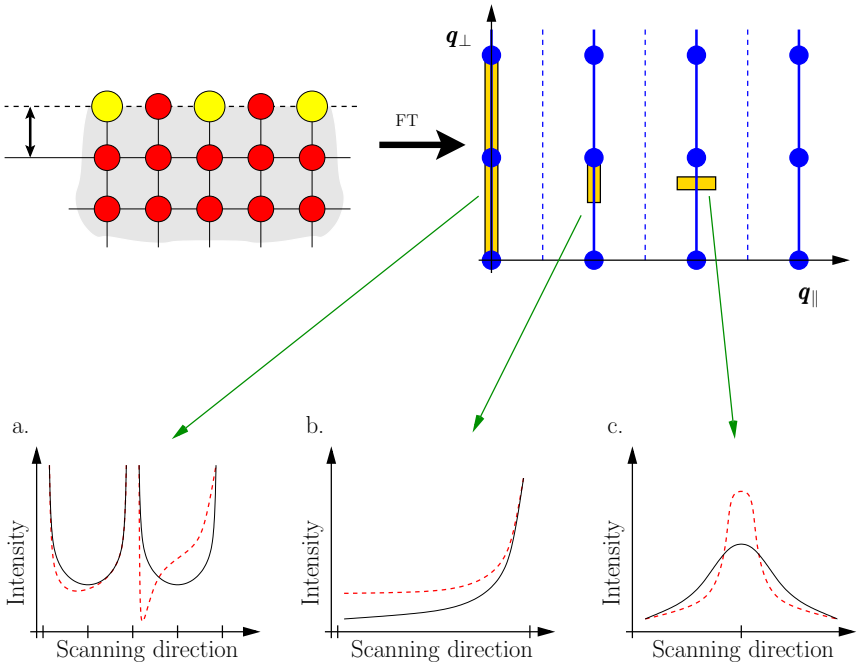

Figure 2.7: Information coded on the rods as described in the text. Shown are typical intensity changes for scans along the portion of the rods depicted. The dashed red curve shows the modifications of the intensity due to an expanded top layer (a.), monolayer surface ordering (b.) and different order parameters of the ordered surface (c.).

2.3 Results for Ni-10%Al(110)

2.3.1 Bulk phase diagram

Al and Ni exhibit fcc structure, whereby their lattice constants at room temperature deviate considerably from each other,

$$a_{\mathrm{Al}} = 7.65\text{a.u.}, \qquad a_{\mathrm{Ni}} = 6.65\text{a.u.}. \tag{2.20}$$

At stoichiometric composition NiAl crystallizes in Cesium Chloride CsCl structure (B2). The B2 structure consists of two interpenetrating simple cubic lattices, occupied with Al and Ni atoms, respectively. The underlying lattice (the lattice of atomic positions irrespective of the occupation of the lattice sites with Al or Ni) is thus bcc.

At a composition of *ca.* 75% Ni the alloy forms in a relatively small range of concentrations a fcc-based Cu_3Au ($L1_2$) structure, the so-called γ' structure, see Fig. 2.8. Interestingly, the γ' structure remains ordered up to the melting temperature of 1385° C of the Ni_3Al alloy. At higher concentrations a rather broad two-phase region of the $L1_2$-ordered γ' phase and the disordered γ phase exists. Further information on the NiAl phase diagram can be found in [6,7,8,9].

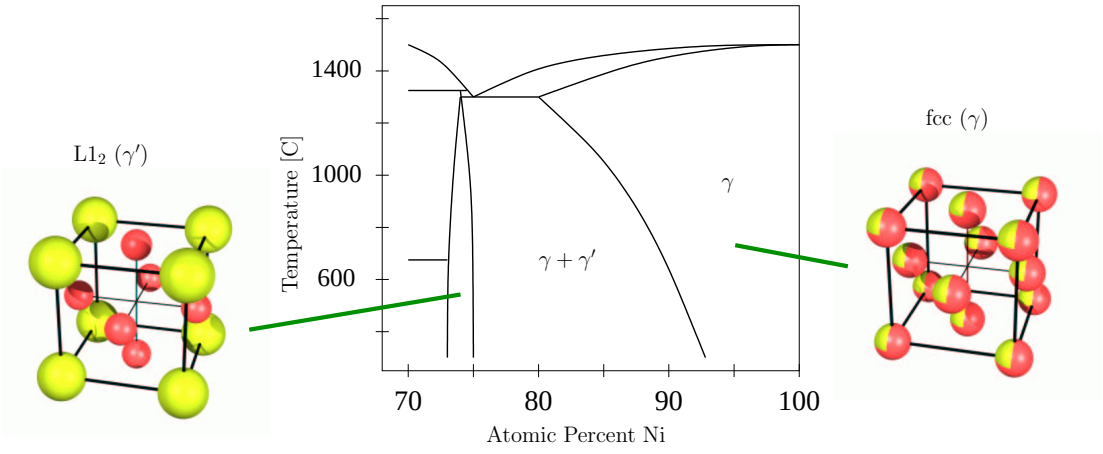

Figure 2.8: Nickel-rich part of the NiAl phase diagram.

2.3.2 Behavior of surfaces of the Ni-rich NiAl-alloy

Literature survey

- Schulthess *et al.* [10] examined the (111) surface of Ni-10%Al using low-energy ion scattering spectroscopy with 1000 eV He ions. At 700° C the authors find a concentration of $c_{\mathrm{Al}} = 21(\pm 1)\%$ in the surface layer, at 800° C the concentration of Al is $c_{\mathrm{Al}} = 25(\pm 1)\%$. The Al concentration of $c_{\mathrm{Al}} = 25(\pm 1)\%$ does not change when the sample is cooled down to 400° C.

Furthermore, the authors also performed first-principles calculations on the surface behavior of Ni-10%Al(111) using the coherent potential approximation implemented within the layer Korringa-Kohn-Rostocker multiple scattering formalism using a modified single-site implementation [11,12,13]. Neglecting the effect of local relaxations, the authors find a concentration of $c_{\mathrm{Al}} = 25\%$. They conclude that this Al concentration corresponds to an ordered $L1_2$ structure within the surface.

- Polak *et al.* [14,15] examined the behavior of the (110) surface of Ni-9%Al using low-energy Auger electron spectroscopy. They find that Al segregates to the surface and that the absolute value for the concentration of Al in the top surface layer depends on temperature. The Al concentration in the first layer increases with temperature from *ca.* 500° C to 750° C. The authors conclude from the time scale for the segregation of Al into the surface upon heating (measured at annealed samples) that the enrichment of Al in the surface is reversible. Thus the Al concentration in the top layer should decrease when the sample is cooled again (In this context of measuring time scales at annealed surface samples the equilibration studies at the surface of Fe-Al by Hammer *et al.* might be interesting [16]).

  This behavior is explained by the free energy concentration expansion method [17] as a competition between short-range order tendencies in the bulk material and the tendency of Al to segregate into the surface.

Results from experiments by H. Reichert

The (110) surface of a $Ni_{90}Al_{10}$ single crystal was prepared in a standard UHV procedure. Numerous cycles of sputtering and high-temperature annealing were applied to remove carbon and sulfur impurities from the bulk material. For the measurements the sample was mounted in an *in-situ* UHV chamber. The temperature dependent gracing angle surface x-ray studies were carried out at the National Synchrotron Light Source (NSLS) using beamline X16A equipped with a $(2 + 2)$ surface diffractometer allowing surface-sensitive in-plane and out-of-plane scans [18].

Fig. 2.9a depicts the structure of a $L1_2(110)$ layer and of a $D0_{22}(110)$ layer. In reciprocal space, Fig. 2.9b , the presence of such an ordered layer gives rise to additional rods, dashed lines in Fig. 2.9b, which emerge at characteristic in-plane positions. This superlattice intensity is constant normal to the surface, if the order is restricted to one monolayer only, and develops characteristic modulations, if more than one ordered layer is involved [1]. Thus surface sensitive observations of an in-plane superlattice intensity and measurements of its intensity distribution normal to the surface gives evidence for the presence of surface order and for the number of layers involved.

After *in-situ* sputtering of the sample surface no such in-plane superlattice intensity corresponding to an $L1_2$-ordered surface could be detected. However, upon heating to 1050 K the $(01L)$ superlattice rod indeed emerged. The inset of Fig. 2.10 shows the in-plane Bragg profile recorded at $L = 0.5$. The width of the peak corresponds to a coherent domain size of 50 nm. The distribution of the in-plane integrated (and background corrected)

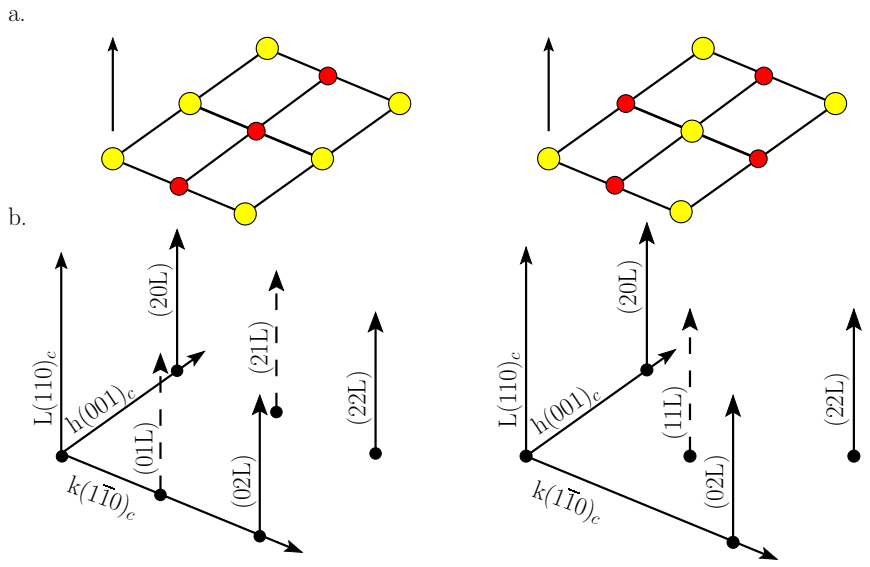

Figure 2.9: The structure of the simplest possible decorations of the fcc (110) surface with 50% Al in the first layer and no like atoms on nearest-neighbor sites correspond to cuts through the $L1_2$ (left) and the $D0_{22}$ (right) structure. The corresponding surface rods are also shown.

intensity along the rod $(01L)$ is depicted in Fig. 2.10 together with model calculations. Note that the intensity at $L = 1$ is due to the (011) bulk reflection, the associated fundamental fcc-rod is shown as black line. In contrast to the calculated intensity for the disordered surface, the experimental intensity levels off at an intensity level which is virtually constant as a function of L, thereby giving evidence for additional surface scattering which originated from a monolayer only. This qualitative argument was confirmed by model calculations by Reichert also shown in Fig. 2.10.

The x-ray studies of H. Reichert thus showed that an $L1_2$ ordered monolayer emerged on top of disordered fcc bulk (see Fig. 2.11 for a model of the $L1_2$ ordered surface). Since the surface intensity shows no temperature dependence and remains constant in particular upon cooling, it must be concluded that the ground state configuration of the $Ni_{90}Al_{10}(110)$ system consists of a phase separated $(\gamma - \gamma')$ bulk structure which coexists with a γ' monolayer at the (110) surface.

A similar behavior as for $Ni_{90}Al_{10}(110)$, namely segregation of Al into the surface and surface ordering, was also observed for the (111) surface [19]. However, upon heating to 1050 K, sulfur diffusion into the surface seemed to have destroyed the surface order, hence the crystal could not be used for further experiments.

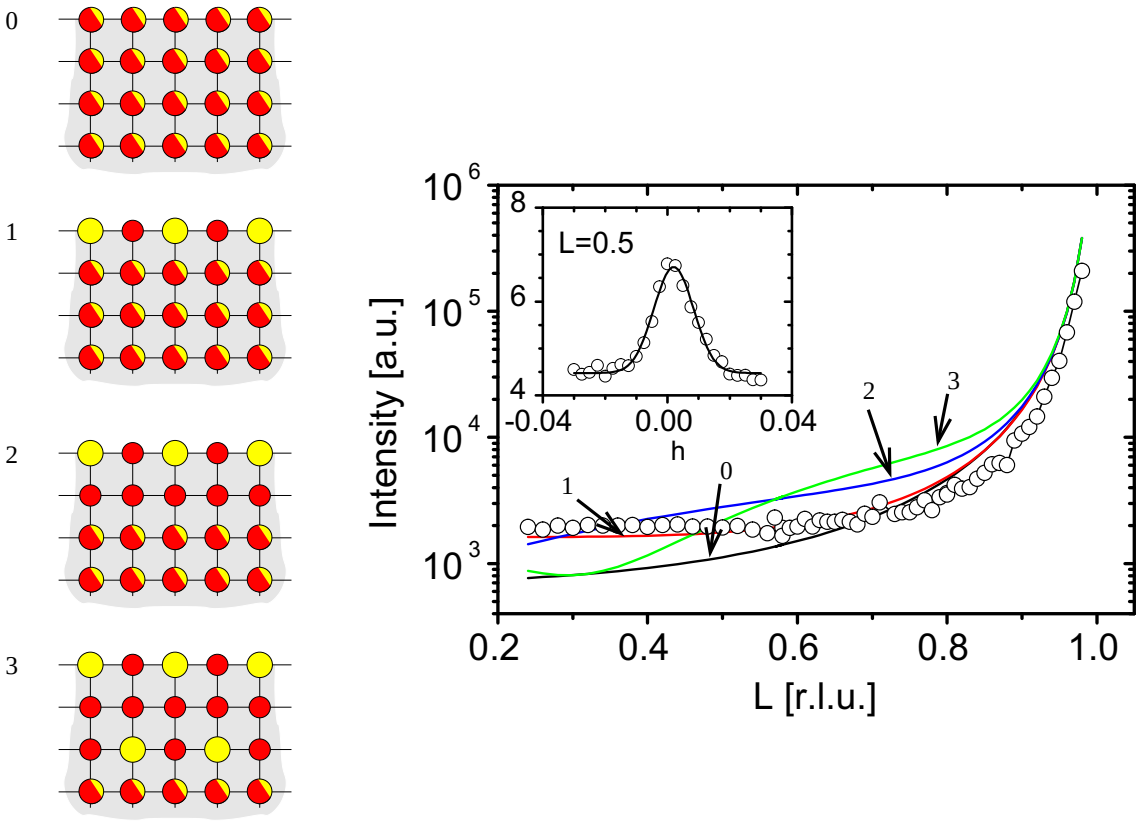

Figure 2.10: Measured intensity distribution along the $(01L)$ surface rod corrected for background and geometrical effects (circles). Model calculations including 0, 1, 2, and 3 layers of the ordered $L1_2$ structure on the disordered bulk material are also shown. The inset shows an in-plane scan through the $(01L)$ truncation rod at $L = 0.5$ r.l.u. The intensities are given on a logarithmic scale in arbitrary units, the x-axis are given in reciprocal lattice units.

a. b.

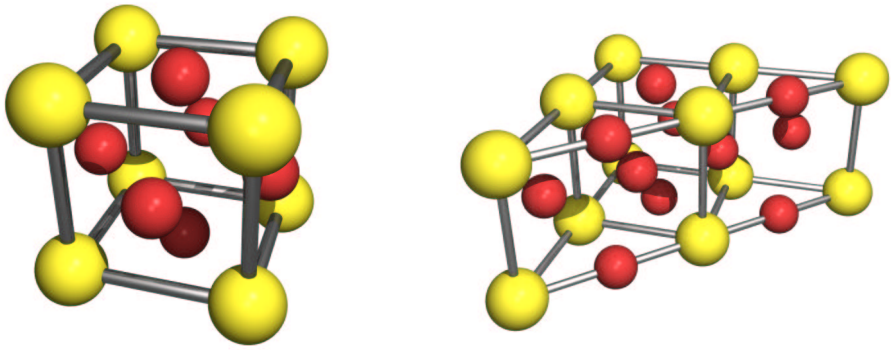

Figure 2.11: The $L1_2$ structure (a) cut along the (110) plane (b).

Chapter 3

Electron theory

The Hamilton operator $\hat{H}$ of a non-relativistic many-body system containing nuclei and electrons is given by,

$$\hat{H} = \hat{T}_e + \hat{T}_Z + \hat{V}_{ee} + \hat{V}_{eZ} + \hat{V}_{ZZ} \tag{3.1}$$

$$= \hat{H}_e + \hat{T}_Z + \hat{V}_{ZZ}\,, \tag{3.2}$$

where the kinetic energy of the electrons is given as,

$$\hat{T}_e = \sum_i \frac{\boldsymbol{p}_i^2}{2m_e}\,, \tag{3.3}$$

with the momentum operator $\boldsymbol{p}_i$ and the mass m_e of the electrons. For the nuclei with momentum operator $\boldsymbol{P}_n$ and masses M_n the kinetic is written as,

$$\hat{T}_Z = \sum_n \frac{\boldsymbol{P}_n^2}{2M_n}\,. \tag{3.4}$$

The Coulomb interaction between the electrons, $\hat{V}_{ee}$, the nuclei with charge Z_n and the electrons, $\hat{V}_{eZ}$, and the nuclei themselves, $\hat{V}_{ZZ}$ are:

$$\hat{V}_{ee} = \frac{1}{2}\sum_{ij} \frac{e^2}{|\boldsymbol{r}_i - \boldsymbol{r}_j|}\,, \tag{3.5}$$

$$\hat{V}_{eZ} = -\frac{1}{2}\sum_{in} \frac{Z_n e^2}{|\boldsymbol{r}_i - \boldsymbol{R}_n|}\,, \tag{3.6}$$

$$\hat{V}_{ZZ} = \frac{1}{2}\sum_{nm} \frac{Z_n Z_m e^2}{|\boldsymbol{R}_m - \boldsymbol{R}_n|}\,. \tag{3.7}$$

3.1 Adiabatic approximation for the nuclei

The masses of the nuclei M_n are 3 to 5 orders of magnitude larger than the electron mass m_e. If the ratio M_n/m_e is further increased by increasing all masses of the nuclei to

infinity, $M_n \to \infty$, the positions of the nuclei are fixed at $\boldsymbol{R}_n$ and the kinetic energy of the nuclei drops out. Taking $M_n \to \infty$ is equivalent to setting $\hbar \to 0$ and thus the quantum mechanical character of the nuclei is simply neglected.

For a given set of fixed nuclei positions $\{\boldsymbol{R}_n\}$, the eigenvalues E_α of the electron eigenstates $|\phi_\alpha\rangle$ are calculated as,

$$\hat{H}_e \, |\phi_\alpha\rangle = E_\alpha \, |\phi_\alpha\rangle \ , \tag{3.8}$$

and depend parametrically on the positions of the nuclei,

$$E_\alpha = E_\alpha \left(\{\boldsymbol{R}_n\}\right) . \tag{3.9}$$

From the ground state energy of the electrons $E_0 = E_0 \left(\{\boldsymbol{R}_n\}\right)$, we define an effective potential for the nuclei,

$$V_{Z,eff} \left(\{\boldsymbol{R}_n\}\right) = \hat{V}_{ZZ} \left(\{\boldsymbol{R}_n\}\right) + E_0 \left(\{\boldsymbol{R}_n\}\right) , \tag{3.10}$$

that allows to calculate, *e.g.*, forces on the nuclei,

$$\boldsymbol{F}_m = -\nabla_m V_{Z,eff} \left(\{\boldsymbol{R}_n\}\right) . \tag{3.11}$$

We can thus relax a certain set of nuclei positions into the configuration with the minimum energy, *e.g.*, to calculate bond lengths and angles in molecules or lattice constants and tetragonal distortions in crystals.

3.1.1 Born-Oppenheimer approximation

If we now assume that the real nuclei move so slowly that the electrons at any time are fully relaxed in their ground state $E_0 \left(\{\boldsymbol{R}_n\}\right)$, we can write down an approximate Hamilton operator for the movement of the nuclei [20],

$$\hat{H}_Z = \hat{T}_Z + V_{Z,eff} \, . \tag{3.12}$$

Temperature induced deviations of the nuclei positions from their ideal minimum energy lattice sites in a crystal are generally small. Thus often an harmonic expansion of $V_{Z,eff}$ is a good approximation, and we are left with a relatively easy to handle harmonic oscillator. In phonon calculations this is the standard procedure [21,22,23,24,25].

For "ab-initio" molecular dynamics one usually looks at the nuclei as classical point masses and integrates classical equations of motions of point masses in the effective potential $V_{Z,eff}$.

3.2 Density functional theory

Assume for the moment that we are interested in finding the electronic wavefunction for a given set of fixed nuclei positions. For N_e electrons this means $3N_e$ variables. For numerical implementations we need to sample each variable on a grid of k points [26], resulting in at

least k^{3N_e} numbers that need to be stored in a computer. If we sample with $k = 100$, a nowadays high-end computer with 10 Gigabytes of memory and double precision numbers of 64 bit size can handle a three-electron problem (This consideration is not completely realistic, as the many-body wavefunctions need to be antisymmetric. One may be able to take this into account for numerical purposes).

In other words, for crystals or medium sized molecules, where we often have to deal with hundreds of electrons, we need to simplify the many-electron problem before we can even think of starting a real calculation.

Two theorems of Hohenberg and Kohn [27,28] will turn out to be enormously helpful.

1. From the external potential $v_{ext}(\boldsymbol{r})$ applied to a many-electron system one can calculate the ground state density $n_0(\boldsymbol{r})$ with the help of Schrödinger's equation. Also, from the ground state density $n_0(\boldsymbol{r})$ one can (apart from a constant) determine the external potential $v_{ext}(\boldsymbol{r})$ acting on the many-electron system. This means that all ground state properties of a system, such as the ground state energy, can be calculated from the knowledge of the ground state density $n_0(\boldsymbol{r})$ alone. Thus there exists a functional $E[n_0]$ that allows us to calculate,

$$E_0(\{\boldsymbol{R}_m\}) = E[n_0]\,. \tag{3.13}$$

2. For a given external potential $v_{ext}(\boldsymbol{r})$, the functional $E[n]$ is minimum only for the ground state density,

$$E[n] \geq E[n_0]\,. \tag{3.14}$$

The benefits of the two theorems are obvious. They tell us that in principle we can calculate the ground state energy of a many-electron system from the knowledge of the density n_0 alone, and n_0 is a function of just three variables irrespective of the number of electrons in the system compared to the $3N_e$ variables of the wavefunction.

All observables of excited states are, via the Schrödinger equation, given as a functional of the external potential applied to the system, *e.g.*, $E_\alpha(\{\boldsymbol{R}_m\}) = E_\alpha[v_{ext}]$. From theorem 1. we conclude that observables of all excited states are a functional of the ground state density alone,

$$E_\alpha(\{\boldsymbol{R}_m\}) = E_\alpha[n_0]\,. \tag{3.15}$$

At first glance this means that we should forget about the wavefunction concept in quantum mechanics! But we simply do not know how to calculate, *e.g.*, excited states via $E_\alpha[n_0]$, and nobody knows how to define an excited state from a density alone without the concept of a wavefunction. In order to benefit from the theorems 1. and 2. one needs an instruction on how to calculate $E_0(\{\boldsymbol{R}_m\}) = E[n_0]$. As we will see in the next section, the only known way so far to calculate $E_0(\{\boldsymbol{R}_m\}) = E[n_0]$ uses one-electron wave functions. This means that for practical implementations one did not manage to get rid of the wavefunction concept yet (A one-particle wavefunction still is much better than a many-particle wavefunction from a computational point of view, as it is, like the density, a function of 3 variables).

3.3 Kohn-Sham equations

For the calculation of $F[n] = T_e[n] + V_{ee}[n]$ we neither know the kinetic energy of the electrons as a functional of the density,

$$T_e[n] = \langle\phi|\, T_e\, |\phi\rangle \ , \tag{3.16}$$

nor the expectation value for the interaction of the electrons,

$$V_{ee}[n] = \langle\phi|\, V_{ee}\, |\phi\rangle \ . \tag{3.17}$$

Kohn and Sham replaced these quantities by their known one-electron expression,

$$T_{KS}[n] = \sum_{\alpha}^{N_e} \langle\psi_\alpha|\, \hat{T}_e\, |\psi_\alpha\rangle = \sum_{\alpha}^{N_e} \langle\psi_\alpha|\, -\frac{\hbar^2}{2m_e}\triangle\, |\psi_\alpha\rangle \ , \tag{3.18}$$

$$E_H[n] = \sum_{\alpha}^{N_e} \langle\psi_\alpha|\, \hat{V}_{ee}\, |\psi_\alpha\rangle = \sum_{\alpha}^{N_e} \langle\psi_\alpha|\, \frac{e^2}{2}\int dV' \frac{n\,(\boldsymbol{r}')}{|\boldsymbol{r}-\boldsymbol{r}'|}\, |\psi_\alpha\rangle \ , \tag{3.19}$$

where ψ_α are one-particle wavefunctions that are solutions of a one-particle Schrödinger equation with an effective, yet undetermined, potential v_{eff}. In this way the many-electron system is mapped on a system of non-interacting electrons in an effective potential. The difference to the many-electron wavefunction observables is hidden in the expression $E_{xc}[n]$ that is called, in accordance with historic considerations like, *e.g.*, the Hartree and the Hartree-Fock equations, exchange-correlation functional,

$$F[n] = T_e[n] + V_{ee}[n] = T_{KS}[n] + E_H[n] + E_{xc}[n]\,. \tag{3.20}$$

For the moment we assume $E_{xc}[n]$ to be known, but it should be noted that the difficulties of finding an explicit expression for $F[n]$ have just been called $E_{xc}[n]$.

Clearly the wave function ϕ has to be antisymmetric, which will result in very complicated constraints for the ground state density n_0. Implicitly we already obeyed the Pauli-Principle for the one-electron wave functions of non-interacting electrons in Eq. (3.18) and Eq. (3.19) by assuming that each one-particle state may be occupied by only one electron. We thus made an implicit Ansatz for possible allowed ground state densities,

$$n\,(\boldsymbol{r}) = \sum_{\alpha}^{N_e} |\psi_\alpha\,(\boldsymbol{r})\,|^2\,. \tag{3.21}$$

The variational principle for the ground state density $n\,(\boldsymbol{r})$ from theorem 2 of the previous section,

$$\delta_{n(\boldsymbol{r})}\left(E[n] - \mu\int dV n\,(\boldsymbol{r})\right) = 0\,, \tag{3.22}$$

(where we coupled the constraint of having $N_e = \int dV n(\boldsymbol{r})$ electrons in the system with a Lagrange parameter μ) results with the help of Eq. (3.21) in the form of an effective one-electron Schrödinger equation,

$$\left(-\frac{\hbar^2}{2m_e}\triangle + v_{eff}\right)\psi_\alpha = \epsilon_\alpha \psi_\alpha \,. \tag{3.23}$$

When we take into account that the ground state density of the real many-electron system and the hypothetical system of non-interacting electrons must be the same, the effective potential v_{eff} is given by,

$$\begin{aligned} v_{eff} &= \frac{\delta}{\delta n}\left(E_H[n] + E_{xc}[n] + \int dV n(\boldsymbol{r})\, v_{ext}(\boldsymbol{r})\right) \\ &= v_H[n] + v_{xc}[n] + v_{ext}\,, \end{aligned} \tag{3.24}$$

where the nuclei-electron interaction is contained in v_{ext}.

Obviously the effective potential v_{eff} depends on the density n. Thus each electron moves in an effective potential generated by the density of all electrons. Therefore, in order to calculate the ground state density of a many-electron system we need to solve Eqs. (3.21, 3.23, 3.24), the Kohn-Sham equations [29], simultaneously, *e.g.*, in an iterative fashion.

3.4 Local density approximation

All considerations of the previous sections will be of practical use only if a good approximation for the exchange-correlation energy E_{xc} can be found. To date, no approximation that seems to give accurate energies for all external potentials v_{ext} was found, and the search for E_{xc} as well as the search for a relativistic formulation of density functional theory is in fact a challenging problem [30].

We will restrict ourselves to the simplest and oldest approximation of E_{xc}, the local density approximation [29] that was used for the remainder of this work. The functional E_{xc} is approximated as,

$$E_{xc} \approx E_{xc}^{\mathrm{LDA}}[n] = \int dV n(\boldsymbol{r})\, \epsilon_{xc}(n(\boldsymbol{r}))\,, \tag{3.25}$$

where $\epsilon_{xc}(n)$ is the exchange correlation energy density of a homogenous electron gas of density n [31,32,33,34,35,24].

3.5 Implementation of the Kohn-Sham equations

All ab-initio calculations for this work were carried out using the mixed-basis pseudopotential package [36,24]. For numerical efficiency, the one-electron Kohn-Sham wavefunctions

of the core electrons were kept fixed to their atomic values in all calculations. The valence electrons thus interact with an effective potential generated by the frozen core electrons and the nuclei. The one-electron wavefunctions of the valence electrons are represented in a mixed-basis consisting of plane waves and some localized atomic-like orbitals. In order to allow a numerically feasible representation of the valence wavefunctions, the effective potential generated by the frozen core and the nuclei is replaced by a much softer, norm-conserving pseudopotential. The pseudopotential exhibits the same valence wavefunctions outside the pseudopotential radius, where bonds to other atoms are formed, but no knots and no fast oscillations inside the pseudopotential radius. This means that the representation of the valence wavefunctions for the pseudopotential requires fewer plane waves but the chemical behavior, *e.g.*, the bond formation, is the same as for the effective frozen core potential. We list a selection of puclications [37,38,39,40,41,42,43,44,45,46,47,48,49,50,51, 52,53,54,55,56] dealing with the mixed-basis representation and with pseudopotentials.

Chapter 4

Many-body potentials

4.1 Energetics in an alloy

Coupling an alloy to a heat bath induces different possible excitations, which we separate in two coupled parts (Sec. 3.1.1): Excitations of the electronic system and movements of the nuclei.

Excitations of the electrons cannot fully be taken into account by the conventional density functional theory as described in chapter 3, however, several authors assumed that E_{xc} is independent of temperature which allows to couple a heat bath by a simple Fermi smearing function to the electrons [57,58] (Also more general approaches exist that take into account the temperature dependence of E_{xc} explicitly). We will neglect excitations of the electrons as we believe that these excitations will only slightly modify the phase diagram at the experimental temperatures that we are interested in, however, if necessary we can always test this approximation by applying a Fermi smearing directly in our calculations.

Neglecting electronic excitations, the model alloy we are now dealing with can be fully specified by the movement and the positions of the nuclei. Phonon calculations show that a treatment of the nuclei as classical point masses is an excellent approximation down to relatively low temperatures, *e.g.*, the experimental measuring temperatures, and rather heavy nuclei, where Al and Ni are heavy elements compared to hydrogen. The nuclei in the alloy thus move in an "effective" classical potential mediated via the electrons and direct nucleus-nucleus Coulomb interaction. A number m is attached to every nucleus, $\boldsymbol{r}_m$ specifies its position, and an integer σ_m defines the type of atom at the position $\boldsymbol{r}_m$.

In this chapter we show that the energy of an alloy can be uniquely expanded in many-body potentials. We will first introduce the necessary definitions and then proceed with the proof. An example for the expansion of effective pair interactions in many-body potentials will also be given. In chapter 5 we then will link the many-body potentials derived in this chapter to the expansion coefficients of the well-known cluster expansion [59]. To approach the cluster expansion from the many-body potentials will allow us to determine the dependence of the expansion coefficients on the position of the atoms.

4.2 Many-body potential expansion

Let $E(M)$ be the total energy of a M particle system,

$$E(M) = E(X_1, X_2, X_3, \ldots, X_M) \;, \tag{4.1}$$

where the position $\boldsymbol{r}_n$ and the species σ_n of atom n is denoted with $X_n = \{\boldsymbol{r}_n, \sigma_n\}$. As the order of $X_1, X_2, \ldots, X_M$ in $E(M)$ may not be relevant for the energy, $E(M)$ is a symmetric (even) function of the $\{X_n\}$ with respect to the exchange of two arguments, see Fig. 4.1.

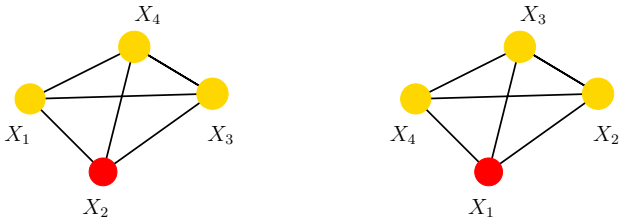

Figure 4.1: There is no unique order for labeling the atoms of a system. In this example, the energy of the four particle system thus may not depend on the order of the arguments and we therefore have to demand $E(X_1, X_2, X_3, X_4) = E(X_4, X_1, X_2, X_3)$.

We define the summation operator $\mathfrak{S}_M^{(N)}$ that sums over all pairwise different arguments of a function $f(X_{m_1}, \ldots, X_{m_N})$ with N arguments in a M particle system,

$$\mathfrak{S}_M^{(N)} = \frac{1}{N!} \sum_{m_1 \neq}^{M} \sum_{m_2 \neq}^{M} \cdots \sum_{\neq m_N}^{M} \;. \tag{4.2}$$

As $E(M)$ is an even function,

$$E(M) = \mathfrak{S}_M^{(M)} E(M) \;. \tag{4.3}$$

4.2.1 Definition of $W^{(N)}$

In order to expand the energy $E(M)$ in many-body potentials, we introduce intermediate quantities $W^{(N)}$. The N particle functions $W^{(N)}$ that are generated from $E(M)$ do depend only on $N \leq M$ of the M particles. We define the set of all points,

$$\alpha_M = \{X_1, X_2, X_3, \ldots, X_M\} \,, \tag{4.4}$$

and the subset,

$$\alpha_N = \{X_1, X_2, X_3, \ldots, X_N\} \,, \tag{4.5}$$

with $N \leq M$. The operator,

$$\lim_{\alpha_M \setminus \alpha_N \to \infty} E(X_1, X_2, X_3, \ldots, X_M) \;, \tag{4.6}$$

leaves the positions of the set $\alpha_N = \{X_1, X_2, X_3, \ldots, X_N\}$ located at finite distances from the origin and takes the positions of the set $\alpha_M \backslash \alpha_N = \{X_{N+1}, \ldots, X_M\}$ to infinite distances from the origin in such a way that also the distances between the positions from set $\{X_{N+1}, \ldots, X_M\}$ are infinite.

We define functions $W^{(N)}$,

$$W^{(N)}\left(X_1, X_2, \ldots, X_N\right) = \lim_{\alpha_M \backslash \alpha_N \to \infty} E\left(M\right) \,, \tag{4.7}$$

that are invariant when the order of the arguments is changed $X_i \leftrightarrow X_j$ and thus are even functions,

$$W^{(N)} = \mathfrak{S}_N^{(N)} W^{(N)} \,. \tag{4.8}$$

For $N \leq M$ particles, $W^{(N)}\left(X_1, X_2, \ldots, X_N\right)$ just corresponds to the energy of the N-particle system,

$$E\left(N\right) = W^{(N)}\left(X_1, X_2, \ldots, X_N\right) \,. \tag{4.9}$$

Other definitions of $W^{(N)}$

Depending on the physical context, we can derive functions of fewer than M variables from $E(M)$ in other ways than with the operator $\lim_{\alpha_M \backslash \alpha_N \to \infty} E\left(X_1, X_2, X_3, \ldots, X_M\right)$. For example, let us think of an even probability distribution $\rho(M)$ of M particles. Then an operator that performs an integration over all coordinates contained in the set $\alpha_M \setminus \alpha_N$ results in functions $W^{(N)}$,

$$W^{(N)}\left(X_1, X_2, \ldots, X_N\right) = \int_{-\infty}^{\infty} dV_{(\alpha_M \backslash \alpha_N)}\, \rho\left(X_1, X_2, X_3, \ldots, X_M\right) \,, \tag{4.10}$$

that can be interpreted in a physical picture. For instance, if $\rho(M)$ is the probability distribution of M particles, then $W^{(1)}\left(X_1\right)$ would be the probability density to find a particle at $\boldsymbol{r}_1$.

4.2.2 Expansion of $W^{(N)}$ in many-body potentials $V^{(N)}$

Before we expand the energy $E\left(M\right)$, we start with the expansion of the energy of a N particle subset of the M particle system. We expand $E\left(N\right)$ in many-body potentials $V^{(L)}$ (and thereby implicitly define the many-body potentials),

$$\begin{aligned} W^{(N)}\left(X_1, X_2, \ldots, X_N\right) = V^{(0)} + \sum_{m_1}^{N} V^{(1)}(X_{m_1}) + \frac{1}{2} \sum_{m_1 \neq}^{N} \sum_{m_2}^{N} V^{(2)}(X_{m_1}, X_{m_2}) + \ldots \\ \ldots + \frac{1}{N!} \sum_{m_1 \neq}^{N} \sum_{m_2 \neq}^{N} \cdots \sum_{\neq m_N}^{N} V^{(N)}(X_{m_1}, X_{m_2}, \ldots, X_{m_N}) \,. \end{aligned} \tag{4.11}$$

In short form Eq. (4.11) looks like,

$$W^{(N)} = \sum_{L=0}^{N} \mathfrak{S}_N^{(L)} V^{(L)} \,. \tag{4.12}$$

In order to calculate the many-body potentials $V^{(L)}$, we will invert Eq. (4.12). As we will see, the inversion of Eq. (4.12) requires the evaluation of $\mathfrak{S}_M^{(N)} W^{(N)}$, $N \leq M$. In a next step we therefore extend the summation on the right hand side of Eq. (4.12) formally from particle L to N and rewrite Eq. (4.12),

$$\begin{aligned} W^{(N)}\left(X_1, X_2, \ldots, X_N\right) &= \sum_{L=0}^{N} \frac{1}{L!} \sum_{m_1 \neq}^{N} \cdots \sum_{\neq m_L}^{N} V^{(L)}(X_{m_1}, X_{m_2}, \ldots, X_{m_L}) \\ &= \sum_{m_1 \neq}^{N} \cdots \sum_{\neq m_N}^{N} \left(\sum_{L=0}^{N} \frac{1}{L!} \frac{1}{(N-L)!} V^{(L)}(X_{m_1}, X_{m_2}, \ldots, X_{m_L}) \right) . \end{aligned} \tag{4.13}$$

To be able to calculate the sum of $W^{(N)}$ over all N particle subsets of the M particles, we rewrite Eq. (4.13) with new labels,

$$W^{(N)}\left(X_{m_1}, X_{m_2}, \ldots, X_{m_N}\right) = \sum_{l_1 \neq}^{N} \cdots \sum_{\neq l_N}^{N} \left(\sum_{L=0}^{N} \frac{1}{L!} \frac{1}{(N-L)!} V^{(L)}(X_{m_{l_1}}, X_{m_{l_2}}, \ldots, X_{m_{l_L}}) \right) . \tag{4.14}$$

The index m now labels the particles, while the index l labels the order of the arguments in $W^{(N)}$. The manipulations allow us to calculate the sum over all contributions $W^{(N)}$ contained in the M particle system in terms of the many-body potentials $V^{(L)}$ with ($M \geq$

N),

$$
\begin{aligned}
&\frac{1}{N!}\sum_{m_1\neq}^{M}\cdots\sum_{\neq m_N}^{M} W^{(N)}\left(X_{m_1},X_{m_2},\ldots,X_{m_N}\right)\\
&=\frac{1}{N!}\sum_{m_1\neq}^{M}\cdots\sum_{\neq m_N}^{M}\left(\sum_{l_1\neq}^{N}\cdots\sum_{\neq l_N}^{N}\left(\sum_{L=0}^{N}\frac{1}{L!}\frac{1}{(N-L)!}V^{(L)}(X_{m_{l_1}},X_{m_{l_2}},\ldots,X_{m_{l_L}})\right)\right)\\
&=\frac{1}{N!}\sum_{m_1\neq}^{M}\cdots\sum_{\neq m_N}^{M}\left(\sum_{L=0}^{N}\frac{1}{L!}\frac{1}{(N-L)!}V^{(L)}(X_{m_1},X_{m_2},\ldots,X_{m_L})\right)\\
&\quad+\frac{1}{N!}\sum_{m_1\neq}^{M}\cdots\sum_{\neq m_N}^{M}\left(\sum_{L=0}^{N}\frac{1}{L!}\frac{1}{(N-L)!}V^{(L)}(X_{m_2},X_{m_1},\ldots,X_{m_L})\right)\\
&\quad+\ldots\\
&\quad+\frac{1}{N!}\sum_{m_1\neq}^{M}\cdots\sum_{\neq m_N}^{M}\left(\sum_{L=0}^{N}\frac{1}{L!}\frac{1}{(N-L)!}V^{(L)}(X_{m_N},X_{m_{N-1}},\ldots,X_{m_{N-L+1}})\right)\\
&=\frac{N!}{N!}\sum_{m_1\neq}^{M}\cdots\sum_{\neq m_N}^{M}\left(\sum_{L=0}^{N}\frac{1}{L!}\frac{1}{(N-L)!}V^{(L)}(X_{m_1},X_{m_2},\ldots,X_{m_L})\right)\\
&=\sum_{L=0}^{N}\frac{1}{L!}\frac{1}{(N-L)!}\frac{(M-L)!}{(M-N)!}\sum_{m_1\neq}^{M}\cdots\sum_{\neq m_L}^{M} V^{(L)}(X_{m_1},X_{m_2},\ldots,X_{m_L})\\
&=\sum_{L=0}^{N}\frac{1}{L!}\binom{M-L}{N-L}\sum_{m_1\neq}^{M}\cdots\sum_{\neq m_L}^{M} V^{(L)}(X_{m_1},X_{m_2},\ldots,X_{m_L})\,.
\end{aligned}
\tag{4.15}
$$

The short form of Eq. (4.15) reads,

$$
\mathfrak{S}_M^{(N)}W^{(N)}=\sum_{L=0}^{N}\binom{M-L}{N-L}\mathfrak{S}_M^{(L)}V^{(L)}\,. \tag{4.16}
$$

For the determination of the many-body potentials $V^{(L)}$ from the contributions $W^{(N)}$ we need to invert Eq. (4.16). The inversion of Eq. (4.16) can be achieved by:

$$
\mathfrak{S}_M^{(N)}V^{(N)}=\sum_{L=0}^{N}a_{MN}^{(L)}\mathfrak{S}_M^{(L)}W^{(L)}\,. \tag{4.17}
$$

To calculate the coefficients $a_{MN}^{(L)}$ we insert Eq. (4.16),

$$\begin{aligned}\mathfrak{S}_M^{(N)} V^{(N)} &= \sum_{L=0}^{N} a_{MN}^{(L)} \mathfrak{S}_M^{(L)} W^{(L)} \\ &= \sum_{L=0}^{N} a_{MN}^{(L)} \sum_{K=0}^{L} \binom{M-K}{L-K} \mathfrak{S}_M^{(K)} V^{(K)} \\ &\overset{\text{Eq. (A.1)}}{=} \sum_{K=0}^{N} \sum_{L=K}^{N} a_{MN}^{(L)} \binom{M-K}{L-K} \mathfrak{S}_M^{(K)} V^{(K)} \,. \end{aligned} \tag{4.18}$$

Eq. (4.18) is solved by:

$$\delta_{NK} = \sum_{L=K}^{N} a_{MN}^{(L)} \binom{M-K}{L-K} \,. \tag{4.19}$$

Eq. (4.19) will be used for the determination of the coefficients $a_{MN}^{(L)}$ in the following sections.

We note that Eq. (4.17) allows only the calculation of $E^{(N)} = \mathfrak{S}_M^{(N)} V^{(N)}$. However, we are interested in the potential $V^{(N)}$ itself. In the next section we will see that symmetry requirements for the many-body potentials will help us to determine $V^{(N)}$ from $E^{(N)}$.

4.2.3 Symmetry of the many-body potentials $V^{(N)}$

For the determination of the many-body potential $V^{(N)}$ we note that,

$$E^{(N)}\left(X_1, \ldots, X_N\right) = \frac{1}{N!} \sum_{m_1 \neq}^{N} \ldots \sum_{\neq m_N}^{N} V^{(N)}\left(X_{m_1}, \ldots, X_{m_N}\right) \,, \tag{4.20}$$

is invariant when the order of two coordinates in $E^{(N)}$ is changed, $X_i \leftrightarrow X_j$, and thus $E^{(N)}$ is an even function. Let us assume for the moment that the potential $V^{(N)}$ itself is in general not an even function,

$$V^{(N)}\left(X_1, \ldots, X_i, \ldots, X_j, \ldots, X_N\right) \neq V^{(N)}\left(X_1, \ldots, X_j, \ldots, X_i, \ldots, X_N\right) \,. \tag{4.21}$$

We define the symmetric (even) potential,

$$V_S^{(N)} = \mathfrak{S}_N^{(N)} V^{(N)} \,, \tag{4.22}$$

that fulfills,

$$V_S^{(N)}\left(X_1, \ldots, X_i, \ldots, X_j, \ldots, X_N\right) = V_S^{(N)}\left(X_1, \ldots, X_j, \ldots, X_i, \ldots, X_N\right) \,. \tag{4.23}$$

We rewrite the symmetric potential $V_S^{(N)}$ in analogy to Eq. (4.13) to be able to sum over all M particles in the system,

$$V_S^{(N)}(X_{m_1}, X_{m_2}, \ldots, X_{m_N}) = \frac{1}{N!} \sum_{l_1 \neq}^{N} \ldots \sum_{\neq l_N}^{N} V^{(N)}(X_{m_{l_1}}, X_{m_{l_2}}, \ldots, X_{m_{l_N}}) \,. \tag{4.24}$$

With the help of the symmetric potential $V_S^{(N)}$ we define,

$$\begin{aligned}
E_S^{(N)} &= \frac{1}{N!}\sum_{m_1\neq}^{M}\cdots\sum_{\neq m_N}^{M} V_S^{(N)}\left(X_{m_1},\ldots,X_{m_N}\right)\\
&\overset{\text{Eq. (4.22)}}{=} \frac{1}{N!}\sum_{m_1\neq}^{M}\cdots\sum_{\neq m_N}^{M}\left(\frac{1}{N!}\sum_{l_1}^{N}\cdots\sum_{l_N}^{N} V^{(N)}\left(X_{m_{l_1}},\ldots,X_{m_{l_N}}\right)\right)\\
&= \frac{1}{N!}\frac{1}{N!}\Bigg(\sum_{m_1\neq}^{M}\sum_{m_2\neq}^{M}\cdots\sum_{\neq m_N}^{M} V^{(N)}\left(X_{m_1},X_{m_2},\ldots,X_{m_N}\right)\\
&\qquad + \sum_{m_1\neq}^{M}\sum_{m_2\neq}^{M}\cdots\sum_{\neq m_N}^{M} V^{(N)}\left(X_{m_2},X_{m_1},\ldots,X_{m_N}\right)+\ldots\\
&\qquad + \sum_{m_1\neq}^{M}\sum_{m_2\neq}^{M}\cdots\sum_{\neq m_N}^{M} V^{(N)}\left(X_{m_N},X_{m_{N-1}},\ldots,X_{m_1}\right)\Bigg)\\
&= \frac{1}{N!}\frac{1}{N!}N!\Big(\sum_{m_1\neq}^{M}\sum_{m_2\neq}^{M}\cdots\sum_{\neq m_N}^{M} V^{(N)}\left(X_{m_1},X_{m_2},\ldots,X_{m_N}\right)\Big)\\
&= E^{(N)}\,.
\end{aligned} \tag{4.25}$$

This means that the symmetrization operation of Eq. (4.22) leaves $E^{(N)}$ invariant. In other words this means that we can always choose an even potential for the calculation of $E^{(N)}$. In case that a given potential is not even, we can use the symmetrization operation of Eq. (4.22) to define an even potential.

4.2.4 Determination of the coefficients $a_{NN}^{(L)}$

For the following it is assumed that all potentials are even,

$$V^{(N)} = V_S^{(N)} = \mathfrak{S}_N^{(N)} V^{(N)}\,. \tag{4.26}$$

As we will see in the following, Eq. (4.26) uniquely lays down the many-body potentials. Now Eq. (4.17) allows us to calculate $V^{(N)}$,

$$V^{(N)} = \mathfrak{S}_N^{(N)} V^{(N)} = \sum_{L=0}^{N} a_{NN}^{(L)} \mathfrak{S}_N^{(L)} W^{(L)}\,. \tag{4.27}$$

Thus for the determination of the many-body potentials we need Eq. (4.19) for the case $M = N$, which reads,

$$\delta_{NK} = \sum_{L=K}^{N} a_{NN}^{(L)} \binom{N-K}{L-K}\,. \tag{4.28}$$

In order to solve Eq. (4.28) we introduce $J = N - L$ and make use of $\binom{N-K}{L-K} = \binom{N-K}{N-L}$,

$$\delta_{NK} = \sum_{J=0}^{N-K} a_{NN}^{(N-J)} \binom{N-K}{J} . \tag{4.29}$$

Eventually $Q = N - K$ is replaced,

$$\delta_{0,Q} = \sum_{J=0}^{Q} a_{NN}^{(N-J)} \binom{Q}{J} , \tag{4.30}$$

which shows that $a_{NN}^{(N-J)}$ does not depend on N but solely on J.

The solution of Eq. (4.30) is,

$$a_{NN}^{(N-J)} = (-1)^J , \quad N \geq J . \tag{4.31}$$

Proof.

We verify the base case for Eq. (4.31) for $Q = 0$ and $Q = 1$. For $Q = 0$ one finds $a_{NN}^{(N)} = 1$. From $Q = 1$ one finds $a_{NN}^{(N-1)} = -1$. We assume that Eq. (4.31) is true for $Q \geq 1$. By manipulating Eq. (4.30) for $Q + 1$ we show that Eq. (4.31) is true:

$$\begin{aligned}
0 &= \sum_{J=0}^{Q+1} a_{NN}^{(N-J)} \binom{Q+1}{J} \\
&= \sum_{J=0}^{Q} a_{NN}^{(N-J)} \binom{Q+1}{J} + a_{NN}^{(N-(Q+1))} \\
&= 1 + \sum_{J=1}^{Q} a_{NN}^{(N-J)} \left(\binom{Q}{J} + \binom{Q}{J-1} \right) + a_{NN}^{(N-(Q+1))} \\
&\overset{\text{Eq. (4.30)}}{=} \sum_{J=1}^{Q} a_{NN}^{(N-J)} \binom{Q}{J-1} + a_{NN}^{(N-(Q+1))} \\
&= \sum_{J=0}^{Q-1} a_{NN}^{(N-(J+1))} \binom{Q}{J} + a_{NN}^{(N-(Q+1))} \\
&\overset{\text{Eq. (4.31)}}{=} \sum_{J=0}^{Q-1} -a_{NN}^{(N-J)} \binom{Q}{J} + a_{NN}^{(N-(Q+1))} \\
&\overset{\text{Eq. (4.30)}}{=} a_{NN}^{(N-Q)} + a_{NN}^{(N-(Q+1))} \\
\Rightarrow \quad & a_{NN}^{(N-(Q+1))} = -a_{NN}^{(N-Q)}
\end{aligned}$$

■ (4.32)

Thus, the many-body potential $V^{(N)}$ is uniquely determined from Eq. (4.27) and Eq. (4.31):

$$V^{(N)} = \sum_{L=0}^{N} a_{NN}^{(L)} \mathfrak{S}_N^{(L)} W^{(L)} = \sum_{L=0}^{N} (-1)^{(N-L)} \mathfrak{S}_N^{(L)} W^{(L)} \,, \tag{4.33}$$

and we can rewrite the energy of the M particle system,

$$E\left(M\right) = \sum_{N=0}^{M} E^{(N)} = \sum_{N=0}^{M} \mathfrak{S}_M^{(N)} V^{(N)} \,. \tag{4.34}$$

Eq. (4.33) allows to calculate the many-body potential expansion for any given energy $E\left(M\right)$. The even many-body potentials are thereby uniquely determined and the expansion of $E\left(M\right)$ is exact. In the following chapters the many-body potential expansion will be linked to the cluster expansion.

4.3 Limitations for the form of the many-body potential

In the definition of the contributions $W^{(N)}$ in Eq. (4.7) we assumed that $W^{(N)}\left(X_1, \ldots, X_N\right)$ is indeed independent of $\{X_{N+1}, \ldots, X_M\}$. In this section we show that this assumption is not only reasonable as it is fulfilled for all commonly used energy parametrizations, but that it needs to be fulfilled for any energy of a physical system.

In the limit $M \to \infty$ we demand that the total energy $E\left(M\right)$ is an extensive function,

$$\lim_{M\to\infty} \frac{E\left(\lambda M\right)}{E\left(M\right)} = \lambda \,, \tag{4.35}$$

where λM is a positive integer number and we assume that the distribution of the particles in space is "isotropic enough". We now demand that the condition Eq. (4.35) is met not only by the energy $E\left(M\right)$ but also by each energy contribution $E^{(N)}$, $N \leq M$,

$$\lim_{M\to\infty} \frac{E^{(N)}\left(\lambda M\right)}{E^{(N)}\left(M\right)} = \lambda \,. \tag{4.36}$$

Let us define two sets of particles, α_{M_1} and α_{M_2} with $\alpha_{M_1} \cap \alpha_{M_2} = \emptyset$, that are seperated by a plane and contain M_1 and M_2 particles, respectively. From Eq. (4.36) then follows,

$$\frac{\lim\limits_{M_1,M_2\to\infty} \frac{1}{N!} \sum\limits_{m_1}^{\alpha_{M_1}\cup\alpha_{M_2}} \sum\limits_{m_2}^{\alpha_{M_1}\cup\alpha_{M_2}} \cdots \sum\limits_{m_N}^{\alpha_{M_1}\cup\alpha_{M_2}} V^{(N)}}{\lim\limits_{M_1\to\infty} \frac{1}{N!} \sum\limits_{m_1}^{\alpha_{M_1}} \sum\limits_{m_2}^{\alpha_{M_1}} \cdots \sum\limits_{m_N}^{\alpha_{M_1}} V^{(N)} + \lim\limits_{M_2\to\infty} \frac{1}{N!} \sum\limits_{m_1}^{\alpha_{M_2}} \sum\limits_{m_2}^{\alpha_{M_2}} \cdots \sum\limits_{m_N}^{\alpha_{M_2}} V^{(N)}} = 1 \,. \tag{4.37}$$

With the help of Eq. (A.5) we conclude,

$$\frac{\sum_{K=1}^{N-1}\binom{N}{K}\lim_{M_1,M_2\to\infty}\frac{1}{N!}\sum_{m_1}^{\alpha_{M_1}}\cdots\sum_{m_K}^{\alpha_{M_1}}\sum_{m_{K+1}}^{\alpha_{M_2}}\cdots\sum_{m_N}^{\alpha_{M_2}}V^{(N)}}{\lim_{M_1\to\infty}\frac{1}{N!}\sum_{m_1}^{\alpha_{M_1}}\sum_{m_2}^{\alpha_{M_1}}\cdots\sum_{m_N}^{\alpha_{M_1}}V^{(N)}+\lim_{M_2\to\infty}\frac{1}{N!}\sum_{m_1}^{\alpha_{M_2}}\sum_{m_2}^{\alpha_{M_2}}\cdots\sum_{m_N}^{\alpha_{M_2}}V^{(N)}}=0\,. \tag{4.38}$$

Eq. (4.38) states that the contribution of terms of the potential $V^{(N)}$ that include atoms from both sets α_{M_1} and α_{M_2} is vanishing compared to the contribution of terms of the potential $V^{(N)}$ that include only atoms from set α_{M_1} or α_{M_2}. If we assume that the potential $V^{(N)}$ was constant,

$$V^{(N)} = const.\,, \tag{4.39}$$

then the left hand side of Eq. (4.38) clearly would not be zero. Thus the potential $V^{(N)}$ has to vanish when one of the coordinates it contains is taken to infinite distances from the rest of the $3N-1$ coordinates,

$$\lim_{r_{ni}\to\infty} V^{(N)}\left(X_1,\ldots,X_n,\ldots,X_N\right)=0\,, \tag{4.40}$$

with $X_n=\{r_{n1},r_{n2},r_{n3},\sigma_n\}$ in three dimensional space.

4.4 Expansion of effective pair potentials

As many-body potentials $V^{(N)}$ are uniquely defined and the many-body potential expansion is able to exactly describe any form of energy $E(M)$ of a M particle system (where M may be arbitrary large), the many-body potentials form a natural base to compare different potentials that are commonly used in literature, such as, *e.g.*, effective pair potentials.

In the context of effective pair potentials one takes into account that the bondstrength between two atoms $\{X_1,X_2\}$ is influenced by other atoms that are close to the bond between atoms $\{X_1,X_2\}$ giving rise to environment dependent effective pair interactions between atoms $\{X_1,X_2\}$. The results derived in Sec. 4.2 allow us to uniquely expand an effective pair potential in terms of many-body potentials $V^{(N)}$. In this section we derive the many-body potentials $V^{(N)}$ corresponding to a class of effective pair potentials that also contains the well-known Tersoff potential [60].

The energy of M particles is calculated as,

$$E\left(X_1,\ldots,X_M\right)=\frac{1}{2}\sum_{m_1}^{M}\sum_{m_2}^{M}f(\sum_{m_3}^{M}g\left(X_{m_1},X_{m_2},X_{m_3}\right))\,A\left(X_{m_1},X_{m_2}\right)\,. \tag{4.41}$$

The summation is carried out with $m_1\neq m_2$, $m_1\neq m_3$ and $m_2\neq m_3$. The pair potential,

$$A\left(X_{m_1},X_{m_2}\right)=A\left(X_{m_2},X_{m_1}\right)\,, \tag{4.42}$$

is multiplied with the screening function,

$$f(\sum_{m_3}^{M} g\left(X_{m_1}, X_{m_2}, X_{m_3}\right)) = f(\sum_{m_3}^{M} g\left(X_{m_2}, X_{m_1}, X_{m_3}\right)) \,. \tag{4.43}$$

When the position of atom X_i is taken to infinity, we demand,

$$\lim_{X_i \to \infty} g\left(X_{m_1}, X_{m_2}, X_i\right) = 0 \,, \tag{4.44}$$

and,

$$\lim_{X_i \to \infty} A\left(X_{m_1}, X_i\right) = 0 \,. \tag{4.45}$$

For the bond between only two particles to be unscreened, we require,

$$f\left(0\right) = 1 \,. \tag{4.46}$$

For this potential, the N particle energies $W^{(N)}$ are calculated according to Eq. (4.7),

$$W^{(N)} = \frac{1}{2} \sum_{m_1}^{N} \sum_{m_2}^{N} f(\sum_{m_3}^{N} g\left(X_{m_1}, X_{m_2}, X_{m_3}\right)) \, A\left(X_{m_1}, X_{m_2}\right) \,. \tag{4.47}$$

We give the first four terms explicitly,

$$W^{(0)} = 0 \,, \tag{4.48}$$

$$W^{(1)} = 0 \,, \tag{4.49}$$

$$W^{(2)} = A(X_1, X_2) \,, \tag{4.50}$$

$$\begin{aligned} W^{(3)} = {} & f(g(X_1, X_2, X_3))A(X_1, X_2) \\ & + f(g(X_2, X_3, X_1))A(X_2, X_3) \\ & + f(g(X_3, X_1, X_2))A(X_3, X_1) \,, \end{aligned} \tag{4.51}$$

$$\begin{aligned} W^{(4)} = {} & f(g(X_1, X_2, X_3) + g(X_1, X_2, X_4))A(X_1, X_2) \\ & + f(g(X_2, X_3, X_1) + g(X_2, X_3, X_4))A(X_2, X_3) \\ & + f(g(X_3, X_1, X_2) + g(X_3, X_1, X_4))A(X_3, X_1) \\ & + f(g(X_1, X_4, X_2) + g(X_1, X_4, X_3))A(X_1, X_4) \\ & + f(g(X_2, X_4, X_1) + g(X_2, X_4, X_3))A(X_2, X_4) \\ & + f(g(X_3, X_4, X_1) + g(X_3, X_4, X_2))A(X_3, X_4) \,. \end{aligned} \tag{4.52}$$

The many-body potentials $V^{(N)}$ can be derived from $W^{(N)}$ according to Eq. (4.33),

$$\begin{aligned} V^{(N)} &= \sum_{L=0}^{N} (-1)^{(N-L)} \mathfrak{S}_N^{(L)} W^{(L)} \\ &= \sum_{L=0}^{N} \frac{(-1)^{(N-L)}}{L!} \sum_{m_1 \neq}^{N} \cdots \sum_{\neq m_L}^{N} \left(\frac{1}{2} \sum_{l_1}^{L} \sum_{l_2}^{L} f(\sum_{l_3}^{L} g(X_{m_{l_1}}, X_{m_{l_2}}, X_{m_{l_3}})) \, A(X_{m_{l_1}}, X_{m_{l_2}}) \right) \,. \end{aligned} \tag{4.53}$$

We give the first four terms explicitly,

$$V^{(0)} = 0\,, \tag{4.54}$$

$$V^{(1)} = 0\,, \tag{4.55}$$

$$V^{(2)} = A(X_1, X_2)\,, \tag{4.56}$$

$$\begin{aligned} V^{(3)} = {} & (f(g(X_1, X_2, X_3)) - 1)\, A(X_1, X_2) \\ & + (f(g(X_2, X_3, X_1)) - 1)\, A(X_2, X_3) \\ & + (f(g(X_3, X_1, X_2)) - 1)\, A(X_3, X_1)\,, \end{aligned} \tag{4.57}$$

$$\begin{aligned} V^{(4)} = {} & (f(g(X_1, X_2, X_3) + g(X_1, X_2, X_4)) - f(g(X_1, X_2, X_3)) - f(g(X_1, X_2, X_4)) + 1)\, A(X_1, X_2) \\ & + (f(g(X_2, X_3, X_1) + g(X_2, X_3, X_4)) - f(g(X_2, X_3, X_1)) - f(g(X_2, X_3, X_4)) + 1)\, A(X_2, X_3) \\ & + (f(g(X_3, X_1, X_2) + g(X_3, X_1, X_4)) - f(g(X_3, X_1, X_2)) - f(g(X_3, X_1, X_4)) + 1)\, A(X_3, X_1) \\ & + (f(g(X_1, X_4, X_2) + g(X_1, X_4, X_3)) - f(g(X_1, X_4, X_2)) - f(g(X_1, X_4, X_3)) + 1)\, A(X_1, X_4) \\ & + (f(g(X_2, X_4, X_1) + g(X_2, X_4, X_3)) - f(g(X_2, X_4, X_1)) - f(g(X_2, X_4, X_3)) + 1)\, A(X_2, X_4) \\ & + (f(g(X_3, X_4, X_1) + g(X_3, X_4, X_2)) - f(g(X_3, X_4, X_1)) - f(g(X_3, X_4, X_2)) + 1)\, A(X_3, X_4)\,. \end{aligned} \tag{4.58}$$

Chapter 5

Cluster Expansion

In this chapter we separate configurational degrees of freedom from spatial variables for a binary alloy with the help of the many-body potential expansion that was developed in chapter 4. For a binary alloy the site occupation σ_m takes the value $\sigma_m = 1$, if we have an atom A (the atom A itself is denoted with $i = 1$) at position $\boldsymbol{r}_m$, while it takes the value $\sigma_m = -1$, if we have an atom B (the atom B is denoted with $i = -1$) at position $\boldsymbol{r}_m$ (The labels for the occupation of the lattice sites and the atomic species correspond to the one used by Sanchez *et al.* [61]). The considerations for a binary alloy are extended to multicomponent systems in Sec. 5.5.

As is shown in chapter 4, the total energy of a set of A and B atoms can be expanded in contributions from different many-body potentials $V^{(N)}$ (The $V^{(N)}$ are independent of configuration and their surroundings. We use a slightly different notation for the many-body potentials than in chapter 4),

$$\begin{aligned} E &= E^{(0)} + E^{(1)} + E^{(2)} + E^{(3)} + E^{(4)} + \ldots + E^{(N)} + \ldots \\ &= V^{(0)} + \sum_m V^{(1)}_{\sigma_m}(\boldsymbol{r}_m) + \frac{1}{2}\sum_{mn} V^{(2)}_{\sigma_m\sigma_n}(\boldsymbol{r}_m, \boldsymbol{r}_n) \\ &+ \frac{1}{6}\sum_{mnl} V^{(3)}_{\sigma_m\sigma_n\sigma_l}(\boldsymbol{r}_m, \boldsymbol{r}_n, \boldsymbol{r}_l) + \frac{1}{24}\sum_{mnlk} V^{(4)}_{\sigma_m\sigma_n\sigma_l\sigma_k}(\boldsymbol{r}_m, \boldsymbol{r}_n, \boldsymbol{r}_l, \boldsymbol{r}_k) + \ldots \\ &+ \frac{1}{N!}\sum_{m_1\ldots m_N} V^{(N)}_{\sigma_{m_1}\ldots\sigma_{m_N}}(\boldsymbol{r}_{m_1}, \ldots, \boldsymbol{r}_{m_N}) + \ldots . \end{aligned} \tag{5.1}$$

We demand from the potentials to have the following, physically reasonable characteristics:

1. **Center of mass and rotations**
   Each many-body potential $V^{(N)}_{\sigma_{m_1}\ldots\sigma_{m_N}}(\boldsymbol{r}_{m_1}, \ldots, \boldsymbol{r}_{m_N})$ is invariant if the origin of the coordinate system is shifted by $\boldsymbol{r}_S$. Furthermore each part of $V^{(N)}_{\sigma_{m_1}\ldots\sigma_{m_N}}(\boldsymbol{r}_{m_1}, \ldots, \boldsymbol{r}_{m_N})$ of the potential is invariant under simultaneous rotations R (group operation of $O(3)$) of all N coordinates.

$$\begin{aligned} V^{(N)}_{\sigma_{m_1}\ldots\sigma_{m_N}}(\boldsymbol{r}_{m_1}, \ldots, \boldsymbol{r}_{m_N}) &= R^{-1} : V^{(N)}_{\sigma_{m_1}\ldots\sigma_{m_N}}(\boldsymbol{r}_{m_1} - \boldsymbol{r}_S, \ldots, \boldsymbol{r}_{m_N} - \boldsymbol{r}_S) \\ &= V^{(N)}_{\sigma_{m_1}\ldots\sigma_{m_N}}(R : \{\boldsymbol{r}_{m_1} - \boldsymbol{r}_S\}, \ldots, R : \{\boldsymbol{r}_{m_N} - \boldsymbol{r}_S\}) \, . \end{aligned} \tag{5.2}$$

2. **Invariance with respect to pairwise exchange**
   Simultaneous exchange of the type and the positions of two atoms leaves the potentials invariant:

$$V^{(N)}_{\sigma_{m_1}\dots\sigma_{m_i}\dots\sigma_{m_j}\dots\sigma_{m_N}}(\boldsymbol{r}_{m_1},\dots,\boldsymbol{r}_{m_i},\dots,\boldsymbol{r}_{m_j},\dots,\boldsymbol{r}_{m_N}) = V^{(N)}_{\sigma_{m_1}\dots\sigma_{m_j}\dots\sigma_{m_i}\dots\sigma_{m_N}}(\boldsymbol{r}_{m_1},\dots,\boldsymbol{r}_{m_j},\dots,\boldsymbol{r}_{m_i},\dots,\boldsymbol{r}_{m_N}) \tag{5.3}$$

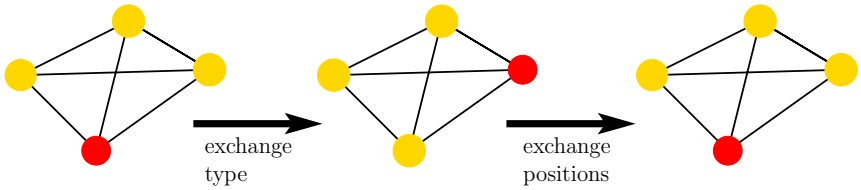

   In chapter 4 it was shown that the potentials $V^{(N)}_{\sigma_{m_1}\dots\sigma_{m_N}}(\boldsymbol{r}_{m_1},\dots,\boldsymbol{r}_{m_N})$ become uniquely defined if they are invariant with respect to pairwise exchange of the type and the positions of two atoms. We refer to functions that are invariant with respect to pairwise exchange of the type and the positions of two atoms, *e.g.*, with respect to exchange of two arguments, as even functions.

3. **Double occupation**
   Two atoms at the same position are not allowed. Therefore we formally demand:

$$V^{(N)}_{\sigma_{m_1}\dots\sigma_{m_i}\dots\sigma_{m_i}\dots\sigma_{m_N}}(\boldsymbol{r}_{m_1},\dots,\boldsymbol{r}_{m_i},\dots,\boldsymbol{r}_{m_i},\dots,\boldsymbol{r}_{m_N}) = 0\,, \tag{5.4}$$

$$\lim_{\|\boldsymbol{r}_{m_i}-\boldsymbol{r}_{m_j}\|\to 0} V^{(N)}_{\sigma_{m_1}\dots\sigma_{m_i}\dots\sigma_{m_j}\dots\sigma_{m_N}}(\boldsymbol{r}_{m_1},\dots,\boldsymbol{r}_{m_i},\dots,\boldsymbol{r}_{m_j},\dots,\boldsymbol{r}_{m_N}) \to \infty\,. \tag{5.5}$$

Examples

- We want that the energy of a system containing zero particles vanishes, hence $V^{(0)} = 0$.
- From 1. we see that $V^{(1)}_{\sigma_m}(\boldsymbol{r}_m) = const.$ as $V^{(1)}_{\sigma_m}(\boldsymbol{r}_m)$ must be invariant with respect to translations.
- From 1. we conclude that $V^{(2)}_{\sigma_m\sigma_n} = V^{(2)}_{\sigma_n\sigma_m}$. Thus $V^{(2)}_{\sigma_n\sigma_m}$ must be a function of $r_{nm} = \|\boldsymbol{r}_n - \boldsymbol{r}_m\|$.
- For any many-body potential $V^{(N)}$ all distances r_{nm} are constant under the transformations described in 1. From the knowledge of all distances, all angles can be constructed. Therefore a many-body potential $V^{(N)}$ can be written as an even function of the $\frac{N(N-1)}{2}$ distances it contains.
- From bullets one to four we see that a three-body potential can be written as a symmetric function of r_{nm}, r_{nk} and r_{mk}. However, contributions to a potential V that fulfill $\frac{\partial}{\partial r_{nm}}\frac{\partial}{\partial r_{mk}}\,V = 0$ are two-body interactions of $V^{(2)}$.

5.1 Separation of configurational and spatial variables

The state of the system at hand is fully specified if all atomic positions ("spatial" variables) and the type of atoms occupying these positions ("configurational" variables) are known. It will turn out that a separation of the spatial and configurational variables will be helpful in order to calculate, *e.g.*, the partition function of a system. For example, one could imagine to confine all atomic positions to lattice sites. The only degree of freedom allowed in this alloy are changes in the occupation, the atoms can be distributed in different ways over the lattice sites. The calculation of the partition sum for such a lattice gas model will turn out to still be a formidable task, which will keep us busy for the most of the remaining pages of this work.

In a first step we will separate the configurational from the spatial variables in the expression for the energy E. Thereby the expression we will obtain for the energy E contains the well known cluster expansion for a binary alloy (see Sec. 5.5), however, in contrast to the known results we will explicitly relate the expansion coefficients of the cluster expansion to the spatial variables (positions of the atoms) and thus establish an explicit link between the cluster expansion method [59] and many-body potentials.

We introduce an operator $\Gamma_i(n) = \frac{1}{2}[1 + i\sigma_n]$ constructed to yield $\Gamma_i(n) = \delta_{i,\sigma_n}$ that allows us to separate configurational from spatial degrees of freedom (This operator was first used by Sanchez *et al.* in the context of the cluster algebra (Sec. 8.2.3) of the cluster variation method [61]). Furthermore, in the following summations and products are assumed to behave well,

$$\sum_{l=1}^{0} m_l = 0\,, \quad \prod_{l=1}^{0} m_l = 1\,. \tag{5.6}$$

We start by rewriting the energy E with the help of $\Gamma_i(n) = \frac{1}{2}[1 + i\sigma_n]$,

$$\begin{aligned} E^{(N)} &= \frac{1}{N!} \sum_{m_1 \ldots m_N} V^{(N)}_{\sigma_{m_1} \ldots \sigma_{m_N}}(\boldsymbol{r}_{m_1}, \ldots, \boldsymbol{r}_{m_N}) \\ &= \frac{1}{N!} \sum_{i_1 \ldots i_N}^{-1,1} \sum_{m_1 \ldots m_N} V^{(N)}_{i_1 \ldots i_N}(\boldsymbol{r}_{m_1}, \ldots, \boldsymbol{r}_{m_N}) \prod_{l=1}^{N} \Gamma_{i_l}(m_l) \qquad (5.7) \\ &= \frac{1}{N!} \sum_{i_1 \ldots i_N}^{-1,1} \sum_{m_1 \ldots m_N} V^{(N)}_{i_1 \ldots i_N}(\boldsymbol{r}_{m_1}, \ldots, \boldsymbol{r}_{m_N}) \prod_{l=1}^{N} \frac{1}{2}[1 + i_l \sigma_{m_l}]. \qquad (5.8) \end{aligned}$$

Using Eq. (5.3) we can now rewrite $E^{(N)}$. We first explicitly illustrate the necessary

manipulations for $N = 2$,

$$
\begin{aligned}
E^{(2)} &= \frac{1}{2}\sum_{m_1}\sum_{m_2} V^{(2)}_{\sigma_{m_1}\sigma_{m_2}}(\boldsymbol{r}_{m_1},\boldsymbol{r}_{m_2}) \\
&= \frac{1}{2^2}\frac{1}{2}\sum_{i_1}^{-1,1}\sum_{i_2}^{-1,1}\sum_{m_1}\sum_{m_2} V^{(2)}_{i_1 i_2}(\boldsymbol{r}_{m_1},\boldsymbol{r}_{m_2})\prod_{l=1}^{2}[1+i_l\sigma_{m_l}] \\
&= \frac{1}{2^2}\frac{1}{2}\Bigg(\sum_{i_1}^{-1,1}\sum_{i_2}^{-1,1}\sum_{m_1}\sum_{m_2} V^{(2)}_{i_1 i_2}(\boldsymbol{r}_{m_1},\boldsymbol{r}_{m_2}) \\
&\quad + \sum_{i_1}^{-1,1}\sum_{i_2}^{-1,1}\sum_{m_1}\sum_{m_2} V^{(2)}_{i_1 i_2}(\boldsymbol{r}_{m_1},\boldsymbol{r}_{m_2}) i_1\sigma_{m_1} \\
&\quad + \sum_{i_1}^{-1,1}\sum_{i_2}^{-1,1}\sum_{m_1}\sum_{m_2} V^{(2)}_{i_1 i_2}(\boldsymbol{r}_{m_1},\boldsymbol{r}_{m_2}) i_2\sigma_{m_2} \\
&\quad + \sum_{i_1}^{-1,1}\sum_{i_2}^{-1,1}\sum_{m_1}\sum_{m_2} V^{(2)}_{i_1 i_2}(\boldsymbol{r}_{m_1},\boldsymbol{r}_{m_2}) i_1 i_2\sigma_{m_1}\sigma_{m_2}\Bigg) \\
&\overset{\text{Eq. (5.3)}}{=} \frac{1}{2^2}\frac{1}{2}\Bigg(\sum_{i_1}^{-1,1}\sum_{i_2}^{-1,1}\sum_{m_1}\sum_{m_2} V^{(2)}_{i_1 i_2}(\boldsymbol{r}_{m_1},\boldsymbol{r}_{m_2}) \\
&\quad + 2\sum_{i_1}^{-1,1}\sum_{i_2}^{-1,1}\sum_{m_1}\sum_{m_2} V^{(2)}_{i_1 i_2}(\boldsymbol{r}_{m_1},\boldsymbol{r}_{m_2}) i_1\sigma_{m_1} \\
&\quad + \sum_{i_1}^{-1,1}\sum_{i_2}^{-1,1}\sum_{m_1}\sum_{m_2} V^{(2)}_{i_1 i_2}(\boldsymbol{r}_{m_1},\boldsymbol{r}_{m_2}) i_1 i_2\sigma_{m_1}\sigma_{m_2}\Bigg) \\
&\quad + \frac{1}{2^2}\frac{1}{2}\sum_{i_1}^{-1,1}\sum_{i_2}^{-1,1}\sum_{m_1}\sum_{m_2} V^{(2)}_{i_1 i_2}(\boldsymbol{r}_{m_1},\boldsymbol{r}_{m_2})[1+2i_1\sigma_{m_1}+i_1 i_2\sigma_{m_1}\sigma_{m_2}]\,. \qquad (5.9)
\end{aligned}
$$

In general, the factor $\prod_{l=1}^{N}\Gamma_{i_l}(m_l) = (\frac{1}{2})^N\prod_{l=1}^{N}[1+i_l\sigma_{m_l}]$ contains $\binom{N}{K} = \frac{N!}{K!(N-K)!}$ products of

the type $\sigma_{m_1}\sigma_{m_2}\ldots\sigma_{m_K}$ of order K. For $E^{(N)}$ we therefore get,

$$\begin{aligned}
E^{(N)} &= \frac{1}{2^N}\frac{1}{N!}\sum_{i_1\ldots i_N}^{-1,1}\sum_{m_1\ldots m_N} V^{(N)}_{i_1\ldots i_N}(\boldsymbol{r}_{m_1},\ldots,\boldsymbol{r}_{m_N})\left(1+\sum_{K=1}^{N}\frac{N!}{K!(N-K)!}\prod_{l=1}^{K} i_l\sigma_{m_l}\right)\\
&= \underbrace{\frac{1}{2^N}\frac{1}{N!}\sum_{i_1\ldots i_N}^{-1,1}\sum_{m_1\ldots m_N} V^{(N)}_{i_1\ldots i_N}(\boldsymbol{r}_{m_1},\ldots,\boldsymbol{r}_{m_N})}_{V^{\binom{0}{N}}}\\
&+ \frac{1}{2^N}\sum_{i_1\ldots i_N}^{-1,1}\sum_{m_1\ldots m_N} V^{(N)}_{\sigma_{m_1}\ldots\sigma_{m_N}}(\boldsymbol{r}_{m_1},\ldots,\boldsymbol{r}_{m_N})\left(\sum_{K=1}^{N}\frac{1}{K!(N-K)!}\prod_{l=1}^{K} i_l\sigma_{m_l}\right)\\
&= V^{\binom{0}{N}}\\
&+ \frac{1}{2^N}\sum_{K=1}^{N}\frac{1}{K!}\sum_{m_1\ldots m_K}\sum_{i_1\ldots i_K}^{-1,1}\left(\prod_{l=1}^{K} i_l\right)\times\\
&\quad\times\left(\frac{1}{(N-K)!}\sum_{m_{K+1}\ldots m_N}\sum_{i_{K+1}\ldots i_N}^{-1,1} V^{(N)}_{i_1\ldots i_N}(\boldsymbol{r}_{m_1},\ldots,\boldsymbol{r}_{m_N})\right)\left(\prod_{l=1}^{K}\sigma_{m_l}\right). \qquad (5.10)
\end{aligned}$$

We define a "reduced" potential,

$$\begin{aligned}
V^{\binom{K}{N}}_{i_1\ldots i_K}(\boldsymbol{r}_{m_1},\ldots,\boldsymbol{r}_{m_K}) &= \qquad (5.11)\\
&\frac{1}{2^N}\frac{1}{(N-K)!}\sum_{m_{K+1}\ldots m_N}\sum_{i_{K+1}\ldots i_N}^{-1,1} V^{(N)}_{i_1\ldots i_N}(\boldsymbol{r}_{m_1},\ldots,\boldsymbol{r}_{m_N}),
\end{aligned}$$

to find that $E^{(N)}$ reads,

$$\begin{aligned}
E^{(N)} &= V^{\binom{0}{N}} \qquad (5.12)\\
&+ \sum_{K=1}^{N}\frac{1}{K!}\sum_{m_1\ldots m_K}\left(\sum_{i_1\ldots i_K}^{-1,1}\left(\prod_{l=1}^{K} i_l\right)V^{\binom{K}{N}}_{i_1\ldots i_K}(\boldsymbol{r}_{m_1},\ldots,\boldsymbol{r}_{m_K})\right)\left(\prod_{l=1}^{K}\sigma_{m_l}\right).
\end{aligned}$$

With the help of,

$$J^{\binom{K}{N}}(\boldsymbol{r}_{m_1},\ldots,\boldsymbol{r}_{m_K}) = \sum_{i_1\ldots i_K}^{-1,1}\left(\prod_{l=1}^{K} i_l\right)V^{\binom{K}{N}}_{i_1\ldots i_K}(\boldsymbol{r}_{m_1},\ldots,\boldsymbol{r}_{m_K}), \qquad (5.13)$$

$$J^{\binom{0}{N}} = V^{\binom{0}{N}}, \qquad (5.14)$$

the contribution $E^{(N)}$ factorizes into the desired only configuration and only coordinate dependent parts,

$$E^{(N)} = J^{\binom{0}{N}} + \sum_{K=1}^{N}\frac{1}{K!}\sum_{m_1\ldots m_K}\underbrace{J^{\binom{K}{N}}(\boldsymbol{r}_{m_1},\ldots,\boldsymbol{r}_{m_K})}_{\text{coordinate dependent}}\times\underbrace{\left(\prod_{l=1}^{K}\sigma_{m_l}\right)}_{\text{configuration dependent}}. \qquad (5.15)$$

5.2 Introduction of clusters

The atomic positions are grouped together into clusters α_K,

$$\alpha_K = \{m_1, m_2, \ldots, m_K\} \,, \tag{5.16}$$

where K denotes the number of points contained within cluster α_K, and the order of the positions included in the cluster is not important,

$$\alpha_K = \{m_1, m_2, \ldots, m_K\} = \{m_2, m_1, \ldots, m_K\} = \ldots \,. \tag{5.17}$$

Furthermore, all elements of α_K are pairwise different. We define the cluster function,

$$\Phi_{\alpha_K} = \prod_{l=1}^{K} \sigma_{m_l} \,, \tag{5.18}$$

l just labels all positions contained in the cluster α_K, and $E^{(N)}$ reads:

$$E^{(N)} = J^{\binom{0}{N}} + \sum_{K=1}^{N} \sum_{\alpha_K} J_{\alpha_K}^{\binom{K}{N}} \Phi_{\alpha_K} \,, \tag{5.19}$$

with the summation,

$$\sum_{\alpha_K} = \frac{1}{K!} \sum_{m_1 m_2 \ldots m_K} \,. \tag{5.20}$$

The factor $\frac{1}{K!}$ from Eq. (5.15) drops out as we sum over every cluster α_K only once and $J_{\alpha_K}^{\binom{K}{N}} = J^{\binom{K}{N}}(\boldsymbol{r}_{m_1}, \ldots, \boldsymbol{r}_{m_K})$. The total energy containing contributions of potentials with up to M points is given by ($E^{(0)} = V^{(0)} = 0$):

$$E = \sum_{N=1}^{M} E^{(N)} = \sum_{N=1}^{M} J^{\binom{0}{N}} + \sum_{N=1}^{M} \sum_{K=1}^{N} \sum_{\alpha_K} J_{\alpha_K}^{\binom{K}{N}} \Phi_{\alpha_K} \tag{5.21}$$

We would like to see the total coupling coefficient J_{α_K} of cluster α_K to the energy. We therefore regroup the above equation using the identity Eq. (A.1),

$$\sum_{N=1}^{M} \sum_{K=1}^{N} A_{KN} b_K = \sum_{N=1}^{M} \sum_{K=N}^{M} A_{NK} b_N \,. \tag{5.22}$$

Thus we get,

$$E = \sum_{N=1}^{M} E^{(N)} = \sum_{N=1}^{M} J^{\binom{0}{N}} + \sum_{N=1}^{M} \sum_{K=N}^{M} \sum_{\alpha_N} J_{\alpha_N}^{\binom{N}{K}} \Phi_{\alpha_N} \,, \tag{5.23}$$

and by defining,

$$J_{\alpha_N} = \sum_{K=N}^{M} J_{\alpha_N}^{\binom{N}{K}} , \tag{5.24}$$

$$J_0 = \sum_{K=1}^{M} J^{\binom{0}{K}} , \tag{5.25}$$

we finally arrive at the desired formula:

$$E = \sum_{N=1}^{M} E^{(N)} = J_0 + \sum_{N=1}^{M} \sum_{\alpha_N} J_{\alpha_N} \Phi_{\alpha_N} . \tag{5.26}$$

Usually one is interested in the limit $M \to \infty$, then M drops out and we write:

$$E = \sum_{N=1} E^{(N)} = J_0 + \sum_{N=1} \sum_{\alpha_N} J_{\alpha_N} \Phi_{\alpha_N} . \tag{5.27}$$

If we sum over coordinates explicitly, we need to replace the summation according to Eq. (5.20) and the formula becomes,

$$E = J_0 + \sum_{N=1} \frac{1}{N!} \sum_{m_1 \ldots m_N} J(\boldsymbol{r}_{m_1}, \ldots, \boldsymbol{r}_{m_N}) \left(\prod_{l=1}^{N} \sigma_{m_l} \right) . \tag{5.28}$$

5.3 From many-body potentials to expansion coefficients

To summarize, the expansion coefficients J_{α_N} that couple the cluster function Φ_{α_N} of cluster $\alpha_N = \{m_1, m_2, \ldots, m_N\}$ to the energy can be derived from a many-body potential expansion as:

$$\begin{aligned} J_{\alpha_N} &= \sum_{K=N} J_{\alpha_N}^{\binom{N}{K}} \\ &= \sum_{K=N} \frac{1}{2^K} \frac{1}{(K-N)!} \sum_{m_{N+1} \ldots m_K} \sum_{i_1 \ldots i_K}^{-1,1} \left(\prod_{l=1}^{N} i_l \right) V_{i_1 \ldots i_K}^{(K)} (\boldsymbol{r}_{m_1}, \ldots, \boldsymbol{r}_{m_N}, \boldsymbol{r}_{m_{N+1}}, \ldots, \boldsymbol{r}_{m_K}) , \end{aligned} \tag{5.29}$$

$$J_0 = \sum_{K=1} J^{\binom{0}{K}} = \sum_{K=1} \frac{1}{2^K} \frac{1}{K!} \sum_{m_1 \ldots m_K} \sum_{i_1 \ldots i_K}^{-1,1} V_{i_1 \ldots i_K}^{(K)} (\boldsymbol{r}_{m_1}, \ldots, \boldsymbol{r}_{m_K}) . \tag{5.30}$$

We note that only potentials $V^{(K)}$ with $K \geq N$ contribute to the expansion coefficient J_{α_N}. By contributions $K > N$ the cluster α_N is embedded into its "gray", averaged surroundings as the sum in Eq.(5.29) runs over all possible occupations of sites not contained in α_N.

5.3.1 Example: Expansion coefficients from pair potentials

A pair potential $V^{(2)}_{\sigma_1\sigma_2}$ containing the pair-cluster $\{\boldsymbol{r}_1, \boldsymbol{r}_2\}$ contributes to the following expansion coefficients:

$$\begin{aligned} J^{\binom{2}{2}}(\boldsymbol{r}_1, \boldsymbol{r}_2) &= \frac{1}{4}\left(V^{(2)}_{1,1}(\boldsymbol{r}_1, \boldsymbol{r}_2) - V^{(2)}_{-1,1}(\boldsymbol{r}_1, \boldsymbol{r}_2) - V^{(2)}_{1,-1}(\boldsymbol{r}_1, \boldsymbol{r}_2) + V^{(2)}_{-1,-1}(\boldsymbol{r}_1, \boldsymbol{r}_2)\right) , \\ J^{\binom{1}{2}}(\boldsymbol{r}_1) &= \frac{1}{4}\sum_m \left(V^{(2)}_{1,1}(\boldsymbol{r}_1, \boldsymbol{r}_m) - V^{(2)}_{-1,-1}(\boldsymbol{r}_1, \boldsymbol{r}_m)\right) , \\ J^{\binom{0}{2}} &= \frac{1}{8}\sum_{nm} \left(V^{(2)}_{1,1}(\boldsymbol{r}_n, \boldsymbol{r}_m) + V^{(2)}_{-1,1}(\boldsymbol{r}_n, \boldsymbol{r}_m) + V^{(2)}_{1,-1}(\boldsymbol{r}_n, \boldsymbol{r}_m) + V^{(2)}_{-1,-1}(\boldsymbol{r}_n, \boldsymbol{r}_m)\right) . \end{aligned} \tag{5.31}$$

If the only interaction in the system is the pair potential, then

$$J^{\binom{2}{2}}(\boldsymbol{r}_1, \boldsymbol{r}_2) = J(\boldsymbol{r}_1, \boldsymbol{r}_2) , \quad J^{\binom{1}{2}}(\boldsymbol{r}_1) = J(\boldsymbol{r}_1) , \quad J^{\binom{0}{2}} = J_0 . \tag{5.32}$$

Note that if the potentials fulfill $V^{(2)}_{1,1} + V^{(2)}_{-1,-1} \approx 2V^{(2)}_{1,-1}$ we expect $J^{\binom{2}{2}}$ to decay faster with distance r_{12} than any component of the potential $V^{(2)}_{\sigma_1\sigma_2}$ alone.

5.3.2 Example: Screening of the pair potentials in NiAl - importance of higher order interactions

The above defined contribution of pair-cluster expansion coefficients can be accessed abinitio by calculating the interaction potentials, here $V^{(2)}_{\mathrm{NiNi}}$, $V^{(2)}_{\mathrm{NiAl}}$ and $V^{(2)}_{\mathrm{AlAl}}$. The contribution of pair potentials to cluster expansion coefficients is shown in Fig. 5.1.

As we will see in chapter 9.1, the total nearest-neighbor pair-cluster expansion coefficient in fcc-NiAl exhibits an energy of approximately $J_{1_2} \approx 90$meV. For the $L1_2$ structure in Ni_3Al the nearest-neighbor distance (calculated using LDA) takes a value of 4.67 a.u.. From Fig. 5.1 we see that the pair potentials alone contribute around 350 meV to J_{1_2}. Therefore the pair potentials in NiAl are screened by *ca.* 75% due to higher order potentials $V^{(N)}$ with $N > 2$.

Note that LDA works so astonishingly well due to the screening effects seen above: The existence of electrons of surrounding atoms that screen a direct bond (and interaction) between two atoms justifies the assumption of a slowly varying charge density made in LDA. Therefore we face the seemingly paradox situation that we can calculate the total pair-cluster expansion coefficient for nearest-neighbors J_{1_2} relatively accurate, but not the contribution $J^{\binom{2}{2}}$ of the pair potentials alone.

5.3.3 Independence of cluster expansion coefficients

After having established the connection between potentials and expansion coefficients, Eq. (5.29), one may wonder whether we can also establish a direct connection between

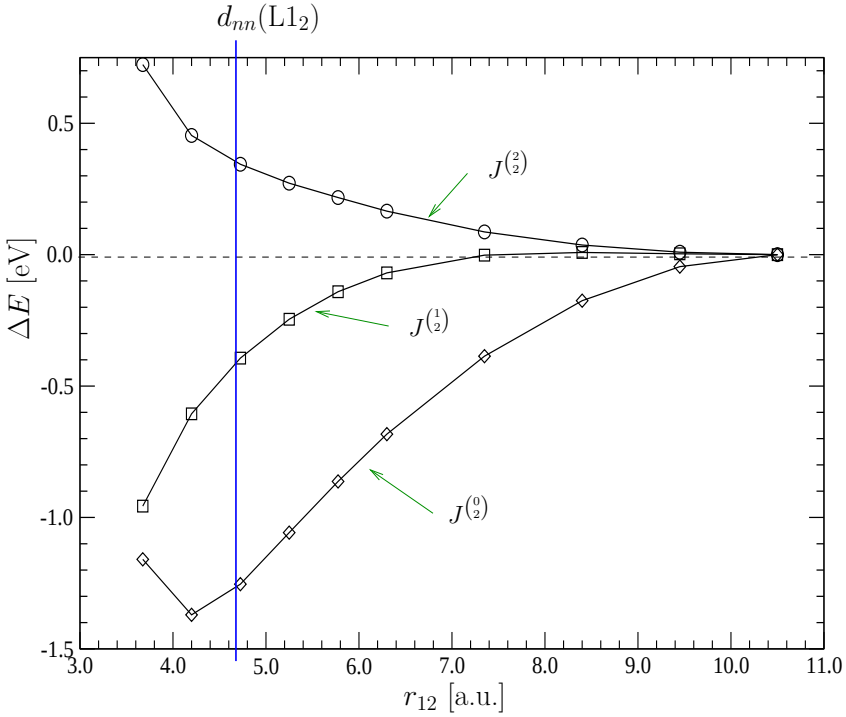

Figure 5.1: Pair cluster expansion coefficients for NiAl. The calculations (marked by symbols) were carried out using local density approximation without spin-polarization for two atoms in a cube of 21 a.u. length. No corrections were made for interactions induced by the periodic boundary conditions, the total energies were shifted to zero at the maximum distance of the atoms (binding energies of dimers calculated within LDA can differ considerably from the real binding energies).

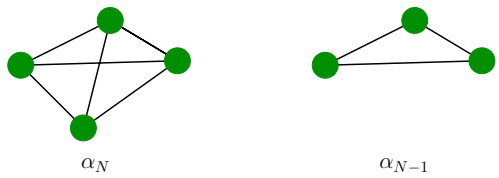

Figure 5.2: The cluster expansion coefficients of cluster α_{N-1} and α_N are in general independent.

different cluster expansion coefficients, *e.g.*, $J_{\alpha_N}^{\binom{N}{K}}$ and $J_{\alpha_{N-1}}^{\binom{N-1}{K}}$. We rewrite the coefficient $J_{\alpha_N}^{\binom{N}{K}}$,

$$\begin{aligned}
J_{\alpha_N}^{\binom{N}{K}} &= \frac{1}{2^K}\frac{1}{(K-N)!}\sum_{m_{N+1}\ldots m_K}\sum_{i_1\ldots i_K}^{-1,1}\left(\prod_{l=1}^{N} i_l\right) V^{(K)}_{i_1\ldots i_K}(\boldsymbol{r}_{m_1},\ldots,\boldsymbol{r}_{m_K}) \\
&= \frac{1}{2^K}\frac{1}{(K-N)!}\underbrace{\left(\sum_{m_{N+1}\ldots m_K}\sum_{i_1\ldots i_{N-1},i_{N+1}\ldots i_K}^{-1,1}\left(\prod_{l=1}^{N-1} i_l\right) V^{(K)}_{i_1\ldots,i_{N-1},1,i_{N+1},\ldots,i_K}(\boldsymbol{r}_{m_1},\ldots,\boldsymbol{r}_{m_K})\right)}_{V_+^{(K)}} \\
&- \frac{1}{2^K}\frac{1}{(K-N)!}\underbrace{\left(\sum_{m_{N+1}\ldots m_K}\sum_{i_1\ldots i_{N-1},i_{N+1}\ldots i_K}^{-1,1}\left(\prod_{l=1}^{N-1} i_l\right) V^{(K)}_{i_1\ldots,i_{N-1},-1,i_{N+1},\ldots,i_K}(\boldsymbol{r}_{m_1},\ldots,\boldsymbol{r}_{m_K})\right)}_{V_-^{(K)}} \\
&= \frac{1}{2^K}\frac{1}{(K-N)!}\left(V_+^{(K)} - V_-^{(K)}\right) . \qquad (5.33)
\end{aligned}$$

Regrouping $J_{\alpha_{N-1}}^{\binom{N-1}{K}}$ in a similar way reveals:

$$J_{\alpha_{N-1}}^{\binom{N-1}{K}} = \frac{1}{2^K}\frac{1}{(K-N+1)!}\sum_{m_N}\left(V_+^{(K)} + V_-^{(K)}\right) , \qquad (5.34)$$

and therefore in general different cluster expansion coefficients cannot be related.

5.3.4 Local quantities

Eq. (5.27) and Eq. (5.28) allow to calculate global quantities, *e.g.*, the energy from the coordinates and the configuration of the system. Sometimes one might also be interested in local quantities, for example, the local energy of an atom close to a surface compared to the energy of an atom in the bulk or the magnetization across an interface. Therefore we split the contribution of each cluster figure α_N contributing to the total energy E in a

symmetric way over all N_{tot} atoms present in the system. If we then sum up all resulting local contributions we obtain the total energy,

$$E = \sum_{m=1}^{N_{tot}} \epsilon_m(\boldsymbol{r}_m)\,. \tag{5.35}$$

The quantities $\epsilon_m(\boldsymbol{r}_m)$ can be viewed as local energies, or, if we look, *e.g.*, at the magnetization instead of the energy, as local magnetic moments. $\epsilon_m(\boldsymbol{r}_m)$ can be derived directly from Eqs. (5.28, 5.27),

$$\epsilon_m(\boldsymbol{r}_m) = \frac{J_0}{N_{tot}} + \sum_{N=1} \frac{1}{N} \sum_{\alpha_N \cap \{m\} \neq \emptyset} J_{\alpha_N}\, \Phi_{\alpha_N}\,, \tag{5.36}$$

where the sum runs over all clusters α_N that contain the site m, $\alpha_N \cap \{m\} \neq \emptyset$.

When we change the occupation σ_m of site $\boldsymbol{r}_m$ from A to B or vice versa, all cluster functions Φ_{α_N} contained in the summation in Eq. (5.36) will also change their sign. We define the spin-flip energy,

$$\Delta\epsilon_m(\boldsymbol{r}_m) = \frac{2}{\sigma_m} \sum_{N=1} \sum_{\alpha_N \cap \{m\} \neq \emptyset} J_{\alpha_N}\, \Phi_{\alpha_N}\,. \tag{5.37}$$

The spin-flip energy is the energy required to replace atom A by atom B on site $\boldsymbol{r}_m$ for, *e.g.*, Monte Carlo simulations, see also Sec. 8.3.

5.4 Introduction of a crystal

We now confine the positions $\boldsymbol{r}_n$ to crystal lattice sites $\boldsymbol{x}_n$ and introduce periodic boundary conditions to the system. The so-defined crystal $\{\boldsymbol{x}_n\}$ with N_0 unit cells, for instance, a cubic crystal with periodic boundary conditions, is assumed to be invariant under the operations $\{R_0|\boldsymbol{t}_0\}$ of space group G_0:

$$\{R_0|\boldsymbol{t}_0\} : \{\boldsymbol{x}_n\} = \{\boldsymbol{x}_n\}\,. \tag{5.38}$$

Again α_K denotes a set of lattice points (a cluster) that we can apply a space group operation to:

$$\{R_0|\boldsymbol{t}_0\} : \alpha_k = \alpha'_k\,. \tag{5.39}$$

From the construction of J_{α_k} we see that,

$$J_{\alpha_K} = J_{\alpha'_K}\,, \tag{5.40}$$

and therefore all clusters in a crystal that can be mapped onto each other have the same cluster expansion coefficient J_{α_K}.

As all atomic positions are confined to lattice sites, the positions $\{\boldsymbol{r}_{m_1}, \boldsymbol{r}_{m_2}, \ldots, \boldsymbol{r}_{m_K}\}$ of the cluster α_K are given by $\alpha_K = \{m_1, m_2, \ldots, m_K\}$. The expansion coefficient J_{α_k} in a crystal is therefore fully specified by $\alpha_K = \{m_1, m_2, \ldots, m_K\}$.

The number of clusters α_K that can be mapped onto each other within the whole crystal are assumed to be $D_{\alpha_K} N_0$, where the multiplicity D_{α_K} tells us how many different pictures of a cluster we can find in one unit cell.

We define ξ_{α_K} as the average of the $D_{\alpha_K} N_0$ cluster functions $\Phi_{\alpha'_K}, \Phi_{\alpha''_K}, \ldots, \Phi_{\alpha'''_K}$ corresponding to clusters $\alpha'_K, \alpha''_K, \ldots, \alpha'''_K$ linked by space group operations,

$$\xi_{\alpha_K} = \frac{1}{D_{\alpha_K} N_0} \sum_{\{R_0|\boldsymbol{t}_0\}} \Phi_{(\{R_0|\boldsymbol{t}_0\}:\alpha_K)} \,. \tag{5.41}$$

The energy can now be written as a sum over clusters β_K that cannot be linked by space group operations ($\{R_0|\boldsymbol{t}_0\} : \beta_K \neq \beta'_K$ for all $\{R_0|\boldsymbol{t}_0\}, \beta_K, \beta'_K$),

$$\left\langle E(\boldsymbol{\sigma}) \right\rangle_U = \frac{E(\boldsymbol{\sigma})}{N_0} = \sum_K \sum_{\beta_K} D_{\beta_K} J_{\beta_K} \xi_{\beta_K} \,. \tag{5.42}$$

In the following $\left\langle F \right\rangle_U = \frac{F}{N_0}$ will be used to denote the unit cell average.

5.5 Generalization for multicomponent systems, orthogonality and completeness

The considerations so far were generalized for multicomponent systems on a lattice by Sanchez *et al.* [59]. Sanchez *et al.* denoted the occupation of the lattice site $\boldsymbol{r}_m$ by σ_m, where σ_m takes values $\pm p, \pm(p-1), \ldots, \pm 1, (0)$ for the $P = 2p$ (or $2p+1$) components.

Orthogonality is defined with respect to the scalar product,

$$(f, g) = \rho_N^0 \mathrm{Tr}^{(N)} f \cdot g \,, \tag{5.43}$$

where $f(\boldsymbol{\sigma}), g(\boldsymbol{\sigma})$ are functions of $\boldsymbol{\sigma}$, the trace operator is defined as,

$$\mathrm{Tr}^{(N)} = \sum_{\sigma_1} \sum_{\sigma_2} \cdots \sum_{\sigma_N} , \tag{5.44}$$

and,

$$\rho_N^0 = P^{-N} \,, \tag{5.45}$$

is a normalization constant. In general, f, g will also depend on the positions $\boldsymbol{r}_m$ of the atoms. A complete orthogonal basis for a multicomponent system can be constructed by

attaching Chebyshev polynomials to every position $\boldsymbol{r}_m$. For each atom position $\boldsymbol{r}_m$ the P orthogonal polynomials $\Theta_v(\sigma_m)$ are defined,

$$\begin{aligned}\Theta_{2u}(\sigma_m) &= \sum_{l=0}^{u} c_l^{(u)} \sigma_m^{2l}\,, \quad u = 0, 1, \ldots, p-1, (p)\,,\\ \Theta_{2u+1}(\sigma_m) &= \sum_{l=0}^{u} d_l^{(u)} \sigma_m^{2l+1}\,, \quad u = 0, 1, \ldots, p-1\,,\end{aligned} \tag{5.46}$$

with the coefficients $c_l^{(u)}$ and $d_l^{(u)}$ defined by the orthogonality relation,

$$(\Theta_{v_1}, \Theta_{v_2}) = \frac{1}{P} \sum_{\sigma_m=-p}^{p} \Theta_{v_1}(\sigma_m)\Theta_{v_2}(\sigma_m) = \delta_{v_1 v_2}\,. \tag{5.47}$$

For the case of binary alloys the basis reads:

$$\Theta_0(\sigma_m) = 1\,, \quad \Theta_1(\sigma_m) = \sigma_m\,. \tag{5.48}$$

The $\Theta_v(\sigma_m)$ obey the following completeness relation,

$$\sum_{v=0}^{P-1} \Theta_v(i_1)\Theta_v(i_2) = P\delta_{i_1 i_2}\,, \quad i_1, i_2 \in \{\pm p, \pm(p-1), \ldots, \pm 1, (0)\}\,. \tag{5.49}$$

Using the many-body potential expansion derived in chapter 4, we extend the cluster expansion of the energy for a multicomponent system with arbitrary positions in analogy to the binary alloy. We begin by rewriting the energy,

$$\begin{aligned} E &= E^{(0)} + E^{(1)} + E^{(2)} + E^{(3)} + E^{(4)} + \ldots + E^{(N)} + \ldots \\ &= V^{(0)} + \sum_m V^{(1)}_{\sigma_m}(\boldsymbol{r}_m) + \frac{1}{2}\sum_{mn} V^{(2)}_{\sigma_m\sigma_n}(\boldsymbol{r}_m, \boldsymbol{r}_n) \\ &+ \frac{1}{6}\sum_{mnl} V^{(3)}_{\sigma_m\sigma_n\sigma_l}(\boldsymbol{r}_m, \boldsymbol{r}_n, \boldsymbol{r}_l) + \frac{1}{24}\sum_{mnlk} V^{(4)}_{\sigma_m\sigma_n\sigma_l\sigma_k}(\boldsymbol{r}_m, \boldsymbol{r}_n, \boldsymbol{r}_l, \boldsymbol{r}_k) + \ldots \\ &+ \frac{1}{N!}\sum_{m_1\ldots m_N} V^{(N)}_{\sigma_{m_1}\ldots\sigma_{m_N}}(\boldsymbol{r}_{m_1}, \ldots, \boldsymbol{r}_{m_N}) + \ldots\,. \end{aligned} \tag{5.50}$$

The expression for the energy is formally identical to Eq. (5.1), however, the occupations σ_m now take values $\pm p, \pm(p-1), \ldots, \pm 1, (0)$. With the help of the completeness relation Eq. (5.49) the contribution $E^{(N)}$ is rewritten,

$$\begin{aligned} E^{(N)} &= \frac{1}{N!}\sum_{m_1\ldots m_N} V^{(N)}_{\sigma_{m_1}\ldots\sigma_{m_N}}(\boldsymbol{r}_{m_1}, \ldots, \boldsymbol{r}_{m_N}) \\ &= \frac{1}{N!}\sum_{m_1\ldots m_N}\sum_{i_1\ldots i_N} V^{(N)}_{i_1\ldots i_N}(\boldsymbol{r}_{m_1}, \ldots, \boldsymbol{r}_{m_N}) \prod_{l=1}^{N} \delta_{i_l,\sigma_{m_l}} \\ &= \frac{1}{N!}\sum_{m_1\ldots m_N}\sum_{i_1\ldots i_N} V^{(N)}_{i_1\ldots i_N}(\boldsymbol{r}_{m_1}, \ldots, \boldsymbol{r}_{m_N}) \prod_{l=1}^{N} \left(\frac{1}{P}\sum_{v=0}^{P-1} \Theta_v(i_l)\Theta_v(\sigma_{m_l})\right)\,, \end{aligned} \tag{5.51}$$

where i_l takes values $\pm p, \pm(p-1), \ldots, \pm 1, (0)$. The first Chebyshev polynomial $\Theta_0 = 1$ is occupation independent. We define,

$$\Delta\left(i_l, \sigma_{m_l}\right) = \sum_{v=1}^{P-1} \Theta_v(i_l)\Theta_v(\sigma_{m_l})\,, \tag{5.52}$$

and rewrite Eq. (5.51),

$$E^{(N)} = \frac{1}{N!}\frac{1}{P^N} \sum_{m_1 \ldots m_N} \sum_{i_1 \ldots i_N} V^{(N)}_{i_1 \ldots i_N}(\boldsymbol{r}_{m_1}, \ldots, \boldsymbol{r}_{m_N}) \prod_{l=1}^{N} \left(1 + \Delta\left(i_l, \sigma_{m_l}\right)\right)\,. \tag{5.53}$$

Since the many-body potentials are invariant with respect to arbitrary permutations S_N of the arguments, we can sort the product in Eq. (5.53),

$$\begin{aligned} E^{(N)} &= \frac{1}{N!}\frac{1}{P^N} \sum_{m_1 \ldots m_N} \sum_{i_1 \ldots i_N} V^{(N)}_{i_{(S_N:1)} \ldots i_{(S_N:N)}}(\boldsymbol{r}_{m_{(S_N:1)}}, \ldots, \boldsymbol{r}_{m_{(S_N:N)}}) \prod_{l=1}^{N} \left(1 + \Delta\left(i_{(S_N:l)}, \sigma_{m_{(S_N:l)}}\right)\right) \\ &= \frac{1}{N!}\frac{1}{P^N} \sum_{m_1 \ldots m_N} \sum_{i_1 \ldots i_N} V^{(N)}_{i_1 \ldots i_N}(\boldsymbol{r}_{m_1}, \ldots, \boldsymbol{r}_{m_N}) \prod_{l=1}^{N} \left(1 + \Delta\left(i_{(S_N:l)}, \sigma_{m_{(S_N:l)}}\right)\right) \\ &= \frac{1}{N!}\frac{1}{P^N} \sum_{m_1 \ldots m_N} \sum_{i_1 \ldots i_N} V^{(N)}_{i_1 \ldots i_N}(\boldsymbol{r}_{m_1}, \ldots, \boldsymbol{r}_{m_N}) \left(1 + \sum_{K=1}^{N} \binom{N}{K} \prod_{l=1}^{K} \Delta\left(i_l, \sigma_{m_l}\right)\right)\,. \end{aligned} \tag{5.54}$$

In analogy to Eq. (5.12) we define a reduced potential,

$$V^{\binom{K}{N}}_{i_1 \ldots i_K}(\boldsymbol{r}_{m_1}, \ldots, \boldsymbol{r}_{m_K}) = \frac{1}{P^N}\frac{1}{(N-K)!} \sum_{m_{K+1} \ldots m_N} \sum_{i_{K+1} \ldots i_N} V^{(N)}_{i_1 \ldots i_N}(\boldsymbol{r}_{m_1}, \ldots, \boldsymbol{r}_{m_N})\,, \tag{5.55}$$

to find that $E^{(N)}$ reads,

$$\begin{aligned} E^{(N)} &= V^{\binom{0}{N}} \\ &+ \sum_{K=1}^{N} \frac{1}{K!} \sum_{m_1 \ldots m_K} \left(\sum_{i_1 \ldots i_K} V^{\binom{K}{N}}_{i_1 \ldots i_K}(\boldsymbol{r}_{m_1}, \ldots, \boldsymbol{r}_{m_K})\right) \left(\prod_{l=1}^{K} \Delta\left(i_l, \sigma_{m_l}\right)\right)\,. \end{aligned} \tag{5.56}$$

We rewrite $\prod_{l=1}^{K} \Delta\left(i_l, \sigma_{m_l}\right)$,

$$\begin{aligned} \prod_{l=1}^{K} \Delta\left(i_l, \sigma_{m_l}\right) &= \prod_{l=1}^{K} \left(\sum_{v_l=1}^{P-1} \Theta_{v_l}(i_l)\Theta_{v_l}(\sigma_{m_l})\right) \\ &= \sum_{v_1 \ldots v_K=1}^{P-1} \left(\prod_{l=1}^{K} \Theta_{v_l}(i_l)\right) \left(\prod_{l=1}^{K} \Theta_{v_l}(\sigma_{m_l})\right)\,. \end{aligned} \tag{5.57}$$

Thus $E^{(N)}$ becomes,

$$E^{(N)} = V^{\binom{0}{N}} + \sum_{K=1}^{N} \frac{1}{K!} \sum_{m_1 \ldots m_K} \sum_{v_1 \ldots v_K=1}^{P-1} \left(\sum_{i_1 \ldots i_K} \left(\prod_{l=1}^{K} \Theta_{v_l}(i_l) \right) V_{i_1 \ldots i_K}^{\binom{K}{N}}(\boldsymbol{r}_{m_1}, \ldots, \boldsymbol{r}_{m_K}) \right) \left(\prod_{l=1}^{K} \Theta_{v_l}(\sigma_{m_l}) \right) . \tag{5.58}$$

By defining,

$$J_{v_1 \ldots v_K}^{\binom{K}{N}}(\boldsymbol{r}_{m_1}, \ldots, \boldsymbol{r}_{m_K}) = \sum_{i_1 \ldots i_K} \left(\prod_{l=1}^{K} \Theta_{v_l}(i_l) \right) V_{i_1 \ldots i_K}^{\binom{K}{N}}(\boldsymbol{r}_{m_1}, \ldots, \boldsymbol{r}_{m_K}) , \tag{5.59}$$

$$J^{\binom{0}{N}} = V^{\binom{0}{N}} , \tag{5.60}$$

the product factorizes into only configuration and only coordinate dependent parts,

$$E^{(N)} = J^{\binom{0}{N}} + \sum_{K=1}^{N} \frac{1}{K!} \sum_{m_1 \ldots m_K} \sum_{v_1 \ldots v_K=1}^{P-1} \underbrace{J_{v_1 \ldots v_K}^{\binom{K}{N}}(\boldsymbol{r}_{m_1}, \ldots, \boldsymbol{r}_{m_K})}_{\text{coordinate dependent}} \times \underbrace{\left(\prod_{l=1}^{K} \Theta_{v_l}(\sigma_{m_l}) \right)}_{\text{configuration dependent}} \tag{5.61}$$

As $J_{v_1 \ldots v_K}^{\binom{K}{N}}(\boldsymbol{r}_{m_1}, \ldots, \boldsymbol{r}_{m_K})$ is invariant with respect to permutations of arguments,

$$J_{v_1 \ldots v_N}^{\binom{K}{N}}(\boldsymbol{r}_{m_1}, \ldots, \boldsymbol{r}_{m_K}) = J_{v_{(S_K:1)} \ldots v_{(S_K:K)}}^{\binom{K}{N}}(\boldsymbol{r}_{m_{(S_K:1)}}, \ldots, \boldsymbol{r}_{m_{(S_K:K)}}) , \tag{5.62}$$

we can introduce a cluster in analogy to Eq. (5.17),

$$\alpha_K = \{m_1, m_2, \ldots, m_K\} , \tag{5.63}$$

that only contains pairwise different elements. Furthermore the order of the elements in the cluster α_K is not important, in other words $m_1 < m_2 < \ldots < m_K$. We also group the indices $v_1, v_2, \ldots, v_K$ together,

$$\nu_K = \{v_1, v_2, \ldots, v_K\} , \quad v_l \in \{\pm P - 1, \ldots, 1\} . \tag{5.64}$$

However, in contrast to the elements of cluster α_K the elements in ν_K do not need to be pairwise different. Furthermore, also the order of the elements is important. Each element v_l can adopt all values $P, \ldots, 1$ irrespective of the values of the other elements of ν_K. Eventually we define the cluster function $\Phi_{(\alpha,\nu)_K}$,

$$\Phi_{(\alpha,\nu)_K} = \prod_{l=1}^{K} \Theta_{v_l}(\sigma_{m_l}) , \tag{5.65}$$

and rewrite $E^{(N)}$ in cluster form,

$$E^{(N)} = J^{\binom{0}{N}} + \sum_{K=1}^{N} {\sum_{\alpha_K}}' \sum_{\nu_K} J_{(\alpha,\nu)_K}^{\binom{K}{N}} \Phi_{(\alpha,\nu)_K} , \tag{5.66}$$

where we marked the sum over α_K as a reminder that the sum has to be taken over all possible pairwise different elements of α_K with $m_1 < m_2 < \ldots < m_K$. The total energy containing contributions of potentials with up to M points is given as ($E^{(0)} = V^{(0)} = 0$):

$$E = \sum_{N=1}^{M} E^{(N)} = \sum_{N=1}^{M} J^{\binom{0}{N}} + \sum_{N=1}^{M} \sum_{K=1}^{N} {\sum_{\alpha_K}}' \sum_{\nu_K} J^{\binom{K}{N}}_{(\alpha,\nu)_K} \Phi_{(\alpha,\nu)_K} \,. \tag{5.67}$$

We rearrange this equation using the identity Eq. (A.1),

$$E = \sum_{N=1}^{M} E^{(N)} = \sum_{N=1}^{M} J^{\binom{0}{N}} + \sum_{N=1}^{M} \sum_{K=N}^{M} {\sum_{\alpha_N}}' \sum_{\nu_N} J^{\binom{N}{K}}_{(\alpha,\nu)_N} \Phi_{(\alpha,\nu)_N} \,, \tag{5.68}$$

and define the cluster expansion coefficients,

$$J_{(\alpha,\nu)_N} = \sum_{K=N}^{M} J^{\binom{N}{K}}_{(\alpha,\nu)_N} \,, \tag{5.69}$$

$$J_0 = \sum_{K=1}^{M} J^{\binom{0}{K}} \,. \tag{5.70}$$

This eventually leads us to the desired formula for a multicomponent system:

$$E = \sum_{N=1}^{M} E^{(N)} = J_0 + \sum_{N=1}^{M} {\sum_{\alpha_N}}' \sum_{\nu_N} J_{(\alpha,\nu)_N} \Phi_{(\alpha,\nu)_N} \,. \tag{5.71}$$

5.6 Energy of formation

For the calculation of a binary alloy phase diagram we need the cluster expansion of the energy of formation,

$$\big\langle E_f(\boldsymbol{\sigma}) \big\rangle_U = \big\langle E(\boldsymbol{\sigma}) \big\rangle_U - x \big\langle E(A) \big\rangle_U - (1-x) \big\langle E(B) \big\rangle_U \,. \tag{5.72}$$

The cluster expansion of $E(A)$ and $E(B)$ is given by,

$$\big\langle E(A) \big\rangle_U = \sum_K \sum_{\beta_K} D_{\beta_K} J_{\beta_K} \,, \tag{5.73}$$

$$\big\langle E(B) \big\rangle_U = \sum_K \sum_{\beta_K} D_{\beta_K} J_{\beta_K} (-1)^K \,. \tag{5.74}$$

Assume a cluster expansion for a crystal that has only one lattice site in the primitive unit cell of the underlying lattice. From the symmetry considerations above we know that the expansion coefficient J_0 coupled to the empty cluster $\xi_0 = 1$ is constant in the whole

system. Also the expansion coefficient J_1 coupled to the point-cluster $\xi_1 = \frac{1}{N_0}\sum_{m=1}^{N_0}\sigma_m$ is the same for all lattice sites.

Inserting Eq. (5.73), Eq. (5.74) in Eq. (5.72) and making use of $x = c_A = \frac{1+\xi_1}{2}$, we find:

$$\left\langle E_f(\boldsymbol{\sigma})\right\rangle_U = \sum_K \sum_{\beta_K} D_{\beta_K} J_{\beta_K} [\, \xi_{\beta_K} - \frac{1+(-1)^K}{2}\xi_0 - \frac{1-(-1)^K}{2}\xi_1 \,] \,. \tag{5.75}$$

The contribution of the clusters β_0 and β_1 to $E_f(\boldsymbol{\sigma})$ vanishes identically. This means that $E_f(\boldsymbol{\sigma})$ is independent of the empty- and the point-cluster, and thus the empty- and the point-cluster cannot appear in a cluster expansion of $E_f(\boldsymbol{\sigma})$.

If we deal with a crystal lattice that has $M = \sum_{\beta_1} D_{\beta_1}$ lattice sites in each of the N_0 unit cells, the summation over point-clusters in Eq. (5.75) becomes,

$$\sum_{\beta_1} D_{\beta_1} J_{\beta_1} \left(\xi_{\beta_1} - \xi_1\right) \,, \tag{5.76}$$

with $\xi_1 = \frac{1}{M}\sum_{\beta_1} D_{\beta_1}\xi_{\beta_1}$.

A transformation,

$$J_{\beta_1} \rightarrow J_{\beta_1} + J_1 \,, \tag{5.77}$$

leaves,

$$\begin{aligned} \sum_{\beta_1} D_{\beta_1} \left(J_{\beta_1} + J_1\right) \left(\xi_{\beta_1} - \xi_1\right) &= \sum_{\beta_1} D_{\beta_1} J_{\beta_1} \left(\xi_{\beta_1} - \xi_1\right) + J_1 \sum_{\beta_1} D_{\beta_1} \left(\xi_{\beta_1} - \xi_1\right) \\ &= \sum_{\beta_1} D_{\beta_1} J_{\beta_1} \left(\xi_{\beta_1} - \xi_1\right) + J_1 (M\xi_1 - M\xi_1) \,, \end{aligned} \tag{5.78}$$

invariant and therefore does not change $\left\langle E_f(\boldsymbol{\sigma})\right\rangle_U$.

Note that J_0 and J_1 can be calculated from the total energy of the elements with $\left\langle E_f(A)\right\rangle_U = \left\langle E_f(B)\right\rangle_U = 0$,

$$\left\langle E(A)\right\rangle_U = \left\langle E_f(A)\right\rangle_U + MJ_1 + J_0 \,, \tag{5.79}$$

$$\left\langle E(B)\right\rangle_U = \left\langle E_f(B)\right\rangle_U - MJ_1 + J_0 \,, \tag{5.80}$$

and therefore,

$$J_1 = \frac{1}{2M}\left(\left\langle E(A)\right\rangle_U - \left\langle E(B)\right\rangle_U\right) \,, \tag{5.81}$$

$$J_0 = \frac{1}{2}\left(\left\langle E(A)\right\rangle_U + \left\langle E(B)\right\rangle_U\right) \,. \tag{5.82}$$

5.7 Taylor expansion of the cluster expansion coefficients

Let the vectors $\{\boldsymbol{u}_m\}$ be displacements of the atomic positions $\{\boldsymbol{r}_m\}$ from their ideal lattice positions $\{\boldsymbol{x}_m\}$, $\boldsymbol{r}_m = \boldsymbol{u}_m + \boldsymbol{x}_m$. For a given cluster $\beta_K = \{m_1, m_2, \ldots, m_K\}$ we can Taylor-expand the coefficient J_{β_K} from Eq. (5.29) around the lattice sites $\{\boldsymbol{x}_{m_1}, \boldsymbol{x}_{m_2}, \ldots, \boldsymbol{x}_{m_K}\}$ in the deviations $\{\boldsymbol{u}_{m_1}, \boldsymbol{u}_{m_2}, \ldots, \boldsymbol{u}_{m_K}\}$.

For example, $J^{\binom{1}{2}}$ is a function of $r_{nm} = \|(\boldsymbol{u}_n - \boldsymbol{u}_m) + (\boldsymbol{x}_n - \boldsymbol{x}_m)\| = \|\boldsymbol{u}_{nm} + \boldsymbol{x}_{nm}\|$. Its Taylor expansion can hence be written as,

$$\begin{aligned} J^{\binom{1}{2}}(\boldsymbol{u}_{nm} + \boldsymbol{x}_{nm}) &= J^{\binom{1}{2}}(\boldsymbol{x}_{nm}) + \sum_{i=1}^{3} \left(\frac{\partial J^{\binom{1}{2}}(\boldsymbol{x}_{nm})}{\partial u_{i,nm}} \right) u_{i,nm} \\ &\quad + \frac{1}{2} \sum_{i,j=1}^{3} \left(\frac{\partial}{\partial u_{i,nm}} \frac{\partial}{\partial u_{j,nm}} J^{\binom{1}{2})}(\boldsymbol{x}_{nm}) \right) u_{i,nm} u_{j,nm} + \ldots \\ &= J^{\binom{1}{2}}_{0,nm} + \sum_{i=1}^{3} J^{\binom{1}{2}}_{1,i,nm} u_{i,nm} + \frac{1}{2} \sum_{i,j=1}^{3} J^{\binom{1}{2}}_{2,ij,nm} u_{i,nm} u_{j,nm} + \ldots . \end{aligned} \tag{5.83}$$

The coefficient $\sum_m J^{\binom{1}{2}}_{0,nm}$ represents the contribution of $J^{\binom{1}{2}}$ to the point-cluster in a rigid lattice cluster expansion as described above. $J^{\binom{1}{2}}_{1,i,nm}$ couples the displacement $\boldsymbol{u}_{nm}$ to the occupation σ_n of lattice site n, $\sum_{mn} \sum_{i=1}^{3} J^{\binom{1}{2}}_{1,i,nm} u_{i,nm} \sigma_n$. The coupling between occupation and displacement in lowest order is often called Kanzaki force [62,63].

5.8 Elastic interactions

For long-ranged elastic interactions we can make some physically motivated approximations in order to simplify their incorporation in the cluster expansion formalism. We assume that the range of interaction of the elastic interactions is large compared to the lattice constant of the alloy and that the lattice site occupations of the alloy are homogenous on the length scale we are interested in (The occupation of the lattice sites in the alloy is homogenous if $\xi_1 = \langle \sigma \rangle_U \approxeq \langle \sigma \rangle_{\Delta V}$ is fulfilled for arbitrary, small subvolumes ΔV of V). Then we can write down a pair potential,

$$V^{(2)}_{\sigma_n \sigma_m} = V^{(2)}_{\sigma_n \sigma_m}(\boldsymbol{x}_{nm}, \boldsymbol{u}_{nm}) \ , \tag{5.84}$$

which depends on the distance vector between the two lattice sites $\boldsymbol{x}_n, \boldsymbol{x}_m$, $\boldsymbol{r}_{nm} = \boldsymbol{x}_{nm} + \boldsymbol{u}_{nm}$ and on their occupation σ_n, σ_m. Small displacements $\boldsymbol{u}_{nm}$ of the atoms from their lattice

positions $\boldsymbol{x}_{nm}$ allow a harmonic expansion of the potential. Using Eq. (5.31) we get,

$$\begin{aligned} E_{elast} = \frac{1}{2}\sum_{nm} V^{(2)}_{\sigma_n\sigma_m} \approx & \sum_{nm}\left(J^{\binom{0}{2}}_{0,nm} + J^{\binom{1}{2}}_{0,nm}\sigma_m + \frac{1}{2}J^{\binom{2}{2}}_{0,nm}\sigma_n\sigma_m\right) \\ & + \sum_{i}\sum_{nm}\left(J^{\binom{0}{2}}_{1,i,nm} + J^{\binom{1}{2}}_{1,i,nm}\sigma_m + \frac{1}{2}J^{\binom{2}{2}}_{1,i,nm}\sigma_n\sigma_m\right)u_{i,nm} \\ & + \frac{1}{2}\sum_{ij}\sum_{nm}\left(J^{\binom{0}{2}}_{2,ij,nm} + J^{\binom{1}{2}}_{2,ij,nm}\sigma_m + \frac{1}{2}J^{\binom{1}{2}}_{2,ij,nm}\sigma_n\sigma_m\right)u_{i,nm}u_{j,nm}\,. \end{aligned} \tag{5.85}$$

So far literature suggests that the expansion coefficients in Eq. (5.85) possess a simple configuration dependence, *e.g.*, they are either constant or depend only on the average concentration c. In the picture of a cluster expansion, Eq. (5.29), a Taylor expansion could also be carried out for many-body potentials, a generalization of Eq. (5.85) is thus straightforward.

For every configuration $\boldsymbol{\sigma}$ of the crystal we can now calculate the elastic relaxation energy E^{rel}_{elast} based on the condition of mechanical equilibrium,

$$\frac{\partial E_{elast}}{\partial u_{i,nm}} = 0\,, \tag{5.86}$$

or we could think of incorporating the effect of phonons in phase diagram calculations. Using Eq. (5.85) the condition for mechanical equilibrium becomes a linear equation, which is commonly solved or approximated in reciprocal space [63,64,65,66,67,68,69]. Obviously E^{rel}_{elast} depends purely on the configuration $\boldsymbol{\sigma}$ and can thus be cluster expanded on a rigid lattice, see Sec. 5.4. However, as is pointed out in the citations given above, the solution to Eq. (5.86) shows a singularity in reciprocal space for $\boldsymbol{k} \to 0$.

5.9 The Russian school

Often in Russian literature the site occupations are labeled as,

$$c_n = \begin{cases} 1 & \text{if species } A \text{ occupies site } n\,, \\ 0 & \text{if species } B \text{ occupies site } n\,. \end{cases} \tag{5.87}$$

In terms of the scalar product defined in Sec. 5.5, this represents a non-orthogonal basis that can be mapped on the common, orthogonal basis by,

$$c_n = \frac{1}{2}(1+\sigma_n)\,. \tag{5.88}$$

For example, the N-body expansion coefficients $W\left(\boldsymbol{r}_{m_1},\ldots,\boldsymbol{r}_{m_N}\right)$ in the Russian notation are expanded in clusters as,

$$\begin{aligned}
E &= \sum_N \frac{1}{N!} \sum_{m_1 \ldots m_N} W\left(\boldsymbol{r}_{m_1},\ldots,\boldsymbol{r}_{m_N}\right) c_{m_1} \ldots c_{m_N} \\
&= \sum_N \frac{1}{N!} \sum_{m_1 \ldots m_N} W\left(\boldsymbol{r}_{m_1},\ldots,\boldsymbol{r}_{m_N}\right) \frac{1}{2}(1+\sigma_{m_1}) \ldots \frac{1}{2}(1+\sigma_{m_N}) \\
&= \sum_N \frac{1}{2^N} \frac{1}{N!} \sum_{m_1 \ldots m_N} W\left(\boldsymbol{r}_{m_1},\ldots,\boldsymbol{r}_{m_N}\right) \left(1 + \sum_{K=1}^{N} \frac{N!}{K!\ (N-K)!} \prod_{l=1}^{K} \sigma_{m_l}\right) \\
&\overset{(5.28)}{=} J_0 + \sum_{K=1} \frac{1}{K!} \sum_{m_1 \ldots m_K} J\left(\boldsymbol{r}_{m_1},\ldots,\boldsymbol{r}_{m_K}\right) \left(\prod_{l=1}^{K} \sigma_{m_l}\right) .
\end{aligned} \tag{5.89}$$

We can identify the expansion coefficients of the cluster expansion,

$$J_0 = \sum_N \frac{1}{2^N} \frac{1}{N!} \sum_{m_1 \ldots m_N} W\left(\boldsymbol{r}_{m_1},\ldots,\boldsymbol{r}_{m_N}\right) , \tag{5.90}$$

and for $1 \leq K \leq N$,

$$J\left(\boldsymbol{r}_{m_1},\ldots,\boldsymbol{r}_{m_K}\right) = \frac{1}{2^N} \frac{1}{(N-K)!} \sum_{m_{K+1} \ldots m_N} W\left(\boldsymbol{r}_{m_1},\ldots,\boldsymbol{r}_{m_K},\boldsymbol{r}_{m_{K+1}},\ldots,\boldsymbol{r}_{m_N}\right) . \tag{5.91}$$

Chapter 6

Cluster Expansion in confined geometry

In chapter 5 we were dealing with the most general expressions for the cluster expansion of a two component system. We will now use these results for restricted geometries, *e.g.*, for the description of surfaces and alloys in contact with a substrate.

6.1 Breaking the symmetry at a surface

We start with a situation where we confine all atomic positions $\boldsymbol{r}_n$ to lattice sites $\boldsymbol{x}_n$. The lattice is invariant under space group operations G_0. A surface is introduced into the above defined crystal by cutting it along a plane without modifying the relative positions of the lattice sites on each side of the cut.

The surface disrupts the symmetry of the bulk system, we do not have translational invariance orthogonal to the surface anymore and we also have another point group symmetry. Altogether we are left with a space group of a two-dimensional system only. However, the considerations from section 5.4 are perfectly valid for the space group of the surface G_S, where G_S is a subgroup of the bulk space group G_0 and the symmetry operations of G_S are given by $\{R_S|\boldsymbol{t}_S\}$.

We label all clusters with a vector (L, α_K), where L denotes the number of successive layers L from the surface to the cluster (L, α_K) (the number of successive layers L is defined by, *e.g.*, the lattice site contained in cluster (L, α_K) closest to the surface) and α_K labels the clusters in each layer L as described in section 5.4. Furthermore, we denote the number of $2d$ unit cells of the undecorated, empty lattice in each layer parallel to the surface with N_S and the number of clusters linked by symmetry operations of G_S with $D_{(L,\alpha_K)}N_S$, see Eq. (5.39). Since there exist no group operations that link clusters (L, α_K) and $(L', \alpha'_{K'})$ located in different layers, $L \neq L'$, the multiplicities are independent of L, $D_{\alpha_K} = D_{(L,\alpha_K)}$.

We know that the influence of the surface on the interaction energies decays with the distance from the surface. Hence, when we look at clusters located far away from the surface, the cluster expansion coefficients of clusters connected by operations of G_0 not

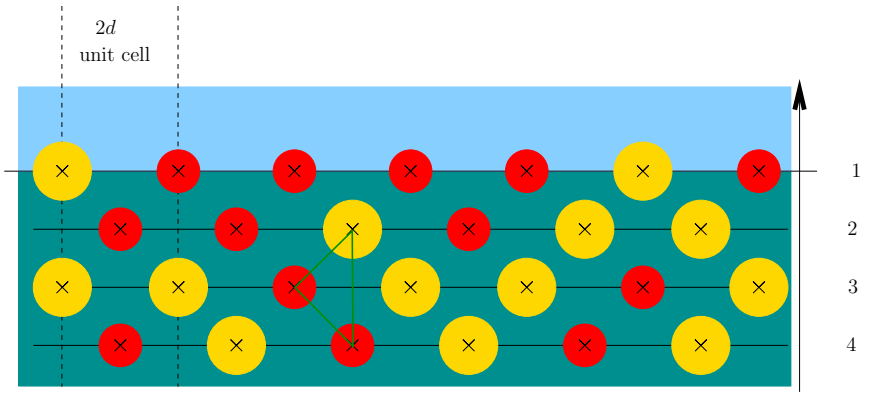

Figure 6.1: Illustration for the definition of the layer L, the $2d$ unit cell of the surface and a cluster $(2, \alpha_3)$.

contained in G_S are the same.

6.1.1 Broken bond model

We denote all clusters in the system with a surface (space group G_S) that could be linked by a symmetry operation of the bulk space group G_0 (the space groups of the system before it was cut into two parts) with $\{(L, \gamma_K), (L', \gamma'_K), \ldots\}$, as in section 5.4. Let us also assume that we know the cluster interactions $J^{BB}_{\gamma_K} = J_{L,\gamma_K}$ in the system without surface, *e.g.*, the interactions deeply beneath the surface, $L \to \infty$. The subset of $\{(L, \gamma_K), (L', \gamma'_K), \ldots\}$ that consists of clusters which can also be linked by group operations of G_S is denoted as $\{(L, \alpha_K(\gamma_K)), (L, \alpha'_K(\gamma_K)), \ldots\}$. γ_K is a prototype cluster of the set $\{(L, \gamma_K), (L', \gamma'_K), \ldots\}$ that can be used to generate the clusters in set $\{(L, \alpha_K(\gamma_K)), (L, \alpha'_K(\gamma_K)), \ldots\}$ by space group operations from G_S (only clusters in the same layer L can be linked by a group operation of G_S).

In the broken bond model we assume that the bulk cluster interactions are not modified in the surface ($J^{BB}_{\gamma_K} = J^{BB}_{\alpha_K(\gamma_K)}$ independent of α_K and L) and the energy of the system with a surface is calculated as,

$$\left\langle E^{BB}(\boldsymbol{\sigma}) \right\rangle_U = \frac{E^{BB}(\boldsymbol{\sigma})}{N_S} = \sum_L \sum_K \sum_{\alpha_K} D_{\alpha_K} J^{BB}_{\alpha_K(\gamma_K)} \xi_{(L,\alpha_K)} \,, \tag{6.1}$$

with,

$$\xi_{(L,\alpha_K)} = \frac{1}{D_{\alpha_K} N_S} \sum_{\{R_S|\boldsymbol{t}_S\}} \Phi_{(\{R_S|\boldsymbol{t}_S\}:(L,\alpha_K))} \,. \tag{6.2}$$

The summation is carried out over clusters α_K that cannot be connected by symmetry operations of G_S. The average $\left\langle E^{BB}(\boldsymbol{\sigma}) \right\rangle_U$ depicts the in-plane average of the $2d$ surface unit cell.

6.1.2 Surface modifications

In general, the cluster expansion for a surface can be written as,

$$\begin{aligned}\left\langle E^{(S)}(\boldsymbol{\sigma})\right\rangle_U &= \frac{E^{(S)}(\boldsymbol{\sigma})}{N_S} = \sum_L \sum_K \sum_{\alpha_K} D_{\alpha_K} J_{(L,\alpha_K)} \xi_{(L,\alpha_K)} \\ &= \sum_L \sum_K \sum_{\alpha_K} D_{\alpha_K} \left(J^{BB}_{\alpha_K(\gamma_K)} + \Delta J_{(L,\alpha_K)} \right) \xi_{(L,\alpha_K)} \\ &= \left\langle E^{BB}(\boldsymbol{\sigma})\right\rangle_U + \underbrace{\sum_L \sum_K \sum_{\alpha_K} D_{\alpha_K} \Delta J_{(L,\alpha_K)} \xi_{(L,\alpha_K)}}_{\text{surface modifications } \left\langle \Delta E^{(S)}(\boldsymbol{\sigma})\right\rangle_U} \\ &= \left\langle E^{BB}(\boldsymbol{\sigma})\right\rangle_U + \left\langle \Delta E^{(S)}(\boldsymbol{\sigma})\right\rangle_U . \end{aligned} \tag{6.3}$$

Deep in the material surface modifications to the interactions will vanish,

$$\lim_{L\to\infty} \Delta J_{(L,\alpha_K)} = 0 \, , \tag{6.4}$$

therefore the surface modification energy $\left\langle \Delta E^{(S)}(\boldsymbol{\sigma})\right\rangle_U$ is located at the surface.

6.1.3 Surface energy of the elements

When we cut bulk material into two parts, we first break bonds and second allow a redistribution of the electrons at the surface that induce modifications of the surface interactions. We define the span ΔL_{α_K} of a cluster. The span ΔL_{α_K} tells us how many layers parallel to the surface are connected by the cluster α_K (*i.e.* a pair-cluster fully contained within one layer parallel to the surface has $\Delta L_{\alpha_2} = 0$). When the bulk material is cut into parts two surfaces are generated and ΔL_{α_K} clusters of type α_K are cut. In the case of pure A, all correlations are $\xi_{\alpha_K} = 1$, for the case of pure B, all correlations are $\xi_{\alpha_K} = (-1)^K$. Thus the contribution of the broken bonds to the surface energy of the elements is given as,

$$\left\langle E^{BB}_{sf}(A)\right\rangle_U = \frac{1}{2} \sum_K \sum_{\alpha_K} \Delta L_{\alpha_K} D_{\alpha_K} J^{BB}_{\alpha_K(\gamma_K)} \, , \tag{6.5}$$

$$\left\langle E^{BB}_{sf}(B)\right\rangle_U = \frac{1}{2} \sum_K \sum_{\alpha_K} \Delta L_{\alpha_K} D_{\alpha_K} J^{BB}_{\alpha_K(\gamma_K)} (-1)^K \, . \tag{6.6}$$

In addition, there are contributions to the surface energies due to surface modifications of the cluster expansion coefficients,

$$\left\langle \Delta E^{(S)}(A)\right\rangle_U = \sum_L \sum_K \sum_{\alpha_K} D_{\alpha_K} \Delta J_{(L,\alpha_K)} \, , \tag{6.7}$$

$$\left\langle \Delta E^{(S)}(B)\right\rangle_U = \sum_L \sum_K \sum_{\alpha_K} D_{\alpha_K} \Delta J_{(L,\alpha_K)} (-1)^K \, . \tag{6.8}$$

The total surface energy finally is equal to the sum of broken bond contributions and surface modifications,

$$\left\langle E_{sf}(A)\right\rangle_U = \frac{1}{2}\sum_K\sum_{\alpha_K}\Delta L_{\alpha_K} D_{\alpha_K} J^{BB}_{\alpha_K(\gamma_K)} + \sum_L\sum_K\sum_{\alpha_K} D_{\alpha_K}\Delta J_{(L,\alpha_K)}\,, \tag{6.9}$$

$$\left\langle E_{sf}(B)\right\rangle_U = \frac{1}{2}\sum_K\sum_{\alpha_K}\Delta L_{\alpha_K} D_{\alpha_K} J^{BB}_{\alpha_K(\gamma_K)}(-1)^K + \sum_L\sum_K\sum_{\alpha_K} D_{\alpha_K}\Delta J_{(L,\alpha_K)}(-1)^K\,. \tag{6.10}$$

6.1.4 Energy of formation for a surface

We split the energy of formation of a surface into two parts, the broken bond part and the energy of formation due to surface modifications:

$$\begin{aligned}\left\langle E_f^{(S)}(\boldsymbol{\sigma})\right\rangle_U &= \left\langle E^{(S)}(\boldsymbol{\sigma})\right\rangle_U - x\left\langle E^{(S)}(A)\right\rangle_U - (1-x)\left\langle E^{(S)}(B)\right\rangle_U \\ &= \left\langle E_f^{(BB)}(\boldsymbol{\sigma})\right\rangle_U + \left\langle \Delta E_f^{(S)}(\boldsymbol{\sigma})\right\rangle_U\,,\end{aligned} \tag{6.11}$$

with,

$$\left\langle E_f^{(BB)}(\boldsymbol{\sigma})\right\rangle_U = \left\langle E^{(BB)}(\boldsymbol{\sigma})\right\rangle_U - x\left\langle E^{(BB)}(A)\right\rangle_U - (1-x)\left\langle E^{(BB)}(B)\right\rangle_U\,, \tag{6.12}$$

$$\left\langle \Delta E_f^{(S)}(\boldsymbol{\sigma})\right\rangle_U = \left\langle \Delta E^{(S)}(\boldsymbol{\sigma})\right\rangle_U - x\left\langle \Delta E^{(S)}(A)\right\rangle_U - (1-x)\left\langle \Delta E^{(S)}(B)\right\rangle_U\,, \tag{6.13}$$

and,

$$\left\langle E^{(BB)}(A)\right\rangle_U = \sum_L\sum_K\sum_{\alpha_K} D_{\alpha_K} J^{BB}_{\alpha_K(\gamma_K)}\,, \tag{6.14}$$

$$\left\langle E^{(BB)}(B)\right\rangle_U = \sum_L\sum_K\sum_{\alpha_K} D_{\alpha_K} J^{BB}_{\alpha_K(\gamma_K)}(-1)^K\,, \tag{6.15}$$

$$\left\langle \Delta E^{(S)}(A)\right\rangle_U = \sum_L\sum_K\sum_{\alpha_K} D_{\alpha_K}\Delta J_{(L,\alpha_K)}\,, \tag{6.16}$$

$$\left\langle \Delta E^{(S)}(B)\right\rangle_U = \sum_L\sum_K\sum_{\alpha_K} D_{\alpha_K}\Delta J_{(L,\alpha_K)}(-1)^K\,. \tag{6.17}$$

In order to calculate the layer averaged concentration x we assume that our system contains N_L layers and that the undecorated $2d$ unit cell in each layer contains M lattice sites,

$$x = \frac{1}{N_L}\sum_L x_L = \frac{1}{2}\left(1 + \frac{1}{N_L}\sum_L\left(\frac{1}{M}\sum_{\alpha_1} D_{\alpha_1}\xi_{(L,\alpha_1)}\right)\right)\,. \tag{6.18}$$

For the broken bond contribution $\left\langle E_f^{(BB)}(\boldsymbol{\sigma})\right\rangle_U$ the interactions are independent of the layer, $J^{BB}_{(L,\alpha_K)} = J^{BB}_{\alpha_K}$. Therefore we again obtain the same result as for the bulk case in section 5.6: J_0^{BB} and ΔJ_1^{BB} do not contribute to $\left\langle E_f^{(BB)}(\boldsymbol{\sigma})\right\rangle_U$.

For $\left\langle \Delta E_f^{(S)}(\boldsymbol{\sigma}) \right\rangle_U$ we can also adopt the bulk considerations. By labeling not only different positions in the unit cell but also different layers with M, the same considerations valid for the bulk also hold for a surface: A layer independent shift of the energy of the point-clusters,

$$\Delta J_{(L,\alpha_1)} \to \Delta J_{(L,\alpha_1)} + \Delta J_1 \,, \tag{6.19}$$

as well as the energy of the empty cluster ΔJ_0 does not change $\left\langle \Delta E_f^{(S)}(\boldsymbol{\sigma}) \right\rangle_U$. We thus can specify the energies of point-clusters $\Delta J_{(L,\alpha_1)}$ only up to an arbitrary constant. For the cluster expansion of a surface this problem can be resolved by demanding,

$$\lim_{L\to\infty} \Delta J_{(L,1)} = 0 \,, \tag{6.20}$$

however, for the cluster expansion of a system with a finite number of layers, *e.g.*, a slab, no such prescription can be given.

6.1.5 The case of a thin film

For the extraction of cluster coefficients from ab-initio calculations, one often has to simulate the behavior of a surface by a slab containing a finite number of layers. This free standing thin film has two "surfaces", and often also a point group operation that inverts the direction normal to the surface (the z-axis $\boldsymbol{e}_z$):

$$\{R_S|\boldsymbol{t}_S\}\,\boldsymbol{e}_z = -\boldsymbol{e}_z \,. \tag{6.21}$$

This group operation thus matches clusters on different sides of the slab. This has to be taken into account for the multiplicities D_{α_K} of the degenerate cluster expansion coefficients $J_{(L,\alpha_K)}$. Apart from this geometric considerations, the considerations for the cluster expansion of a surface also hold for a film.

6.1.6 A potentials point of view

Up to now we discussed the surface modified interactions based only on symmetry considerations. However, the potential defined in Eq. (5.1) does not depend on whether we look at a surface or at bulk material. We therefore can derive the surface modified interactions from Eq. (5.1) directly.

We look at a situation where we confine all atomic positions $\{\boldsymbol{r}_m\}$ to lattice sites $\{\boldsymbol{x}_m\}$. The positions that were erased by cutting the surface (the atomic positions above the surface) are denoted as "erased bulk sites" E (see Fig. 6.2). The remaining positions, occupied by atoms, are the "alloy" positions and form the set A where each position either belongs to set A or E, $A \cap E = \emptyset$. In order to obtain the cluster expansion coefficients of the bulk alloy for the broken bond description of the surface, we extend the summation over the alloy lattice sites contained in E above the surface. Now the summation over m_i runs over lattice sites beneath and in the surface (set A) as well as over lattice sites above

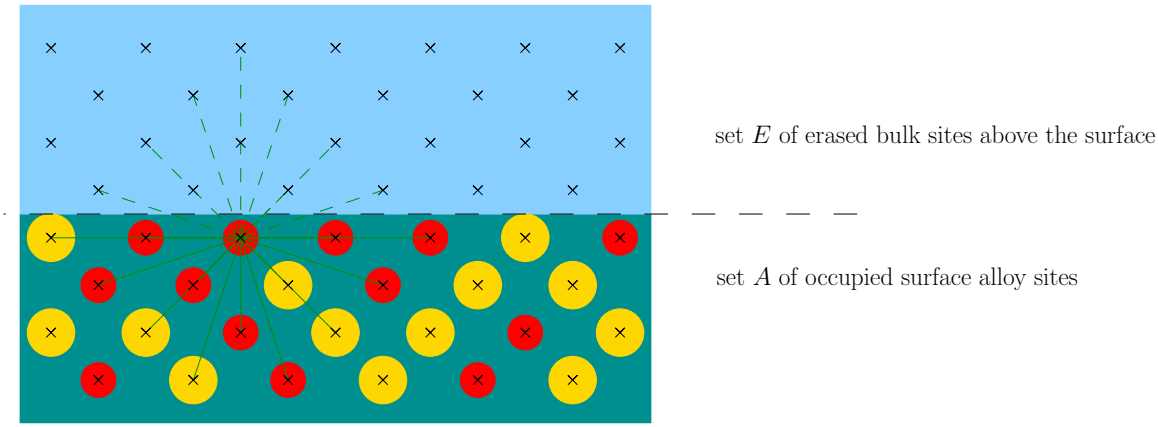

Figure 6.2: Set E of erased sites above the surface and set A of occupied alloy sites.

the surface (set E), $A \cup E$. The positions of cluster α_K are completely within or beneath the surface, $\alpha_N \subseteq A$. The summation over the set $A \cup E$ is simply a summation over all lattice sites of a bulk crystal, and we thus get the bulk cluster expansion coefficients (broken bond interactions) from,

$$J^{BB}_{\alpha_N} = \sum_{K=N} \frac{1}{2^K} \frac{1}{(K-N)!} \sum_{m_{N+1}\ldots m_K}^{A\cup E} \sum_{i_1\ldots i_K}^{-1,1} \left(\prod_{l=1}^{N} i_l \right) V^{(K)}_{i_1\ldots i_K}(\boldsymbol{r}_{m_1}, \ldots, \boldsymbol{r}_{m_N}, \boldsymbol{r}_{m_{N+1}}, \ldots, \boldsymbol{r}_{m_K}) \,,$$

with,

$$\alpha_N = \{m_1, \ldots, m_N\} \subseteq A \,. \tag{6.22}$$

For the actual cluster expansion coefficients at the surface, only positions occupied by atoms (set A) contribute to the many-body potentials. The total surface modified expansion coefficients $J_{(L,\alpha_N)}$ thus have to be calculated as,

$$J_{(L,\alpha_N)} = \sum_{K=N} \frac{1}{2^K} \frac{1}{(K-N)!} \sum_{m_{N+1}\ldots m_K}^{A} \sum_{i_1\ldots i_K}^{-1,1} \left(\prod_{l=1}^{N} i_l \right) V^{(K)}_{i_1\ldots i_K}(\boldsymbol{r}_{m_1}, \ldots, \boldsymbol{r}_{m_N}, \boldsymbol{r}_{m_{N+1}}, \ldots, \boldsymbol{r}_{m_K}) \,,$$

and,

$$\alpha_N = \{m_1, \ldots, m_N\} \subseteq A \,. \tag{6.23}$$

Using Eq. (A.5) we can also write an explicit formula for the modifications of the expansion

coefficients induced by the surface:

$$\begin{aligned}\Delta J_{(L,\alpha_N)} &= J_{(L,\alpha_N)} - J^{BB}_{\alpha_N} \\ &= -\sum_{K=N} \frac{1}{2^K} \frac{1}{(K-N)!} \sum_{M=1}^{K-N} \binom{K-N}{M} \times \\ &\quad \sum_{m_{N+1}\ldots m_{K-M}}^{A} \sum_{m_{K-M+1}\ldots m_K}^{E} \sum_{i_1\ldots i_K}^{-1,1} \left(\prod_{l=1}^{N} i_l \right) V^{(K)}_{i_1\ldots i_K}(\boldsymbol{r}_{m_1}, \ldots, \boldsymbol{r}_{m_N}, \boldsymbol{r}_{m_{N+1}}, \ldots, \boldsymbol{r}_{m_K}) \,.\end{aligned} \tag{6.24}$$

We see that surface modifications $\Delta J_{(L,\alpha_N)}$ of a N point-cluster are due to potentials $V^{(K)}$ with $K > N$.

6.1.7 Surface description using pair potentials

Assume that we model an alloy with a surface solely with pair potentials, as it is often done in classical molecular dynamics simulations. From the previous section we know that for such a situation the pair-cluster expansion coefficients are not modified in the surface, $\Delta J_{(L,\alpha_2)} = 0$. The modification of a point-cluster in layer L located at $\boldsymbol{r}_1$ can be calculated from Eq. (6.24),

$$\begin{aligned}\Delta J_{(L,\{\boldsymbol{r}_1\})} &= -\frac{1}{4} \sum_{m}^{E} \sum_{i_1 i_2}^{-1,1} (i_1)\, V^{(2)}_{i_1 i_2}(\boldsymbol{r}_1, \boldsymbol{r}_m) \\ &= \frac{1}{4} \sum_{m}^{E} \left[V^{(2)}_{-1-1}(\boldsymbol{r}_1, \boldsymbol{r}_m) - V^{(2)}_{11}(\boldsymbol{r}_1, \boldsymbol{r}_m) \right] \,,\end{aligned} \tag{6.25}$$

where we took into account that $V^{(2)}_{-1,1}(\boldsymbol{r}_1, \boldsymbol{r}_m) = V^{(2)}_{1,-1}(\boldsymbol{r}_1, \boldsymbol{r}_m)$. When we cut the pure bulk A or B into parts, we introduce two surfaces. The surface energies can be calculated by counting the broken bonds,

$$E_{sf}(A) = \frac{1}{2} \sum_{m_1}^{A} \sum_{m_2}^{E} V^{(2)}_{11}(\boldsymbol{r}_{m_1}, \boldsymbol{r}_{m_2}) \,, \tag{6.26}$$

$$E_{sf}(B) = \frac{1}{2} \sum_{m_1}^{A} \sum_{m_2}^{E} V^{(2)}_{-1-1}(\boldsymbol{r}_{m_1}, \boldsymbol{r}_{m_2}) \,, \tag{6.27}$$

and therefore,

$$\sum_{(L,\beta_1)}^{A} \Delta J_{(L,\beta_1)} = \frac{1}{2} \left[E_{sf}(B) - E_{sf}(A) \right] \,. \tag{6.28}$$

Hence the total surface modifications can be attributed to the difference of the surface energies alone.

When we embed a single atom B (A) into pure bulk A (B), the change in energy is calculated by means of Eq. (5.31) as,

$$\begin{aligned}\Delta E^{A\to B} &= -2J^{\binom{1}{2}}(\boldsymbol{r}_1) - 2\sum_m^A J^{\binom{2}{2}}(\boldsymbol{r}_1,\boldsymbol{r}_m)\\ &= \sum_m^A \left[V^{(2)}_{-11}(\boldsymbol{r}_1,\boldsymbol{r}_m) - V^{(2)}_{11}(\boldsymbol{r}_1,\boldsymbol{r}_m)\right] , \qquad (6.29)\\ \Delta E^{B\to A} &= \sum_m^A \left[V^{(2)}_{-11}(\boldsymbol{r}_1,\boldsymbol{r}_m) - V^{(2)}_{-1-1}(\boldsymbol{r}_1,\boldsymbol{r}_m)\right] . \qquad (6.30)\end{aligned}$$

In order to get the bulk limit, the sum runs over the set $A \cup E$,

$$\begin{aligned}\Delta E^{A\to B}_{\text{bulk}} &= \sum_m^{A\cup E} \left[V^{(2)}_{-11}(\boldsymbol{r}_1,\boldsymbol{r}_m) - V^{(2)}_{11}(\boldsymbol{r}_1,\boldsymbol{r}_m)\right] , \qquad (6.31)\\ \Delta E^{B\to A}_{\text{bulk}} &= \sum_m^{A\cup E} \left[V^{(2)}_{-11}(\boldsymbol{r}_1,\boldsymbol{r}_m) - V^{(2)}_{-1-1}(\boldsymbol{r}_1,\boldsymbol{r}_m)\right] , \qquad (6.32)\end{aligned}$$

and we thus can write the surface modifications as,

$$\begin{aligned}\Delta E^{A\to B} &= \Delta E^{A\to B}_{\text{bulk}} + \underbrace{\sum_m^E \left[V^{(2)}_{11}(\boldsymbol{r}_1,\boldsymbol{r}_m) - V^{(2)}_{-11}(\boldsymbol{r}_1,\boldsymbol{r}_m)\right]}_{\Delta E^{A\to B}_{sf}} , \qquad (6.33)\\ \Delta E^{B\to A} &= \Delta E^{B\to A}_{\text{bulk}} + \underbrace{\sum_m^E \left[V^{(2)}_{-1-1}(\boldsymbol{r}_1,\boldsymbol{r}_m) - V^{(2)}_{-11}(\boldsymbol{r}_1,\boldsymbol{r}_m)\right]}_{\Delta E^{B\to A}_{sf}} . \qquad (6.34)\end{aligned}$$

When $\Delta E^{A\to B}_{sf} < 0$, a single atom B embedded into a pure crystal A will segregate spontaneously to the surface. Atoms B will also segregate spontaneously to the surface in the case of a dilute alloy where the concentration of atoms B is small enough so that interactions between the B atoms are small compared to $\Delta E^{B\to A}$).

We see that segregation tendencies cannot be derived from $\Delta J_{(L,\beta_1)}$ alone. We also must take into account terms directly related to the energy of formation, such as $V^{(2)}_{-11}$. This reflects Miedema's empirical rules for surface segregation [70,71]. According to Miedema surface segregation depends on the heat of formation of the alloy (in a pair potential description presented through $V^{(2)}_{-11}$), the surface energy of the elements (here $\Delta J_{(L,\beta_1)}$) and relaxation effects for size mismatched components at the surface.

Are Pair Potentials sufficient for NiAl ?

Fig. 6.3 shows the difference of pair potentials from dimer calculations in NiAl. We see that $\left[V^{(2)}_{\mathrm{AlAl}}(\boldsymbol{r}_1,\boldsymbol{r}_2) - V^{(2)}_{\mathrm{NiAl}}(\boldsymbol{r}_1,\boldsymbol{r}_2)\right]$ is strictly positive, therefore $\Delta E_{sf}^{Al\to Ni} > 0$ and we thus expect no segregation of Ni to any, *e.g.*, $(100), (110), \ldots$, surface of Al. The situation is more difficult for $\Delta E_{sf}^{Ni\to Al}$: If we take into account that the bond length between Ni and Al is at least ≈ 4.5 a.u., it seems that the integral of $\left[V^{(2)}_{\mathrm{NiNi}}(\boldsymbol{r}_1,\boldsymbol{r}_m) - V^{(2)}_{\mathrm{NiAl}}(\boldsymbol{r}_1,\boldsymbol{r}_m)\right]$ over $\boldsymbol{r}_m$ is positive (approximating the sum over m in Eq. (6.33)) and therefore from pair potentials one would expect no segregation of Al. However, as we will see in the following chapter of this thesis, Al segregates into the Ni surface.

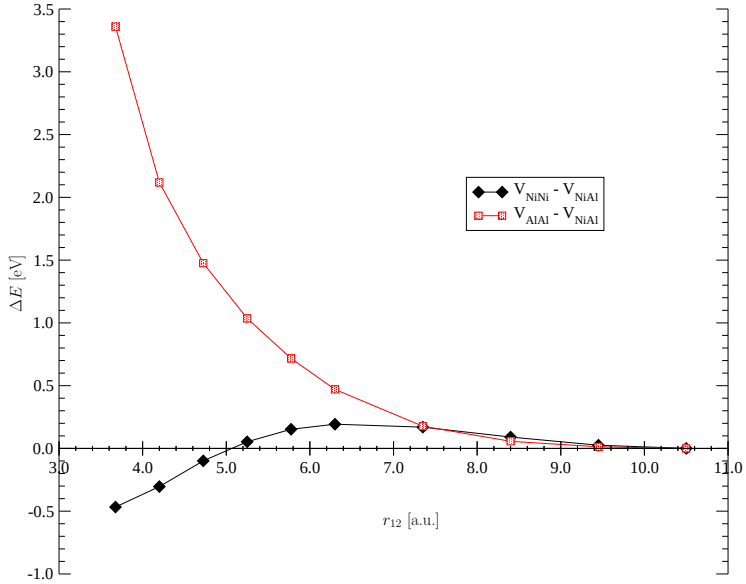

Figure 6.3: Difference of pair potentials calculated for dimers in LDA. See also caption of Fig. 5.1.

6.2 Alloying on top of a substrate

Let us look at a ternary system consisting of the alloy components A and B which we will again denote with the occupation $\sigma_m = 1$ and $\sigma_m = -1$, respectively, and a component that forms the substrate, see Fig. (6.4), denoted with $\sigma_m = 0$.

The total energy can be formally calculated as in Eq. (5.1),

$$\begin{aligned} E &= E^{(0)} + E^{(1)} + E^{(2)} + E^{(3)} + E^{(4)} + \ldots + E^{(N)} + \ldots \\ &= \sum_N \frac{1}{N!} \sum_{m_1 \ldots m_N}^{A\cup S} V^{(N)}_{\sigma_{m_1}\ldots\sigma_{m_N}}(\boldsymbol{r}_{m_1},\ldots,\boldsymbol{r}_{m_N})\,, \end{aligned} \tag{6.35}$$

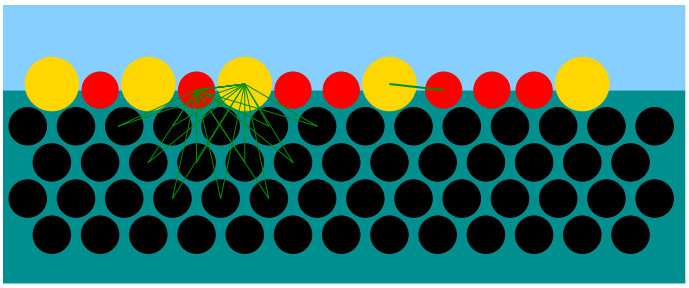

Figure 6.4: Alloy atoms on top of a substrate. Shown are direct pair interactions between alloy atoms and pair interactions between alloy atoms by three-body interactions between alloy and substrate atoms.

with atomic positions $\boldsymbol{r}_m$ that may now be occupied by three different species, $1, -1, 0$.

We know that the alloy forms on top of the substrate, in other words, the set of substrate positions S is occupied by substrate atoms, while the set of alloy positions A is occupied by atoms A and B, with $A \cap S \in \emptyset$. We use Eq. (A.5) to rewrite Eq. (6.35),

$$
\begin{aligned}
E^{(N)} &= \frac{1}{N!} \sum_{m_1}^{A\cup S} \sum_{m_2}^{A\cup S} \cdots \sum_{m_N}^{A\cup S} V^{(N)}_{\sigma_{m_1}\ldots\sigma_{m_N}}(\boldsymbol{r}_{m_1},\ldots,\boldsymbol{r}_{m_N}) \\
&= \frac{1}{N!} \sum_{K=0}^{N} \binom{N}{K} \sum_{m_1,\ldots,m_{N-K}}^{A} \sum_{m_{N-K+1},\ldots,m_N}^{S} V^{(N)}_{\sigma_{m_1}\ldots\sigma_{m_N}}(\boldsymbol{r}_{m_1},\ldots,\boldsymbol{r}_{m_N}) \qquad (6.36) \\
&= \sum_{K=0}^{N} \frac{1}{(N-K)!} \sum_{m_1,\ldots,m_{N-K}}^{A} \frac{1}{K!} \sum_{m_{N-K+1},\ldots,m_N}^{S} V^{(N)}_{\sigma_{m_1}\ldots\sigma_{m_N}}(\boldsymbol{r}_{m_1},\ldots,\boldsymbol{r}_{m_N}) \qquad (6.37) \\
&= \sum_{K=0}^{N} \frac{1}{(N-K)!} \sum_{m_1,\ldots,m_{N-K}}^{A} W^{\binom{N-K}{N}}_{\sigma_{m_1}\ldots\sigma_{m_{N-K}}}(\boldsymbol{r}_{m_1},\ldots,\boldsymbol{r}_{m_{N-K}}) \qquad (6.38) \\
&= \sum_{K=0}^{N} \frac{1}{K!} \sum_{m_1,\ldots,m_K}^{A} W^{\binom{K}{N}}_{\sigma_{m_1}\ldots\sigma_{m_K}}(\boldsymbol{r}_{m_1},\ldots,\boldsymbol{r}_{m_K})\,, \qquad (6.39)
\end{aligned}
$$

where the effective alloy interaction $W^{\binom{K}{N}}_{\sigma_{m_1}\ldots\sigma_{m_K}}$ is given as,

$$
W^{\binom{K}{N}}_{\sigma_{m_1}\ldots\sigma_{m_K}}(\boldsymbol{r}_{m_1},\ldots,\boldsymbol{r}_{m_K}) = \frac{1}{(N-K)!} \sum_{m_{K+1},\ldots,m_N}^{S} V^{(N)}_{\sigma_{m_1}\ldots\sigma_{m_K},0\ldots0}(\boldsymbol{r}_{m_1},\ldots,\boldsymbol{r}_{m_N})\,, \qquad (6.40)
$$

and we took into account that all substrate positions are always occupied by substrate atoms, while the alloy positions present in $W^{\binom{K}{N}}_{\sigma_{m_1}\ldots\sigma_{m_K}}$ can be occupied only by A or B atoms. Using Eq. (A.1) we rewrite the total energy Eq. (6.35) in pseudo binary form,

$$
E = \epsilon^{(0)} + \epsilon^{(1)} + \epsilon^{(2)} + \epsilon^{(3)} + \epsilon^{(4)} + \ldots + \epsilon^{(N)} + \ldots\,, \qquad (6.41)
$$

with,

$$\epsilon^{(N)} = \frac{1}{N!} \sum_{K=N} \sum_{m_1,\ldots,m_N}^{A} W^{\binom{N}{K}}_{\sigma_{m_1}\ldots\sigma_{m_N}}(\boldsymbol{r}_{m_1},\ldots,\boldsymbol{r}_{m_N}) \tag{6.42}$$

$$= \frac{1}{N!} \sum_{m_1,\ldots,m_N}^{A} W^{(N)}_{\sigma_{m_1}\ldots\sigma_{m_N}}(\boldsymbol{r}_{m_1},\ldots,\boldsymbol{r}_{m_N})\,, \tag{6.43}$$

and $\sigma_{m_1}\ldots\sigma_{m_N}$ takes only values $+1$ and -1 as the summations are carried out only over the set of alloy positions.

The effective pseudo binary potential,

$$W^{(N)}_{\sigma_{m_1}\ldots\sigma_{m_N}}(\boldsymbol{r}_{m_1},\ldots,\boldsymbol{r}_{m_N}) = \sum_{K=N} W^{\binom{N}{K}}_{\sigma_{m_1}\ldots\sigma_{m_N}}(\boldsymbol{r}_{m_1},\ldots,\boldsymbol{r}_{m_N})\,, \tag{6.44}$$

can now be used to get the effective cluster expansion coefficients for the case of an alloy on a substrate by making use of Eq. (5.29), Eq. (6.40) and Eq. (6.44),

$$J_{\alpha_N} = \sum_{K=N} J^{\binom{N}{K}}_{\alpha_N} \tag{6.45}$$

$$= \sum_{K=N} \frac{1}{2^K} \frac{1}{(K-N)!} \sum_{m_{N+1}\ldots m_K}^{A} \sum_{i_1\ldots i_K}^{-1,1} \left(\prod_{l=1}^{N} i_l\right) W^{(K)}_{i_1\ldots i_K}(\boldsymbol{r}_{m_1},\ldots,\boldsymbol{r}_{m_N},\boldsymbol{r}_{m_{N+1}},\ldots,\boldsymbol{r}_{m_K})$$

$$= \sum_{K=N} \frac{1}{2^K} \frac{1}{(K-N)!} \sum_{m_{N+1}\ldots m_K}^{A} \sum_{i_1\ldots i_K}^{-1,1} \left(\prod_{l=1}^{N} i_l\right) \sum_{L=K} W^{\binom{K}{L}}_{i_1\ldots i_K}(\boldsymbol{r}_{m_1},\ldots,\boldsymbol{r}_{m_K})$$

$$= \sum_{K=N} \sum_{L=K} \frac{1}{2^K} \frac{1}{(K-N)!} \frac{1}{(L-K)!} \times$$

$$\sum_{i_1\ldots i_K}^{-1,1} \left(\prod_{l=1}^{N} i_l\right) \sum_{m_{N+1}\ldots m_K}^{A} \sum_{m_{K+1},\ldots,m_L}^{S} V^{(L)}_{i_1\ldots i_K,0\ldots0}(\boldsymbol{r}_{m_1},\ldots,\boldsymbol{r}_{m_L})\,, \tag{6.46}$$

where the cluster α_N contains only alloy atoms,

$$\alpha_N = \{m_1,\ldots,m_N\} \subseteq A\,. \tag{6.47}$$

As for the case of a surface, also in the case of an alloy on a substrate, only potentials $V^{(L)}$ with $L > N$ contribute to substrate modifications of the cluster coefficient J_{α_N}.

The occupation independent interaction coefficient of the empty cluster J_0 can also be derived with Eq. (5.29),

$$J_0 = \sum_{K=0} \sum_{L=K} \frac{1}{2^K} \frac{1}{K!} \frac{1}{(L-K)!} \sum_{i_1\ldots i_K}^{-1,1} \sum_{m_1\ldots m_K}^{A} \sum_{m_{K+1},\ldots,m_L}^{S} V^{(L)}_{i_1\ldots i_K,0\ldots0}(\boldsymbol{r}_{m_1},\ldots,\boldsymbol{r}_{m_L})\,, \tag{6.48}$$

and we formally obtain Eq. (5.27) for the cluster expansion of a binary alloy,

$$E = \sum_N \epsilon^{(N)} = J_0 + \sum_{N=1} \sum_{\alpha_N} J_{\alpha_N} \, \Phi_{\alpha_N} \ , \tag{6.49}$$

where, as pointed out above, only clusters α_N fully contained in set A contribute to the energy E.

6.2.1 Substrate induced interactions

An effective pair potential $W^{(2)}_{\sigma_1\sigma_2}$ containing the pair-cluster $\{\boldsymbol{r}_1, \boldsymbol{r}_2\}$ contributes to $J^{\binom{2}{2}}(\boldsymbol{r}_1, \boldsymbol{r}_2)$,

$$\begin{aligned} J^{\binom{2}{2}}(\boldsymbol{r}_1, \boldsymbol{r}_2) &= \frac{1}{4}\left(W^{(2)}_{1,1}(\boldsymbol{r}_1, \boldsymbol{r}_2) - W^{(2)}_{-1,1}(\boldsymbol{r}_1, \boldsymbol{r}_2) - W^{(2)}_{1,-1}(\boldsymbol{r}_1, \boldsymbol{r}_2) + W^{(2)}_{-1,-1}(\boldsymbol{r}_1, \boldsymbol{r}_2)\right) \qquad (6.50) \\ &= \frac{1}{4}\left(V^{(2)}_{1,1}(\boldsymbol{r}_1, \boldsymbol{r}_2) - V^{(2)}_{-1,1}(\boldsymbol{r}_1, \boldsymbol{r}_2) - V^{(2)}_{1,-1}(\boldsymbol{r}_1, \boldsymbol{r}_2) + V^{(2)}_{-1,-1}(\boldsymbol{r}_1, \boldsymbol{r}_2)\right) \\ &\quad + \frac{1}{4}\sum_m^S \left(V^{(3)}_{1,1,0}(\boldsymbol{r}_1, \boldsymbol{r}_2, \boldsymbol{r}_m) - V^{(3)}_{-1,1,0}(\boldsymbol{r}_1, \boldsymbol{r}_2, \boldsymbol{r}_m)\right) \\ &\qquad + \frac{1}{4}\sum_m^S \left(-V^{(3)}_{1,-1,0}(\boldsymbol{r}_1, \boldsymbol{r}_2, \boldsymbol{r}_m) + V^{(3)}_{-1,-1,0}(\boldsymbol{r}_1, \boldsymbol{r}_2, \boldsymbol{r}_m)\right) \\ &\quad + \frac{1}{8}\sum_{m,n}^S \left(V^{(4)}_{1,1,0,0}(\boldsymbol{r}_1, \boldsymbol{r}_2, \boldsymbol{r}_m, \boldsymbol{r}_n) - V^{(4)}_{-1,1,0,0}(\boldsymbol{r}_1, \boldsymbol{r}_2, \boldsymbol{r}_m, \boldsymbol{r}_n)\right) \\ &\qquad + \frac{1}{8}\sum_{m,n}^S \left(-V^{(4)}_{1,-1,0,0}(\boldsymbol{r}_1, \boldsymbol{r}_2, \boldsymbol{r}_m, \boldsymbol{r}_n) + V^{(4)}_{-1,-1,0,0}(\boldsymbol{r}_1, \boldsymbol{r}_2, \boldsymbol{r}_m, \boldsymbol{r}_n)\right) \\ &\quad + \ldots \ . \qquad (6.51) \end{aligned}$$

Now we see how the contribution $J^{\binom{2}{2}}$ to the effective interaction coefficient can be split into two parts: purely alloy interactions from pair potentials and substrate mediated interactions from three-body, four-body, and higher order potentials.

Thus any description of an alloy on top of a substrate based on pair potentials will not allow substrate modifications of the pair coefficient J_2.

6.2.2 Crystal lattice sites

Let us again confine all atomic positions, the ones of the substrate as well as the ones of the alloy, to crystal lattice sites. Then the cluster expansion coefficients can be labeled by the cluster α_N alone, any explicit dependence on coordinates $\boldsymbol{r}_m$ vanishes, and all considerations of section 5.4 are valid.

In the case of a monolayer of an alloy on top of a substrate we see from Eq. (6.46) that only two-dimensional clusters must be taken into account to characterize the energy of the system. Thus the system is effectively a two-dimensional system.

6.3 Partial coverage of a substrate by a single atomic species

We now look at a substrate partially covered by atoms A as a an alloy on top of a substrate consisting of atoms A and vacancies ("atomic" species B). Eq. (6.46) is thus valid for the description of a partially covered substrate. By noting that the vacancies may not

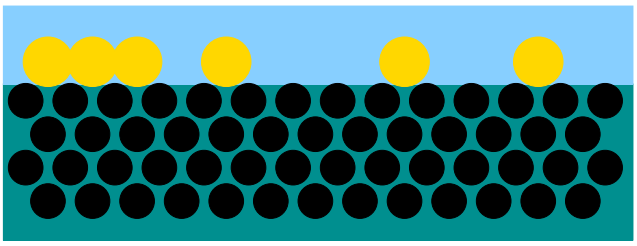

Figure 6.5: For partial surface coverage empty sites are considered to be the atomic species "vacancies" denoted with B.

contribute in the multi-body potentials,

$$\sum_{i_1 \ldots i_K}^{-1,1} \left(\prod_{l=1}^{N} i_l \right) V^{(L)}_{i_1 \ldots i_K, 0 \ldots 0}(\boldsymbol{r}_{m_1}, \ldots, \boldsymbol{r}_{m_L}) = V^{(L)}_{1 \ldots 1, 0 \ldots 0}(\boldsymbol{r}_{m_1}, \ldots, \boldsymbol{r}_{m_L}) \,, \tag{6.52}$$

for example, all many-body potentials that contain at least one component of species B vanish, we can further simplify the expression for the energetics of the system:

$$\begin{aligned} J_{\alpha_N} &= \sum_{K=N} J^{\binom{N}{K}}_{\alpha_N} && (6.53) \\ &= \sum_{K=N} \frac{1}{2^K} \frac{1}{(K-N)!} \sum_{m_{N+1} \ldots m_K}^{A} W^{(K)}_{1 \ldots 1}(\boldsymbol{r}_{m_1}, \ldots, \boldsymbol{r}_{m_N}, \boldsymbol{r}_{m_{N+1}}, \ldots, \boldsymbol{r}_{m_K}) \\ &= \sum_{K=N} \frac{1}{2^K} \frac{1}{(K-N)!} \sum_{m_{N+1} \ldots m_K}^{A} \sum_{L=K} W^{\binom{K}{L}}_{1 \ldots 1}(\boldsymbol{r}_{m_1}, \ldots, \boldsymbol{r}_{m_K}) \\ &= \sum_{K=N} \sum_{L=K} \frac{1}{2^K} \frac{1}{(K-N)!} \frac{1}{(L-K)!} \sum_{m_{N+1} \ldots m_K}^{A} \sum_{m_{K+1}, \ldots, m_L}^{S} V^{(L)}_{1 \ldots 1, 0 \ldots 0}(\boldsymbol{r}_{m_1}, \ldots, \boldsymbol{r}_{m_L}) \,, && (6.54) \end{aligned}$$

where the cluster α_N contains only alloy positions,

$$\alpha_N = \{m_1, \ldots, m_N\} \subseteq A \,. \tag{6.55}$$

The occupation independent interaction coefficient of the empty cluster J_0 can also be derived using Eq. (5.29),

$$J_0 = \sum_{K=0} \sum_{L=K} \frac{1}{2^K} \frac{1}{K!} \frac{1}{(L-K)!} \sum_{m_1 \ldots m_K}^{A} \sum_{m_{K+1},\ldots,m_L}^{S} V^{(L)}_{1\ldots1,0\ldots0}(\boldsymbol{r}_{m_1}, \ldots, \boldsymbol{r}_{m_L}) \,. \tag{6.56}$$

The benefits of a two component description (atoms A and vacancies B) of a real one component system (atoms A) will only show up when we can, for physical reasons, restrict the positions of the atoms (and thus the positions of the vacancies) to periodic "lattice sites" on top of the substrate.

6.3.1 Substrate induced interactions

An effective pair potential $W^{(2)}_{\sigma_1\sigma_2}$ containing the pair-cluster $\{\boldsymbol{r}_1, \boldsymbol{r}_2\}$ contributes to $J^{\binom{2}{2}}(\boldsymbol{r}_1, \boldsymbol{r}_2)$,

$$\begin{aligned} J^{\binom{2}{2}}(\boldsymbol{r}_1, \boldsymbol{r}_2) &= \frac{1}{4} W^{(2)}_{1,1}(\boldsymbol{r}_1, \boldsymbol{r}_2) \\ &= \frac{1}{4} V^{(2)}_{1,1}(\boldsymbol{r}_1, \boldsymbol{r}_2) + \frac{1}{4} \sum_{m}^{S} V^{(3)}_{1,1,0}(\boldsymbol{r}_1, \boldsymbol{r}_2, \boldsymbol{r}_m) + \frac{1}{8} \sum_{m,n}^{S} V^{(4)}_{1,1,0,0}(\boldsymbol{r}_1, \boldsymbol{r}_2, \boldsymbol{r}_m, \boldsymbol{r}_n) + \ldots \end{aligned} \tag{6.57}$$

In the case of partial substrate coverage, the expansion coefficients are obtained as the sum of interatomic potentials.

6.3.2 Relation between expansion coefficients

Different from our findings in section 5.3.3, it is possible to find a relation between the expansion coefficients if the B "atoms" are vacancies. Using Eq. (6.54) we see,

$$J^{\binom{N-1}{K}}_{\alpha_{N-1}}(m_1, m_2, \ldots, m_{N-1}) = \frac{1}{K-N+1} \sum_{m_N}^{A} J^{\binom{N}{K}}_{\alpha_N}(m_1, m_2, \ldots, m_{N-1}, m_N) \,. \tag{6.58}$$

This relation can be employed for the practical cluster expansion of the energetics of a partially covered substrate in order to reduce the number of ab-initio calculations required to extract converged expansion coefficients J_{α_N}.

Chapter 7

Practical Cluster Expansion

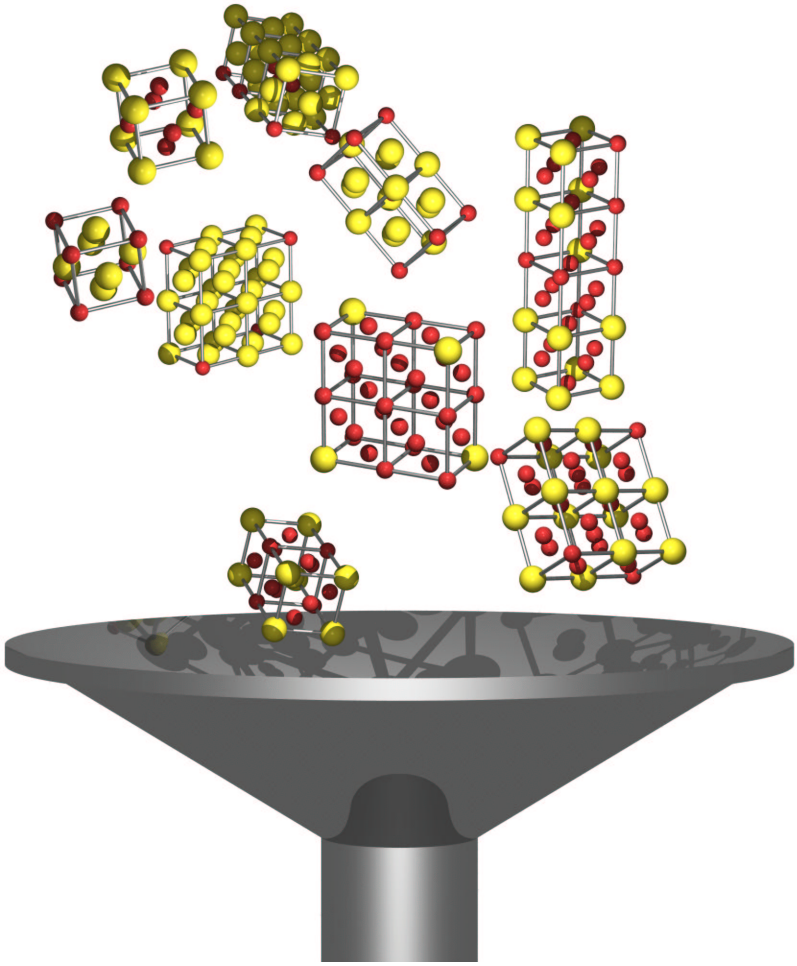

Figure 7.1: How does one extract expansion coefficients from information available from ab-initio calculations?

Due to enormous efforts required for ab-initio calculations, neither the many-body potentials $V^{(N)}$ can be calculated directly nor does anybody know how to parameterize them in a sufficiently accurate way. The amount of information at hand for phase diagram calculations is thus limited.

Generally one therefore only calculates the energies of relaxed configurations $\boldsymbol{\sigma}$ that correspond to periodic decorations of an underlying lattice with atoms A and B. A relaxed configuration is a configuration where all forces acting on the atoms as well as the shape of the unit cell are optimized into the mechanical equilibrium in the sense of Eqs. (3.11, 5.86),

$$-\nabla_m E(\boldsymbol{\sigma}) = 0\,, \tag{7.1}$$

where $E(\boldsymbol{\sigma})$ is the total energy of configuration $\boldsymbol{\sigma}$. Eq. (7.1) defines the "fully relaxed" energy of configuration $\boldsymbol{\sigma}$. This "fully relaxed" state is in general not uniquely defined, as we only require a necessary condition for a minimum to be fulfilled. One hence has to constrain the search for "fully relaxed" configurations:

- We start from a configuration $\boldsymbol{\sigma}$ where all positions $\boldsymbol{r}_m$ form an ideal underlying lattice, *e.g.*, fcc or bcc.

- According to Eq. (7.1) we then search for the "closest" local minimum by optimizing the volume of the unit cell, then the shape of the unit cell and eventually relaxing the forces on the atoms. This procedure (volume optimization, shape optimization, force minimization) is repeated until the energy does not change anymore. In most cases the resulting relaxed positions do not depend on the procedure used for the relaxation, however, sometimes, *e.g.*, minimizing forces before optimizing the volume of the unit cell may lead to different local minima.

- When the positions of the atoms $\boldsymbol{r}_m$ in the relaxed state deviate too much from the initial ideal lattice positions so that in a topological sense the initial ideal lattice positions and the relaxed positions form a different lattice, then this structure will not be used for the cluster expansion.

  For example, the fcc- based $L1_1$ structure in NiAl spontaneously relaxes into the bcc-based B2 structure when its c/a ratio is optimized, via a so-called bain deformation. Thus we will not use the $L1_1$ structure for the cluster expansion of NiAl on an underlying fcc lattice.

- It is then assumed that the fully relaxed energies $E^{fr}(\boldsymbol{\sigma})$ can be mapped onto the configuration $\boldsymbol{\sigma}$ alone via cluster expansion, see Sec. 5.4,

  $$\left\langle E^{fr}(\boldsymbol{\sigma})\right\rangle_U = \sum_{\beta_K} D_{\beta_K} J^{fr}_{\beta_K} \xi_{\beta_K}\,, \tag{7.2}$$

  where the multiplicities D_{β_K} are calculated from the symmetry of the ideal undistorted underlying lattice. The different procedures that exist to obtain the expansion coefficients $J^{fr}_{\beta_K}$ from a set of energies $\{E^{fr}(\boldsymbol{\sigma})\}$ will be summarized in the next section.

- Some authors also obtained cluster expansion coefficients J_{β_K} from "unrelaxed" configurations, *i.e.*, all energies $E^{un}(\boldsymbol{\sigma})$ were calculated with all atoms at ideal lattice sites at a given lattice constant. The term "volume relaxed" refers to expansion coefficients J_{β_K} that were obtained from configurations that were calculated with all atoms at ideal lattice sites of the underlying lattice at the volume that yielded the lowest energy $E^{vr}(\boldsymbol{\sigma})$ for each configuration. The energy of the "unrelaxed" or the "volume relaxed" configurations are sometimes also termed chemical energy.

- Since the cluster expansion is linear in the expansion coefficients J_{β_K} we can split the expansion coefficients into three different contributions,

$$J^{fr}_{\beta_K} = J^{un}_{\beta_K} + \Delta J^{vr}_{\beta_K} + \Delta J^{fr}_{\beta_K}\,, \tag{7.3}$$

  where $J^{un}_{\beta_K}$ originates from the cluster expansion of unrelaxed configurations $E^{un}(\boldsymbol{\sigma})$, $\Delta J^{vr}_{\beta_K}$ is due to a cluster expansion of the volume relaxation energy $E^{vr}(\boldsymbol{\sigma}) - E^{un}(\boldsymbol{\sigma})$ and $\Delta J^{fr}_{\beta_K}$ is due to the cluster expansion of the remaining relaxation energy, $E^{fr}(\boldsymbol{\sigma}) - E^{vr}(\boldsymbol{\sigma})$.

- The ab-initio calculations for fully relaxed configurations are time consuming, therefore sometimes "volume relaxed" or "unrelaxed" input configurations for the construction of the expansion coefficients are used. However, if one looks at a system that has various structures close in energy to the ground state structure, not fully calculating the mechanical equilibrium might result in the wrong ground state for a given concentration and thus the calculation of the phase diagram is not possible.

- Some systems have different underlying lattices at different compositions, such as NiAl, where the B2 structure at stoichiometric composition is formed on an underlying bcc lattice while the $L1_2$ structure at 75% Ni is formed on an fcc lattice. The recipe of fully relaxing the structures will for some configurations result in fcc based structures, for others in bcc based structures and for some in underlying structures that are neither fcc nor bcc.

  However, in order to calculate, for example, the fcc based part of the phase diagram along the lines of the above reasoning, we need to construct $J^{fr}_{\beta_K}$ on an underlying fcc lattice. Since in principle we cannot calculate $E^{fr}(\boldsymbol{\sigma})$ for every configuration based on a fcc lattice (as some configurations, such as the $L1_1$ structure will relax into, for example, bcc based configurations) the energies of the configurations available do not form a complete set. Hence we cannot uniquely construct the coefficients $J^{fr}_{\beta_K}$ because the completeness relation, Eq. (5.49), that the cluster expansion is based on is not fulfilled. In other words, we have a certain degree of freedom when we construct the interaction coefficients $J^{fr}_{\beta_K}$ for fcc based NiAl. Interestingly, to the best knowledge of the author, this has not been noticed or mentioned in literature so far.

7.1 Extracting expansion coefficients from ab-initio data

Let us assume that we have a set of N_{in} ab-initio calculated energies $E_i = \left\langle E\left(\boldsymbol{\sigma}_i\right)\right\rangle_U$ for different configurations $\boldsymbol{\sigma}_i$ at hand. For the moment, the energies can correspond to fully relaxed, volume relaxed or unrelaxed configurations. All configurations are assumed to have the same underlying lattice.

We now need to find the expansion coefficients J_{β_K} that reproduce the energies E_i,

$$E_i \approx \sum_{\beta_K} D_{\beta_K} J_{\beta_K} \xi_{i\,\beta_K} \,, \tag{7.4}$$

sufficiently well, whereby we wrote $\xi_{i\,\beta_K}$ for the correlation matrix $\xi_{i\,\beta_K} = \xi_{\beta_K}\left(\boldsymbol{\sigma}_i\right)$. Obviously, we only need to solve a simple system of linear equations. However, the sum over clusters β_K is yet unrestricted. Thus we need to first select a finite set of clusters that we use for the construction of the interaction coefficients J_{β_K}.

The following sections deal with the selection of clusters that best approximate the finite set of energies $\{E_i\}$ whereas Eq. (5.29) in general requires an infinite set of input energies in order to extract the in general also infinitely many cluster expansion coefficients.

7.1.1 Selection of clusters

There is no universal rule which cluster one should take into account for the fit and which not. Usually one starts with some pairs and a few compact three- and four-body clusters, then adds more and more pairs and many-body clusters. Clusters that turn out, according to the inversion procedure described below, to have a smaller absolute energy than a certain energy cut-off ϵ are not taken into account for the fit. The cut-off energy ϵ is linked to the numerical accuracy one expects from the cluster expansion, where the numerical accuracy, for example, may be characterized by the average error,

$$\mathfrak{e} = \sqrt{\frac{\sum_i^{N_{\text{in}}} \left(E_i - E_i^{\text{CE}}\right)^2}{N_{\text{in}}}} \,, \tag{7.5}$$

where $E_i^{\text{CE}} = \sum_{\beta_K} D_{\beta_K} J_{\beta_K} \xi_{i\,\beta_K}$ corresponds to the energies of the various configurations calculated with a finite set of cluster coefficients. The lower limit for the numerical error $\mathfrak{e}$ is given by the accuracy of the energy E_i of the input configurations.

One way to guess the importance of a cluster is to define a purely empirical measure $\mathcal{M}$ for every cluster. One measure could, *e.g.*, be the sum of all bond lengths included in a cluster, or the square of all bond lengths included in a cluster. One then sorts the clusters according to their measure $\mathcal{M}$ in order to judge whether a cluster is important or not.

Many authors provide information on how to find the best possible choice of clusters for a given system. See the citations in the following section. In general, the cluster expansion of fully relaxed structures requires far more interaction coefficients (around 20 to 50 for

bulk material) than the cluster expansion of unrelaxed or volume relaxed input structures (approximately 10 to 20 for bulk material) for fits with comparable accuracy.

7.1.2 Inversion procedure

If we simply fit the same number of clusters N_{CE} to the number of calculated input structures, $N_{\mathrm{CE}} = N_{\mathrm{in}}$, we only need to invert Eq. (7.4),

$$J_{\beta_K} = \frac{1}{D_{\beta_K}} \sum_i E_i \left(\boldsymbol{\xi}^{-1}\right)_{i\,\beta_K} , \tag{7.6}$$

where we require $\|\boldsymbol{\xi}\| \neq 0$. Historically, the first ab-initio cluster expansion [72] was carried out accordingly.

Nowadays it is common sense to use, where possible, more input structures than clusters in order to fit in the inversion procedure. There are various approaches how to extract converged interaction coefficients from ab-initio calculations. Actually there seem to be as many recipes for the extraction of interaction coefficients as there are authors working in this field and rarely someone dares to compare two recipes. We will try to quickly outline the general ideas behind most inversion procedures. We define a function,

$$\mathcal{W}\left(J_{\beta_K}\right) = \sum_i \omega_i \left(E_i - E^0\left(\boldsymbol{\sigma}_i\right) - \sum_{\beta_K} D_{\beta_K} J_{\beta_K} \xi_{i\,\beta_K} \right)^2 + \sum_{\beta_K} f_{\beta_K}\left(J_{\beta_K}\right) . \tag{7.7}$$

The function $\mathcal{W}$ is minimized with respect to the interaction coefficients J_{β_K}, where often the minimization of $\mathcal{W}$ is carried out with implicit constraints on the interaction coefficients J_{β_K}.

- The prefactors ω_i in Eq. (7.7) allow to weigh different structures according to their importance, *e.g.*, one can assign to ground state structures a higher weight in order to make sure that the ground states are correctly reproduced in phase diagram calculations [73,74,75].

- The energies $E^0\left(\boldsymbol{\sigma}_i\right)$ are approximations to the energies E_i that, *e.g.*, contain the correct long-ranged elastic behavior of structure $\boldsymbol{\sigma}_i$, such as the "constituent strain" in [73,64,76,77] or the broken-bond approximation for surface energies. In practice, a good empirical approximation $E^0\left(\boldsymbol{\sigma}_i\right)$ to the energies E_i can drastically reduce the numbers (and magnitude) of cluster expansion coefficients J_{β_K} required for an accurate fit, which makes the cluster expansion more reliable.

- The factors $f_{\beta_K}\left(J_{\beta_K}\right)$ allow to weight the interaction coefficients themselves, *e.g.*, one assigns to long-ranged pair-cluster coefficients a high weight such as,

$$f^{(1)}_{\beta_2} = D_{\beta_2} J^2_{\beta_2} r^{\lambda}_{\beta_2} , \tag{7.8}$$

(r_{β_2} is the length of cluster β_2 and λ an empirical decay constant) to enforce a quick decay of the pair expansion coefficients with respect to their lengths. Zunger *et al.* [73,64,78,77], *e.g.*, define a smoothness criterion in order to ensure a smooth behavior of the pair interactions in reciprocal space. The factors f_{β_K} (J_{β_K}) also make it possible to fit more cluster expansion coefficients J_{β_K} than input energies E_i are available.

- Ceder *et al.* [74] confine the search for the minimum of $\mathcal{W}$ to values of J_{β_K} that reproduce all energies E_i and the difference energies $\|E_i - E_j\|$ within certain error bars, see next section.

- Recently Ceder *et al.* [79] proposed a more elaborate fitting algorithm in the context of automatic phase diagram calculations that starts from a minimal set of clusters and structures and that automatically picks new clusters and structures to yield the best cluster expansion possible. Thereby the best possible cluster expansion minimizes the cross-validation score. The cross-validation score is identical to the predictive error $\mathfrak{e}_{pred}$ that is defined in Eq. (7.23).

7.2 Procedures used in this work

Two stages of cluster expansion procedures were used in this work. First, physically motivated weights and limits when optimizing $\mathcal{W}$ which are described in the next subsection. Second, statistical averaging was used to extract more reliable expansion coefficients, as will be described in section 7.2.3.

7.2.1 Cluster expansion coefficients for bulk material

Following Ceder *et al.* [74] two sets of inequalities were implemented in the fitting procedure.

1. The fitted energy E_i^{CE} of any structure may not deviate more than $\delta_i^{(1)}$ from the ab-initio calculated input energy E_i,

$$E_i - \delta_i^{(1)} \leq E_i^{\mathrm{CE}} \leq E_i + \delta_i^{(1)} \,. \tag{7.9}$$

   To make sure that the possible ground state structures are well reproduced, an empirical temperature kT is introduced. $\delta_i^{(1)}$ for the input structure i is then calculated from a Boltzmann factor,

$$\delta_i^{(1)} = \delta_0^{(1)} \exp\left(\frac{E_i - E_0}{kT}\right) \,, \tag{7.10}$$

   where $\delta_0^{(1)}$ and kT are parameters that can be used to control the fit and E_0 corresponds to the input structure with the lowest energy at the composition of structure i.

2. The correct energetic order of structures that exhibit identical compositions is enforced. Let E_i, E_{i+1} be the energies of two (energetically) successive structures from the subset of input structures that are of the same composition. We require,

$$|E_i - E_{i+1}| - \delta_i^{(2)} \leq |E_i^{\mathrm{CE}} - E_{i+1}^{\mathrm{CE}}| \leq |E_i - E_{i+1}| + \delta_i^{(2)} \,. \tag{7.11}$$

$\delta_i^{(2)}$ for input structure i is calculated also from a Boltzmann factor,

$$\delta_i^{(2)} = \delta_0^{(2)} \exp\left(\frac{E_i - E_0}{kT}\right) \,, \tag{7.12}$$

where $\delta_0^{(2)}$ is a free parameter to control the fit.

The smoothness criterion of the mixed-space cluster expansion of Zunger *et al.* is equivalent to weighing the square of the absolute values of the pair expansion coefficients dependent on their length r_{β_K} [73]. We have used this real-space formulation of the reciprocal-space cluster expansion by applying weights in the form of,

$$f_{\beta_2}^{(1)} = c_1 D_{\beta_2} J_{\beta_2}^2 r_{\beta_2}^{\lambda_1} \,, \tag{7.13}$$

to the pair-cluster expansion coefficients. The parameters c_1 and λ_1 are parameters used to stabilize the fit.

Above weights $f_{\beta_2}^{(1)}$ are limited to pairs only. Suppression of the pair-cluster expansion coefficients by weighing them may result in an overestimation of the expansion coefficients of many-body clusters. Therefore, and to enforce short-ranged expansion coefficients for all clusters, another empirical weight is introduced. Let d_l be the distance between two neighboring layers orthogonal to the $l = (110)$, $l = (100)$ or $l = (111)$ direction. Let $\Delta L_{\beta_K}^{nl}$ be the number of layers orthogonal to, *e.g.*, the $l = (110)$ direction that a picture of a cluster spans, where the cluster has $n = 1 \ldots D_{\beta_K}$ pictures in each unit cell (the multiplicity of the cluster is D_{β_K}). We define the new weight,

$$f_{\beta_K}^{(2)} = c_2 \sum_{n=1}^{D_{\beta_K}} \sum_{l} (d_l \, \Delta L_{\beta_K}^{nl})^{\lambda_2} J_{\beta_K}^2 \,, \tag{7.14}$$

where the sum runs over $l = (110)$, $l = (100)$ and $l = (111)$. This new weight is,

- similar to the weight $f_{\beta_K}^{(2)}$ for pairs as is shown in Fig. 7.2 and seems to work equivalently for pairs,
- defines a weight for many-body clusters that seems to work well,
- and gives smooth broken bond surface energetics from bulk cluster expansions.

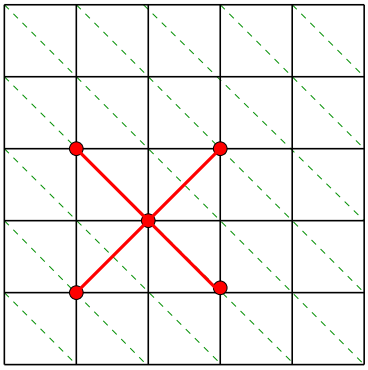

Figure 7.2: Comparison between the weights $f^{(1)}$ and $f^{(2)}$ for a second nearest-neighbor pair-cluster expansion coefficient. Four equivalent pairs exist in the square lattice. Two of them span two successive (11) planes, two of them do not cross any (11) plane. The weight $f^{(1)}$ is calculated as $f^{(1)} = c_1 4(\sqrt{2})^{\lambda_1} J_{2_2}^2$ and $f^{(2)} = c_2 2(2\frac{\sqrt{2}}{2})^{\lambda_2} J_{2_2}^2$. For the second nearest-neighbor pair the weights thus are the same if $2c_1 = c_2$.

For cluster expansions carried out in this work we mainly used weights $f^{(2)}_{\beta_K}$, however, we checked the expansion coefficients also with weights $f^{(1)}_{\beta_K}$ and a mixture of weights $f^{(1)}_{\beta_K}$ and $f^{(2)}_{\beta_K}$.

The total function,

$$\mathcal{W} = \sum_i \omega_i \left(E_i - \sum_{\beta_K} D_{\beta_K} J_{\beta_K} \xi_{i\,\beta_K} \right)^2 + c_1 \sum_{\beta_2} D_{\beta_2} J_{\beta_2}^2 r_{\beta_2}^{\lambda_1} + c_2 \sum_{\beta_K} \sum_{n=1}^{D_{\beta_K}} \sum_l (d_l\, \Delta L_{\beta_K}^{nl})^{\lambda_2} J_{\beta_K}^2 \,, \tag{7.15}$$

is minimized subject to the constraints of Eqs. (7.9, 7.11) using a quadratic programming method. The parameters $\{\omega_i\}, \delta_0^{(1)}, \delta_0^{(2)}, kT, c_1, \lambda_1, c_2$ and λ_2 are used to stabilize the fit.

According to Eq. (5.75) we can simply replace,

$$\xi_{\beta_K} \;\rightarrow\; \xi_{\beta_K} - \frac{1+(-1)^K}{2}\xi_0 - \frac{1-(-1)^K}{2}\xi_1 \,, \tag{7.16}$$

for every input structure to fit the energies of formation instead of the total energies E_i. Thereby we automatically fulfill $E_f(A) = E_f(B) = 0$, and as was explained in Sec. 5.6 we do not need to take J_0 and J_1 into account for the fit.

7.2.2 Cluster expansion coefficients for surface material

The principles for cluster expanding the energetics of a surface are the same as for bulk material, see Sec. 6.1. At a surface one faces simply a problem of numbers. Due to the broken translational symmetry orthogonal to the surface and the fewer point group

operations of the empty surface lattice compared to the bulk we expect that much more cluster expansion coefficients are required for a cluster expansion of the surface.

For the cluster expansion of the surface we define a function similar to $\mathcal{W}$ from Eq. (7.7). We identify,

$$E^0\left(\boldsymbol{\sigma}_i\right) = \left\langle E^{BB}\left(\boldsymbol{\sigma}_i\right)\right\rangle_U , \tag{7.17}$$

with the broken bond energy from Eq. (6.1). The remaining task is thus to calculate the surface modifications $\Delta J_{(L,\beta_K)}$ of the expansion coefficients.

In order to stabilize the expansion we define, in complete analogy to the bulk, limits for the allowed errors of the fit controlled by parameters $\delta_0^{(1)}, \delta_0^{(2)}, kT$.

The surface modifications will vanish deeply within the material. We assume that the surface modifications decay smoothly by weighing them according to their distance from the surface,

$$f_{(L,\beta_K)} = c\, D_{\beta_K} \exp\left(\lambda L\right)\, \Delta J^2_{(L,\beta_K)} , \tag{7.18}$$

where c, λ are parameters to control the fit.

With the same reasoning as for the bulk case we fit the energy of formation of the surface energies instead of the input energies directly.

7.2.3 Statistical averaging

The cluster expansion coefficients which we numerically extract from our ab-initio calculations, $J_\alpha^{(num)}$, consist of different parts,

$$J_\alpha^{(num)} = J_\alpha + \Delta J_\alpha^{(incomp)} + \Delta J_\alpha^{(input)} + \Delta J_\alpha^{(noise)} . \tag{7.19}$$

Thereby J_α are the true cluster expansion coefficients of a fully converged cluster expansion, the remaining terms are perturbations due to different factors.

- $\Delta J_\alpha^{(incomp)}$
  The finite set of clusters which we use to construct the cluster expansion is in general incomplete. This means that we set some expansion coefficients to zero which in reality have a finite value. This finite value may show up in the other expansion coefficients as an error $\Delta J_\alpha^{(incomp)}$.

- $\Delta J_\alpha^{(input)}$
  If the set of input structures and corresponding ab-initio energies is not large enough, no accurate expansion coefficients $J_\alpha^{(num)}$ can be extracted from this set of structures. Also, if the structures are chosen in such a way that the correlation matrix $\xi_{i\beta_K}$ is ill-defined, it cannot be inverted properly. If, for example, the determinant of the correlation matrix $\|\xi_{i\beta_K}\| = 0$, the minimum of Eq. (7.15) (and thus the expansion coefficients) is determined by the empirical weights $f^{(1)}$ and $f^{(2)}$. Also, if $\|\xi_{i\beta_K}\| \approx 0$, small numerical errors of the input energies E_i may induce large errors of the expansion coefficients.

- $\Delta J_\alpha^{(noise)}$
  Noise on the input ab-initio data will directly show up in the expansion coefficients. This can be handled relatively easily if a large enough set of input structures is available to allow for simple averaging.

The errors $\Delta J_\alpha^{(incomp)}$ and $\Delta J_\alpha^{(input)}$ are directly related. For example, let us assume that all input energies E_i were calculated using a unit cell with basis vectors $\boldsymbol{A}_1, \boldsymbol{A}_2, \boldsymbol{A}_3$. Then all pair-correlation functions $\xi_{\Delta \boldsymbol{x}}$ between two lattice sites i, j separated by a vector $\Delta \boldsymbol{x} = \Delta \boldsymbol{x}_0 + \sum_{i=1}^{3} m_i \boldsymbol{A}_i$ (with m_i integer numbers) are the same,

$$\xi_{\Delta \boldsymbol{x}} = \xi_{\Delta \boldsymbol{x}_0} = \xi_{(\Delta \boldsymbol{x}_0 + \sum_{i=1}^{3} m_i \boldsymbol{A}_i)} \,. \tag{7.20}$$

A correlation matrix $\xi_{i\beta_K}$ that contains the pair-correlation functions of two such pairs thus contains two identical rows and has determinant zero. The minimum of $\mathcal{W}$, Eq. (7.15), is then defined only by the empirical weights $f^{(1)}$ and $f^{(2)}$. The resulting cluster expansion coefficients are not a result of a fit to ab-initio calculations but are determined by empirical parameters.

Obviously the detailed choice of the calculated input energies E_i as well as the choice of clusters is important to guarantee reliable cluster expansion coefficients that can be used not only to describe the energies of the input structures E_i but even more important that predict accurate energies for structures not included in the set of ab-initio calculated input structures. Here we present some procedures that can be used to check for an accurate predictive power of a cluster expansion. First we discuss different measures to quantify the quality of the cluster expansion, subsequently we discuss the practical implementation used for the cluster expansions performed in this work.

- Not enough clusters or a choice of clusters that are not relevant simply leads to a large error in the fitted structures,

$$\mathfrak{e}_{fit} = \sqrt{\frac{\sum_i^{N_{\text{in}}} \left(E_i - E_i^{\text{CE}}\right)^2}{N_{\text{in}}}} \,, \tag{7.21}$$

  and therefore also to large errors in $J_\alpha^{(num)}$.

- If one tries to fit too many clusters to few structures (often hidden) linear dependencies between the correlations of the clusters in the different structures lead to unreliable results for $J_\alpha^{(num)}$. The validity of the expansion coefficients can be checked by calculating the energies of some structures not used to construct the interaction coefficients, thus by calculating,

$$\mathfrak{e}_{check} = \sqrt{\frac{\sum_i^{N_{\text{check}}} \left(E_i - E_i^{\text{CE}}\right)^2}{N_{\text{check}}}} \,, \tag{7.22}$$

  where none of the structures used to calculate $\mathfrak{e}_{check}$ is used to construct $J_\alpha^{(num)}$.

- Not enough or the "wrong" input structures will also lead to large errors $\mathfrak{e}_{check}$.

In order to quantify the quality of a cluster expansion we should calculate $\mathfrak{e}_{fit}$ and $\mathfrak{e}_{check}$. However, to calculate values for $\mathfrak{e}_{check}$ we need to ab-initio calculate a number N_{check} of energies that are not used in the construction of the cluster expansion but only for checking the quality of it. To not loose the information contained in the N_{check} structures for the cluster expansion fit, we used a fitting procedure that is able to include all the structures available in the cluster expansion fit but still provides a measure similar to $\mathfrak{e}_{check}$.

7.2.4 Flowchart of the cluster expansion procedure

For a given set of a total of N ab-initio calculated energies, we proceeded as follows to extract converged $J_\alpha^{(num)}$.

1. **Chose a set of clusters**
   A given set of clusters used in the cluster expansion procedure is compared to another set of clusters by comparing the measures $\mathfrak{e}_{fit}$ and $\mathfrak{e}_{pred}$ ($\mathfrak{e}_{pred}$ is defined below) for both sets of clusters. In this way the best possible set of clusters for a given system is determined.

2. **Construct N cluster expansion fits to all combinations of $N-1$ input structures**
   For the set of clusters chosen in 1., the function $\mathcal{W}$ is minimized N times for all possible combinations of $N-1$ input energies from the set of the N ab-initio calculated input energies available. From each of the N fits the energy of the one structure not used to construct the cluster expansion is predicted. We define the average prediction error from the N fits for each of their missing structure,

$$\mathfrak{e}_{pred} = \sqrt{\frac{\sum_i^N \left(E_i - E_i^{\mathrm{CE}}\right)^2}{N}}\,. \tag{7.23}$$

   Clearly $\mathfrak{e}_{pred}$ is smaller when the N cluster expansions on average are better converged. Thus the weights defined in the two above sections for the bulk and the surface fit are optimized to yield a minimum for $\mathfrak{e}_{pred}$. $\mathfrak{e}_{pred}$ and $\mathfrak{e}_{check}$ are related, both help to quantify the predictive power of the cluster expansion. Also experience shows,

$$\mathfrak{e}_{pred} \approx \mathfrak{e}_{check} > \mathfrak{e}_{fit}\,, \tag{7.24}$$

   and thus we automatically optimize $\mathfrak{e}_{check}$ and $\mathfrak{e}_{fit}$ when we optimize $\mathfrak{e}_{pred}$.

   To uncover hidden dependencies between the cluster expansion coefficients, we investigate correlations between cluster expansion coefficients from the N different fits by calculating,

$$\chi_{\alpha_K\beta_M} = D_{\alpha_K} D_{\beta_M} \left(\sum_l^N \frac{J_{\alpha_K}^{(l)} J_{\beta_M}^{(l)}}{N} - \overline{J}_{\alpha_K} \overline{J}_{\beta_M} \right)\,, \tag{7.25}$$

where the index $l = 1, \ldots, N$ labels the different fits and $\overline{J}_{\alpha_K} = \sum_l^N \frac{J_{\alpha_K}^{(l)}}{N}$ are the average expansion coefficients from the fits. Again, the set of clusters and weights for the fitting procedure is chosen to minimize the average squared correlations $\chi^2_{\alpha_K \beta_M}$.

The averaged expansion coefficients $\overline{J}_{\alpha_K}$ are found to give stable fits with small errors $\mathfrak{e}_{fit}$ and $\mathfrak{e}_{pred}$. Numbers for J_{α_K} provided in the following chapters correspond to $\overline{J}_{\alpha_K}$.

3. **Interaction space fit**
   The expansion coefficients $J_{\alpha_K}^{(l)}$ of the N fits define a subspace that would collapse into one vector J_{α_K} if all N fits were converged. We pick the optimum vector from the interaction space spanned by the N sets $J_{\alpha_K}^{(l)}, l = 1 \ldots N$ by defining,

$$J_{\alpha_K} = \sum_{l=1}^{N} a_l J_{\alpha_K}^{(l)} \,, \tag{7.26}$$

   and optimizing,

$$\mathfrak{e}_{pred} = \sqrt{\frac{\sum_i^N \left(E_i - E_i^{\mathrm{CE}}\right)^2}{N}} \,, \tag{7.27}$$

   with respect to a_l, where we demand (in order to stay in a physically reasonable interaction subspace),

$$a_l > 0 \,. \tag{7.28}$$

4. **Checks**
   The predictive power of the expansion is then again checked with few energies not from the set of the N structures used in the procedure above by calculating $\mathfrak{e}_{check}$.

Altogether, with this procedure we calculate three sets of cluster expansion coefficients:

- **direct**
  The set of expansion coefficients obtained from minimizing $\mathcal{W}$ with all N input structures directly.

- **average**
  The average expansion coefficients $\overline{J}_{\alpha_K}$ from N fits to $N-1$ input structures.

- **interaction space**
  The optimized expansion coefficients according to 3.

These three sets of expansion coefficients are the same for a converged cluster expansion. Thus, in case they deviate from each other this is another hint that the cluster expansion is not well converged. All numbers for expansion coefficients given in this work are average expansion coefficients. They compared well with expanison coefficients obtained from the two other procedures but produced more stable expansion coefficients when the number of input structures was varied.

Chapter 8

Temperature effects

When we are able to describe the energetics in an alloy, we know immediately how to calculate, in principle, the temperature dependence of the expectation values of all observables with the help of the partition sum of the system. Again, as for the solution of the many-particle Schrödinger equation in chapter 3, the direct calculation of the partition sum is simply not feasible for systems containing more than a few lattice sites. We present two methods, the Cluster Variation Method (CVM) based on the work of Kikuchi [80] and the Monte Carlo (MC) Method, for the calculation of phase diagrams and temperature dependent observables that avoid the direct calculation of the partition sum.

In the following the ensemble average of observable X will be denoted with $\langle X \rangle_T$, whereas the unit cell average will be denoted with $\langle X \rangle_U$ according to previous chapters.

8.1 Characterizing the state of order

First, let us quickly think of the information we are interested in and the information we can extract from experiments, see also the following section 8.5.1. We need to find appropriate expressions to define and measure the changes that occur, for example, when we heat up a system or change the concentration of one atomic species. Substitutional alloys are fully described when we know which site is occupied by what type of atom, namely, when we know the configuration $\boldsymbol{\sigma}$. However, neither the detailed configuration can be accessed by experiment nor some 10^{23} numbers can be handled in theory. Therefore we define averages that can, at least partly, be accessed by experiments and that still can answer questions, for example, whether the system is "ordered" or not. We define two types of parameters,

- Long-range order:
  This is the more intuitive definition of order, taking into account that many ground state structures of alloys need to be described by unit cells that contain different sublattices that are preferentially occupied by a certain atomic species. One example would be the Ni_3Al-$L1_2$ structure: The simple cubic positions are occupied by Al atoms while the face centers are occupied by Ni atoms. Thus, if we label the four atomic positions in the $L1_2$ unit cell from one to four, their Ni concentrations would

be $c_1 = 0$ and $c_2 = c_3 = c_4 = 1$. If we heat up the system, some of the Ni atoms exchange sites with some Al atoms until the probability of finding a Ni atom is the same on all lattice sites, *e.g.*, $c_1 = c_2 = c_3 = c_4 = \frac{3}{4}$. We define a long-range order parameter as a weighed sum over sublattice concentrations c_l of a given structure,

$$\Theta = w_0 + \sum_l w_l c_l \,, \tag{8.1}$$

that fulfills,

$$\Theta = \begin{cases} 1 & \text{perfectly ordered system at } T = 0, \\ 0 & \text{completely disordered system at high temperature } T. \end{cases} \tag{8.2}$$

For the $L1_2$ structure an appropriate definition of a long-range order parameter would thus be,

$$\Theta_{L1_2} = \frac{1}{3}(c_2 + c_3 + c_4 - 3c_1) = \frac{1}{3}(3 - 4c_1) \,. \tag{8.3}$$

The long-range order parameters can also be expressed by the point correlation of the respective sublattice l by using,

$$c_l = \frac{1}{2}(\langle \sigma_l \rangle_{_T} + 1) \,. \tag{8.4}$$

Note that the calculation of c_l or $\langle \sigma_l \rangle_{_T}$ involves averaging over the whole sample. Hence, from the long-range order parameters we cannot learn about local order, for example, whether in the system there are ordered domains or not.

- Short-range order:
  Let us assume that we have an atom A on site m_1. We then want to know the probability to find an atom A on site m_2 located at distance vector $\boldsymbol{r}_{12}$ from site m_1. Questions like this cannot be answered from the knowledge of the long-range order as the long-range order averages over all distances between atoms. Hence, the term short range order comprises pair- and many-body probabilities. The pair- and many-body probabilities are equivalent (see Sec. 8.2.3) to pair- and many-body cluster correlation functions (see Sec. 5.4 for definitions),

$$\xi_{\alpha_K} = \frac{1}{D_{\alpha_K} N_0} \sum_{\{R_0|\boldsymbol{t}_0\}} \Phi_{(\{R_0|\boldsymbol{t}_0\}:\alpha_K)} \,.$$

  In x-ray scattering experiments one usually measures the Warren-Cowley short-range order parameters which are equivalent to pair-correlations, see Sec. 8.5.1.

8.2 The Cluster Variation method

We start from a model crystal where all atomic positions are ideally confined to lattice sites $\boldsymbol{x}_m$. The only allowed excitations are thus the occupations of the lattice sites with

either A or B atoms. The state of the crystal can be fully specified by the configuration $\boldsymbol{\sigma}$ alone, see section 5.4, and the energy is given by $E(\boldsymbol{\sigma})$.

Once we have calculated the partition sum,

$$Z = \sum_{\boldsymbol{\sigma}} \exp\left(-\frac{E\left(\boldsymbol{\sigma}\right)}{kT}\right) \overset{(5.44)}{=} \mathrm{Tr}\exp\left(-\frac{E\left(\boldsymbol{\sigma}\right)}{kT}\right), \tag{8.5}$$

we are able to calculate the probability of finding the system in a certain configuration,

$$\rho(\boldsymbol{\sigma}) = \frac{\exp\left(-\frac{E(\boldsymbol{\sigma})}{kT}\right)}{Z}. \tag{8.6}$$

Note that the summation over all configurations in Z implicitly includes the sum over all possible concentrations. The free energy F can be derived from the knowledge of the partition function,

$$F = -kT\ln Z\,. \tag{8.7}$$

Following references [81,82,83] we define a functional for the free energy,

$$\begin{aligned}\mathcal{F} &= -kT\mathrm{Tr}\left(\rho\ln\frac{\exp(-\frac{E(\rho)}{kT})}{\rho}\right)\\ &= \mathrm{Tr}\rho E\left(\rho\right) - kT\mathrm{Tr}\rho\ln\rho\\ &= U[\rho] - TS[\rho]\,.\end{aligned} \tag{8.8}$$

As the logarithm fulfills,

$$\frac{1}{2}\left(\ln x + \ln y\right) \leq \ln\left(\frac{x+y}{2}\right), \tag{8.9}$$

the logarithm of an expectation value of an observable X, with $\mathrm{Tr}\rho = 1$, is greater or equal to the expectation value of the logarithm $\ln X$,

$$\mathrm{Tr}\left(\rho\ln X\right) \leq \ln\mathrm{Tr}\left(\rho X\right). \tag{8.10}$$

Therefore,

$$\mathcal{F}[\rho] \geq F\,, \tag{8.11}$$

where $\mathcal{F}[\rho] = F$ is fulfilled in thermal equilibrium for $\rho = \frac{\exp\left(-\frac{E(\rho)}{kT}\right)}{Z}$ and we thus have a recipe to calculate ρ in thermal equilibrium without calculating Z,

$$F = \underset{\rho}{Min!}\,\mathcal{F}[\rho]\,. \tag{8.12}$$

8.2.1 The internal energy

We rewrite the functional for the internal energy of an ensemble by using the cluster expansion of section 5.4,

$$U[\rho] = \mathrm{Tr}\rho E\left(\rho\right) = N_0\sum_K\sum_{\beta_K} D_{\beta_K} J_{\beta_K}\left\langle\xi_{\beta_K}\right\rangle_T. \tag{8.13}$$

8.2.2 The configurational entropy

In the cluster variation method, the entropy functional,

$$S = -k\mathrm{Tr}\left(\rho\left(\sigma\right)\ln\rho\left(\sigma\right)\right)\,, \tag{8.14}$$

can be expressed as [84,59]:

$$S = -k\mathrm{Tr}\left(\rho\left(\sigma\right)\ln\rho\left(\sigma\right)\right) = \sum_{K}\sum_{\beta_K}\Omega_{\beta_K}\,, \tag{8.15}$$

where the Ω_{β_K} are defined by,

$$-k\mathrm{Tr}^{(\alpha_L)}\left(\rho_{\alpha_L}\ln\rho_{\alpha_L}\right) = \sum_{K,\beta_K\subset L,\alpha_L}\Omega_{\beta_K}\,. \tag{8.16}$$

A hierarchy for CVM approximations can hence be defined by neglecting the terms Ω_{β_K} for clusters larger than given basic clusters $\{\alpha_{max}\}$ (The basic clusters are also sometimes called maximum clusters). The entropy is then approximated by

$$S = \sum_{K,\beta_K}^{\{\alpha_{max}\}}\Omega_{\beta_K}\,. \tag{8.17}$$

Combining Eq. (8.16) and Eq. (8.17) we can write the entropy as,

$$S = -k\sum_{L,\alpha_L}^{\{\alpha_{max}\}}a_{\alpha_L}\mathrm{Tr}^{(\alpha_L)}\left(\rho_{\alpha_L}\ln\rho_{\alpha_L}\right)\,, \tag{8.18}$$

where the a_{α_L} are geometric coefficients defined by,

$$\sum_{K\beta_K\supset L\alpha_L}^{\{\alpha_{max}\}}a_{\alpha_L} = 1\,. \tag{8.19}$$

8.2.3 Cluster algebra

The free energy is minimized with respect to the correlations $\left\langle\xi_{\alpha_N}\right\rangle_T$. We therefore write the cluster probabilites ρ_{α_L} as a function of the correlations $\left\langle\xi_{\alpha_N}\right\rangle_T$ [61].

1. As in chapter 5, we introduce the occupation variable σ_n:

$$\sigma_n = \begin{cases} +1 & \text{if species } i=+1 \text{ is at site } n\,, \\ -1 & \text{if species } i=-1 \text{ is at site } n\,. \end{cases} \tag{8.20}$$

2. Define $\Gamma_i(n)$:

$$\Gamma_i(n) = \frac{1}{2}(1+i\sigma_n)\,. \tag{8.21}$$

3. The probability to find a cluster α_L with occupation $\boldsymbol{\sigma}_L = \{i_1, i_2, \ldots . i_L\}$ in the occupation $\boldsymbol{\sigma}$ of the whole crystal with N_0 unit cells can be written as:

$$\rho_{\alpha_L}(\boldsymbol{\sigma}_L, \boldsymbol{\sigma}) = \rho_{\alpha_L}(i_1, i_2, \ldots, i_L) = \Big\langle \frac{1}{N_0} \sum_{\alpha_L} \Gamma_{i_1}(m_1)\Gamma_{i_2}(m_2)\ldots\Gamma_{i_L}(m_L) \Big\rangle_T , \quad (8.22)$$

where the sum runs over all clusters $\alpha_L = \{m_1, m_2, \ldots, m_L\}$ related by a space group operations in the system with N_0 unit cells.

4. Define the K-body correlations ξ_{α_K}, Eq. (5.18), for the cluster $\alpha_K = \{m_1, m_2, \ldots, m_K\}$:

$$\xi_{\alpha_K} = \frac{1}{D_{\alpha_K} N_0} \sum_{\{R_0|\boldsymbol{t}_0\}} \Phi_{(\{R_0|\boldsymbol{t}_0\}:\alpha_K)} . \quad (8.23)$$

5. Using Eq. (8.21) the probabilities are then expanded into the correlations,

$$\rho_{\alpha_L}(\boldsymbol{\sigma}_L, \boldsymbol{\xi}) = \frac{1}{2^L} \left(1 + \sum_{\beta_K} V(\boldsymbol{\sigma}_L)_{\alpha_L \beta_K} \langle \xi_{\beta_K} \rangle_T \right) . \quad (8.24)$$

Note that the matrix $V(\boldsymbol{\sigma}_L)_{\alpha_L \beta_K}$ needs to be calculated only once for a given set $\boldsymbol{\sigma}_L, \alpha_L$ and β_K.

We can now rewrite the free energy functional,

$$\mathcal{F} = N_0 \left(\sum_{\beta_K} D_{\beta_K} J_{\beta_K} \langle \xi_{\beta_K} \rangle_T + kT \sum_{\beta_K}^{\{\alpha_{max}\}} b_{\beta_K} \mathrm{Tr}^{(\beta_K)} \rho_{\beta_K} \ln \rho_{\beta_K} \right) , \quad (8.25)$$

(the sum over β_K runs only over one unit cell) as a function of the correlations $\mathcal{F} = \mathcal{F}\left(\{ \langle \xi_{\alpha_K} \rangle_T \} \right)$ and therefore,

$$F = \underset{\rho}{Min!}\, \mathcal{F}[\rho] = \underset{\{\langle \xi_{\beta_K} \rangle_T\}}{Min!}\, \mathcal{F}\left(\{ \langle \xi_{\beta_K} \rangle_T \} \right) . \quad (8.26)$$

The minimization must be carried out with the constraint,

$$0 \leq \rho(\boldsymbol{\sigma}_K, \boldsymbol{\xi})_{\beta_K} \leq 1 . \quad (8.27)$$

8.2.4 The Bragg-Williams approximation (BW)

The basic cluster (the set of basic clusters) defines the range of correlations that are taken into account for the system in question. Within a given cluster variation approximation, correlations of pair-clusters that are too large to be contained in the basic cluster therefore fulfill:

$$\xi_{\alpha_2}^{\mathrm{BW}} = \langle \sigma_n \sigma_m \rangle_T = \langle \sigma_n \rangle_T \langle \sigma_m \rangle_T = \langle \xi_{n_1} \rangle_T \langle \xi_{m_1} \rangle_T , \quad (8.28)$$

where BW indicates that the pair $\alpha_2 = \{n, m\}$ is not contained in the basic cluster and ξ_{n_1}, ξ_{m_1} refer to correlations of point-clusters at lattice sites n, m.

The contribution of the BW pairs to the free energy functional can be written as,

$$E_{\mathrm{BW}} = \sum_{\alpha_2}^{\mathrm{BW}} D_{\alpha_2} J_{\alpha_2} \left\langle \xi_{\alpha_2}^{\mathrm{BW}} \right\rangle_T = \frac{1}{2} \sum_{n,m}^{\mathrm{BW}} D_{nm} J_{nm} \left\langle \xi_{n_1} \right\rangle_T \left\langle \xi_{m_1} \right\rangle_T , \tag{8.29}$$

with $J_{nm} = J_{\alpha_2}$ for $\alpha_2 = \{n, m\}$.

Originally, the BW approximation [85] was introduced with the point-cluster that contains only one atomic site as basic cluster. Then all pair energies are written as in Eq. (8.29).

8.2.5 Minimization of the free energy

In the following the index BW means pair-clusters that are not contained in the the maximum or basic cluster. If not indexed, the clusters are assumed to be contained in the basic cluster, summations are to be taken over all clusters contained in the basic cluster, including the point-clusters.

The 1. derivative

For clusters α_K that are not point-clusters, we have:

$$g_{\alpha_K} = \frac{\partial(\mathcal{F}/N_0)}{\partial \left\langle \xi_{\alpha_K} \right\rangle_T} = D_{\alpha_K} J_{\alpha_K} - kT \sum_{\beta_L} \frac{a_{\beta_L}}{2^L} \sum_{\boldsymbol{\sigma}_{\beta_L}} V\left(\boldsymbol{\sigma}_{\beta_L}\right)_{\alpha_K \beta_L} \ln \rho_{\beta_L}\left(\boldsymbol{\sigma}_{\beta_L}, \boldsymbol{\xi}\right) , \tag{8.30}$$

where we took into account, that $\sum_{\boldsymbol{\sigma}_{\beta_L}} V\left(\boldsymbol{\sigma}_{\beta_L}\right)_{\alpha_K \beta_L} = 0$ [61]. The derivatives for the point-clusters (labeled with their lattice sites n_1, m_1) are modified:

$$\begin{aligned} g_{n_1} = \frac{\partial(\mathcal{F}/N_0)}{\partial \left\langle \xi_{n_1} \right\rangle_T} =& D_{n_1} J_{n_1} + \sum_{m_1} D_{n_1 m_1} J_{n_1 m_1} \left\langle \xi_{m_1} \right\rangle_T \\ & - kT \sum_{\beta_L} \frac{a_{\beta_L}}{2^L} \sum_{\boldsymbol{\sigma}_{\beta_L}} V\left(\boldsymbol{\sigma}_{\beta_L}\right)_{n_1 \beta_L} \ln \rho_{\beta_L}\left(\boldsymbol{\sigma}_{\beta_L}, \boldsymbol{\xi}\right) , \end{aligned} \tag{8.31}$$

where we took into account that $D_{n_1 m_1} J_{n_1 m_1} = D_{m_1 n_1} J_{m_1 n_1}$.

The 2. derivative

Starting with clusters that contain more than one site, we find:

$$H_{\alpha_K \beta_L} = \frac{\partial^2(\mathcal{F}/N_0)}{\partial \left\langle \xi_{\alpha_K} \right\rangle_T \partial \left\langle \xi_{\beta_L} \right\rangle_T} = -kT \sum_{\kappa_M} \frac{a_{\kappa_M}}{2^{2M}} \sum_{\boldsymbol{\sigma}_{\kappa_M}} V_{\kappa_M \alpha_K}\left(\boldsymbol{\sigma}_{\kappa_M}\right) V_{\kappa_M \beta_L}\left(\boldsymbol{\sigma}_{\kappa_M}\right) \frac{1}{\rho_{\kappa_M}\left(\boldsymbol{\sigma}_{\kappa_M}, \boldsymbol{\xi}\right)} . \tag{8.32}$$

This relation also holds for mixed derivatives $H_{n_1\beta_L}$ between point- and non-point-clusters. For $H_{n_1m_1}$ we find:

$$H_{n_1m_1} = \frac{\partial^2(\mathcal{F}/N_0)}{\partial\langle\xi_{n_1}\rangle_T\partial\langle\xi_{m_1}\rangle_T} = D_{n_1m_1}J_{n_1m_1} - kT\sum_{\kappa_M}\frac{a_{\kappa_M}}{2^{2M}}\sum_{\boldsymbol{\sigma}_{\kappa_M}} V_{\kappa_M n_1}(\boldsymbol{\sigma}_{\kappa_M})\, V_{\kappa_M m_1}(\boldsymbol{\sigma}_{\kappa_M})\,\frac{1}{\rho_{\kappa_M}(\boldsymbol{\sigma}_{\kappa_M},\boldsymbol{\xi})}\,. \tag{8.33}$$

Minimization technique

The (local) minimization condition for the free energy is (subscripts omitted):

$$\boldsymbol{g}(\langle\boldsymbol{\xi}\rangle_T) = 0\,. \tag{8.34}$$

A Taylor expansion to first order around the i^{th} input $\langle\boldsymbol{\xi}^{(i)}\rangle_T$ in an iteration cycle:

$$\boldsymbol{g}(\langle\boldsymbol{\xi}\rangle_T) = \boldsymbol{g}(\langle\boldsymbol{\xi}^{(i)}\rangle_T) + \boldsymbol{H}(\langle\boldsymbol{\xi}\rangle_T - \langle\boldsymbol{\xi}^{(i)}\rangle_T) = \boldsymbol{g}^{(i)} + \boldsymbol{H}(\langle\boldsymbol{\xi}\rangle_T - \langle\boldsymbol{\xi}^{(i)}\rangle_T) \tag{8.35}$$

is used to construct the next input vector $\langle\boldsymbol{\xi}^{(i+1)}\rangle_T$ (The Hessian $\boldsymbol{H}$ is calculated at $\langle\boldsymbol{\xi}^{(i)}\rangle_T$):

$$\langle\boldsymbol{\xi}^{(i+1)}\rangle_T = \langle\boldsymbol{\xi}^{(i)}\rangle_T - \boldsymbol{H}^{-1}\boldsymbol{g}^{(i)}\,. \tag{8.36}$$

This is the Newton-Raphson scheme. Due to the factor $\frac{1}{\rho_{\kappa_M}}$ in Eq. (8.32) the inversion of $\boldsymbol{H}$ becomes a problem at low temperatures, when some probabilities approach zero, $\lim_{kT\to 0}\rho_{\kappa_M} = 0$.

The natural iteration method

Another minimization procedure, the so-called natural iteration method [86,87], is also often used to calculate the equilibrium free energy. The natural iteration method is tedious to implement and converge for the relatively large maximum clusters used for the surface calculations. Although it was not used in this work, we will quickly sketch how it works. The central quantity in the natural iteration method are the probabilities of the various possible occupations of the maximum cluster. From these probabilities all probabilities for the occupation of smaller clusters can be obtained. The constraint that the sum over all probabilities that the maximum cluster can have must be equal to one, is coupled to the free energy with the help of a Lagrange multiplier. Starting from an initial guess for the probabilities of the maximum cluster, the iteration then consists of an inner and an outer loop (called minor and major iteration). The inner loop finds the Lagrange multipliers for given probabilities, the outer loop finds the minimum of the free energy with respect to the probabilities.

8.2.6 Calculation of phase diagrams

The free energy $\mathcal{F}$ is coupled to particle reservoirs of particles A and B. The Legendre transformation of $\mathcal{F}$ with respect to N_1 and N_2 is the grand potential $\mathcal{G}$,

$$\mathcal{G} = \mathcal{F} - \mu_{\mathrm{A}} N_{\mathrm{A}} - \mu_{\mathrm{B}} N_{\mathrm{B}} = \mathcal{F} - \Delta\mu(N_{\mathrm{A}} - N_{\mathrm{B}}) - \mu(N_{\mathrm{A}} + N_{\mathrm{B}})\,, \tag{8.37}$$

with,

$$\Delta\mu = \frac{1}{2}(\mu_{\mathrm{A}} - \mu_{\mathrm{B}})\,, \quad \mu = \frac{1}{2}(\mu_{\mathrm{A}} + \mu_{\mathrm{B}})\,. \tag{8.38}$$

Let there be M lattice sites in each of the N_0 unit cells of the underlying lattice. The total number of particles in the system is constant, $MN_0 = N_1 + N_2$,

$$\mathcal{G} = \mathcal{F} - \Delta\mu(N_1 - N_2) - \mu M N_0\,. \tag{8.39}$$

After minimization of $\mathcal{G}$ with respect to the correlations $\left\langle \xi_{\alpha_K} \right\rangle_T$, the thermodynamic equilibrium values of the correlations are functions of $T, \Delta\mu, \mu$. However, as,

$$\frac{\partial(\mathcal{G} + \mu M N_0)}{\partial\left\langle \xi_{\alpha_K} \right\rangle_T} = \frac{\partial\mathcal{G}}{\partial\left\langle \xi_{\alpha_K} \right\rangle_T}\,, \tag{8.40}$$

the thermodynamic equilibrium values of the correlations depend only on T and $\Delta\mu$,

$$\left\langle \xi_{\alpha_K} \right\rangle_T = \left\langle \xi_{\alpha_K}\left(T, \Delta\mu\right) \right\rangle_T\,. \tag{8.41}$$

Thus the chemical potential μ just induces a constant energy change that does not depend on the thermodynamic state of the system. In what follows we will thus assume $\mu = 0$ and,

$$\mathcal{G} = \mathcal{F} - \Delta\mu(N_1 - N_2)\,. \tag{8.42}$$

For the calculation of a phase diagram, we calculate the minimum value $\mathcal{G}$ with a given (set of) long-range order parameter(s) Θ_i that characterizes phase i,

$$\mathcal{G} = \mathcal{G}\left(\Theta_i\right)\,. \tag{8.43}$$

Practically the long-range order parameter of a given phase can be imposed only for a certain range of T and $\Delta\mu$ as $\mathcal{G}$ can only be minimized if it has at least a local minimum compatible with the order parameter Θ_i.

In the phase diagram the phase i with the lowest possible value of $\mathcal{G}\left(\Theta_i\right)$ is realized. A phase transition can occur if two different long-range order parameters yield the same $\mathcal{G}$,

$$\mathcal{G}\left(\Theta_i\right) = \mathcal{G}\left(\Theta_j\right)\,. \tag{8.44}$$

The classification of phase transitions in first and second order is carried out according to textbook thermodynamics [88].

Surface phase diagrams

In this work the calculation of surface phase diagrams within the cluster variation approach was realized with slabs that contain a finite number of layers parallel to the surface layer. In principle each layer can have different long-range order parameters as well as different cluster expansion coefficients. However, once the long-range order parameters in the slab are specified, the calculation of the phase diagram works exactly as described in the previous section for the bulk case.

8.2.7 Extensions for phonons

The CVM equations can be extended so that the entropy and energy contributions due to oscillations of the atoms around their ideal lattice sites are taken into account. Two different approaches exist:

- Kikuchi [89,90,91,92,93] extends the phase space of the CVM by introducing probabilities for the displacement of the atoms from their ideal lattice sites. Higher order probabilities (corresponding to higher order clusters) are also required, *e.g.*, $\rho\left(\boldsymbol{r}_1, \boldsymbol{r}_2\right)$ is the probability to find one atom displaced at $\boldsymbol{r}_1$ when the other is at $\boldsymbol{r}_2$.

  The now continuous CVM equations must be solved on a discrete mesh and the numerical effort required is dramatic.

- Finel [94] assumed that the potential for displacements of the atoms from their ideal lattice site is purely harmonic, leading to a Gaussian distribution of the displacement probabilities in a cluster. This Gaussian distribution can be integrated analytically, and the resulting equations are only slightly more complicated than the traditional CVM equations.

However, to the best knowledge of the author, no such extension to the CVM was used in the ab-initio modeling of phase diagrams.

8.3 The Monte Carlo method

In the CVM method one models the free energy in a restricted phase space given by the basic cluster $\alpha_{\max}$. In contrast, with the Monte Carlo method one tries not to model the free energy at all, but one takes into account that in thermal equilibrium the minimum of the free energy is characterized by the Boltzmann distribution,

$$\rho(\boldsymbol{\sigma}) = \frac{\exp\left(-\frac{E(\boldsymbol{\sigma})}{kT}\right)}{Z}\,. \tag{8.45}$$

Thus the probabilities for two states are given by,

$$\frac{\rho(\boldsymbol{\sigma}_1)}{\rho(\boldsymbol{\sigma}_2)} = \frac{\exp\left(-\frac{E(\boldsymbol{\sigma}_1)}{kT}\right)}{\exp\left(-\frac{E(\boldsymbol{\sigma}_2)}{kT}\right)}\,, \tag{8.46}$$

and the energies of the configurations can be calculated from a cluster expansion, see section 5.4.

In the traditional Monte Carlo approach one randomly generates a configuration $\boldsymbol{\sigma}_2$ by slightly modifying configuration $\boldsymbol{\sigma}_1$, *e.g.*, by exchanging the occupations at two lattice sites. This change is accepted if $E(\boldsymbol{\sigma}_1) > E(\boldsymbol{\sigma}_2)$ or it is accepted with probability $\frac{\rho(\boldsymbol{\sigma}_1)}{\rho(\boldsymbol{\sigma}_2)}$ if $E(\boldsymbol{\sigma}_1) < E(\boldsymbol{\sigma}_2)$. The procedure is repeated until all correlations do not change anymore. One then assumes that the correlations approached their equilibrium value. See [95,96,97] for a detailed introduction.

8.4 Excitations not included in the lattice gas model

Various authors modeled the influence of phonons and electronic excitations on the phase diagram. Due to the complexity of the problem, a wealth of approximations is used and a variety of assumptions are made, leading to sometimes contradicting conclusions. We restrict ourselves to cite some typical approaches [57,58,98,99,100,101,102,103,104,105].

8.5 Inversion of the CVM equations

The free energy functional of the CVM explicitly depends on the correlations $\left\langle \xi_{\beta_K} \right\rangle_T$ and the expansion coefficients J_{β_K}. Consider that we know all correlations at a given temperature from experiment. Then we use Eq. (8.30),

$$0 = \frac{\partial(\mathcal{F}/N_0)}{\partial\left\langle \xi_{\alpha_K} \right\rangle_T} = D_{\alpha_K} J_{\alpha_K} - kT \sum_{\beta_L} \frac{a_{\beta_L}}{2^L} \sum_{\boldsymbol{\sigma}_{\beta_L}} V(\boldsymbol{\sigma}_{\beta_L})_{\alpha_K \beta_L} \ln \rho_{\beta_L}(\boldsymbol{\sigma}_{\beta_L}, \boldsymbol{\xi}) \ ,$$

in order to derive the expansion coefficients [106,107,108]. The minimum condition can be used to extract expansion coefficients from all methods with an explicit free energy functional, *e.g.*, the random phase approximation [109] and its extensions, such as the ring approximation [110]. Inversion of the Monte Carlo method is possible by a trial and error method similar to the Monte Carlo method itself: Values for the expansion coefficients are guessed and optimized until they reproduce in a Monte Carlo simulation the experimentally observed correlations [111,7,95,108].

In general, the main problem consists in determining a complete set of accurate correlations from experiment. For example, from x-ray experiments only pair-correlations can be extracted, and expansion coefficients extracted from information on only pair-correlations are not unique [112].

8.5.1 Information from x-ray experiments

We show that from x-ray experiments only pair-correlations can be extracted (in kinematic approximation) with the help of Eq. (2.7) for the scattered intensity,

$$\begin{aligned} I = |A|^2 &= |A_0|^2 \left(\frac{e^2}{mc^2}\frac{1}{R_0}\right)^2 \sum_{nm} f_n(\boldsymbol{q})\, f_m^*(\boldsymbol{q}) \exp\left(i\boldsymbol{q}\left(\boldsymbol{r}_n - \boldsymbol{r}_m\right)\right) \\ &= |A_0|^2 \left(\frac{e^2}{mc^2}\frac{1}{R_0}\right)^2 \sum_{nm} \left(f_0(\boldsymbol{q}) + f_1(\boldsymbol{q})\,\sigma_n\right)\left(f_0^*(\boldsymbol{q}) + f_1^*(\boldsymbol{q})\,\sigma_m\right) \exp\left(i\boldsymbol{q}\left(\boldsymbol{r}_n - \boldsymbol{r}_m\right)\right) \\ &= |A_0|^2 \left(\frac{e^2}{mc^2}\frac{1}{R_0}\right)^2 \sum_{nm} \left(|f_0|^2 + 2\mathcal{R}\left(f_0 f_1\right)\sigma_n + |f_1|^2\sigma_n\sigma_m\right) \cos\left(\boldsymbol{q}\left(\boldsymbol{r}_n - \boldsymbol{r}_m\right)\right)\,, \end{aligned} \tag{8.47}$$

where we took into account that the atomic form factors $f_n(\boldsymbol{q})$ are purely atomic quantities that depend only on the occupation of lattice site n and on the momentum transfer $\boldsymbol{q}$. A cluster expansion of $f_n(\boldsymbol{q})$ thus contains only terms up to first order, $f_n(\boldsymbol{q}) = f_0(\boldsymbol{q}) + f_1(\boldsymbol{q})\,\sigma_n$.

For a periodic crystal with N lattice sites we can further simplify the above expression,

$$\begin{aligned} I = |A_0|^2 \left(\frac{e^2}{mc^2}\frac{1}{R_0}\right)^2 N\Bigg(&|f_0|^2 \sum_n \cos\left(\boldsymbol{q}\left(\boldsymbol{r}_n - \boldsymbol{r}_0\right)\right) \\ &+ 2\mathcal{R}\left(f_0 f_1\right)\left(\frac{1}{N}\sum_m \sigma_m\right)\sum_n \cos\left(\boldsymbol{q}\left(\boldsymbol{r}_n - \boldsymbol{r}_0\right)\right) \\ &+ |f_1|^2 \frac{1}{N}\sum_{nm} \sigma_n\sigma_m \cos\left(\boldsymbol{q}\left(\boldsymbol{r}_n - \boldsymbol{r}_m\right)\right)\Bigg) \\ = |A_0|^2 \left(\frac{e^2}{mc^2}\frac{1}{R_0}\right)^2 N\Bigg(&\left(|f_0|^2 + 2\mathcal{R}\left(f_0 f_1\right)\langle\sigma\rangle\right)\sum_n \cos\left(\boldsymbol{q}\left(\boldsymbol{r}_n - \boldsymbol{r}_0\right)\right) \\ &+ |f_1|^2 \sum_n \langle\sigma\sigma\left(\boldsymbol{r}_n - \boldsymbol{r}_0\right)\rangle \cos\left(\boldsymbol{q}\left(\boldsymbol{r}_n - \boldsymbol{r}_0\right)\right)\Bigg)\,, \end{aligned} \tag{8.48}$$

with the pair-correlations,

$$\langle\sigma\sigma\left(\boldsymbol{r}_n - \boldsymbol{r}_0\right)\rangle = \frac{1}{N}\sum_m \sigma_{n+m}\sigma_m\,. \tag{8.49}$$

The pair-correlation in a completely disordered alloy is given by,

$$\langle\sigma\sigma\left(\boldsymbol{r}_n - \boldsymbol{r}_0\right)\rangle = \langle\sigma\rangle\langle\sigma\rangle\,. \tag{8.50}$$

We see that the intensity of the fundamental rods of the disordered alloy changes quadratically with $\langle\sigma\rangle$,

$$I = |A_0|^2 \left(\frac{e^2}{mc^2}\frac{1}{R_0}\right)^2 \; N\Big(|f_0|^2 + 2\mathcal{R}\,(f_0 f_1)\,\langle\sigma\rangle + |f_1|^2\langle\sigma\rangle\langle\sigma\rangle\Big) \sum_n \cos\left(\boldsymbol{q}\,(\boldsymbol{r}_n - \boldsymbol{r}_0)\right) \,. \tag{8.51}$$

The intensity difference between an ordered structure, giving rise to superstructure rods, and the disordered alloy reads,

$$\begin{aligned}\Delta I &= |A_0|^2 \left(\frac{e^2}{mc^2}\frac{1}{R_0}\right)^2 \; N|f_1|^2 \sum_n \left(\langle\sigma\sigma\,(\boldsymbol{r}_n - \boldsymbol{r}_0)\,\rangle - \langle\sigma\rangle\langle\sigma\rangle\right) \cos\left(\boldsymbol{q}\,(\boldsymbol{r}_n - \boldsymbol{r}_0)\right) \\ &= |A_0|^2 \left(\frac{e^2}{mc^2}\frac{1}{R_0}\right)^2 \; N|f_1|^2 \left(1 - \langle\sigma\rangle\langle\sigma\rangle\right) \sum_n \alpha_n \cos\left(\boldsymbol{q}\,(\boldsymbol{r}_n - \boldsymbol{r}_0)\right) \,, \end{aligned} \tag{8.52}$$

with the Warren-Cowley short-range order parameters (see, *e.g.*, [78] and citations therein),

$$\alpha_n = \frac{\langle\sigma\sigma\,(\boldsymbol{r}_n - \boldsymbol{r}_0)\,\rangle - \langle\sigma\rangle\langle\sigma\rangle}{1 - \langle\sigma\rangle\langle\sigma\rangle} \,. \tag{8.53}$$

To extract from experimentally obtained short-range order parameters effective pair interactions a mean-field (point as maximum cluster, see also Sec. 8.2.4) treatment of the CVM equations, the Krivoglaz-Clapp-Moss formula, was commonly used [113,114]. The effective pair interactions obtained in this way are from measurements at one concentration and thus are usually concentration (and also temperature) dependent. Due to higher experimental resolution nowadays an inversion of theories including short-range order as described in Sec. 8.5 is used. As was noted by Sanchez [115,108], measuring the short-range order parameters α_n for a set of different concentrations and temperatures allows to indirectly extract the contribution of many-body correlations. Also, multiple scattered photons (not included in the scattering theory developed in this section) carry information about many-body correlations that could be used to extract information about many-body correlations from experiment.

Chapter 9

The (110) surface of Ni90%-Al

We know from the x-ray experiments performed by H. Reichert (Sec. 2.3.2) that Al segregates into the surface of $Ni_{90}Al_{10}$, forming an ordered monolayer in the surface. We want to understand why Al segregates into the surface and what are the reasons that an ordered monolayer is formed on top of a disordered material.

As we will see, a simple size effect due to the mismatch of the lattice constants of Al and Ni (experiment: $a_{\mathrm{Al}} = 7.65$ a.u., $a_{\mathrm{Ni}} = 6.65$ a.u.) is not responsible for the segregation of Al into the surface. The segregation seems to be driven by general modifications of the electronic structure at the surface. By means of the bond charge density and the covalent bond energy E_{cov} we try to characterize these electronic modifications.

However, since by definition the surface is just the end of bulk material, surface properties always depend on the underlying bulk. Therefore, and in order to see if the surface of NiAl can be described by a simple extrapolation of the bulk properties, we look at fcc-based NiAl bulk material first.

A glance at the band structures

Ni and Al are metals that simply display different behavior. While Al is often approximated as free electron gas which is reflected in the parabolas of the band structure in Fig. 9.1, Ni shows localized atomic d-states that form narrow bands in Fig. 9.1 which allow a description of parts of its behavior in terms of atomic orbitals, their overlaps and matrix elements. When Al and Ni atoms are mixed, we do not expect that the free electron gas limit nor the atomic orbitals description can fully capture the relevant physics. Before even getting started we already see that a detailed physical interpretation in terms of known "historic" expressions such as tight-binding matrix elements or properties of the free electron gas will not be possible.

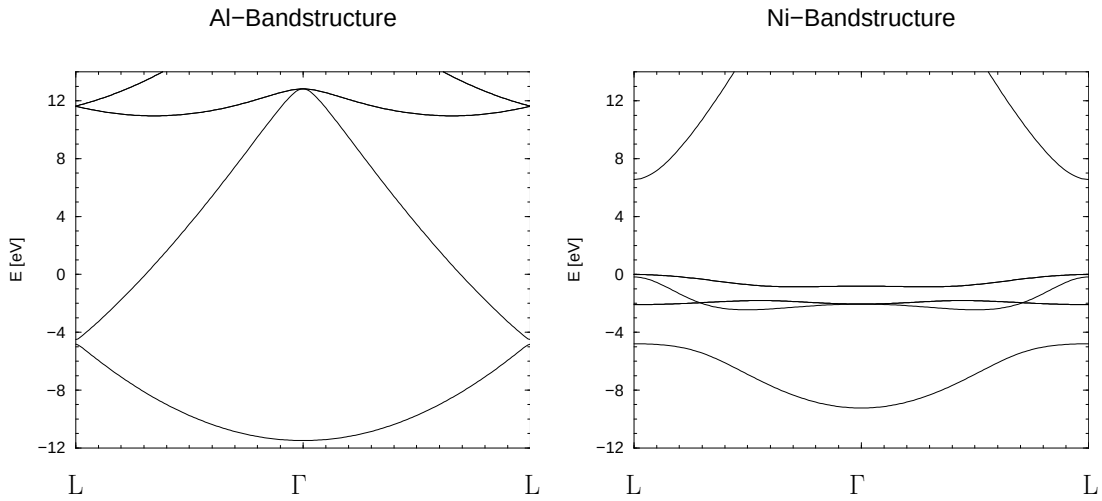

Figure 9.1: Band structure of Al and Ni.

9.1 NiAl bulk material

In order to characterize the fcc-based part of the NiAl phase diagram, 75 structures were fully relaxed (See chapter 7 for a definition of the term fully relaxed, and appendix B for computational details). The structures were chosen according to the following criteria:

- ground state structures and structures that appear in the fcc-based part of the phase diagram of NiAl [8]
- ground state structures that appear in other binary fcc-based compounds than NiAl, see [116,117]
- other artifical structures that might, from an intuitive point of view, be relevant in NiAl
- structures based on large unit cell that allow to check the convergence of long-ranged pair interactions, where long-ranged means 10 to 30 nearest-neighbor
- artifical structures especially designed to lift accidental degeneracies for certain cluster figures in the other structures considered so far.

Among the 75 originally considered structures were 58 that turned out to be stable with atomic positions relatively close to ideal fcc positions when they were fully relaxed. These 58 structures were used to construct the cluster expansion.

As one does not know apriori which clusters are relevant for a certain system, we started from a minimum set of clusters (three pairs, the nearest-neighbor triangle, the nearest-neighbor tetrahedron) that we extended in a systematic trial-and-error fashion

until the convergence of the cluster expansion was satisfying (average errors per atom for the fully relaxed CE: $\mathfrak{e}_{fit} = 13$ meV, $\mathfrak{e}_{pred} = 35$ meV. The prediction error is much larger than the mean average error from the fit as some structures among the 58 structures seem to be necessary to achieve a good cluster expansion, these structures cannot be predicted satisfactorily). For the pair-clusters the trial-and-error scheme is simple: Just add longer and longer pairs until their expansion coefficients do only slightly improve $\mathfrak{e}_{fit}$ and make $\mathfrak{e}_{pred}$ worse. To generate the three- and four-body clusters we started from the smallest cluster that contains $N-1$ sites, *e.g.*, the nearest-neighbor pair for the three-body clusters and the nearest-neighbor triangle for the four-body interactions. We then added one additional site that was a nearest-neighbor site to at least one of the sites already contained in the $N-1$ body cluster. Each of these clusters was then evaluated for its relevance in the cluster expansion. We also tested the most compact five, six and seven sites clusters. For NiAl, the contribution of five point- and higher clusters seems to be irrelevant.

Note that we used much more structures than it is commonly assumed in literature to be sufficient for an accurate cluster expansion. The reason is that we needed to have a very well converged cluster expansion for an accurate broken bond model of the surface energetics. This is the basis to extract well converged surface modified expansion coefficients according to the scheme used in Sec. 7.2.2.

Fig. 9.2 shows the clusters used for the cluster expansion in NiAl and depicts the respective energies that we calculated from the fully relaxed structures. The general features of the CE in NiAl are clearly the strong, positive and thus ordering, nearest-neighbor interaction and the relatively quickly decaying remaining cluster expansion coefficients. Other results published on fcc-based NiAl cluster expansion coefficients (cluster expansions from unrelaxed and volume relaxed energies from "LMTO-ASA" calculations [116,118], from "KKR-CPA-GPM" calculations [119,11] and from mixed-basis pseudopotential calculations [9], inverse Cluster Variation and inverse Monte-Carlo calculations based on diffuse x-ray scattering [6] and inverse Monte-Carlo calculations from diffuse neutron scattering experiments [7]) also show the strong ordering nearest-neighbor pair coefficient. However, the absolute values of the expansion coefficients deviate from the ones presented here. For the theoretical considerations this is due to the fewer and unrelaxed or volume relaxed input structures that were used, on the other hand, the extraction of accurate interaction coefficients from experiment is difficult [112].

9.1.1 Relaxation: No simple atomic size effect

The relaxation behavior which we found in the Ni-rich part with more than 75% Ni in NiAl can be characterized by three examples.

- If we look at a single Al atom dissolved in Ni bulk, we find that the relaxations of the Ni atoms surrounding the Al atom are small. Also the relaxation energy of $\Delta E = 13$ meV for each single Al atom embedded into Ni is small. The distance between the Al atom and the surrounding Ni atoms is $d = 4.63$ a.u. (from a fully

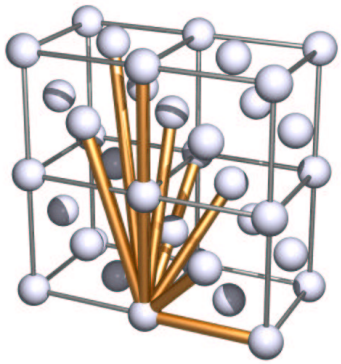

sorted according to their length

$j_{1_2} = 88$ meV
$j_{2_2} = 10$ meV
$j_{3_2} = 6$ meV
$j_{4_2} = 7$ meV
$j_{5_2} = -7$ meV
$j_{6_2} = -3$ meV
$j_{7_2} = 0$ meV
$j_{8_2} = 10$ meV
$j_{9_2} = 4$ meV
$j_{10_2} = 1$ meV

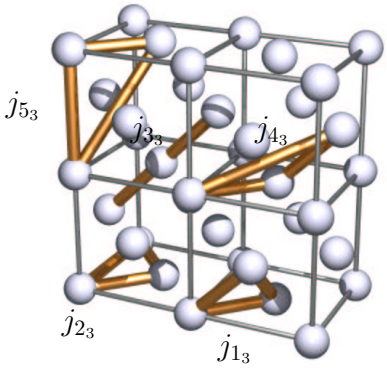

$j_{1_3} = 19$ meV
$j_{2_3} = -2$ meV
$j_{3_3} = -6$ meV
$j_{4_3} = 0$ meV
$j_{5_3} = 2$ meV

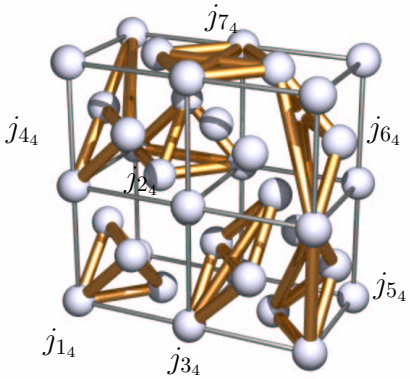

$j_{1_4} = -8$ meV
$j_{2_4} = 0$ meV
$j_{3_4} = -4$ meV
$j_{4_4} = -1$ meV
$j_{5_4} = -1$ meV
$j_{6_4} = 2$ meV
$j_{7_4} = 8$ meV

Figure 9.2: Figures used in the cluster expansion and respective interaction coefficients.

	Name	c/a	
$NiAl_5$	-	0.96	fcc
$NiAl_3$	Z3	0.97	fcc
$NiAl_2$	$\beta 2$	0.56	bcc
NiAl	$L1_0$	$1/\sqrt{2}$	bcc
Ni_2Al_2	Z2	0.77	bcc
Ni_2Al	$\beta 1$	$1/\sqrt{2}$	bcc
Ni_3Al	Z1	$\approx 1/\sqrt{2}$	bcc
Ni_5Al	-	0.88	-
$(NiAl)_1Al_3$	-	0.99	fcc
$(NiAl)_1Ni_3$	-	1.00	fcc

Figure 9.3: A single layer of Al atoms drives five layers of Ni atoms nearly into a bcc based lattice, while the elements Ni as well as Al are both fcc based. The last two lines give the c/a ratios for structures that contain instead of one layer of pure Al or Ni, one layer that contains 50% Al and 50%Ni. The c/a ratios of these structures are very close to an ideal fcc lattice.

relaxed $Ni_{107}Al$ calculation). The difference to the nearest-neigbor distance in Ni ($d = 4.61$ a.u.) is merely 0.5%, compared to the difference of 15.3% relative to the ideal Al lattice. Thus the larger Al atom does not strongly deform the Ni lattice. If we look at Al as an ideal electron gas, this means that the gas is compressed relative to its optimum state in pure Al. If we would assume that the "atomic size" is a quantity that is maintained when elements form compounds, we would expect larger relaxations. Therefore, for the moment it appears that we do not deal with a size effect, but Al can, without much relaxation, be dissolved in a matrix of Ni atoms.

- When we place two Al atoms on nearest-neighbor sites in otherwise pure Ni, we find that the fully relaxed energy of this configuration is high as well as the relaxations and the relaxation energy are large. This means that Al atoms on nearest-neighbor sites strongly repell each other. Let us try to give some very simple arguments to explain this behavior in the context of an ideal electron gas: Two Al atoms on nearest-neigbor sites in Ni are closer at each other than in pure Al. Thus their electron densities add up to a higher electron density, the energy increases.

- Finally we look at layered structures built from periodic layers of Al and Ni. Table 9.3 provides some examples for the calculated lowest energy c/a ratios for layered structures along the (100) direction. The bain deformation along the (100) direction transforms the perfect fcc lattice for $c/a = 1$ into a bcc lattice for $c/a = 1/\sqrt{2} \approx 0.71$. We also classfied whether a structure is more or less still a fcc-based structure or already a bcc-based structure.

To summarize, while isolated Al atoms in Ni do not cause large relaxation effects, Al atoms on nearest-neighbor sites or even Al atoms in layers introduce large structural relaxations that are accompanied by considerable energy relief when the system is relaxed from ideal fcc positions into the force and stress free mechanical equilibrium. However, Al atoms on nearest-neighbor positions are energetically very unfavorable and their contribution to the partition sum at relevant temperatures is very small. Fig. 9.4 summarizes the relaxation behavior for the 58 fcc-stable structures used for the cluster expansion. In Fig. 9.5 we compare the energies of formation in the Ni-rich part to a heterogeneous mixture of pure Ni and the $L1_2$ structure at the same composition. When we plot the difference between the respective energy of formation $E_f(\boldsymbol{\sigma}, x)$ of structure $\boldsymbol{\sigma}$ (structure $\boldsymbol{\sigma}$ has composition x) and the heterogeneous mixture [1],

$$\Delta E_f(\boldsymbol{\sigma}, x) = E_f(\boldsymbol{\sigma}, x) - \left(\frac{1-x}{1-x_{\mathrm{L1_2}}}\right) E_f(\mathrm{L1_2}, x_{\mathrm{L1_2}}) \ , \tag{9.2}$$

some structures are found with $\Delta E_f(\boldsymbol{\sigma}, x) < 0$. These structures are more stable than the heterogeneous mixture. Some of them should appear in the experimental phase diagram Fig. 2.8. The fact that none of the structures with $\Delta E_f(\boldsymbol{\sigma}, x) < 0$ is observed experimentally is probably due to the slow kinetics at the low temperatures where the ground state structure should exist.

[1] The energy of a heterogeneous mixture of the $L1_2$ structure and pure Ni is given by,

$$E(x) = aE(\mathrm{L1_2}, x_{\mathrm{L1_2}}) + bE(\mathrm{Ni}) \ . \tag{9.1}$$

The coefficients a and b are linear functions of the average composition x that are determined from $x = ax_{\mathrm{L1_2}} + bx_{\mathrm{Ni}}$ and $E(x = x_{\mathrm{L1_2}}) = E(\mathrm{L1_2}, x_{\mathrm{L1_2}})$ and $E(x = 1) = E(\mathrm{Ni})$. If we take into account $E_f(\mathrm{Ni}) = 0$ we arrive at Eq. (9.2).

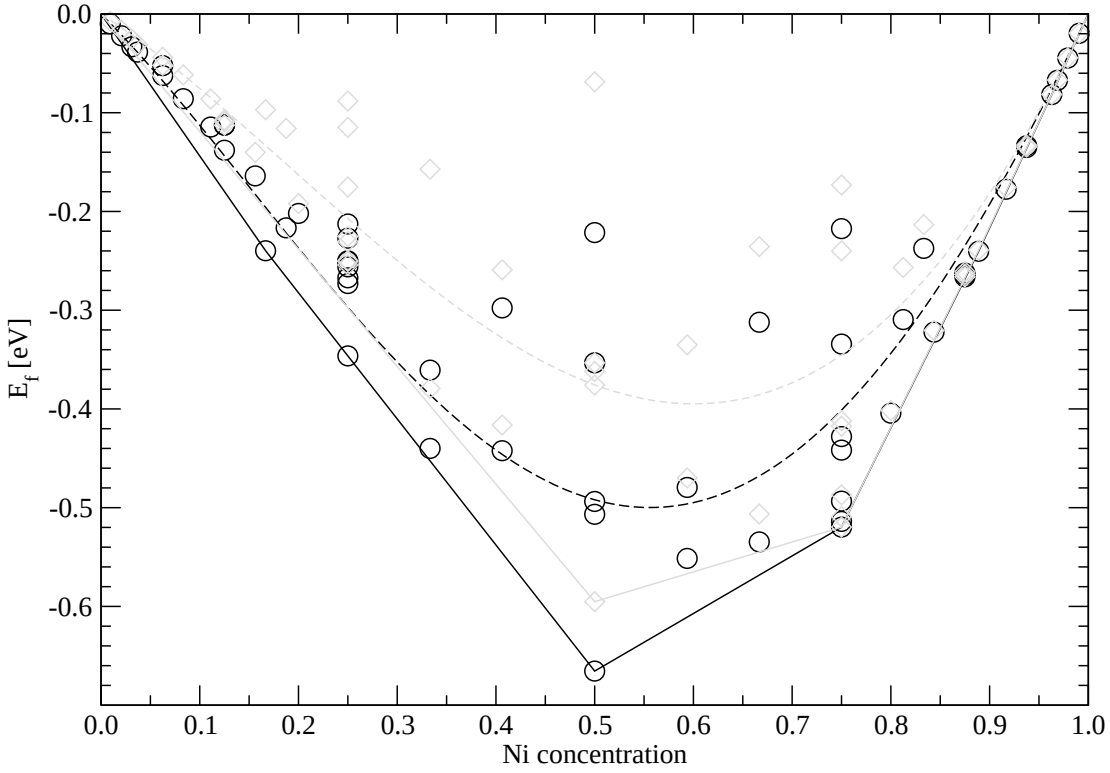

Figure 9.4: Fully relaxed (○) and volume relaxed (◇) energies of formation per atom for 58 structures used in the cluster expansion. The straight lines are a convex hull to the lowest lying energies of the fully relaxed (black) and volume relaxed (gray) structures. The dashed lines correspond to the energy of the random alloy where one assumes that all correlations fully separate into point-correlations, $\xi_{\alpha_K} = \xi_1^K$, and the energy is calculated as $E(\xi_1) = \sum_K \sum_{\alpha_K} D_{\alpha_K} J_{\alpha_K} \xi_1^K$. Since there are energies of 58 structures shown, fully relaxed and volume relaxed, one cannot connect each fully relaxed structure with its volume relaxed counterpart from the graph alone. However, note that the relaxation energy for energetically relevant structures below the energy of the random alloy is in general small in the part of the phase diagram we are interested in, namely Ni $> 75\%$. At a concentration of Ni $\approx 90\%$ relaxations seem to be negligible.

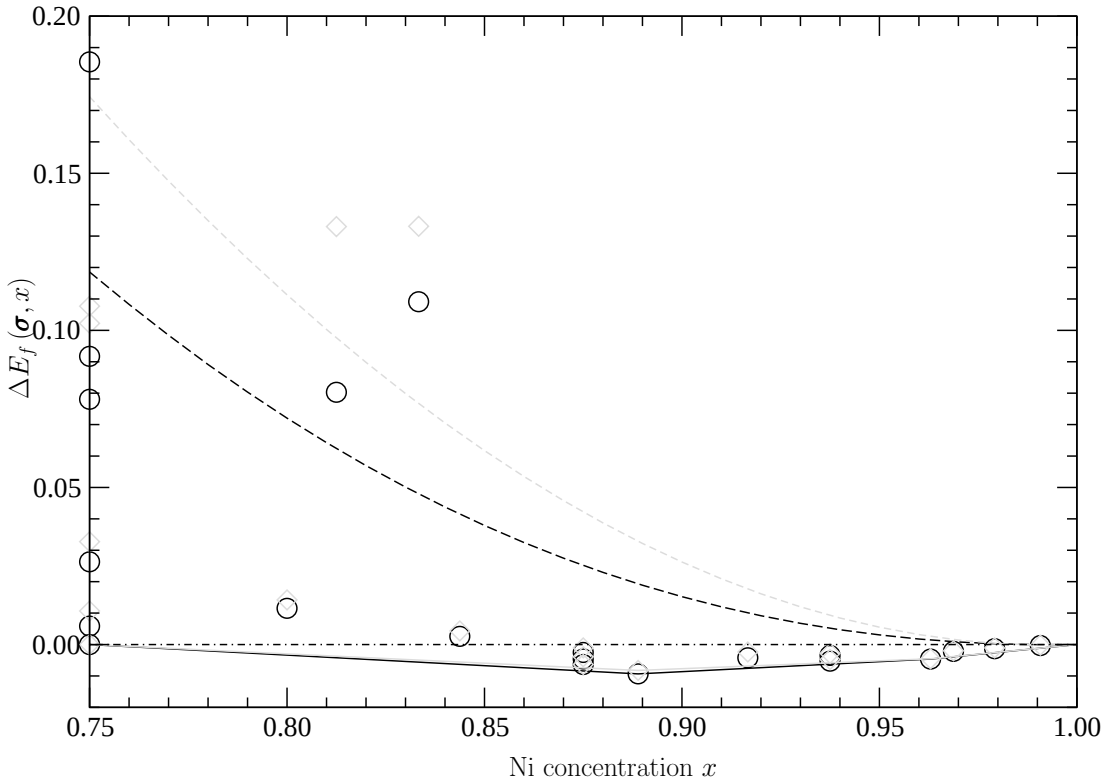

Figure 9.5: Fully relaxed (○) and volume relaxed (◇) energies of formation for structures with a concentration of $c_{\mathrm{Ni}} \geq 0.75$ compared to a mixture of the $\mathrm{L1_2}$ structure and pure Ni, $\Delta E_f(\boldsymbol{\sigma}, x) = E_f(\boldsymbol{\sigma}, x) - \left(\frac{1-x}{1-x_{\mathrm{L1_2}}}\right) E_f(\mathrm{L1_2}, x_{\mathrm{L1_2}})$. See caption of Fig. 9.4 for further details. One sees how small the relaxation energies of relevant structures for a concentration $c_{\mathrm{Ni}} \geq 0.75$ really are. A ground state structure $\mathrm{Ni_8Al}$ is observed with an energy of around 8 meV (≈ 100 K) less than the homogeneous mixture (This structure might be destabilized when magnetism is taken into account. It has the same structure as the $\mathrm{NbNi_8}$ alloy, see [116]. The D7-$\mathrm{Ni_7Al}$ structure [120] at $x = 7/8 = 0.875$ is unstable compared to a heterogeneous mixture of the $\mathrm{NbNi_8}$ structure and the $\mathrm{L1_2}$ structure and thus not a ground state structure according to our calculations).

9.2 The (110) surface

Let us, to begin with, just guess whether a single Al atom will segregate to the surface of Ni. So far we looked at an Al atom in Ni as a compressed electron gas. An Al atom in the surface has more space for its electrons as some of the electrons may slightly leak out into the vacuum. Hence, according to this oversimplified reasoning an Al atom in the surface would have a lower energy and from this argument Al would segregate into the surface. The same conclusion, namely that we expect the segregation of Al, also can be drawn from the surface energy of the elements. We calculated the surface energy of the (110) surface of Ni to be 1.50 eV, whereas the surface energy of Al is just 0.80 eV, this intuitively being in favor of the segregation of Al (The limited power of this argument is discussed in Sec. 6.1.7).

On the other hand, we know from the bulk cluster expansion that the nearest-neighbor pair-interaction coefficient dominates fcc-based NiAl. This means that it is energetically favorable for a single Al atom to be completely surrounded by Ni atoms on nearest-neighbor sites. If we bring such a single Al atom from the bulk to the surface, some of the Ni-Al bonds must be broken, leading to a higher energy. Thus Al would not segregate according to this simple broken bond picture (See again Sec. 6.1.7 for the limited power of the argument given here).

9.2.1 Characterization from ab-initio calculations

In oder to see which of the above considerations is correct, we will first discuss the behavior of the NiAl (110) surface with Ni$>$ 75% from direct ab-initio calculations. For all calculations we used slabs with 9 (110) layers, see Fig. 9.6. The lateral lattice constant of the slab unit cells was kept fixed at 6.60 a.u. (corresponding to the ab-initio interpolated lattice constant of $Ni_{90}Al_{10}$) in order to mimic the underlying bulk material. The extension of the slab unit cell orthogonal to the (110) layers was 50 a.u. in all calculations. All slab calculations were carried out with configurations that had an inversion center or a mirror plane in the central layer of the slab. The k-point mesh was chosen to be close to the k-point mesh used in the bulk calculations. A grid of two k-points was used orthogonal to the layers (Basically one k-point is enough as one assumes that the distance between the periodically arranged slabs is large enough that they do not interact and no dispersion is present). All other parameters were kept the same as in the bulk calculations, see appendix B. The atoms of the various configurations of the slabs were all moved along the forces acting on them until the forces were so small that the energy change corresponding to completely vanishing forces was smaller than the assumed accuracy of the calculations of $\approx$ 1mRy for the complete unit cell of the slab. This was achieved for smaller maximum forces than 2mRy/(a.u.).

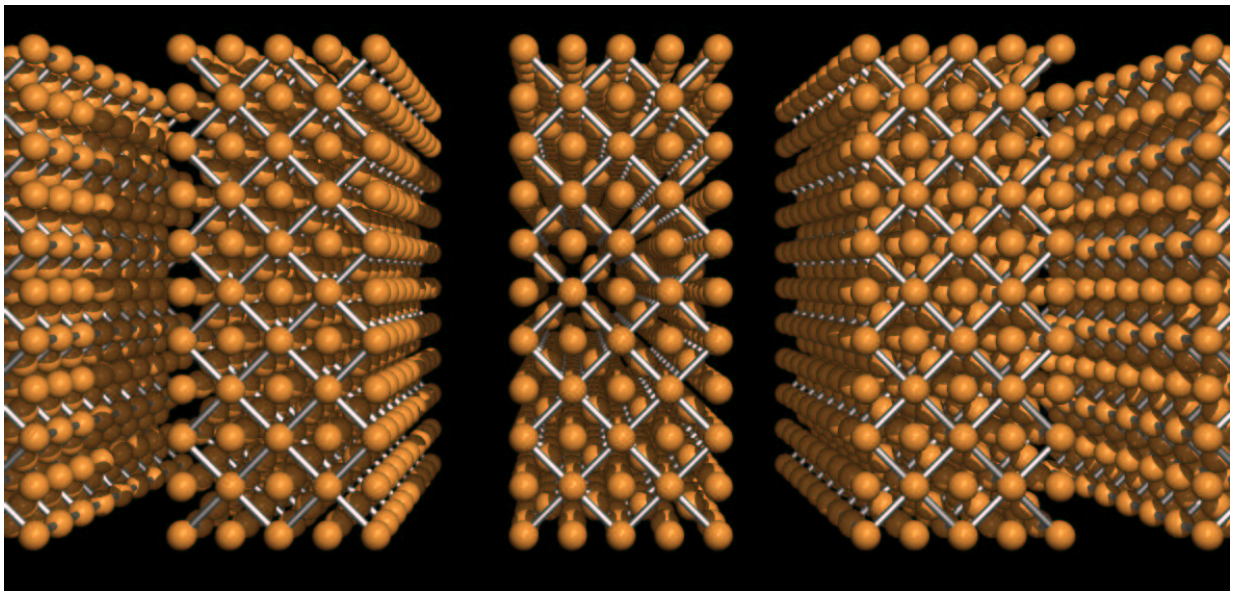

Figure 9.6: A periodic arrangement of 9-layered slabs was used to simulate the surface behavior.

Segregation of Aluminum

In Fig. 9.7 we sketched the changes when we bring a single Al atom into the (110) surface of Ni. From the corresponding ab-initio data we see that according to the ab-initio calculations Al segregates spontaneously into the surface. It is also clear that from a broken bond model due to the strong ordering nearest-neighbor pair-interaction coefficient segregation of Al is energetically unfavorable. The broken bond model thus cannot be used even for a qualitative description of the surface energetics of NiAl.

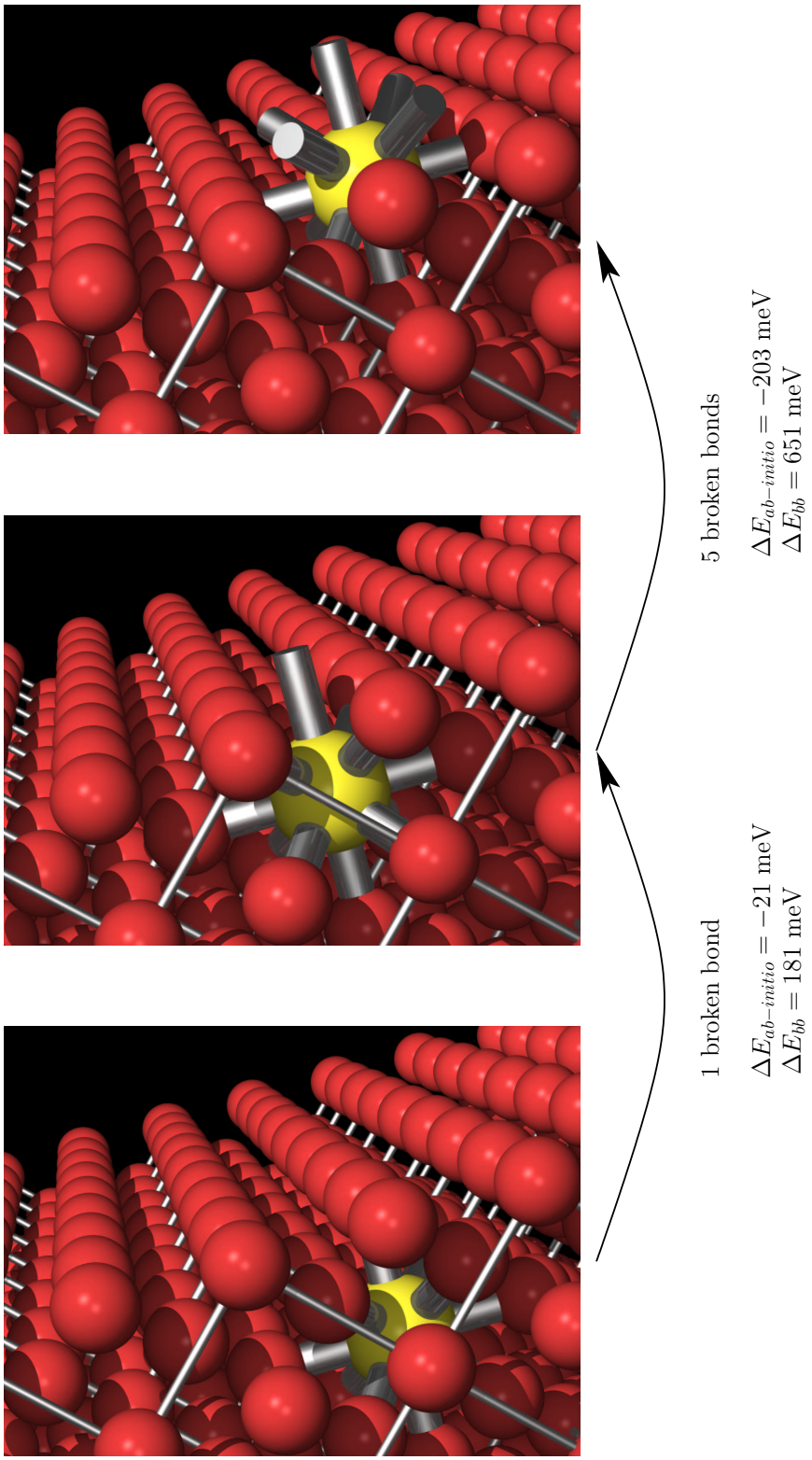

Figure 9.7: Models showing the segregation of a single Al atom into the (110) surface of Ni. Also shown are the broken nearest-neighbor bonds of the Al atom. Given are the energy differences between the shown configurations as calculated from ab-initio data and from broken bond configurations. The simulation of a "single" Al atom within the surface was modeled by calculations for a $(2 \times 6/\sqrt{2})$ surface unit cell where the Al-Al interaction is already very small. As mentioned before, also the configuration of the 9-layered slabs

Surface concentration of Aluminum

Let us assume for the moment that the strong nearest-neighbor interaction is qualitatively preserved in the surface; we will justify this assumption later. We then can guess the Al surface concentration with the lowest energy from a glance at the (110) surface of a fcc crystal (see Fig. 9.8). In the (110) surface each atom has two nearest-neighbor bonds and two second nearest-neighbor bonds to other surface atoms. If we assume that the energy related to the second nearest-neighbor interaction coefficient is small compared to the dominating nearest-neighbor interaction coefficient, the energetics in the surface is determined by the occupation of chains along the nearest-neighbor bonds within the surface. The lowest energy configuration of one such chain is the one with the most nearest-neighbor bonds between Ni and Al atoms, or in other words, the Al surface concentration with the lowest energy is expected to be 50%. Fig. 9.8 illustrates a situation where we bring an additional Al atom into a surface that already contains 50% Al. The extra Al atom is strongly repelled by the repulsive nearest-neighbor interaction coefficients between two Al atoms. Note that this also holds for the second layer and some sites in the third layer, as nearest-neighbor bonds in the fcc (110) surface stretch down into the third layer.

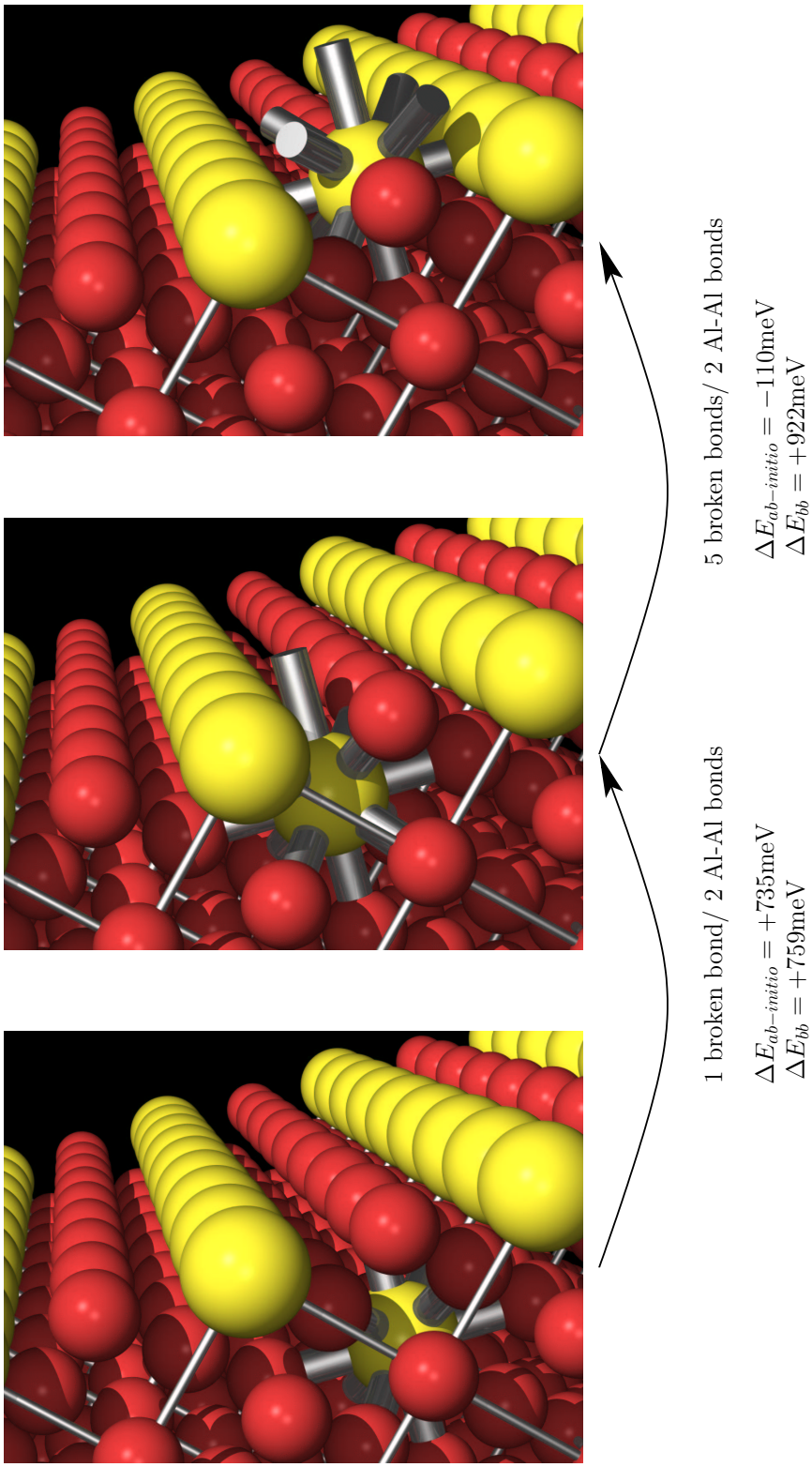

Figure 9.8: Models showing the segregation of a single Al atom into a fcc (110) surface covered by an $L1_2$-ordered monolayer of NiAl. Also shown are the broken nearest-neighbor bonds of the Al atom. Given are the energy differences between the shown configurations as calculated from ab-initio data and from broken bond configurations. The calculations were carried out for $(2 \times 6/\sqrt{2})$ surface unit cells.

Ordering in the surface

If the above said is true, the ordering mechanisms in the surface are simple.

- Al segregates into the surface until a concentration of 50% Al is reached.
- Due to the strong nearest-neighbor interaction further Al atoms are stopped in the third layer.
- The Al atoms order in chains on every second site along the nearest-neighbor bonds.

$\Rightarrow$ The surface is ordered.

but: Is it really that simple?

If we look at one isolated chain with antiferromagnetic nearest-neighbor interactions, we note that this is nothing else but a $1d$ Ising model. We know from textbook physics that long-range ordering cannot be established for the $1d$ Ising chain for finite temperatures. Therefore the weak interaction between the chains formed by nearest-neighbor bonds in the surface might be decisive for the order formed in the surface. We take a closer look at different possible ordered surface monolayers.

$L1_2$ versus $D0_{22}$ ordering in the surface There are in principle only two different ways to arrange the Ni-Al nearest-neighbor chains in the surface, corresponding to a cut through the $L1_2$ or the $D0_{22}$ structure, see Fig. 9.9. In other words, if one takes one step along the second-nearest-neighbor bond in the surface one may either find the same atomic species or the other atomic species than the one that was on the site one started from.

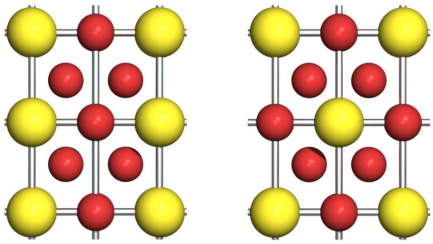

Figure 9.9: Surface ordering without nearest-neighbor sites occupied by atoms of the same type. The model on the left hand side illustrates the $L1_2$ surface coverage, on the right hand side the surface ordering corresponding to a cut through a $D0_{22}$ structure is shown. The calculated energy difference per surface site is $E_{L1_2} - E_{D0_{22}} = 13$ meV for a non-spin-polarized calculation with 9 layers and $E_{L1_2} - E_{D0_{22}} = 9$ meV in the spin polarized calculation. We also calculated the energy difference for a 19 layer slab with one monolayer of ordered NiAl on top. We find $E_{L1_2} - E_{D0_{22}} = 23$ meV for the 19 layer slab. All sites inside the slab from the 2^{nd} to the 8^{th} layer (and from the 2^{nd} to the 18^{th}layer for the 19 layer slab) were occupied by Ni atoms.

Going from $L1_2$ to $D0_{22}$ ordering Fig. 9.10 shows the energies which we calculated for various structures when going from the $D0_{22}$ to $L1_2$ surface ordering. Obviously the energy is increasing with the number of Al atoms that occupy second-nearest-neighbor sites in the surface.

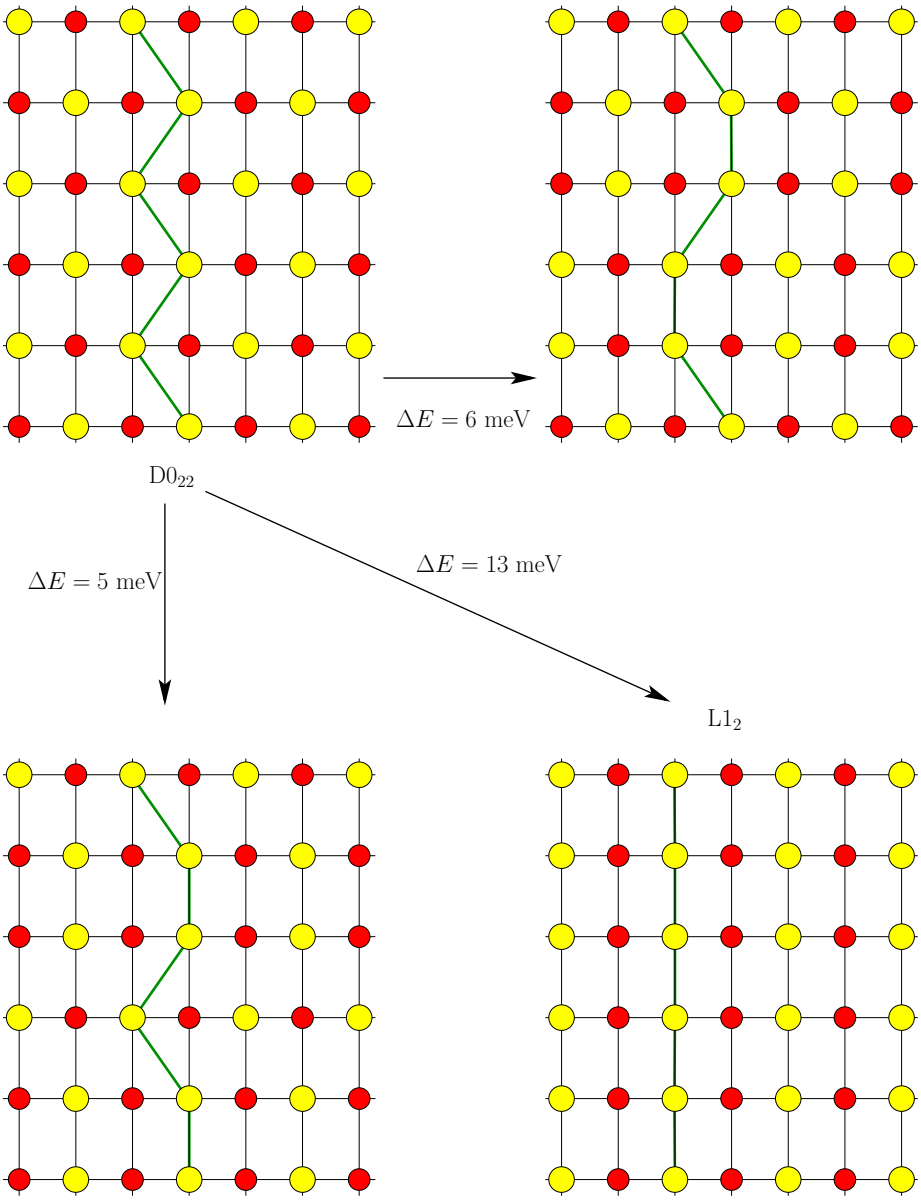

Figure 9.10: Calculated energy change per surface atom when the $D0_{22}$ structure is transformed into the $L1_2$ structure in the ordered surface monolayer. All atoms outside the surface layer are Ni atoms. The thick line in the structures is a guide for the eye only.

The importance of the bulk concentration Depending on the chemical potential in the bulk and thus on the bulk Ni concentration, we expect that the concentration of Al atoms in the first, second and third subsurface layer changes. We calculated the energies for possible subsurface concentrations with either a $L1_2$ or a $D0_{22}$ ordering in the surface. We find that the energetically favored type of order of the surface monolayer, $L1_2$ or $D0_{22}$, depends on the subsurface concentration, see Fig. 9.11. Hence, according to the ab-initio calculations, the type of surface order should depend on the bulk Ni concentration.

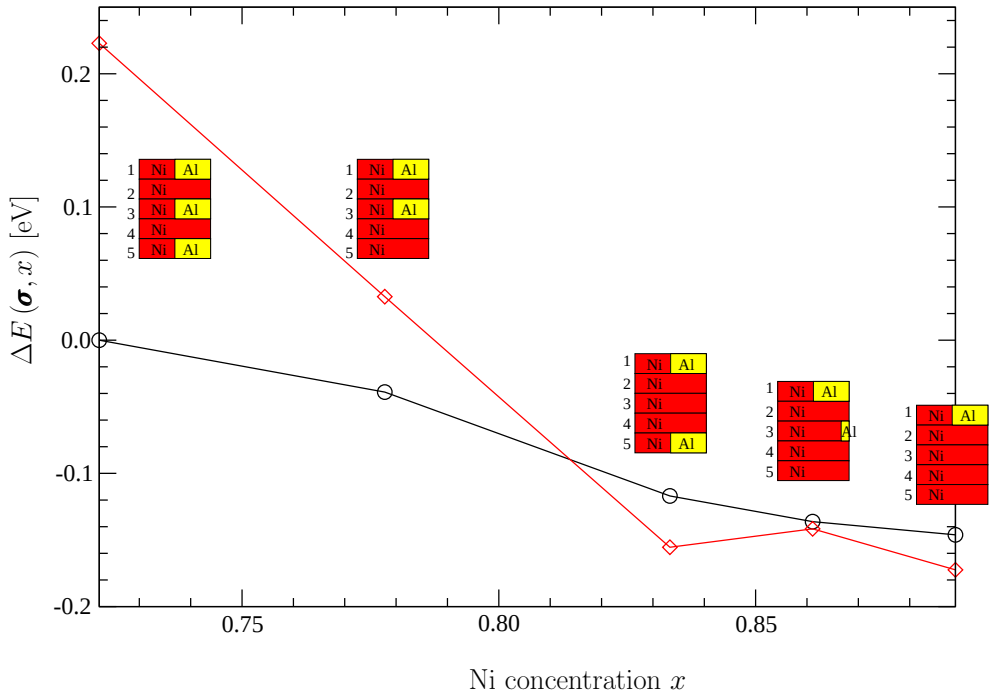

Figure 9.11: Difference energy of various $L1_2$ (○) and $D0_{22}$ (◊) ordered surfaces compared to a mixture of a pure Ni and a $L1_2$-ordered slab with 9 layers (and two surfaces), $\Delta E\,(\boldsymbol{\sigma}, x) = E_f\,(\boldsymbol{\sigma}, x) - \left(\frac{1-x}{1-x_{L1_2}}\right) E_f\,(L1_2, x_{L1_2})$. Shown are the Al concentrations in the first five layers for each $L1_2$- and $D0_{22}$-ordered slab. The fact that $\Delta E\,(\boldsymbol{\sigma}, x) < 0$ means that the mixture of a pure Ni and a $L1_2$-ordered slab is energetically less favorable than a slab configuration with 50% Al segregated into the first layer.

Relaxation effects at the surface The relaxation behavior at the surface is similar to the bulk, namely Al atoms on nearest-neighbor sites strongly repel each other and thus introduce large geometrical relaxations and relaxation energies. Moreover, since the strong nearest-neighbor interaction of the bulk is qualitatively preserved at the surface, configurations with Al atoms on nearest-neighbor sites are energetically unfavorable and the contribution of configurations with Al atoms on nearest-neighbor sites to the partition sum is small. Most surface decorations without Al atoms on nearest-neighbor sites dis-

play relatively moderate geometrical relaxations and relaxation energies, as shown by the example in Tab. 9.1. Although the relaxation energies for the surface are not negligible, their contribution to the total energy was found to be small so that the basic findings, such as segregation of Al into the surface and the strong nearest-neighbor interaction in the surface, were qualitatively also present in data from unrelaxed structural energies.

layer	relaxation (%)
1-1	2.4
1-2	-10.2
2-2	0.0
2-3	5.2
3-3	0.3
3-4	-1.2

Table 9.1: Calculated interlayer and intralayer relaxations compared to the ideal lattice constant of the $L1_2$ structure in a 9-layer slab ordered in $L1_2$ structure. The larger Al atoms stick out of the surface. The relaxation energy per surface site is $E_{rel} = 0.05$ eV which is $\approx 10\%$ of the energy of formation per atom for the $L1_2$ structure. The calculated relaxations compare well with experimental data [121].

9.2.2 Note on finite size effects, limited accuracy and possible conclusions

The ab-initio surface (slab) calculations are a compromise between available CPU time, limited accuracy of the density functional calculations (performed in local density approximation without spin polarization) and the accuracy required for the description of the surface energetics. Current implementations of the Kohn-Sham equations, LDA or GGA, still require relatively slow varying charge densities which might limit the accuracy available from surface energy calculations. Furthermore, numerical details such as the k-space integration and the quality of the basis functions used (here: the number of plane waves) needs to be chosen in order to guarantee fast and accurate calculations.

Note that the extraction of energies from 9-layered slabs in principle limits conclusions for the surface modifications of the expansion coefficients $\Delta J_{(L,\alpha_K)}$ to clusters that are located not more than 5 layers away from the surface. For a metal the surface modifications of the interactions should be effectively screened and approach their bulk values within such a small number of layers. Also, configurations that induce large relaxations at the surface and that might alter interactions deeper beneath the surface seem to be not relevant for the investigated surface. By comparing the energies of a few calculations for thicker slabs with the 9-layered slabs we showed that indeed 9 layers seem to be enough. Furthermore, the surface energy of Ni and Al was systematically converged with the number of layers involved for slabs with up to 40 layers thickness, and 9-layered Ni and Al slabs were found

to have a reasonably accurate surface energy. Fig. 9.12 shows the energy of formation for all slab configurations that were later used for the cluster expansion of the surface.

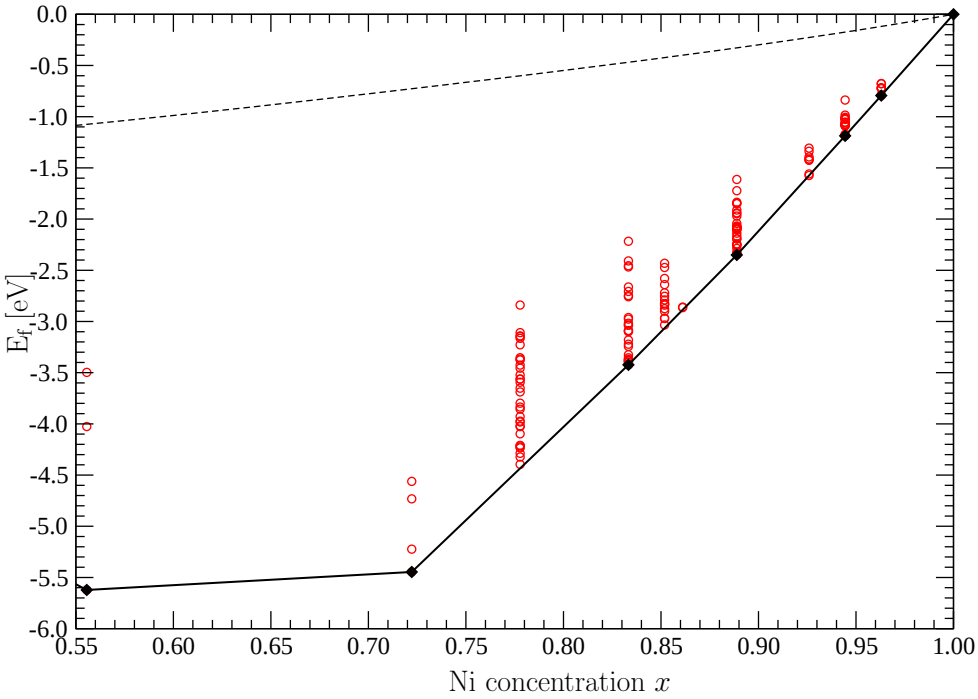

Figure 9.12: Energy of formation for a single column of atoms in the slab (9 atoms) of all ab-initio calculated relaxed slab configurations (○). The black line connects the ground states found from the ab-initio calculations. The dashed line corresponds to the random alloy. Compared to the bulk calculations, see Fig. 9.4, the random alloy is a worse approximation for the surface, reflecting the tendency of Ni90%-Al to form an inhomogeneous, *e.g.*, segregated and ordered surface. In Fig. 9.13 the ground states are discussed.

Fig. 9.13 shows the energy difference to a phase separated mixture of the $L1_2$ structure and pure Ni, namely,

$$\Delta E\left(\boldsymbol{\sigma}, x\right) = E_f\left(\boldsymbol{\sigma}, x\right) - \left(\frac{1-x}{1-x_{\mathrm{L1_2}}}\right) E_f\left(\mathrm{L1_2}, x_{\mathrm{L1_2}}\right) , \tag{9.3}$$

where the perfect $L1_2$-ordered 9-layered slab has a concentration of $x_{\mathrm{L1_2}} = \frac{13}{18}$.

We see that the $D0_{22}$ surface ordered slab has an energy lower than the mixture of a pure Ni slab and a completely $L1_2$-ordered slab. Besides the completely $L1_2$-ordered slab and the $D0_{22}$-ordered surface layer on pure underlying Ni, three more ground states were found from the ab-initio calculations. They are depicted as GS_3, GS_4 and GS_5.

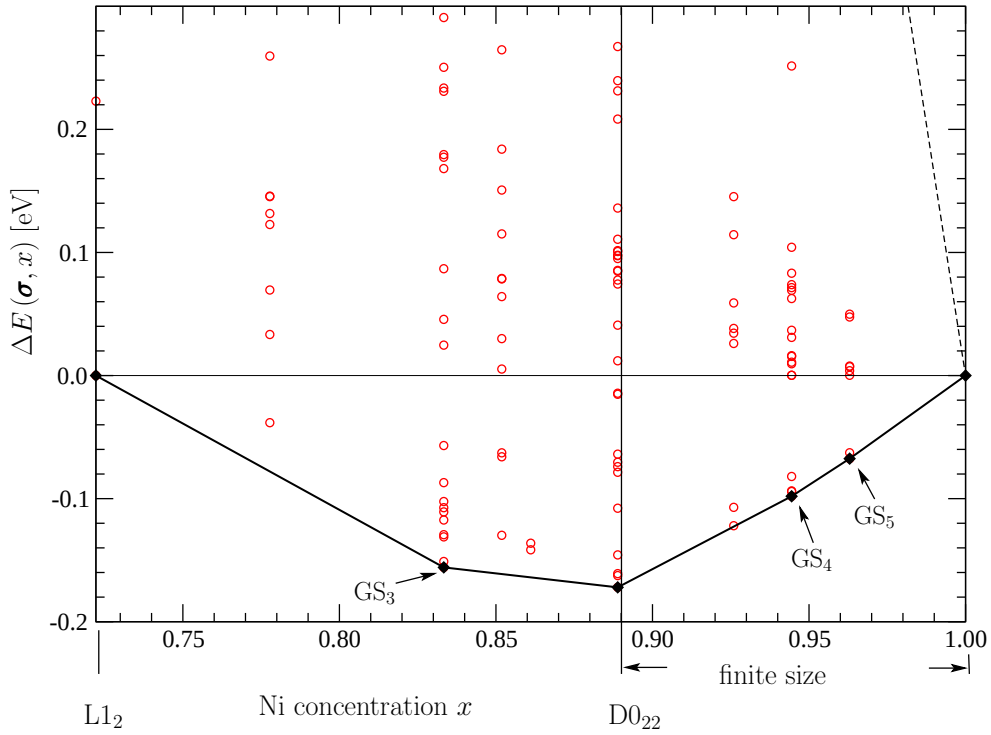

Figure 9.13: Shown are the same quantities as in Fig. 9.12, however the y-axis is calculated as $\Delta E\,(\boldsymbol{\sigma}, x)$, Eq. (9.3). Further explanations see text.

- GS_3 corresponds to a $D0_{22}$-ordered surface with 50% Al in the fifth layer (ordered in $D0_{22}$ structure) of an otherwise pure Ni slab.
- GS_4 corresponds to a surface coverage of 1/4 Al and otherwise pure Ni ($(2 \times 4/\sqrt{2})$ surface unit cell), whereas GS_5 corresponds to a surface coverage of 1/6 Al and otherwise pure Ni ($(2 \times 6/\sqrt{2})$ surface unit cell).

The ground states GS_4 and GS_5 are ground states only in the 9-layered system but not in a semi-infinite system: Slabs with Ni-concentrations higher than $x = \frac{8}{9}$ cannot exhibit a surface concentration of 50% Al or more (with a mirror plane in the center of the slab) in the 9-layered slabs. In order to check whether the ground states GS_4 and GS_5 are ground states of a semi-infinite system, the slab was coupled to a dilute NiAl bulk material with few, approximately 1% Al atoms dissolved in the bulk. We then calculated the energy gained if we bring an Al atom from the bulk reservoir into the surface in such a way that the ground states GS_4 and GS_5 are transformed into a $D0_{22}$-ordered surface layer. Table 9.2 shows that indeed the energy is lowered and therefore in the case of a semi-infinite system even in the limit $c_{\mathrm{Al}} \to 0$ we predict the first surface layer to be ordered in $D0_{22}$ structure with an Al-concentration of 50% for $T \to 0$.

Last but not least, we see that the energy of the $L1_2$ and the $D0_{22}$ surface coverage are close together. The preferred lower energy structure thereby depends on the details

	energy gain
GS_4	243 meV
GS_5	252 meV
pure Ni	273 meV

Table 9.2: Energy gained per atom if isolated Al atoms are brought from the Ni-bulk material into the surface in order to transform different surface ordered states into a $D0_{22}$-ordered surface state. The energy of an isolated Al atom in Ni was obtained from a $Ni_{107}Al$ calculation.

of the Al concentration profile beneath the surface. In contrast, the repulsive interaction between Al atoms on nearest-neighbor sites in the bulk and at the surface as well as the segregation tendency of the Al atoms are displayed in all calculations. The significance of the results obtained so far thus seems to be different: From the ab-initio calculations we conclude that the surface concentration is 50% and that the Ni and Al atoms order on nearest-neighbor sites in the surface. However, in order to judge whether we expect an $L1_2$- or a $D0_{22}$-ordered surface seems to be at the limits of the accuracy of our calculations.

9.3 Cluster Expansion of the surface energetics

For the cluster expansion of the surface the same clusters as for the bulk were used, see Fig. 9.2. The (110) surface of a fcc crystal is invariant under point group operations of D_{2h}. Furthermore in a slab with 9 layers that is not translationally invariant orthogonal to the surface, the interaction coefficients can be different in the first 5 layers. Altogether, from the bulk cluster expansion with 23 different cluster figures (point-cluster with zero energy included) 374 energetically different clusters in the 9-layered slab are derived.

The fact that the interaction coefficients are not the same at each lattice site but different in each layer in contrast to the bulk material, makes the construction of the surface modified interaction coefficients from ab-initio calculated total energy data even more complicated: From total energy calculations the interaction coefficients need to be extracted and located in different layers. Therefore, in order to extract converged surface modified interactions from the slab energies directly, we believe that we would need far more than 374 ab-initio calculated energies of slab configurations.

For the cluster expansion of the surface we thus assumed that the modifications of the interaction coefficients are located in the first three layers and that the cluster coefficients from the fourth surface layer onwards take their bulk values. The 154 slab calculations used for the cluster expansion thus focused on correlations in the first three layers. From the 112 clusters in the first three layers in a trial and error procedure the ones that did not improve $\mathfrak{e}_{fit}$ and $\mathfrak{e}_{pred}$ were sorted out. Finally we used 69 clusters to describe the surface modifications. The mean average error per atom was $\mathfrak{e}_{fit} = 6.2$ meV and the average prediction error $\mathfrak{e}_{pred} = 9.5$ meV. In comparison, the slab energies calculated from the bulk

expansion coefficients ("broken bond" model) deviated on average $\mathfrak{e}_{BB} = 84.5$ meV per atom from the ab-initio energies, with large scatters from this average error from 0.1 meV to 220 meV depending on the surface configuration. Fig. 9.14 shows the ab-initio calculated energies in comparison to the cluster expanded energies.

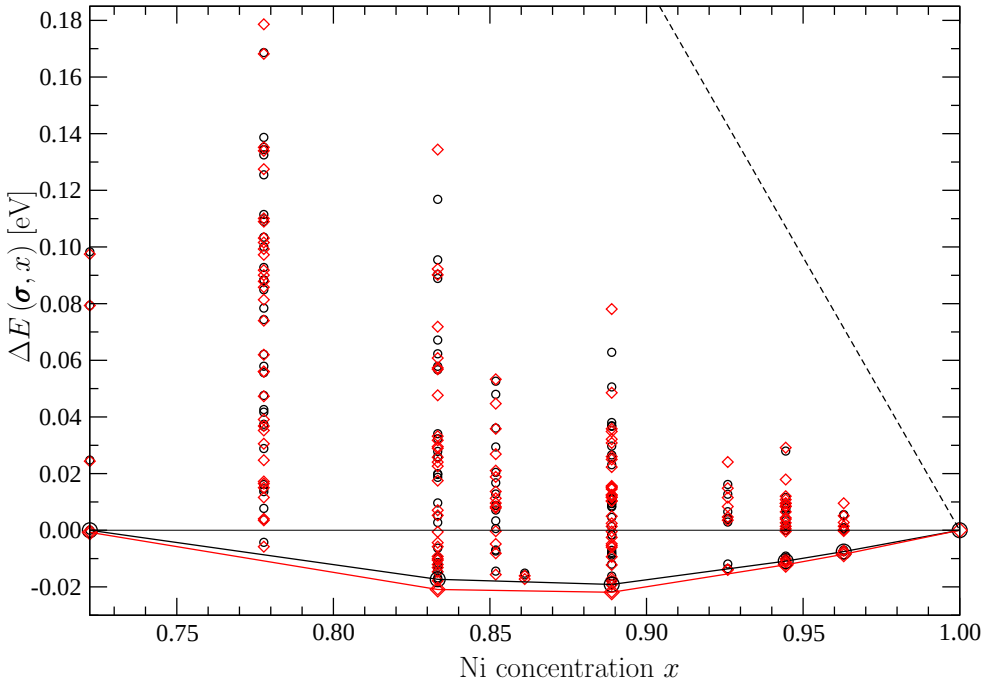

Figure 9.14: Comparison of the ab-initio calculated energies (○) with the cluster expanded energies (◇). The dashed line corresponds to the energy of the random alloy, the straight lines connect the ground states found among the ab-initio and the cluster expanded energies. The ground state structures found from the ab-initio and the cluster expanded energies are the same. The y-axis shows energies per atom given in comparison to a mixture of the $L1_2$-ordered slab and the pure fcc-Ni slab, see Eq. (9.3).

The energies of structures with energy $\Delta E(\boldsymbol{\sigma}, x) \approx 0$ are very well described by the cluster expansion, even the complicated competition between $L1_2$ and $D0_{22}$ surface ordering which is due to modifications of three- and four-body cluster expansion coefficients can be accurately reproduced.

Fig. 9.15 summarizes the modifications of the expansion coefficients for the nearest-neighbor pairs and for the point-cluster found from the cluster expansion. The large point-cluster (4.4 times larger than the bulk nearest-neighbor interaction coefficient) together with the strong nearest-neighbor interaction coefficient in the surface (40% higher than in the bulk) drives the segregation of Al into the surface. At the same time, the strong nearest-

neighbor interaction in the surface prevents nearest-neighbor sites to be occupied with the same type of atoms, and the segregation into the surface is stopped at 50%, quantitatively confirming the picture that we already derived from the analysis of the ab-initio data in the previous sections.

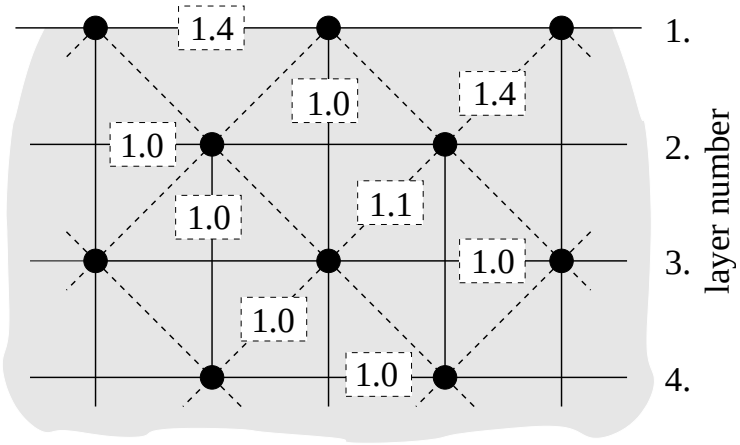

Figure 9.15: Modification of the expansion coefficients of the nearest-neighbor pair-cluster relative to its bulk value of 88 meV. The modification of the point-cluster was 0.38 eV in the first, −0.04 eV in the second and 0.004 eV in the third layer.

Absolute values of the expansion coefficients

The absolute values of the modified surface cluster expansion coefficients depend on the bulk cluster coefficients and on the choice of surface clusters that are allowed to be modified in the surface.

From the bulk calculations it had been possible to extract more expansion coefficients in order to achieve better convergence of the bulk expansion coefficients. This would require to use at least 10-20 more pair interaction coefficients and also more three- and four-body clusters. This increase of the total number of expansion coefficients used in the bulk leads to an enormous increase of the total number of different expansion coefficients in the slabs. As the number of ab-initio calculations and the CPU time required for the slabs was already at the limit of "what could be done", the bulk cluster expansion was cut at a reasonable number of clusters, Fig. 9.2, where the total number of the expansion coefficients were already quite well converged, especially to yield a good quantitative description of the bulk material.

The choice of clusters that are allowed to be modified in the surface is a non-trivial task, as many cluster expansion coefficients, *e.g.*, in the third or fourth layer, will change only by a quite small amount, and one must judge whether one allows them to slightly change or not to change at all. Given the finite accuracy of the bulk cluster expansion used for the broken bond guess, even clusters in the center of the slab will look like they need

to be slightly modified, just to correct for the finite accuracy of the bulk cluster expansion (Even if the surface modifications to the expansion coefficients vanished completely in the center of the slabs, the description of the energetics of the center of the slabs within the broken bond model is not perfect as the bulk cluster expansion has only finite accuracy. This finite accuracy induces noise in the broken bond approximations of the slab structures which the fitting procedure for the cluster expansion surface modifications tries to fit. This noise then may show up in the surface modified expansion coefficients). At the same time, the number of calculated slab configuration energies is not enough to carry out a direct inversion for the slab expansion coefficients. Each cluster that is modified in the surface thus requires to be checked carefully with respect to the prediction error $\mathfrak{e}_{pred}$ of the cluster expansion. If a cluster lowers the predictive error, it is allowed to be modified in the surface, if it increases or does not change the average prediction error, it is not taken into account.

The numbers for the expansion coefficients obtained in [122] were obtained with a version of the cluster expansion code that calculated only the mean square error $\mathfrak{e}_{fit}$ but not the prediction error $\mathfrak{e}_{pred}$. It turned out that the cluster expansion presented in Fig. 9.15 has a lower prediction error $\mathfrak{e}_{pred}$ by approximately 30% but a higher error $\mathfrak{e}_{fit}$ compared to the numbers provided in [122]. However, it is important to note here that the absolute representation of the energies of the ab-initio calculated structures as well as the energies of many predicted structures seems to be very similar and identical when it comes to the description of the segregation and ordering tendencies in the surface. Also the qualitative modifications of the surface interactions in both cluster expansions are the same.

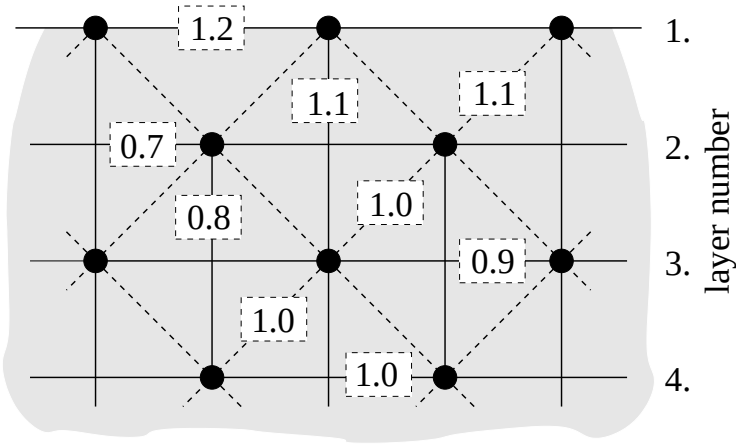

Figure 9.16: Modification of the expansion coefficients of the nearest-neighbor pair-cluster relative to its bulk value of 90 meV according to [122]. The modification of the point-cluster was 0.53 eV in the first, 0.17 eV in the second and 0.03 eV in the third layer.

9.4 Can we understand what is happening at the surface?

The segregation of Al into the surface is driven by the electronic structure in contrast to the segregation induced by atomic relaxation effects, as the effect induced by relaxing the surface atoms does not change the segregation tendencies. In order to understand why Al segregates we need to understand what the modifications of the electronic structure at the surface are.

In the following we discuss different ways in order to quantify the electronic modifications at the surface. However, as we also will see, the system is complicated enough to not let us draw simple conclusions.

9.4.1 Charge density modifications at the surface

Fig. 9.17 and Fig. 9.18 show contour plots of the bond charge density

$$\Delta\rho = \rho_{\text{slab}} - \rho_{\text{atomic}} \,, \tag{9.4}$$

where ρ_{slab} is the full charge density of the slab and ρ_{atomic} is the superimposed charge density of free atoms located at the positions of the respective slab atoms. Plotted is a cut perpendicular to the (110) surface through the atoms that form a (100) layer of the bulk $L1_2$ structure. Blue areas represent $\Delta\rho < 0$, which means that the atoms located there donate some of their charge (we do not deal with an ionic crystal, indeed the atoms donate only the fraction of an electron charge, redistribution of the electrons has the largest effects), and red areas represent $\Delta\rho > 0$. The distribution of the colors was chosen in such way in order to display important features of the bonding behavior.

Fig. 9.17 shows $\Delta\rho$ for a few Al atoms (large blue areas) located within the surface of an otherwise pure Ni crystal. The Ni atoms form flower like bonds to nearest-neighbor sites. In Fig. 9.18 the surface of a $L1_2$ structure is shown. From Fig. 9.17 and Fig. 9.18 it appears that the Al atoms in the first layer are only slightly influenced by the Al atoms in the third and fifth layer which can be seen in Fig. 9.18. The shape of the Al atoms in the third and the fifth layer deviates considerably from the shape of the Al atoms in the first layer. This different shape might be linked to the segregation tendency of Al. Compared to Fig. 9.17 all Ni atoms redistribute their charge as they now form bonds to Al atoms on nearest-neighbor sites. The fourfold symmetry of the $L1_2$ structure can be seen from the charge density of the Ni atoms only in the fifth layer whereas in Fig. 9.17 the Ni atoms seem to have fourfold symmetry in the third layer already.

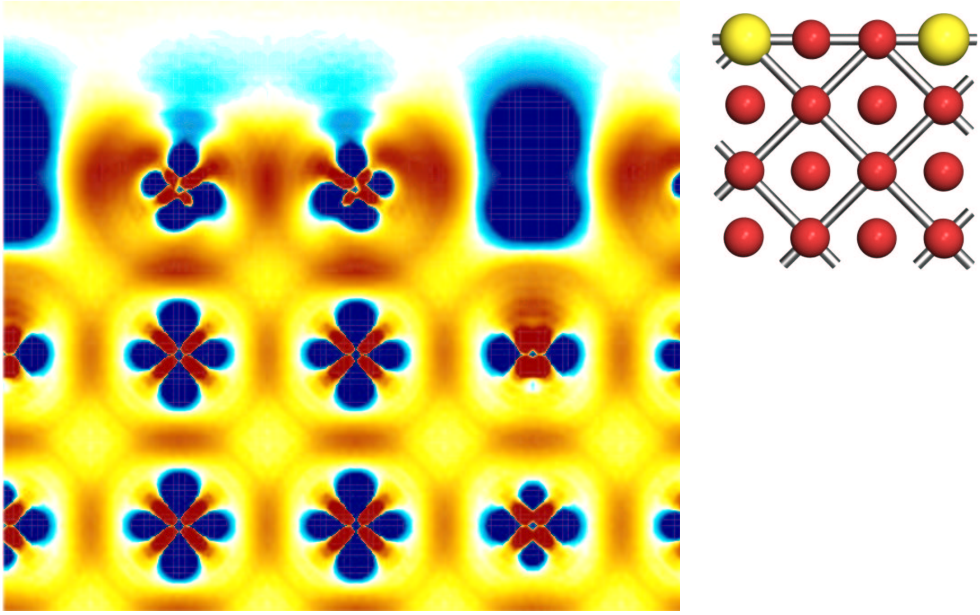

Figure 9.17: Charge density difference plot for a few Al atoms within the (110) surface of a pure Ni crystal. The right side shows the surface and the atoms contained in the plot plane. The larger yellow balls correspond to Al atoms, the smaller red ones to Ni atoms.

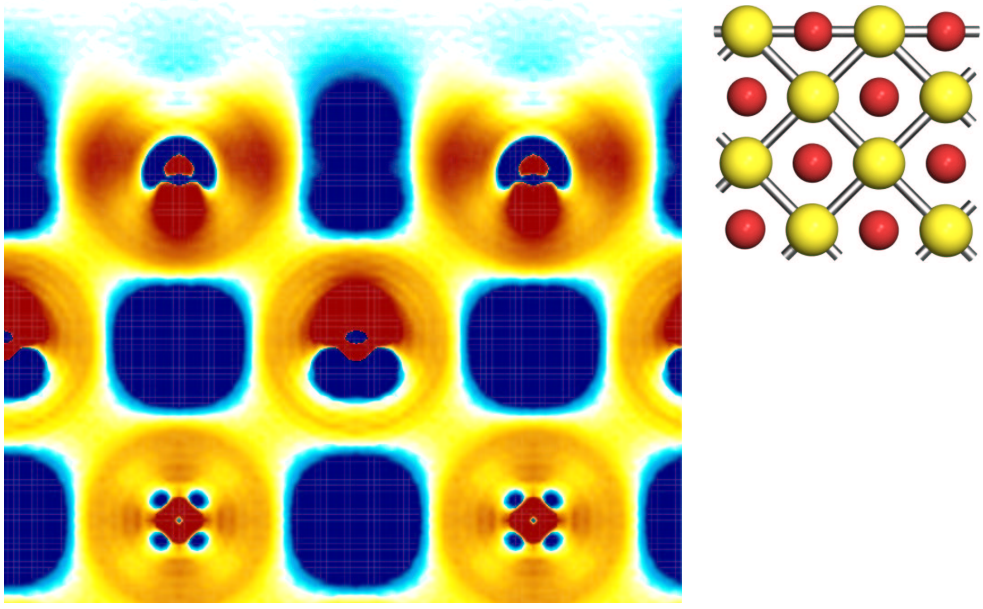

Figure 9.18: Charge density difference plot for the (110) surface of a $L1_2$ structure.

9.4.2 The covalent bond energy at the surface

A more quantitative picture of the surface can be obtained from the covalent bond energy. The covalent bond energy, $E^{cov}_{i\alpha\, j\beta}$, see appendix C, is calculated as an energy-offset-corrected band energy, projected on localized atomic-like orbitals to allow a local interpretation and thus to be able to see surface modifications. We used atomic-like s, p and d functions that were optimized for Al and Ni, respectively, in order to reproduce the $L1_2$ bulk band structure [123,124]. As the band structure at the surface changes, these localized functions are not the optimum localized functions to reproduce the surface band structure. However, in order to keep the matrix elements between different localized functions comparable for the bulk and the surface, we kept the bulk optimized functions also for the surface.

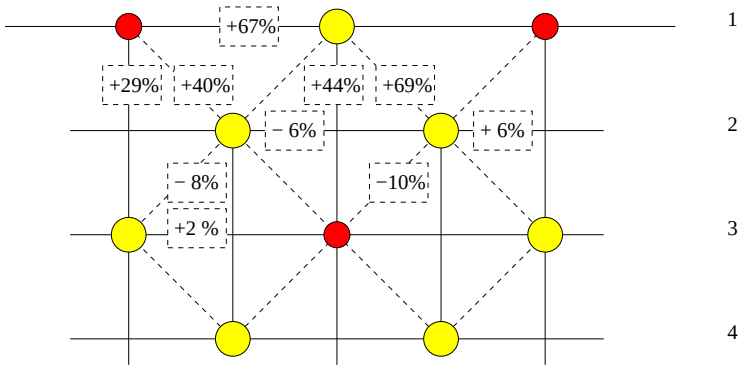

Figure 9.19: Modifications of the total covalent bond energy $\sum_{\alpha\beta} E^{cov}_{i\alpha\, j\beta}$ between atoms on nearest-neighbor ij sites in an $L1_2$-ordered surface relative to their bulk values. The smaller red circles denote Ni atoms, the larger yellow circles Al atoms. The atoms of layers two and four are located half of a lattice constant above the atoms of layer one and three.

Fig. 9.19 summarizes the modifications of the total covalent bond energy at the surface. Obviously, the electronic structure at the surface undergoes strong changes.

In a tight-binding picture the covalent bond energy can in principle be related to many-body potentials via the bond-order potentials, see appendix C and chapter 4. The many-body potentials then are related to cluster expansion coefficients as described in chapter 5. In order to be able to describe the band structure efficiently with only few localized atomic-like functions, these functions were chosen to be non-orthogonal. It turns out that the practical concept of bond-order potentials established so far is based on orthogonal basis functions, and that the task to establish a direct and quantitative link between surface modifications of the covalent bond energy and surface modifications of the cluster expansion coefficients is, if possible at all, well beyond the task of this thesis.

Chapter 10

Finite temperature considerations for the surface

From the previous chapter we learned that Al spontaneously segregates into the surface until a concentration of 50% is reached. At a concentration of 50% Al in the surface we expect the Al and Ni atoms in the first surface layer to form -Ni-Al-Ni-Al- chains along the nearest-neighbor bonds in the surface. From a delicate competition between the energy of a $L1_2$-ordered and a $D0_{22}$-ordered surface we concluded that the actual surface order depends sensitively on the bulk concentration.

In order to compare our results with the experimental findings described in Sec. 2.3.2, we need to understand the behavior of the surface at finite temperatures. We start with some model calculations where we simplified the interactions in order to guarantee that the energies of the $L1_2$-ordered and the $D0_{22}$-ordered surface monolayer are degenerate. For these model interactions we calculate the surface phase diagram for a $L1_2$-ordered surface competing with the disordered A1 surface phase. The detailed competition between $L1_2$-ordered and $D0_{22}$-ordered surface is then approached in the limit of vanishing Al bulk concentration using the $2d$ Ising model. Given the uncertainties of the ab-initio calculations, these considerations will enable us to sketch a surface phase diagram. The surface induced order in the surface found in the model calculations is stabilized with the modifications of the surface expansion coefficients found in Sec. 9.3 due to,

- the surface field (the surface point-cluster) that drives the segregation of Al and thereby changes the surface composition and surface phase [125],

- the increased nearest-neighbor pair expansion coefficient in the surface (together with frustration effects of the fcc bulk-lattice that are not present in the surface [126,127]).

Finally CVM calculations for the disordered surface show that the segregation of Al is, as we expected from the surface energetics, indeed limited to the first surface layer also at finite temperatures.

10.1 Model calculations 1: nearest-neighbor interactions

To describe and understand the finite temperature behavior of the surface we start with model calculations.

- The bulk material is modeled with nearest-neighbor interactions only, $J_{1_2} = 1$.
- Only the point and the nearest-neighbor pair-clusters are used to model the surface. The modifications of the interactions are shown in Fig. 9.16.

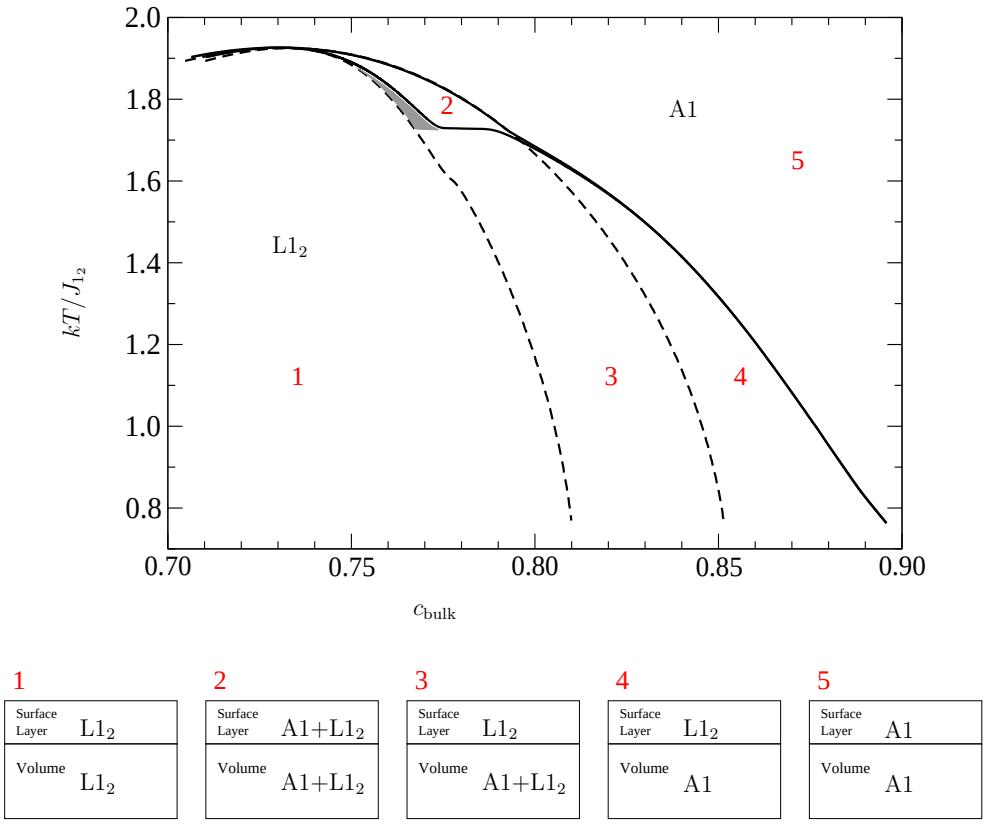

Figure 10.1: Surface phase diagram with surface modified interactions. The straight lines show the surface transition, dashed lines the bulk transitions. The five phases that exist in the shown region are sketched below the graph. The shaded area between phase one and two is due to the finite number of layers used in the calculation and vanishes for a semi-infinite system. In appendix F we explain in detail how the diagram was derived. We show the part of the phase diagram that we could calculate directly with 128 bit numbers in Tetrahedron approximation (see appendix D).

In Fig. 10.1 we show how the phase diagram is modified due to the surface modified interactions. The transition between the ordered $L1_2$ and the disordered phase remains a first order phase transition. However, the ordered phase completely disorders in the bulk and only the surface layer remains ordered at the transition temperature. Fig. 10.2 shows a snapshot of how the order vanishes from the bulk to the surface. The first order transition is located in the surface layer, only the surface concentration changes when we go from the ordered to the disordered phase, the bulk concentration stays the same (The bulk concentration stays the same only for a semi-infinite system, in the model calculations with 101 layers the bulk concentration stays only nearly the same). Thus in the phase diagram of Fig. 10.1 the bulk concentrations for the transition $L1_2 \leftrightarrow L1_2$+ A1 and $L1_2$+ A1 $\leftrightarrow$ A1 are identical, although we are dealing with a first order transition.

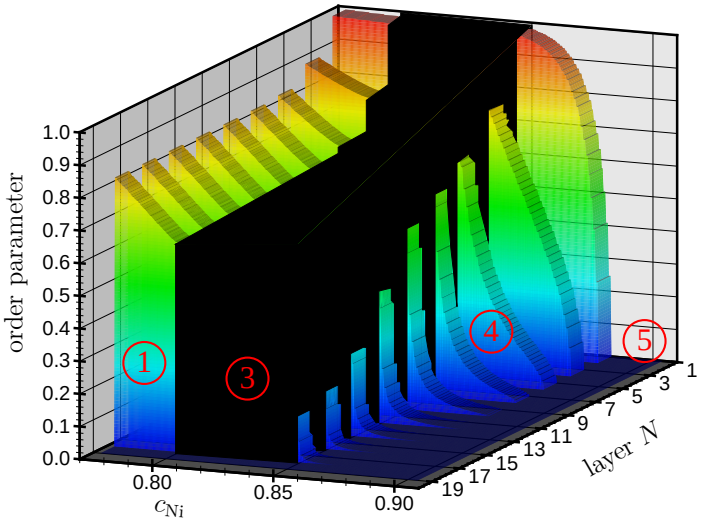

Figure 10.2: Order parameter of the ordered phase for different bulk concentrations calculated at $kT = J_{1_2}$. Also depicted are the phases according to Fig. 10.1. In the region between $c_{\mathrm{Ni}} \approx 0.80 - 0.85$ the Tetrahedron approximation predicts a $L1_2$-A1 two phase region in the bulk (phase 3) where the order parameter is not directly accessible with CVM calculations. The order parameter is calculated as $(c_1^{(l)} - c_2^{(l)})/(c_1^{(l)} + c_2^{(l)})$ from the two sublattice concentrations $c_1^{(l)}, c_2^{(l)}$ of the $L1_2$-ordered (110) surface for each layer l.

Fig. 10.3 shows the surface modified phase diagram calculated with different approximations for the entropy. The transition temperature depends sensitively on the approximation used for the calculation of the entropy. However, all approximations for the entropy display the same general features, namely, an ordered surface layer up to a concentration of $c_{\mathrm{Ni}} = 1$.

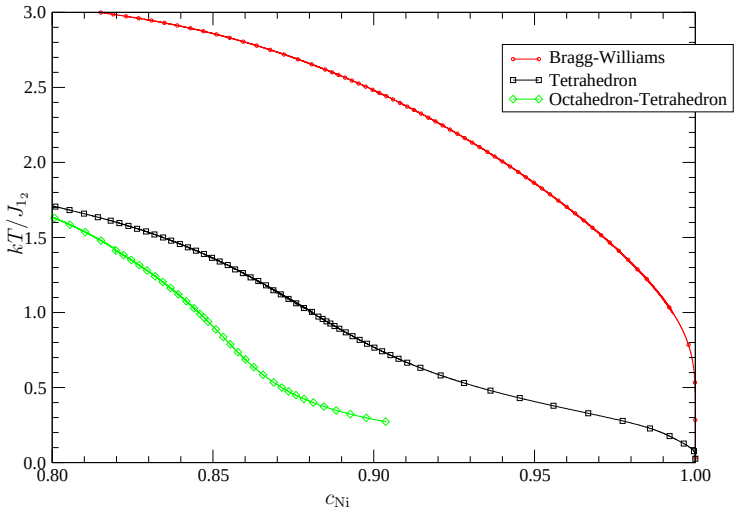

Figure 10.3: Phase diagram calculated with surface modified interactions for different approximations of the entropy (see appendix D) for a 101 layer slab. Shown is the phase separation line between phase four and five from Fig. 10.1. Above a concentration of $c_{\mathrm{Ni}} \approx 0.9$ the differences between the grand potentials Eq. (8.42) for the surface ordered and the disordered phase in Octahedron-Tetrahedron approximation were so small in comparison to the total grand potential of the 101 layer system that we could not calculate the phase diagram anymore (See appendix D for the CVM approximations). Note that for all entropy approximations the step width for not loosing the ordered phase was 500 times denser than the points that are shown. See text for possible problems of a mean-field modeling of this surface.

The (110) surface of an fcc crystal, as shown in Fig. 2.11 and Fig. 9.10, consists of chains of atoms linked by nearest-neighbor bonds. The distance between two of these chains is equivalent to the second-nearest-neighbor bond length in a fcc crystal. In the above calculations only nearest-neighbor interactions were used, there is no direct interaction between the chains. Thus from this point of view, we deal with isolated $1d$ Ising chains in the surface. Imagine a system with a finite number of layers but an infinite surface area at a concentration that allows a surface with perfectly ordered $1d$ Ising chains without Al atoms dissolved in the bulk. In complete analogy to the $1d$ Ising model, any finite temperature will destroy the long-range surface order as, *e.g.*, an Al atom will diffuse into a subsurface layer. Fig. 10.4 illustrates the elemental excitations that destroy the long-range order in the surface.

Thus, the long-range ordered surface found in the above calculations must be stabilized by Al atoms in subsurface layers. In order that the subsurface layers can indeed stabilize the long-range ordered surface, at least the correlations in the subsurface layers must have the periodicity of the ordered surface in thermal average, and not the periodicity of the disordered surface in thermal average. The $\mathrm{L1_2}$ order therefore must decay gradually in the bulk, as can be seen in Fig. 10.2. The order-disorder transition temperature therefore

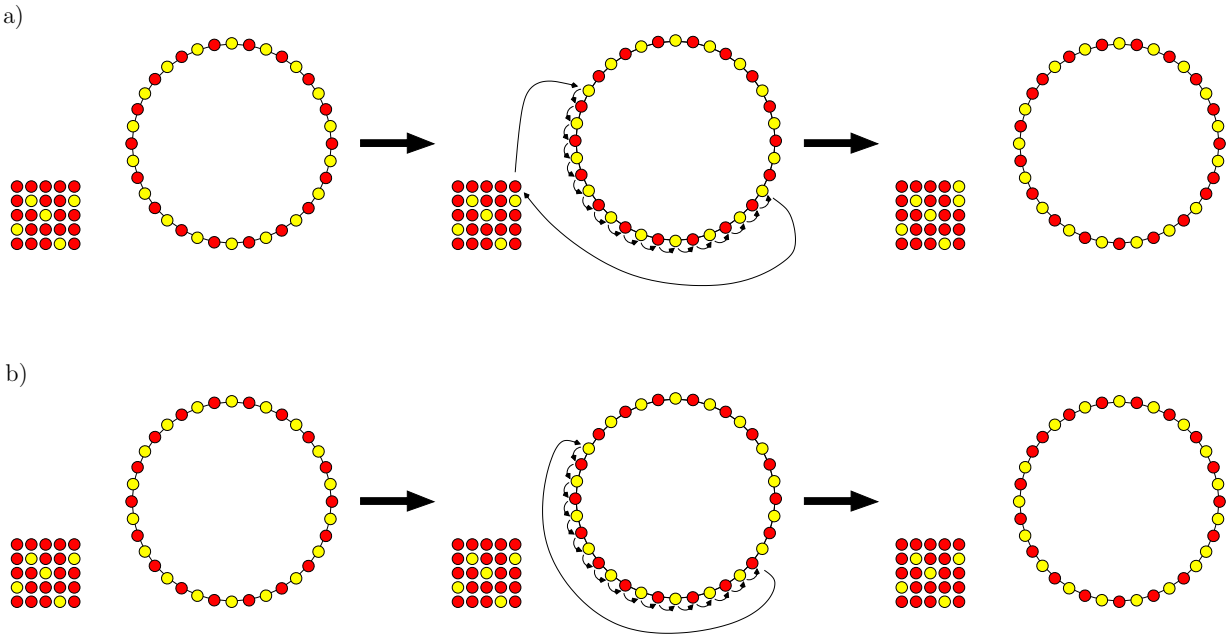

Figure 10.4: Illustration of elemental excitations that destroy the long-range order in the $1d$ surface chains. Shown are $1d$ surface chains with periodic boundary conditions that are coupled to a bulk reservoir, a) shows how one atom from the bulk reservoir that is brought in the chain destroys the long-range order of the chain, b) shows a canonical excitation in the chain that also destroys the long-range order. If we think of the red atoms as spin up, the yellow atoms as spin down and the bulk reservoir coupled with an external field (chemical potential or magnetic field) to the $1d$ surface chains the complete analogy of the $1d$ surface chains and the $1d$ Ising model becomes clear.

depends on the details of the subsurface correlations and how they are described in the different CVM approximations. This explains the differences for the transition temperatures found for the various CVM approximations in Fig. 10.3. Also, as we will see in the next section, the Bragg-Williams approximation is not adequate for the description of the $1d$ Ising chain and thus for the description of the surface phase diagram of NiAl that we are interested in.

10.2 Model calculations 2: the $2d$ Ising model

In the previous section CVM calculations for the fcc (110) surface with nearest-neighbor interactions showed that an ordered surface phase can be stabilized on a disordered volume material in a nearest-neighbor description. However, we also found that the order parameter of the surface ordered phase must not only be different from zero in the very first surface layer, the order must be extended into the bulk material. In this section we show how an ordered surface state can exist solely in the very first layer: The surface ordered

state in the very first layer is stabilized if we take into account the weak coupling between the $1d$ Ising chains in the surface. With the help of the $2d$ plane square Ising model we will derive an upper limit for the order-disorder surface transition temperature in the region of $c_{\mathrm{Ni}} \approx 0.9 - 1.0$ for the ordered surface monolayer phase. An ordered surface state that extends only over the very first surface layer is of interest as the experiment at Ni90%-Al, Sec. 2.3.2, claims to have found an ordered monolayer only and not an order parameter that continously decays into the bulk material.

In the case of a vanishing Al bulk concentration, the ab-initio calculations predict an ordered $\mathrm{D0}_{22}$ monolayer with 50% Al as surface ground state. Let us assume that we look at such a situation, a semi-infinite system with an ordered $\mathrm{D0}_{22}$ monolayer on top and pure Ni in all other layers. If temperature is increased, some of the Al atoms within the surface either exchange sites with Ni atoms within the surface or occupy sites in the underlying bulk material. To simplify the problem, it is assumed that the Al atoms dissolved in the bulk material occupy each site of the semi-infinite bulk lattice with the same probability. The bulk thus just behaves like a particle reservoir for the surface monolayer. Furthermore, according to the ab-initio calculations, the dominating interaction in the surface is the nearest-neighbor pair expansion coefficient. The second-nearest-neighbor pair expansion coefficient is already relatively weak. Its magnitude determines the energy difference between $\mathrm{L1}_2$ and $\mathrm{D0}_{22}$ surface ordering, see Fig. 9.9. For the following model calculation all other expansion coefficients in the surface plane are neglected. Coefficients of cluster figures that reach from the surface layer into layers beneath the surface need not to be taken into account for this consideration, as we assume a bulk concentration of $c_{\mathrm{Al}} \to 0$ and the situation formally corresponds to an alloy monolayer on top of a substrate, Sec. 6.2. Thus in order to model the phase transition in the ordered surface monolayer two expansion coefficients, J_{1_2} and J_{2_2}, are used. This corresponds to the $2d$ Ising model on a square lattice, see Fig. 10.5.

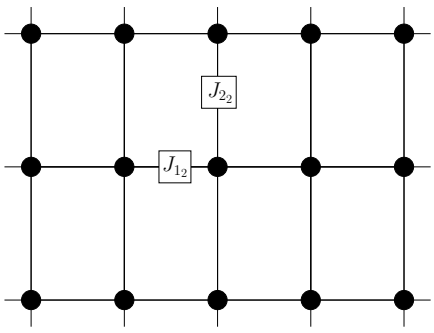

Figure 10.5: The surface plane is approximated as $2d$ Ising model.

A Bragg-Williams treatment of the $2d$ Ising model with external field $H = 0$ yields a transition temperature of,

$$\frac{2J_{1_2}}{kT_c} + \frac{2J_{2_2}}{kT_c} = 1\,. \tag{10.1}$$

For the limit $J_{2_2} \to 0$, the Bragg-Williams approximation predicts a finite transition temperature of $kT_c = 2J_{1_2}$ and thus fails to describe the vanishing transition temperature of the $1d$ Ising model.

Onsager's solution for the $2d$ Ising model [128],

$$\sinh\left(\frac{2J_{1_2}}{kT_c}\right)\sinh\left(\frac{2J_{2_2}}{kT_c}\right) = 1\,, \tag{10.2}$$

remains correct in the limit $J_{2_2} \to 0$, see Fig. 10.6.

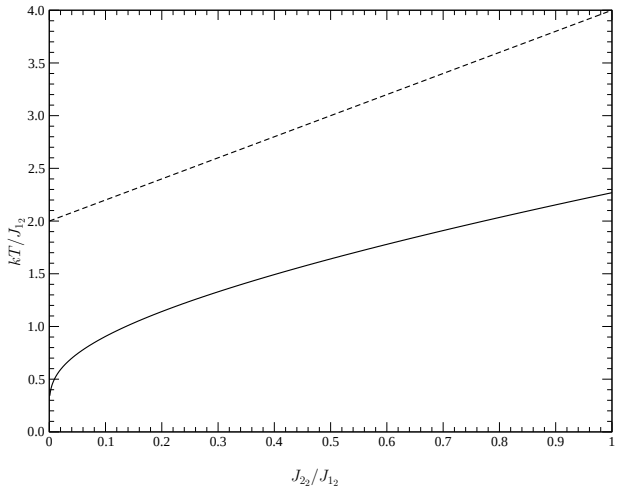

Figure 10.6: Phase transition temperature for the $2d$ Ising model in zero field. The dashed line corresponds to the solution obtained in Bragg-Williams approximation.

In finite field H the energy of the Ising model becomes,

$$U = \sum_{<ij>} J_{1_2}\sigma_i\sigma_j + \sum_{<ij>} J_{2_2}\sigma_i\sigma_j + \sum_i H\sigma_i\,, \tag{10.3}$$

where the sum $< ij >$ runs over all vertical and horizontal nearest-neighbor pairs, respectively. The solution od Onsager was extended for this case [129,130],

$$\sinh\left(\frac{2J_1}{kT_c}\right)\sinh\left(\frac{2J_2}{kT_c}\right) = \cosh\left(\frac{H}{kT_c}\right)\,. \tag{10.4}$$

The required parameters H, J_{1_2} and J_{2_2} are now extracted from ab-initio calculations that were performed for configurations that had Al atoms solely in the first layer. To calculate the field H and the nearest-neighbor interaction J_{1_2} the energy of a dilute Al atom (calculated as a $Ni_{107}Al_1$ crystal) was compared with the energy of four surface structures, one was the perfectly ordered $D0_{22}$ monolayer, one the $L1_2$ monolayer, one had Al atoms on nearest-neighbor sites and one Ni atoms on nearest-neighbor sites, see appendix E. The second-nearest-neighbor interaction corresponding to J_{2_2} was calculated

from the energy difference of the $L1_2$ and the $D0_{22}$ structure. Depending on the detailed structures chosen to extract H and J_{1_2}, H and J_{1_2} were found to take values,

$$J_{1_2} = 100 \ldots 125\text{meV} \;, \quad H = -100 \ldots -155\text{meV} \,, \tag{10.5}$$

whereas the value of $J_{2_2} = 13/2\text{meV}$ was fixed from the energy difference of the $L1_2$ and the $D0_{22}$ surface monolayer. Although the values for J_{1_2} and H depend on the details of the structures chosen for the fit, see Fig. 10.7, the transition temperature was found to be stable,

$$T_c = (60 \pm 10)\text{meV} = (700 \pm 120)\text{K} \,. \tag{10.6}$$

Obviously the energy difference between the $L1_2$-ordered and the $D0_{22}$-ordered surface is

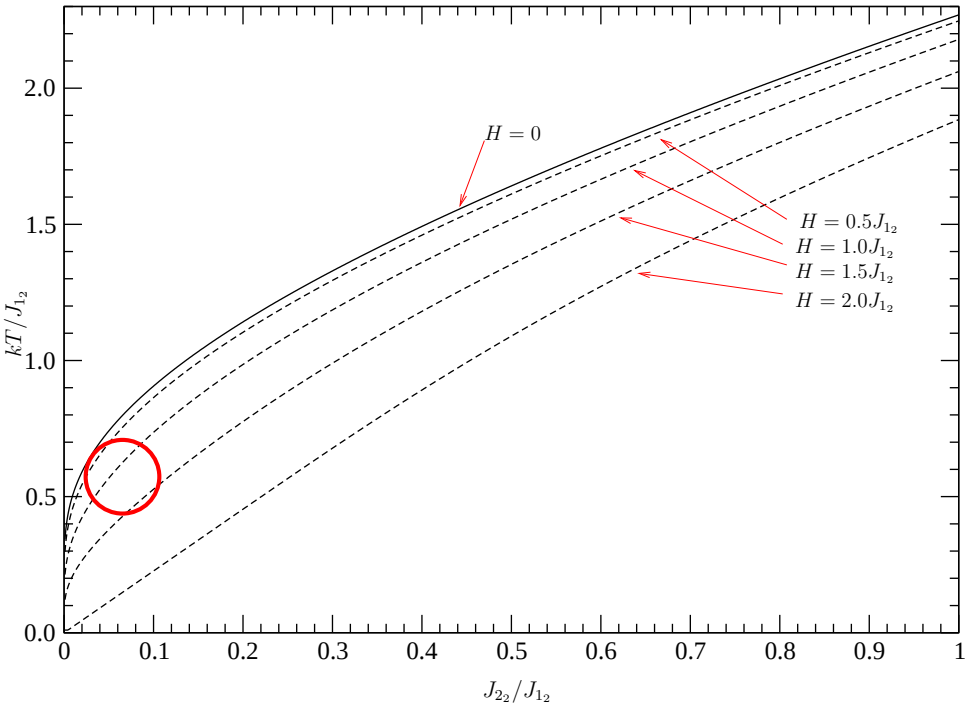

Figure 10.7: Phase transition temperature for the $2d$ Ising model in non-zero field H. The red circle aproximates the region of parameters allowed by the non-spin-polarized ab-initio calculations for slabs with 9 layers.

crucial as this energy difference determines the weak coupling J_{2_2} and thus has a strong influence on the transition temperature. Therefore the energy difference between the $L1_2$-ordered and the $D0_{22}$-ordered surface from calculations with thicker (19 layer) slabs was considered, see Fig. 9.9,

$$J_{2_2} = 23/2\text{meV, 19 layer calculation} \quad \Rightarrow \; T_c = (78 \pm 10)\text{meV} \approx (900 \pm 120)\text{K} \,. \tag{10.7}$$

In the $2d$ Ising model, the calculated phase transition temperature represents an upper limit for the phase transition temperature of the surface: If the concentration of Al in

the disordered A1 phase is increased compared to the assumed concentration $c_{\mathrm{Al}} \to 0$, according to the ab-initio calculations the energy difference between the $L1_2$-ordered and the $D0_{22}$-ordered surface is lowered, see Fig. 9.11. This effectively lowers J_{2_2} and this lowers the critical temperature T_c of the ordered surface phase.

Also the stability of the result that the $L1_2$-ordered surface is higher in energy than the $D0_{22}$-ordered surface,

$$E_{sf}\,(\mathrm{L1_2}) - E_{sf}\,(\mathrm{D0_{22}}) < 0\,, \tag{10.8}$$

has been extensively tested, the calculated energy difference is so small that Eq. (10.8) might be due to the local density approximation or other approximations made in the implementation of the pseudopotential code, such as, for example, the frozen core approximation or approximations made during the calculations (number of plane waves used, k-point sampling,...).

However, even if Eq. (10.8) does not hold, the LDA results should enable us to estimate the energy difference to be smaller than,

$$|E_{sf}\,(\mathrm{L1_2}) - E_{sf}\,(\mathrm{D0_{22}})\,| \lessapprox 40 \text{ meV}\,. \tag{10.9}$$

Furthermore, even if the energy of the $L1_2$-ordered surface should be lower than the energy of the $D0_{22}$-ordered surface, all considerations for $c_{\mathrm{Al}} \to 0$ in the $2d$ Ising model from above remain valid as only the absolute value $|J_{2_2}|$ enters Eq. (10.4).

To summarize, the transition temperature depends sensitively on J_{2_2} and therefore on the energy difference between $L1_2$-ordered and $D0_{22}$-ordered surface, which cannot be calculated better than few 10 meV. Therefore it does not make sense to calculate a detailed phase diagram from the ab-initio data. However, a look at the extreme case $J_{2_2} = 0$, namely the $1d$ Ising model, shows that although there exists no long-range order at finite temperature, this does not mean that the correlations, *e.g.*, the short-range order, along the $1d$ Ising chain also vanishes [131]. We look at the correlations within the surface in the next section.

10.3 The NiAl surface at finite temperature

10.3.1 What could we learn?

We summarize what we know about the surface phase diagram from the ab-initio calculations, the cluster expansion and the CVM model calculations so far.

- On the left hand side of the two-phase region the bulk system is ordered in $L1_2$ structure. Ab-initio calculations showed that for the ground state $T = 0$ K this is also the case for the surface, Sec. 9.2.1.

- For a semi-infinite system the ab-initio calculations predict a $D0_{22}$-ordered surface ground state for a Ni bulk concentration of $c_{\mathrm{Ni}} = 1$, Sec. 9.2.1. The experiment for the Ni90%-Al surface found an ordered $L1_2$ surface structure.

- According to the ab-initio calculations, upon decreasing the Ni bulk concentration, a $L1_2$-ordered surface ground state becomes more stable than the $D0_{22}$-ordered surface ground state, Sec. 9.2.1.

- According to the ab-initio calculations, at an Al bulk concentration of around 10% to 15% the energies of the $L1_2$-ordered and the $D0_{22}$-ordered surface are the same.

- The transition from $L1_2$- to $D0_{22}$-ordered surface ground state might take place in the region of the homogeneously disordered bulk phase or in the two-phase region where the layer dependent order parameter is not accessible by CVM calculations.

- From the strong nearest-neighbor interaction in the surface together with the point interaction that drives the segregation of Al into the surface, we expect that in the surface nearest-neighbor chains that are occupied with Ni and Al on nearest-neighbor sites are formed. For a Ni bulk concentration $c_{\mathrm{Ni}} = 1$ this corresponds to a $1d$ Ising antiferromagnet, Sec. 9.3.

- Since the energy difference for a surface ordered in $L1_2$ or $D0_{22}$ structure is small, the $1d$ nearest-neighbor chains can be only weakly coupled to each other, Sec. 9.2.1. The NiAl surface in the A1 bulk phase diagram region can be thought of as $1d$ Ising antiferromagnetic chains (strong nearest-neighbor interaction in the surface) which are weakly coupled to each other (weak second-nearest-neighbor interaction) to form a $2d$ surface that is linked to a $3d$ bulk reservoir, Sec. 10.2.

- The weak coupling between the $1d$ Ising chains in the surface allows an ordered monolayer on top of the surface, Sec. 10.2. If one neglects the weak coupling between the $1d$ Ising antiferromagnetic chains, the order parameter has to decay continously into the bulk material in order that an ordered surface phase can be formed, Sec. 10.1. The experiment for the Ni90%-Al surface claims to have found an ordered monolayer only.

- The energy difference between the $D0_{22}$-ordered and the $L1_2$-ordered surface is crucial for the transition temperature of the ordered surface monolayer. The ab-initio calculations allow the calculation of this energy difference not as accurate as required.

Therefore we expect a very detailed dependence of the surface long-range parameters and thus on the surface phase diagram on the strength of the coupling between the $1d$ Ising chains. At the same time we cannot expect from the ab-initio calculations to provide the coupling between the $1d$ Ising chains better than $\approx$ 10 meV. However, the short-range order along the $1d$ Ising chains is basically determined from the strong nearest-neighbor interaction between atoms on nearest-neighbor sites in the surface. Detailed changes of the second-nearest-neighbor interaction (the coupling between the $1d$ Ising chains) do not play an important role for the surface short-range order. In the following we thus focus on the short-range order and segregation at the surface.

We also tried hard to calculate a phase diagram from the ab-initio data. However, as the energy differences between the $L1_2$-ordered and the $D0_{22}$-ordered surfaces are small, the calculation of the boundary between ordered and disordered surface requires a very well converged cluster expansion and a large basic cluster in the CVM calculations to properly take into account the frustration of the fcc lattice as well as the unfrustrated surface. On the one hand, the complicated details of the surface modifications together with large basic clusters induce many local minima in the free energy functional, on the other hand the many degrees of freedom induced by the large clusters require the inversion of large matrices in the Newton-Raphson scheme which means an exponentially strong increase in CPU time with cluster size and a loss of accuracy during the iterations of the Newton-Raphson scheme. Knowing that the required accuracy for the determination of the coupling between the $1d$ Ising chains is beyond the capabilites of the local density approximation, the calculated phase diagram would be a mere model phase diagram, and we eventually decided not to proceed with the calculation of the surface phase diagram.

10.3.2 Correlations and segregation at the disordered surface

Fig. 10.8 shows the temperature and concentration dependent surface concentration and nearest-neighbor probability for the first five layers from the surface. The calculations were carried out in Double-Tetrahedron-Octahedron approximation of the CVM equations, the energetics was modeled according to Sec. 9.3 (Pairs larger than the Double-Tetrahedron or the Octahedron were taken into account in Bragg Williams approximation, Sec. 8.2.4). None of the layers was allowed to display long-range order even at low temperatures by prescribing that the Ni concentration in each layer $c_{\mathrm{Ni}}^{(l)}$ is the same for all sublattices in this layer. In this way it is pointed to the common features of a surface that might have a $L1_2$-ordered or a $D0_{22}$-ordered ground state.

It is obvious that the surface layer displays a behavior completely different from the remaining layers: The Al concentration is considerably higher than in the other layers even at high temperatures. Also the pair-correlation function is much higher in the surface. As expected from the ab-initio calculations the strong nearest-neighbor interactions between the first and the second layer and the high Al concentration in the first layer lead to a low Al concentration in the second layer. Even for relatively moderate and low temperatures, the layers from the third layer on behave already like bulk material. At low temperatures the surface concentration approaches $c_{\mathrm{Al}} = 1/2$ in the first layer. However, one must be careful with the segregation behavior at low temperatures as the first layer was not allowed to display order in Fig. 10.8.

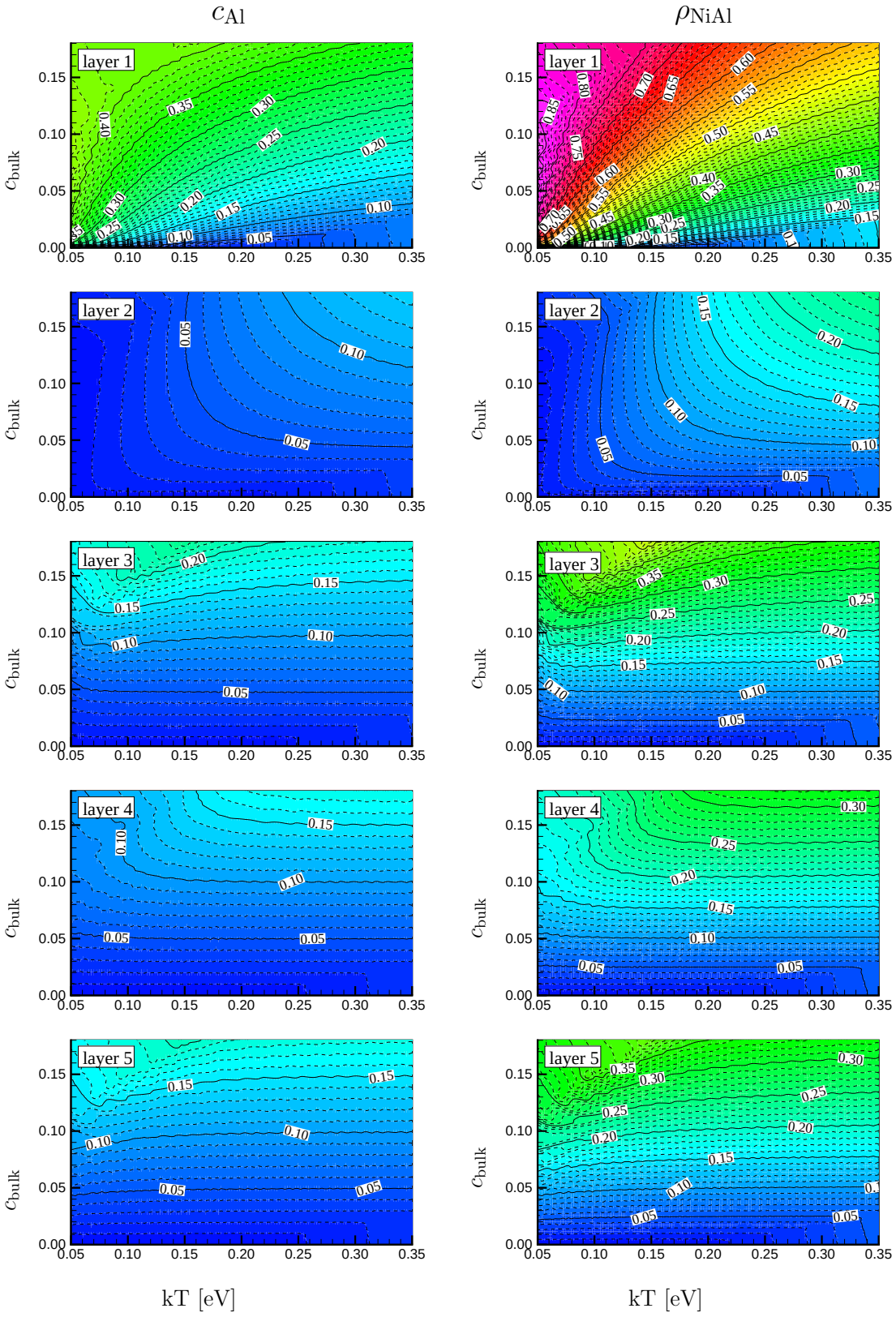

Figure 10.8: Concentration c_{Al} and the probability to find a pair of Ni-Al atoms on nearest-neighbor sites calculated in Double-Tetrahedron-Octahedron approximation.

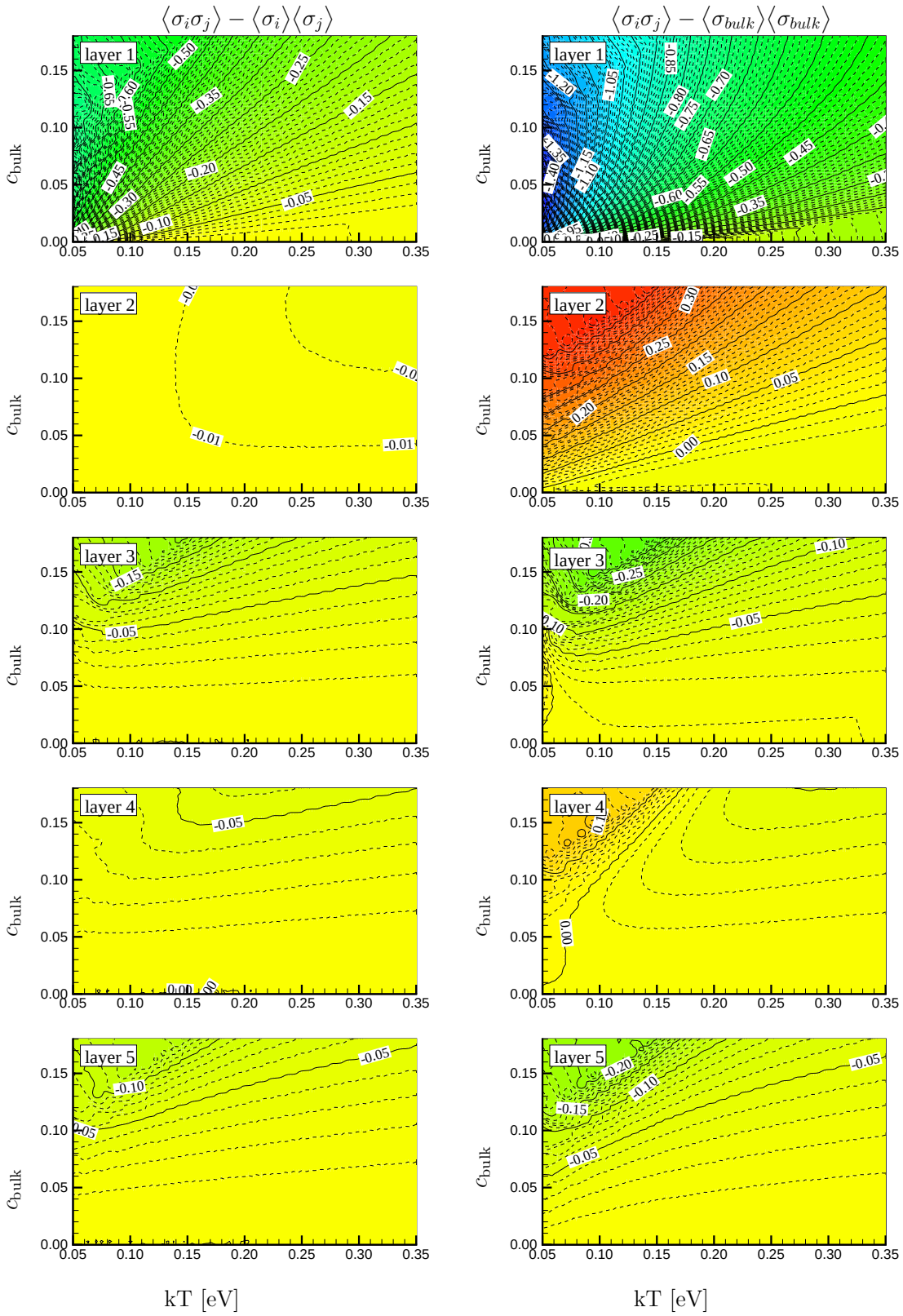

Figure 10.9: Pair correlation function $\langle\sigma_i\sigma_j\rangle - \langle\sigma_i\rangle\langle\sigma_j\rangle$ and comparison to the bulk concentration, $\langle\sigma_i\sigma_j\rangle - \langle\sigma_{bulk}\rangle\langle\sigma_{bulk}\rangle$ for nearest-neighbor pairs in the first five layers of the (110) surface. One sees that from the third layer the left and the right column look very similar, which means that they show bulk behavior. The CVM calculations were carried out in Double-Tetrahedron-Octahedron approximation.

Chapter 11

Summary and conclusions

Ab-initio statistical mechanics for surfaces

In chapters 3 to 8 the concepts of ab-initio statistical mechanics were presented and developed. A hierarchy of approximations and assumptions was introduced in order to deal with the complex behavior found at all levels of the description of a many-body system:

- The complex quantum mechanical many-particle equation was mapped on a system of one-particle equations in density functional theory. For the calculations local density approximation was employed for the one-particle equations since the exact exchange-correlation functional is unknown.
- By taking into account only alloy configurations in mechanical equilibrium, the phase space of the surface was drastically reduced, the surface was looked at as a lattice gas. Excitations such as phonons and excitations of the electronic structure were neglected. The energy of the surface configurations then was mapped on the cluster expansion that in principle contains contributions of infinitely many clusters but that was terminated after a finite number of clusters.
- The calculation of the entropy was simplified by introducing basic maximum clusters in the cluster variation method, in order to circumvent the problem of counting all possible configurations of the surface alloy.

All these approximations and assumptions can, at least in principle, be tested and the theory can be extended in order to include, for example, phonons, excitations of the electronic system or correlations of arbitrary length. Furthermore, although approximations were made, no free parameters were introduced, rules were established to calculate all quantities. Hence the theory is based on first-principles and exhibits ab-initio character. The hierarchy of approximations on different levels is summarized in Fig. 11.1.

Segregation and ordering at Ni90%-Al(110)

Based on ab-initio considerations and finite temperature modeling, chapters 9 and 10, it was found that Al spontaneously segregates into the surface. The segregation is driven by

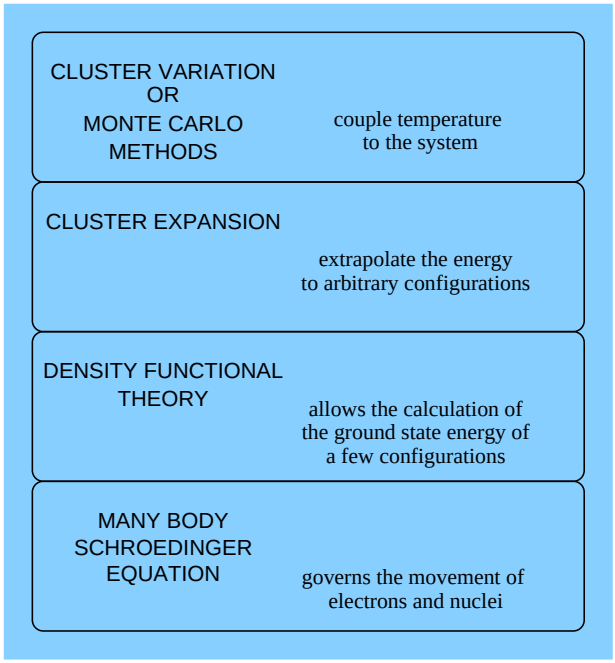

Figure 11.1: Hierarchy in the ab-initio statistical mechanics for the calculation of phase diagrams.

general modifications of the electronic structure in the surface and not by simple relaxation or size effects. The strong nearest-neighbor interaction in the surface stops Al from segregation at a concentration of 50% in the surface monolayer, and subsequently induces ordered Ni-Al-Ni-Al-Ni- chains on nearest-neighbor sites in the surface. The small energy difference that was found among various arrangements of the ordered chains led to the conclusion that in the limit of $c_{\mathrm{Ni}} \rightarrow 1$ the surface must be described as weakly coupled $1d$ antiferromagnetic chains in contact with a particle reservoir. In addition, the energy differences between various arrangements of the chains were small yet important for the order-disorder temperature in the surface so that, due to the limited accuracy of the local-density approximation, a phase diagram expected for the surface can only be sketched. Due to the strong nearest-neighbor interaction in the surface it was found that correlations exist in the disordered surface well above the approximated transition temperature. From the ab-initio calculations it was concluded that the surface modifications of the energetics decay rapidly into the bulk, which was also found for the segregation and correlations in the finite temperature considerations. It is important to point out that the segregation and ordering of Al is essentially limited to the first surface layer.

Comparison of theory and experiment

An increased surface concentration for Al was experimentally observed for various surfaces of Ni90%-Al and confirmed by calculations for the (110) surface. In this context, the

50% Al concentration found by Reichert, see Sec. 2.3.2, for the (110) surface can also be explained. In agreement with the experimental data obtained by Reichert the decrease of the Al concentration in the surface with decreasing temperature, as it was observed by Polak *et al.* [14,15], could not be reproduced.

Due to the limited accuracy of the LDA calculations it can only be speculated about the experimentally observed $L1_2$ surface order. From our calculations we are not able to decide whether the surface at the experimental conditions of 1050 K and a Ni bulk concentration of 90% is ordered in $L1_2$ structure, in $D0_{22}$ structure or whether it is disordered, see chapter 10. However, we expect that at these conditions in the surface chains occupied with Ni and Al atoms on nearest-neighbor sites are formed that lead at least to locally ordered domains.

For a better characterization of the finite temperature surface order the problem needs to be approached from two sides.

- Additional experiments at different temperatures and concentrations could supply vital information on the decay of the order parameter in the bulk material and thus decide whether the surface order is indeed restricted to the first monolayer or if the surface order is a precursor of the $L1_2$-A1 two-phase region that extends deeper and deeper into the bulk at lower and lower Ni concentrations. Further experiments could also exclude or confirm the possibility of a $D0_{22}$-ordered surface at Ni bulk concentrations close to $c_{\mathrm{Ni}} = 1$.

- Additional calculations of higher accuracy for the energy difference between the $D0_{22}$ and the $L1_2$ surface monolayer would supply crucial information in order to support the above scenarios. However, more accurate methods for systems of the size required to model a surface are well beyond reach today.

Appendix A

Ordering the summation in many-body potentials

A.1 Regrouping for different limits

Summation over different limits can be exchanged as,

$$\sum_{N=0}^{M}\sum_{K=0}^{N} A_{KN} = \sum_{K,N}^{0\leq K\leq N\leq M} A_{KN} = \sum_{N,K}^{0\leq N\leq K\leq M} A_{NK} = \sum_{N=0}^{M}\sum_{K=N}^{M} A_{NK}\,. \tag{A.1}$$

A.2 Summation over distinct sets

Consider a function f of N variables,

$$f(x_{m_1}, x_{m_2}, \ldots, x_{m_N})\,, \tag{A.2}$$

which is symmetric,

$$f(x_{m_1}, \ldots, x_{m_i}, \ldots, x_{m_j}, \ldots, x_{m_N}) = f(x_{m_1}, \ldots, x_{m_j}, \ldots, x_{m_i}, \ldots, x_{m_N})\,. \tag{A.3}$$

Summations over the indices m_i are carried out over two subsets, A and S, where $A\cap S = \emptyset$,

$$\sum_{m_1}^{A\cup S}\sum_{m_2}^{A\cup S}\cdots\sum_{m_N}^{A\cup S} f(x_{m_1}, x_{m_2}, \ldots, x_{m_N})\,. \tag{A.4}$$

The summation above can be rewritten as:

$$\begin{aligned}&\sum_{m_1}^{A\cup S}\sum_{m_2}^{A\cup S}\cdots\sum_{m_N}^{A\cup S} f(x_{m_1}, x_{m_2}, \ldots, x_{m_N})\\ &= \sum_{K=0}^{N}\binom{N}{K}\sum_{m_1,\ldots,m_{N-K}}^{A}\ \sum_{m_{N-K+1},\ldots,m_N}^{S} f(x_{m_1}, x_{m_2}, \ldots, x_{m_N})\,,\end{aligned} \tag{A.5}$$

where the sum over all m_i must be carried out for every value of K.

Proof.

For the case of two variables Eq. (A.5) can be verified easily:

$$\begin{aligned}
\sum_{m_1}^{A\cup S}\sum_{m_2}^{A\cup S} f(x_{m_1},x_{m_2}) &= \sum_{m_1}^{A}\sum_{m_2}^{A} f(x_{m_1},x_{m_2}) + \sum_{m_1}^{A}\sum_{m_2}^{S} f(x_{m_1},x_{m_2}) \\
&\quad + \sum_{m_1}^{S}\sum_{m_2}^{A} f(x_{m_1},x_{m_2}) + \sum_{m_1}^{S}\sum_{m_2}^{S} f(x_{m_1},x_{m_2}) \\
&\overset{\text{Eq. (A.3)}}{=} \sum_{m_1}^{A}\sum_{m_2}^{A} f(x_{m_1},x_{m_2}) + 2\sum_{m_1}^{A}\sum_{m_2}^{S} f(x_{m_1},x_{m_2}) + \sum_{m_1}^{S}\sum_{m_2}^{S} f(x_{m_1},x_{m_2}) \\
&= \left(\sum_{m_1}^{A}\sum_{m_2}^{A} + 2\sum_{m_1}^{A}\sum_{m_2}^{S} + \sum_{m_1}^{S}\sum_{m_2}^{S}\right) f(x_{m_1},x_{m_2}) \\
&= \sum_{K=0}^{2}\binom{2}{K} \sum_{m_1,\ldots,m_{2-K}}^{A} \sum_{m_{2-K+1},\ldots,m_2}^{S} f(x_{m_1},x_{m_2})\,. \qquad \text{(A.6)}
\end{aligned}$$

We thus assume that Eq. (A.5) holds for N variables.

For $N+1$ variables we find (the function $f(x_{m_1},x_{m_2},\ldots,x_{m_{N+1}})$ behind the summation

is not explicitly written):

$$
\begin{aligned}
&\sum_{m_1}^{A\cup S}\sum_{m_2}^{A\cup S}\cdots\sum_{m_{N+1}}^{A\cup S} \\
&\qquad = \sum_{K=0}^{N}\binom{N}{K}\sum_{m_1}^{A}\cdots\sum_{m_{N-K}}^{A}\sum_{m_{N-K+1}}^{S}\cdots\sum_{m_N}^{S}\sum_{m_{N+1}}^{A\cup S} \\
&\qquad = \sum_{K=0}^{N}\binom{N}{K}\sum_{m_1}^{A}\cdots\sum_{m_{N-K}}^{A}\sum_{m_{N-K+1}}^{S}\cdots\sum_{m_N}^{S}\sum_{m_{N+1}}^{A} \\
&\qquad + \sum_{K=0}^{N}\binom{N}{K}\sum_{m_1}^{A}\cdots\sum_{m_{N-K}}^{A}\sum_{m_{N-K+1}}^{S}\cdots\sum_{m_N}^{S}\sum_{m_{N+1}}^{S} \\
&\qquad \overset{\text{Eq. (A.3)}}{=} \sum_{K=0}^{N}\binom{N}{K}\sum_{m_1}^{A}\cdots\sum_{m_{N+1-K}}^{A}\sum_{m_{N+1-K+1}}^{S}\cdots\sum_{m_{N+1}}^{S} \\
&\qquad + \sum_{K=0}^{N}\binom{N}{K}\sum_{m_1}^{A}\cdots\sum_{m_{N-K}}^{A}\sum_{m_{N-K+1}}^{S}\cdots\sum_{m_{N+1}}^{S} \\
&\qquad = \binom{(N+1)-1}{0}\sum_{m_1}^{A}\cdots\sum_{m_{N+1}}^{A} \\
&\qquad + \binom{(N+1)-1}{(N+1)-1}\sum_{m_1}^{S}\cdots\sum_{m_{N+1}}^{S} \\
&\qquad + \sum_{K=1}^{(N+1)-1}\left(\binom{(N+1)-1}{K}+\binom{(N+1)-1}{K-1}\right)\sum_{m_1}^{A}\cdots\sum_{m_{(N+1)-K}}^{A}\sum_{m_{(N+1)-K+1}}^{S}\cdots\sum_{m_{(N+1)}}^{S}.
\end{aligned}
\tag{A.7}
$$

We note that,

$$\binom{(N+1)-1}{0} = \binom{N+1}{0} = 1\,, \tag{A.8}$$

$$\binom{(N+1)-1}{(N+1)-1} = \binom{N+1}{N+1} = 1\,, \tag{A.9}$$

$$\binom{(N+1)-1}{K} + \binom{(N+1)-1}{K-1} = \binom{N+1}{K}\,, \tag{A.10}$$

and therefore

$$
\begin{aligned}
&\binom{(N+1)-1}{0} \sum_{m_1}^{A} \cdots \sum_{m_{N+1}}^{A} \\
&+ \binom{(N+1)-1}{(N+1)-1} \sum_{m_1}^{S} \cdots \sum_{m_{N+1}}^{S} \\
&+ \sum_{K=1}^{(N+1)-1} \left(\binom{(N+1)-1}{K} + \binom{(N+1)-1}{K-1} \right) \sum_{m_1}^{A} \cdots \sum_{m_{(N+1)-K}}^{A} \sum_{m_{(N+1)-K+1}}^{S} \cdots \sum_{m_{(N+1)}}^{S} \\
&= \sum_{K=0}^{N+1} \binom{N+1}{K} \sum_{m_1}^{A} \cdots \sum_{m_{(N+1)-K}}^{A} \sum_{m_{(N+1)-K+1}}^{S} \cdots \sum_{m_{(N+1)}}^{S} .
\end{aligned}
$$

■ (A.11)

Appendix B

Computational details

All ab-initio calculations were performed using the mixed-basis pseudopotential package by Meyer, Elsässer and Fähnle [36]. The calculations were run on all machines available, including Intel Pentium and AMD Athlon Linux PCs, Compaq Alpha Unix Workstations, IBM RS6000 AIX Workstations, and also on a Cray SV1, a NEC SX4 and a NEC SX5. The total CPU time required for all calculations presented in this work sums up to more than 2 CPU years on a Cray SV1.

In the mixed-basis representation of the one-electron valence wavefunctions a cut-off for the plane wave energy of `emax=16` Ry was used. One atomic-like localized d-function was attached to every Ni atom. These parameters were the same in all calculations. Furthermore, a simple cubic k-point mesh was chosen using the Moreno-Soler scheme [132] with `nk=12` for the reciprocal space of the simple cubic unit cell. The mesh was kept exactly the same for all calculations that had reciprocal space unit cells that could be sampled with a simple cubic `nk=12` mesh. Unit cells that, for example, had a length of five simple cubic unit cells were calculated with `nk=15`. The energy was then corrected according to the energy difference of the elements between a run with `nk=12` and `nk=15`.

The elements were represented by norm-conserving pseudopotentials with 10 valence electrons for Ni and 3 valence electrons for Al. All calculations were carried out using LDA in the parameterization of Ceperly and Alder [34].

Below some sample input files are given. With the MBPP package [36] one should be able to reproduce all numbers printed in this work.

Sample input file for bulk calculations:

```
struk75
#define VERSION1.0
#define MB_SMALL_TOL
10
  natomax=12  ntype=2  struc=Ni4Al12  source=file coord=c
  vol=1420.0
   2.0            0.0            0.0
   0.0            2.0            0.0
```

```
   0.0            0.0            1.0
  symop=gen
20
  emax=16.000  gmax=20.000  corr=ca
  nloc=1
  itype=1   l=2   fctyp=11   gamma=0.98   rcut=2.2
  ngauss=300
  atom=Ni s=lo 1000 0.02 p=nl 160 0.05 d=nl  160 0.05 znuc=28.0
  atom=Al s=lo 1000 0.02 p=nl 160 0.05 d=nl  160 0.05 znuc=13.0
30
  kpmeth=ms
  nband=53   ifmax=40    nkxyz=12 12 12  shift= 0.5 0.5 0.5
  1.0 0.0 0.0
  0.0 1.0 0.0
  0.0 0.0 1.0
40
  niter=100  scr=at  ifmet=yes intmeth=gauss width=0.1
  broy=yes   spec=ad nitdp=5  nitup=0  ekmix=60.0 alph=0.1
00
```

Input file for the generation of the Al pseudopotential (pe.dat):

```
   pe
 kerker=van
 n=Al c=ca
     0.000     0.000     0.000     0.000     0.000     0.000
    3    3
    3    0     2.000     0.000
    3    1     0.700     0.000
    3    2     0.300     0.000
   1.05000   1.20000   1.40000   0.00000   2.00000
 stop
```

Input file for the generation of the Ni pseudopotential (pe.dat):

```
   pe
 kerker=van
 n=Ni c=car
     0.000     0.000     0.000     0.000     0.000     0.000
    5    3
    3    2    8.6000    0.000
    4    0    0.6000    0.000
    4    1    0.8000    0.000
  -0.20000  -0.20000  -0.80000   0.00000  -0.520
 stop
```

The pt.dat file also required looks like the pe.dat file, just replace `pt` by `pe`, `car` by `ca` and cut the line before `stop` from pe.dat.

Appendix C

The covalent bond energy

In chapter 7 it was shown how cluster expansion coefficients are commonly obtained from ab-initio calculations: One calculates the energies of some reference structures. These energies are mapped on cluster expansion coefficients of a lattice model. The advantage of this procedure is the accuracy of the cluster expansion with respect to the reproducibility and prediction of energies of structures. The drawbacks of the method are:

1. The type and range of clusters required for the cluster expansion must be found from a trial-and-error procedure.

2. No information other than few cluster expansion coefficients from the fit is available. In this context, an approximated behavior of the cluster coefficients with type and range of the clusters would often be helpful.

3. The expansion coefficients of clusters of the same system (the same atoms) cannot be related for different geometries, *e.g.*, bulk and surface cluster expansion coefficients can not be related, expansion coefficients of bcc-based NiAl cannot be related to expansion coefficients of fcc-based Ni_3Al.

Fig. C.1 shows a second path that can be used for the determination of the cluster expansion coefficients and that can help to solve problems 1.-3. The idea behind the second path is to directly relate the electronic structure of the material to the expansion coefficients. In this approach one tries to obtain the cluster expansion coefficients from a parameterization of the electronic structure.

We sketch the steps and approximations required along the second path:

- **From density functional theory to semi-empirical tight-binding:**
  In Sec. C.1 we sketch how the bulk of the physical properties of a system can be cast in few orbitals and an effective repulsive pair-potential. To obtain accurate parameterizations one usually takes non-orthogonal functions for the parameterization of the tight-binding equations. The relative simplicity of the tight-binding equations allows a physical interpretation and understanding of the electronic structure in terms of the covalent bond energy E_{cov}.

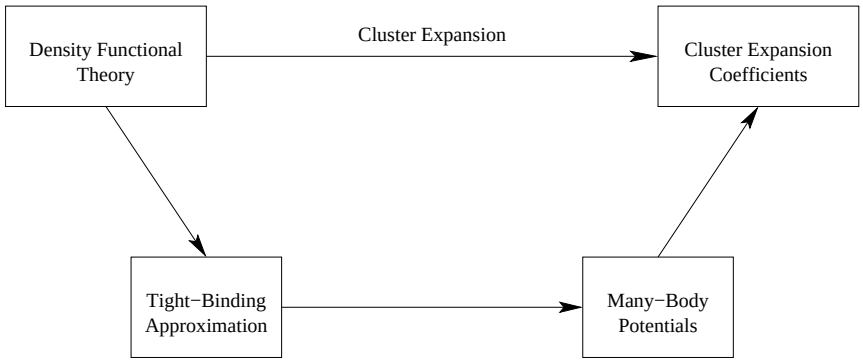

Figure C.1: Two different approaches to obtain cluster expansion coefficients from density functional theory.

- **From semi-empirical tight-binding to many-body potentials:**
  The parameterized Hamilton matrix of the tight-binding approximation can be, in principle, related to many-body potentials via bond-order potentials [133,134,135, 136,137,138,139,140]. The bond-order potentials thereby can be expanded in many-body potentials as described in chapter 4. However, up to now, only few explicit bond-order potentials for non-orthogonal parameterizations were found.

- **From many-body potentials to cluster expansion coefficients:**
  This step was described in chapters 5 and 6.

Approximations involved in the first two steps will make the cluster expansion along the second path less accurate than the traditional cluster expansion approach (and thus this approach will not replace the traditional approach), however, valuable information can be gained on problems 1.-3. and for a general physical understanding of the system.

In the following we introduce the first of the above steps, from density functional theory to semi-empirical tight-binding. The covalent bond energy is discussed as a tool for the quantitative description of the electronic structure of a system. We also address the behavior of the covalent bond energy with respect to basis transformations.

C.1 From ab-initio DFT to semi-empirical tight-binding

The total energy in density functional theory is given as a sum over the occupied one-electron eigenvalues E_ν plus a rest term $D[n]$ that accounts for double counting of the energy due to the effective potential v_{eff}, and that contains $E_H[n]$, $E_{xc}[n]$ and the coupling

to the external potential v_{ext}, see Sec. 3.3,

$$E = \underbrace{\sum_{\nu} f_\nu E_\nu}_{E_{band}} + D[n]\,, \tag{C.1}$$

where f_ν is two for every occupied band and zero otherwise when the spin degree of freedom is not explicitly taken into account.

To derive a tight-binding model from the density functional energy as systematically as possible, it is commonly assumed [141] that $D[n]$ can be approximated by an empirical, repulsive pair-potential,

$$D[n] \Rightarrow E_{rep}\,. \tag{C.2}$$

By expanding the one-electron eigenstates in localized atomic-like functions,

$$|\psi_\nu\rangle = \sum_{i\alpha} c_{i\alpha}^{(\nu)} \left|\varphi^{i\alpha}\right\rangle\,, \tag{C.3}$$

(i indexes the site of the atom that $|\varphi^{i\alpha}\rangle$ is attached to, α specifies the orbital, *e.g.*, $s, p, d, \ldots$ and m), the band energy is rewritten as,

$$E_{band} = \sum_{\nu} f_\nu E_\nu = \sum_{\nu} f_\nu \sum_{j\beta\, i\alpha} \left(c_{j\beta}^{(\nu)}\right)^* c_{i\alpha}^{(\nu)} \left\langle\varphi^{j\beta}\right| \hat{H} \left|\varphi^{i\alpha}\right\rangle\,. \tag{C.4}$$

We define the density matrix,

$$\rho_{i\alpha\, j\beta} = \sum_{\nu} f_\nu \left(c_{j\beta}^{(\nu)}\right)^* c_{i\alpha}^{(\nu)}\,, \tag{C.5}$$

and the Hamilton matrix,

$$H^{i\alpha\, j\beta} = \left\langle\varphi^{i\alpha}\right| \hat{H} \left|\varphi^{j\beta}\right\rangle\,. \tag{C.6}$$

E_{band} is partitioned in physically motivated parts,

$$E_{band} = \underbrace{\sum_{i\neq j,\alpha\,\beta} \rho_{i\alpha\, j\beta} H^{j\beta\, i\alpha}}_{E_{bond}} + \underbrace{\sum_{i\alpha} \rho_{i\alpha\, i\alpha} H^{i\alpha\, i\alpha}}_{E_{prom}} + \underbrace{\sum_{i,\alpha\neq\beta} \rho_{i\alpha\, i\beta} H^{i\beta\, i\alpha}}_{E_{crystal}}\,, \tag{C.7}$$

where the bond energy E_{bond} contains only matrix elements that correspond to bonds between different atoms. The energy of promotion E_{prom} contains only diagonal elements that measure the energy change due to a shift of the matrix elements. $E_{crystal}$ corresponds to the part of the energy induced by modifying the matrix elements on one atom by the surrounding atoms (Note that commonly one assumes that $H^{i\beta\, i\alpha} = 0$ for the free atom as one uses atomic like basis functions that are orthogonal to each other on the same atom).

Altogether, the total energy in tight-binding approximation is now given by,

$$\begin{aligned} E^{TB} &= E_{band} + E_{rep} \\ &= E_{bond} + E_{prom} + E_{crystal} + E_{rep}\,. \end{aligned} \tag{C.8}$$

C.1.1 No gauge invariance of E_{band}

We can add an arbitrary constant potential ΔV to the Hamilton Operator $\hat{H}$ without changing the physics described by $\hat{H}$. Moreover, in calculations with periodic boundary conditions there is no way to find out whether there is a constant shift ΔV added to $\hat{H}$ or not, as no recipes such as "expectation values of $\hat{H}$ have to vanish in infinite distance" can be provided. Although all observables are independent of ΔV (which means that the physics of the system does not change), the band energy changes as all eigenvalues E_ν of the system are shifted,

$$\begin{aligned} \hat{H} &\to \hat{H} + \Delta V \,, \\ E_\nu &\to E_\nu + \Delta V \,, \end{aligned} \tag{C.9}$$

and thus the band energy changes,

$$E_{band} \to E_{band} + \Delta V \left(\sum_\nu f_\nu \right) = E_{band} + \Delta V N_e \,, \tag{C.10}$$

where N_e is the number of electrons contained in the system. As the one-electron wave functions do not change when a constant potential is added, the changes of matrix elements in the localized basis are simply given as,

$$H^{i\alpha\, j\beta} \to H^{i\alpha\, j\beta} + \Delta V \left\langle \varphi^{i\alpha} | \varphi^{j\beta} \right\rangle \,. \tag{C.11}$$

In an orthogonal basis,

$$\left\langle \varphi^{i\alpha} | \varphi^{j\beta} \right\rangle = \delta_{i\alpha, j\beta} \,, \tag{C.12}$$

only the energy of promotion changes,

$$E_{prom} \to E_{prom} + \Delta V N_e \,. \tag{C.13}$$

The energy of promotion is an on-site quantity and has nothing to do with bond formation. Thus the fact that E_{prom} is not uniquely defined is not a problem when we analyze bonds and their behavior in two-center approximation.

However, in a non-orthogonal basis generally off-diagonal matrix elements also change, and E_{bond} and $E_{crystal}$ are not well defined anymore.

C.2 Algebra in a non-orthogonal basis

Following [142] we summarize how to deal with a non-orthogonal basis. Summations have to be carried out over pairwise indices.

We define the overlap matrix,

$$S^{i\alpha\, j\beta} = \left\langle \varphi^{i\alpha} | \varphi^{j\beta} \right\rangle = \left(S^{j\beta\, i\alpha} \right)^* \,. \tag{C.14}$$

For an atomic-like basis, usually the basis is chosen to be orthogonal on each atom (no sum over i here),

$$S^{i\alpha\, i\beta} = \delta^{\alpha\beta}\,. \tag{C.15}$$

We establish a dual, orthogonal basis,

$$\begin{aligned} |\varphi_{i\alpha}\rangle &= \left|\varphi^{j\beta}\right\rangle \left(S^{-1}\right)_{j\beta\, i\alpha}\,, \\ \left\langle\varphi_{i\alpha}|\varphi^{j\beta}\right\rangle &= \left(S^{-1}\right)_{i\alpha\, k\gamma} S^{k\gamma\, j\beta} = \delta^{j\beta}_{i\alpha}\,. \end{aligned} \tag{C.16}$$

When the basis fulfills,

$$\hat{\mathbf{1}} = |\varphi_{i\alpha}\rangle \left\langle\varphi^{i\alpha}\right| = \left|\varphi^{j\beta}\right\rangle \left(S^{-1}\right)_{j\beta\, i\alpha} \left\langle\varphi^{i\alpha}\right|\,, \tag{C.17}$$

it is complete and a vector $|u\rangle$ can be expanded,

$$|u\rangle = u_{i\alpha} \left|\varphi^{i\alpha}\right\rangle = u^{i\alpha} |\varphi_{i\alpha}\rangle \tag{C.18}$$

$$\Rightarrow u^{i\alpha} = S^{i\alpha\, j\beta} u_{j\beta}\,. \tag{C.19}$$

We define a scalar product between two vectors,

$$\langle v|u\rangle = \left(v_{i\alpha}\right)^* S^{i\alpha\, j\beta} u_{j\beta} = \left(v_{i\alpha}\right)^* u^{i\alpha} = \left(v^{i\alpha}\right)^* u_{i\alpha}\,. \tag{C.20}$$

The matrix elements of an operator are given by,

$$H^{i\alpha\, j\beta} = \left\langle\varphi^{i\alpha}\right| \hat{H} \left|\varphi^{j\beta}\right\rangle\,. \tag{C.21}$$

Using Eq. (C.17) we can write down a spectral representation of an operator,

$$\hat{H} = \left|\varphi^{i\alpha}\right\rangle H_{i\alpha\, j\beta} \left\langle\varphi^{j\beta}\right|\,. \tag{C.22}$$

Note that the overlap matrix $\mathbf{S}$ behaves similar to a metric $\mathbf{I}$ in non-euclidian space,

$$I^{i\alpha\, j\beta} = S^{i\alpha\, j\beta}\,, \quad I_{i\alpha\, j\beta} = \left(S^{-1}\right)_{i\alpha\, j\beta}\,, \quad I^{i\alpha}_{j\beta} = \delta^{i\alpha}_{j\beta}\,. \tag{C.23}$$

C.3 The reformulated covalent bond energy

As noted in Sec. C.1.1, the band energy is not invariant when a constant potential ΔV is added to $\hat{H}$. Thus, the values of E_{bond}, E_{prom}, $E_{crystal}$ and E_{rep} obtained for a tight-binding parameterization from density functional calculations with periodic boundary conditions can be shifted by an arbitrary constant. Hence, it is useless to compare their numerical values with other data.

We follow [143,144,124] in order to avoid the ambiguity of the conventional definitions of E_{bond}, E_{prom}, $E_{crystal}$ and E_{rep}. These authors had the following idea: If there is no way to find ΔV, let us define expressions similar to the ones commonly used in tight-binding

parameterizations but invariant under changes of ΔV. This led to the definition of the reformulated covalent bond energy,

$$E_{cov,\,i\alpha\,j\beta} = \rho_{i\alpha\,j\beta}\left[H^{i\alpha\,j\beta} - \frac{1}{2}S^{i\alpha\,j\beta}\left(H^{j\beta\,j\beta} + H^{i\alpha\,i\alpha}\right)\right], \tag{C.24}$$

which is invariant under shifts ΔV.

With the help of $E_{cov,\,i\alpha\,j\beta}$ we can again subdivide the total energy of the system into physically motivated parts,

$$\begin{aligned} E_{cohesive} &= E_{tot} - E^{freeatoms} \\ &= E_{prom} + E_{crystal} + E_{polar} + E_{cov} + \underbrace{E_{rep}}_{D[n]}. \end{aligned} \tag{C.25}$$

The energy of promotion is modified,

$$E_{prom} = \sum_{i\alpha}\left(q_{i\alpha} - q_{i\alpha}^{free\,atoms}\right)H^{i\alpha i\alpha\,(freeatoms)}, \tag{C.26}$$

with the orbital charge that is defined by,

$$q_{i\alpha} = \sum_{j\beta}\rho_{i\alpha\,j\beta}S^{j\beta i\alpha}. \tag{C.27}$$

The crystal field energy becomes,

$$E_{crystal} = \sum_{i\alpha} q_{i\alpha}\left(H^{i\alpha i\alpha} - H^{i\alpha i\alpha\,(free\,atoms)}\right). \tag{C.28}$$

Note that, although $E_{cov,\,i\alpha\,j\beta}$ and E_{prom} are now invariant under shifts ΔV, $E_{crystal}$ is still not. The total polar energy is defined as,

$$E_{polar} = \sum_{i\alpha\beta} E_{cov,\,i\alpha\,i\beta}, \tag{C.29}$$

and the total covalent bond energy is given by,

$$E_{cov} = \sum_{i\neq j,\alpha\beta} E_{cov,\,i\alpha\,j\beta}. \tag{C.30}$$

C.3.1 E_{cov} and basis transformations

In order to be able to compare the covalent bond energy calculated in different basis sets we need to find the transformation properties for E_{cov}. First we note that none of the elements $E_{cov,\,i\alpha\,j\beta}$ is an observable. Thus, if we calculate the matrix element $E_{cov,\,i\alpha\,j\beta}$ we are not able to compare it with a matrix element $E'_{cov,\,i\alpha\,j\beta}$ that was calculated, *e.g.*, in a rotated

coordinate system. Hence, the elements $E_{cov,\,i\alpha\,j\beta}$ calculated in different coordinate systems cannot be compared, but maybe the total covalent bond energy E_{cov} can be compared in different coordinate systems. Before we examine the covalent bond energy E_{cov} under basis transformations, we need to define some quantities. We assume to have two complete basis sets, $\{|\varphi^\alpha\rangle\}$ and $\{|\phi^\alpha\rangle\}$, where α now labels site and orbital,

$$\begin{aligned} |\phi^\alpha\rangle &= \hat{\mathbf{1}}\,|\phi^\alpha\rangle \\ &= \left|\varphi^\beta\right\rangle \langle\varphi_\beta|\phi^\alpha\rangle \\ &= (A^*)^\alpha{}_\beta \left|\varphi^\beta\right\rangle , \\ |\phi_\alpha\rangle = (A^*)_\alpha{}^\beta\,|\varphi_\beta\rangle \ , \quad \langle\phi^\alpha| = A^\alpha{}_\beta \left\langle\varphi^\beta\right| \ , \quad \langle\phi_\alpha| &= A_\alpha{}^\beta \langle\varphi_\beta| \ , \end{aligned} \tag{C.31}$$

with

$$A_\alpha{}^\beta = \left\langle\phi_\alpha|\varphi^\beta\right\rangle . \tag{C.32}$$

Also,

$$\delta_\alpha^\beta = \left\langle\phi_\alpha|\phi^\beta\right\rangle = A_\alpha{}^\gamma \langle\varphi_\gamma| (A^*)^\beta{}_\delta \left|\varphi^\delta\right\rangle = A_\alpha{}^\gamma \left(A^+\right)_\gamma{}^\beta , \tag{C.33}$$

which helps us to show that the trace of the Hamilton matrix is invariant under basis transformation,

$$\langle\phi_\alpha|\,\hat{H}\,|\phi^\alpha\rangle = A_\alpha{}^\gamma\,(A^*)^\alpha{}_\delta\,\langle\varphi_\gamma|\,\hat{H}\,\left|\varphi^\delta\right\rangle = \langle\varphi_\alpha|\,\hat{H}\,|\varphi^\alpha\rangle \ . \tag{C.34}$$

The expansion of the eigenfunctions is given by,

$$|\psi_\nu\rangle = c_\alpha^{(\nu)}\,|\varphi^\alpha\rangle = b_\alpha^{(\nu)}\,|\phi^\alpha\rangle \ . \tag{C.35}$$

The fact that the eigenvalues and occupation of the eigenvalues are invariant under a basis transformation means that the band energy is also invariant under a basis transformation,

$$\begin{aligned} E_{band} = \sum_\nu f_\nu E_\nu &= \sum_\nu f_\nu \sum_{\beta\alpha} \left(c_\beta^{(\nu)}\right)^* c_\alpha^{(\nu)} \left\langle\varphi^\beta\right|\,\hat{H}\,|\varphi^\alpha\rangle \\ &= \sum_\nu f_\nu \sum_{\beta\alpha} \left(b_\beta^{(\nu)}\right)^* b_\alpha^{(\nu)} \left\langle\phi^\beta\right|\,\hat{H}\,|\phi^\alpha\rangle \ . \end{aligned} \tag{C.36}$$

Now let us look at,

$$\begin{aligned} E_{cov} + E_{polar} &= \sum_{\alpha\beta} \rho_{\alpha\beta} \left[H^{\alpha\beta} - \frac{1}{2} S^{\alpha\beta} \left(H^{\beta\beta} + H^{\alpha\alpha}\right)\right] \\ &= E_{band} - \frac{1}{2} \sum_{\alpha\beta} \rho_{\alpha\beta} S^{\alpha\beta} \left(H^{\beta\beta} + H^{\alpha\alpha}\right) \ . \end{aligned} \tag{C.37}$$

The term $\frac{1}{2}\sum_{\alpha\beta}\rho_{\alpha\beta}S^{\alpha\beta}\left(H^{\beta\beta}+H^{\alpha\alpha}\right)$ does not allow proper pairwise contraction of indices, thus in general it will not be invariant under a basis transformation. This means that the covalent bond energy E_{cov} is invariant under a constant shift of the potential, which is an improvement over the band energy E_{band}. However, while E_{band} is invariant under general basis transformations, E_{cov} is not.

C.4 A new covalent bond energy

We need to define a new covalent bond energy that is invariant under constant shifts ΔV of the potential as well as under general basis transformations. We present two possible formulations.

Note that usually the orbitals used for the parameterization of the Hamilton matrix do not form a complete set. For the following we differentiate two cases:

1. The basis transformation maps the incomplete basis set with a one-to-one correspondence on another incomplete basis set that contains the same "kind" of basis functions (Usually a rotation of the coordinate system would be such a basis transformation).

2. The basis transformation maps the incomplete basis set on functions that are not fully contained in the basis set we want to compare the covalent bond energy with. Then either the two basis sets can be extended until a one-to-one correspondence according to 1. can be established. Or the covalent bond energies in the two different basis sets can be compared only approximately.

C.4.1 A modified band energy

We can simply rewrite the total band energy as

$$\begin{aligned} E_{band} &= \sum_{j\beta\, i\alpha} \rho_{i\alpha\, j\beta} \left\langle \varphi^{j\beta} \right| \hat{H} \left| \varphi^{i\alpha} \right\rangle \\ &= \sum_{j\beta\, i\alpha} \rho_{i\alpha}{}^{j\beta} \left\langle \varphi_{j\beta} \right| \hat{H} \left| \varphi^{i\alpha} \right\rangle . \end{aligned} \tag{C.38}$$

If we add a constant potential ΔV to $\hat{H}$, the band energy becomes,

$$E_{band} = \sum_{j\beta\, i\alpha} \rho_{i\alpha}{}^{j\beta} \left(\left\langle \varphi_{j\beta} \right| \hat{H} \left| \varphi^{i\alpha} \right\rangle + \Delta V \delta^{i\alpha}_{j\beta} \right) . \tag{C.39}$$

Only diagonal elements of $H_{j\beta}{}^{i\alpha}$ are modified. Thus we can define a bond energy that is invariant,

$$E_{band} = \underbrace{\sum_{i\neq j, \alpha\,\beta} \rho_{i\alpha}{}^{j\beta} H^{j\beta}{}_{i\alpha}}_{E_{bond}} + \underbrace{\sum_{i\alpha} \rho_{i\alpha}{}^{i\alpha} H^{i\alpha}{}_{i\alpha}}_{E_{prom}} + \underbrace{\sum_{i,\alpha\neq\beta} \rho_{i\alpha}{}^{i\beta} H^{i\beta}{}_{i\alpha}}_{E_{crystal}} . \tag{C.40}$$

In complete analogy to the case of an orthogonal basis, only the energy of promotion E_{prom} changes upon a shift $\hat{H} \to \hat{H} + \Delta V$.

C.4.2 A modified covalent bond energy

Using the invariant $H^{i\alpha}_{i\alpha}$ from Eq. (C.34) it is possible to define an invariant similar to the covalent bond energy. If,

$$\hat{H} \to \hat{H} + \Delta V ,$$

$H_{i\alpha}{}^{i\alpha}$ changes to,

$$H_{i\alpha}{}^{i\alpha} \rightarrow H_{i\alpha}{}^{i\alpha} + N\Delta V \,,$$

where N is the total number of orbitals in the system. If we take into account that the number N_e of electrons in the system is given by,

$$N_e = \sum_{\nu} f_\nu = \sum_{i\alpha\, j\beta} \rho_{i\alpha\, j\beta} S^{i\alpha\, j\beta} \,, \tag{C.41}$$

we can write down a modified covalent bond energy that is invariant under transformations $\hat{H} \rightarrow \hat{H} + \Delta V$ and displays proper transformation behavior under basis transformations,

$$E^{mod}_{cov,\, i\alpha\, j\beta} = \rho_{i\alpha\, j\beta} \left(H^{i\alpha\, j\beta} - \frac{1}{N} S^{i\alpha\, j\beta} H^{k\gamma}{}_{k\gamma} \right) \tag{C.42}$$

$$= \rho_{i\alpha\, j\beta} \left(H^{i\alpha\, j\beta} - \frac{1}{N} S^{i\alpha\, j\beta} H^{k\gamma\, l\delta} \left(S^{-1} \right)_{l\delta\, k\gamma} \right) \,. \tag{C.43}$$

Appendix D

CVM approximations used

In a binary system the number of states a cluster with N sites can be in, namely 2^N, is exponentially growing with N. For the case of a surface that was modeled as a slab with $\approx 50 - 100$ layers, the exponential barrier 2^N and problems when inverting the Hessian, Eq. (8.32), limited the size of feasible maximum clusters to the Double-Tetrahedron-Octahedron approximation, see Fig. (D.1). Smaller maximum clusters were also possible, and calculations were carried out with the octahedron and the tetrahedron as maximum clusters (Tetrahedron-Octahedron approximation) as well as with the tetrahedron as maximum cluster (Tetrahedron approximation) and with a single site or the point as maximum cluster (Bragg-Williams approximation). From bulk calculations [61,145,146,147,148] it is known that the Double-Tetrahedron-Octahedron and the Tetrahedron-Octahedron approximation can handle frustration effects present in the fcc-lattice and yield accurate transition temperatures, see Tab. D.1 .

The calculations were carried out with a CVM code written by Sanchez [149] that was modified to include long-ranged pair-clusters in Bragg-Williams approximation, see Sec. 8.2.4. The code was also modified for low temperature calculations as will be described in the following sections.

Approximation	$kT/12J_{1_2}$
Tetrahedron	0.83544
Double-Tetrahedron	0.84045
Octahedron-Tetrahedron	0.83394
Double-Octahedron-Tetrahedron	0.82981
High-T expansion	0.81627

Table D.1: Critical temperature for the fcc Ising ferromagnet [61].

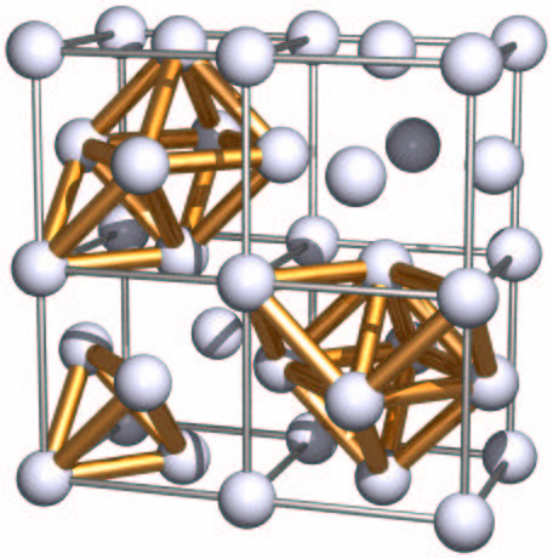

Figure D.1: Maximum clusters used in the CVM calculations were the point as largest cluster for the Bragg-Williams approximation and the tetrahedron for the Tetrahedron approximation. Two maximum clusters, the tetrahedron and the octahedron were used in the Tetrahedron-Octahedron approximation and the double-tetrahedron and the octahedron for the Double-Tetrahedron-Octahedron approximation.

D.1 Low temperature behavior

As has been noted in Sec. 8.2.5, the inversion of the Hessian for the Newton-Raphson scheme becomes a problem at low temperature kT, when the probability for a certain occupation of some cluster κ_M approaches zero,

$$\lim_{kT\to 0} \rho_{\kappa_M} = 0\,. \tag{D.1}$$

First we shown how this problem arises, then a numerical approximation in order to deal with it will be given. More elaborate solutions than the one presented here were developed by other authors [150,151,152].

D.1.1 Statement of the problem

The model for a floating point number in a computer is given as,

$$x = \pm\, a\, 10^n\,, \tag{D.2}$$

where $\pm$ is stored in one bit, a is a fractional with approximately $I = 15$ digits and the exponent n takes integer values from $-308 < n < 307$ for common 64 bit double precision numbers `real(8)`. Some computer systems also provide 128 bit quadruple precision

`real(16)` numbers where a then is a number with approximately $I = 33$ digits and the exponent n can take values from $-4932 < n < 4931$.

When two numbers are added (or subtracted),

$$z = x + y\,, \tag{D.3}$$

the result z can only be different from x if,

$$|\log\left(\frac{y}{x}\right)| \lessapprox I\,. \tag{D.4}$$

Or in other words, the result of a summation of two numbers has an accuracy of only I digits. Thus addition operations in a computer require that the orders of magnitude of the numbers to be added are not too different. This problem is not present in a multiplication.

Termination criterion

In Cluster Variation calculations we numerically minimize the free energy which is done by searching for zeros of the first derivative. The termination criterion for the minimum search will be that the first derivative of the free energy $g_{\alpha_K}(\boldsymbol{\xi})$ of Sec. 8.2.5 fulfills,

$$\epsilon' > |g_{\alpha_K}(\boldsymbol{\xi})| = |D_{\alpha_K} J_{\alpha_K} - kT \sum_{\beta_L} \frac{a_{\beta_L}}{2^L} \sum_{\boldsymbol{\sigma}_{\beta_L}} V(\boldsymbol{\sigma}_{\beta_L})_{\alpha_K \beta_L} \ln \rho_{\beta_L}(\boldsymbol{\sigma}_{\beta_L}, \boldsymbol{\xi})|\,, \tag{D.5}$$

for all clusters α_K. The probabilities $\rho_{\beta_L}(\boldsymbol{\sigma}_{\beta_L})$ are, according to Sec. 8.2.3, linear functions of the correlations $\boldsymbol{\xi}$. Thus small perturbations of order $\boldsymbol{\delta}_\sigma$ of the correlations also induce small perturbations δ_ρ of the probabilities,

$$\rho_{\beta_L}(\boldsymbol{\sigma}_{\beta_L}, \boldsymbol{\xi} + \boldsymbol{\delta}_\sigma) = \rho_{\beta_L}(\boldsymbol{\sigma}_{\beta_L}, \boldsymbol{\xi}) + \delta_\rho\,, \tag{D.6}$$

with,

$$\delta_\sigma \approx \delta_\rho\,. \tag{D.7}$$

If δ_ρ is small compared to $\rho_{\beta_L}(\boldsymbol{\sigma}_{\beta_L}, \boldsymbol{\xi})$, the logarithm in Eq. (D.5) can be expanded,

$$\ln \rho_{\beta_L}(\boldsymbol{\sigma}_{\beta_L}, \boldsymbol{\xi} + \boldsymbol{\delta}_\sigma) \approx \ln \rho_{\beta_L}(\boldsymbol{\sigma}_{\beta_L}, \boldsymbol{\xi}) + \frac{\delta_\rho}{\rho_{\beta_L}(\boldsymbol{\sigma}_{\beta_L}, \boldsymbol{\xi})}\,, \tag{D.8}$$

A crude approximation thus yields an allowed error of the correlations in Eq. (D.5) of,

$$\delta_\sigma \approx \epsilon'\, \rho_{\beta_L}(\boldsymbol{\sigma}_{\beta_L}, \boldsymbol{\xi})\,. \tag{D.9}$$

We see that the lower a probability is, the more accurate the correlations $\boldsymbol{\xi}$ have to be determined before the iteration cycle will terminate. In the next section we will see that the convergence of the free energy itself behaves different from the convergence of its first derivate.

Inversion of the Hessian

In general, in order to invert a matrix we need to multiply and add its elements. According to Sec. 8.2.5, the elements of the Hessian,

$$H_{\alpha_K\beta_L} = -kT \sum_{\kappa_M} \frac{a_{\kappa_M}}{2^{2M}} \sum_{\boldsymbol{\sigma}_{\kappa_M}} V_{\kappa_M\alpha_K}\left(\boldsymbol{\sigma}_{\kappa_M}\right) V_{\kappa_M\beta_L}\left(\boldsymbol{\sigma}_{\kappa_M}\right) \frac{1}{\rho_{\kappa_M}\left(\boldsymbol{\sigma}_{\kappa_M}\right)} ,$$

are linear combinations of $\frac{1}{\rho_{\kappa_M}(\boldsymbol{\xi})}$. Thus, when at low temperatures some probabilities tend to zero while others, *e.g.*, the probability for the ordered ground state configuration, approach one, the summations required to calculate the Hessian and to invert it can, according to Eq. (D.4), only be calculated with the precision I of the floating point numbers. Let us look at an extreme case to see what this means. When one probability ρ_{α_L} is smaller by a factor of 10^{-I} than all other probabilities $\{\rho_{\kappa_M}\}$,

$$\rho_{\alpha_L} < \rho_{\kappa_M}\, 10^{-I} , \tag{D.10}$$

the numerically calculated Hessian would contain only numbers related to ρ_{α_L} because $1/\rho_{\alpha_L}$ enters the Hessian. It then cannot be used to predict a new search vector $\boldsymbol{\xi}$ for the next step of the Newton-Raphson scheme or, in other words, the Newton-Raphson scheme will fail to converge to the solution.

D.1.2 The free energy at low temperatures

The free energy in the Cluster Variation approximation, Eq. (8.25),

$$\mathcal{F} = \sum_{\beta_K} D_{\beta_K} J_{\beta_K} \xi_{\beta_K} + kT \sum_{\beta_K}^{\alpha_{\max}} b_{\beta_K} \mathrm{Tr}\rho_{\beta_K} \ln \rho_{\beta_K} ,$$

approaches a constant finite value $\mathcal{F}_0$ for $kT \to 0$. If the system investigated has an ordered ground state, the system is in this ground state at $kT \to 0$ with probability one whereas the probabilities for all other states of the system are zero.

Now let us look at a slight variation δ of a probability that is zero or at least close to zero. The probabilities are linear functions of the correlation vector ξ, thus a slight variation δ of a probability requires a slight variation of ξ that induces a linear error δU into the energy U,

$$\delta U \propto \delta . \tag{D.11}$$

We can rewrite the expression for the entropy as,

$$(\rho_{\alpha_L} + \delta) \ln (\rho_{\alpha_L} + \delta) = \rho_{\alpha_L} \ln (\rho_{\alpha_L}) + \rho_{\alpha_L} \ln \left(1 + \frac{\delta}{\rho_{\alpha_L}}\right) + \delta \ln \left(1 + \frac{\rho_{\alpha_L}}{\delta}\right) + \delta \ln (\delta) . \tag{D.12}$$

For the inversion of the Hessian $H_{\alpha_K\beta_L}$ we are interested in a variation δ that is much larger than a small probability ρ_{α_L} but that is still small in a numerical sense,

$$\rho_{\alpha_L}/\delta \ll 1 \quad \text{and} \quad \delta \ll 1 , \tag{D.13}$$

The by far largest term is now given by $\delta \ln(\delta)$. We give an example, let $\rho_{\alpha_L} = 10^{-16}$ and $\delta = 10^{-8}$. We find

$$\begin{aligned} \rho_{\alpha_L} \ln(\rho_{\alpha_L}) &\approx -3.7 \times 10^{-15} \\ \rho_{\alpha_L} \ln\left(1 + \frac{\delta}{\rho_{\alpha_L}}\right) &\approx -1.8 \times 10^{-15} \\ \delta \ln\left(1 + \frac{\rho_{\alpha_L}}{\delta}\right) &\approx 1.0 \times 10^{-16} \\ \delta \ln(\delta) &\approx -1.8 \times 10^{-7} \,. \end{aligned} \tag{D.14}$$

In practice, for phase diagram calculations one is interested in a finite convergence criteria ϵ for the numerical minimization of the free energy $\mathcal{F}$ for terminating the Newton-Raphson iteration scheme (and not a convergence criterion for the first derivative of $\mathcal{F}$). For typical applications this may be $\epsilon \approx 10^{-6}$. Thus from the above example we see that small variations δ of very small probabilities ρ_{α_L} would yield, in a numerical sense, the same free energy, $\mathcal{F} \pm \epsilon$. Or in other words, probabilities that are very small compared to the convergence criterion ϵ need, if we are interested in the free energy, not be converged better than δ.

This gives us the possibility to avoid the inversion and calculation problem for the Hessian $H_{\alpha_K \beta_L}$ that was stated in the previous section: Do not allow any of the probabilities $\{\rho_{\kappa_M}\}$ to be smaller than δ, where δ is large enough that the inversion and calculation of $H_{\alpha_K \beta_L}$ can be carried out numerically accurate. At the same time the allowed δ must be small enough to only induce errors of the order ϵ of the termination criterion into the free energy.

Note that, as was pointed out in the previous section, usually one minimizes the free energy by searching zero in the first derivative of the free energy, Eq. (D.5). Due to the logarithm $\ln(\rho_{\alpha_L})$ variations $\rho_{\alpha_L}/\delta \ll 1$ spoil the solution,

$$\ln(\rho_{\alpha_L} + \delta) = \ln(\rho_{\alpha_L}) + \ln\left(1 + \frac{\delta}{\rho_{\alpha_L}}\right) \neq \ln(\rho_{\alpha_L}) + \epsilon' \,. \tag{D.15}$$

Therefore, although the free energy does not change in a numerical sense if we add δ to very small probabilities, due to the divergence of the logarithm at zero, the first derivative is far away from being zero, which would normally tell us that we are not converged. The next section will show how we can still use the zero of the derivative of a (slightly modified) free energy as stopping criteria in a Newton-Raphson scheme.

D.1.3 Adding a hard core potential to the free energy

We simply add a Yukawa term to the free energy,

$$\mathcal{F}_Y = \mathcal{F} + Y \,, \tag{D.16}$$

with,

$$Y = c\, \delta_\rho^2 \sum_{\beta_K}^{\alpha_{\max}} b_{\beta_K} \mathrm{Tr}\left(\frac{\delta_\rho}{\rho_{\beta_K}}\right) \exp\left(-\frac{\rho_{\beta_K}}{\delta_\rho}\right) \,, \tag{D.17}$$

where δ_ρ is the cut-off probability of the order of δ from the previous section and c is a coupling constant of $O(1)$. In order to still have a numerically accurate description of the free energy, Y must be as small as possible in the inversion of the Hessian, thus δ_ρ must be chosen as a numerically very small value.

We give limits for the errors introduced into the free energy by adding the Yukawa term (see Fig. D.2). The Yukawa potential is a strictly positive function Y, with a strictly negative derivative with respect to the probabilities $\{\rho_{\alpha_L}\}$. We denote the probability distribution that minimizes $\mathcal{F}$ with $\boldsymbol{\rho}_0$ and the one that minimizes $\mathcal{F}_Y$ with $\boldsymbol{\rho}_1$. We define a function,

$$\omega(\lambda) = \underset{\boldsymbol{\xi}}{Min!}\left[\mathcal{F} + \lambda Y\right], \quad \lambda \leq 0 \leq 1. \tag{D.18}$$

With the above minimization condition we note that,

$$\frac{d\omega}{d\lambda} = Y\left(\boldsymbol{\xi}(\lambda)\right), \tag{D.19}$$

and thus,

$$\omega(1) = \omega(0) + \int_0^1 Y d\lambda. \tag{D.20}$$

With the help of $\frac{\partial Y}{\partial \lambda} \leq 0$ we find an upper limit for the free energy,

$$\mathcal{F}(\boldsymbol{\rho}_0) = \omega(0) < \omega(1) - Y(1) = \mathcal{F}(\boldsymbol{\rho}_1). \tag{D.21}$$

If we furthermore assume that along the way defined by λ the curvature of the free energy function is positive (which simply means that we are "close" to the minimum of $\mathcal{F}$ which is guaranteed by choosing $\delta_\rho \ll 1$), we can give a lower limit for $\mathcal{F}(\boldsymbol{\rho}_0)$,

$$\begin{aligned}
\mathcal{F}(\boldsymbol{\rho}_1) &\leq \mathcal{F}(\boldsymbol{\rho}_0) + \sum_L \sum_{\alpha_L} \left.\frac{\partial \mathcal{F}}{\partial \xi_{\alpha_L}}\right|_{\xi_{\alpha_L}(\lambda=1)} \left(\xi_{\alpha_L}(\lambda=1) - \xi_{\alpha_L}(\lambda=0)\right) \\
&= \mathcal{F}(\boldsymbol{\rho}_0) - \sum_K \sum_{\beta_K} \sum_{\sigma_{\beta_K}} \frac{\partial Y}{\partial \rho_{\beta_K}} \sum_L \sum_{\alpha_L} \left.\frac{\partial \rho_{\beta_K}}{\partial \xi_{\alpha_L}}\right|_{\xi_{\alpha_L}(\lambda=1)} \left(\xi_{\alpha_L}(\lambda=1) - \xi_{\alpha_L}(\lambda=0)\right) \\
&= \mathcal{F}(\boldsymbol{\rho}_0) - \sum_K \sum_{\beta_K} \sum_{\sigma_{\beta_K}} \frac{\partial Y}{\partial \rho_{\beta_K}} \left(\rho_{\beta_K}(\lambda=1) - \rho_{\beta_K}(\lambda=0)\right)
\end{aligned} \tag{D.22}$$

We do not know $\boldsymbol{\rho}_0$. However, with $\sum_K \sum_{\beta_K} \sum_{\sigma_{\beta_K}} \left.\frac{\partial Y}{\partial \rho_{\beta_K}}\right|_{\boldsymbol{\rho}_1} \rho_{\beta_K}(\lambda=0) < 0$ we have

$$\mathcal{F}(\boldsymbol{\rho}_1) \leq \mathcal{F}(\boldsymbol{\rho}_0) - \sum_K \sum_{\beta_K} \sum_{\sigma_{\beta_K}} \left.\frac{\partial Y}{\partial \rho_{\beta_K}}\right|_{\boldsymbol{\rho}_1} \rho_{\beta_K}(\lambda=1). \tag{D.23}$$

which defines an estimate for a lower bound of $\mathcal{F}$.

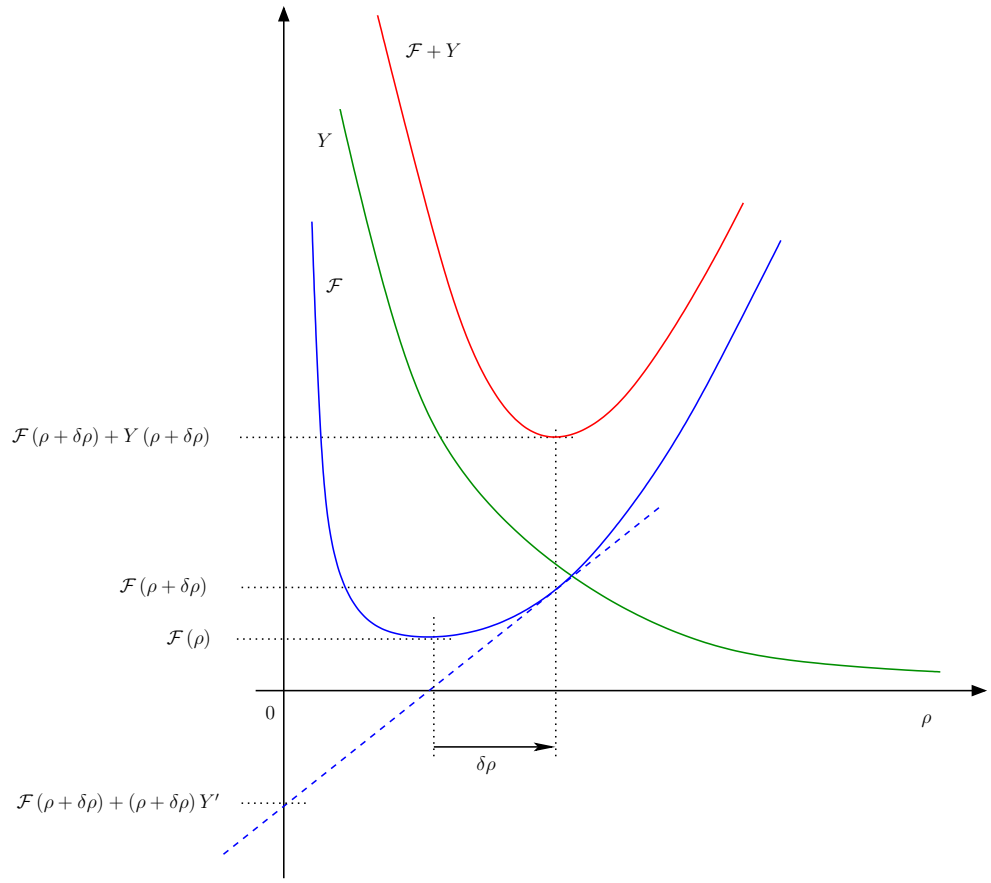

Figure D.2: Schematic representation of the error estimates found for the free energy.

In practice we chose the parameter $c = 1$ and δ_ρ so large that a numerically accurate inversion of the Hessian was possible for the range of temperature that we were interested in but at the same time δ_ρ was chosen as small as possible. For 64 bit double precision numbers we chose $\delta_\rho \approx 10^{-7}$. Depending on the temperature and the approximation for the entropy, the relative error of the free energy defined be the difference of the error bounds Eq. (D.21) and Eq. (D.23), was

$$\epsilon \leq 10^{-5}\,. \tag{D.24}$$

Appendix E

Determination of the parameters for the $2d$ Ising model

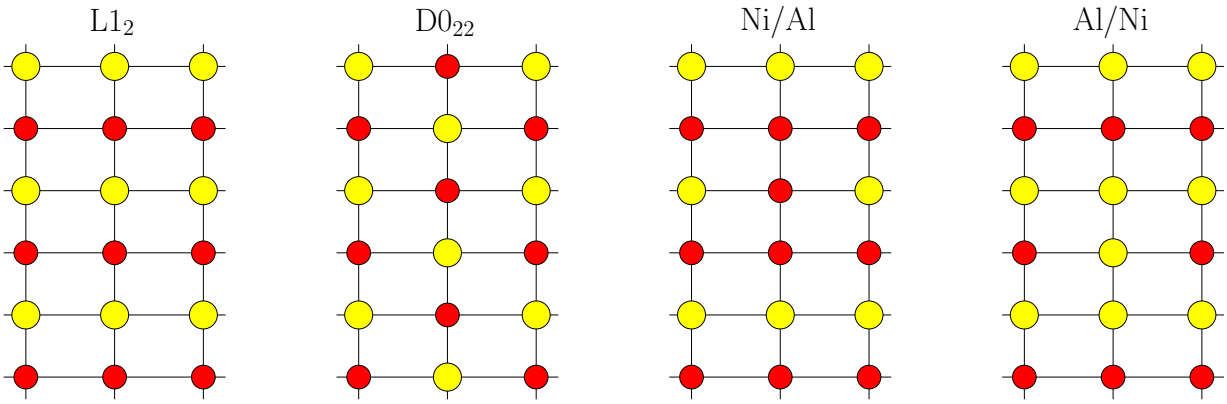

Figure E.1: Surface structures used for the determination of the parameters of the $2d$ Ising model. All layers but the first layer consist of pure Ni.

The parameters J_{1_2}, J_{2_2} and H were determined from a few ab-initio calculated surface structures shown in Fig. E.1. The energy that is gained when a single Al atom is brought into pure Ni material was calculated from a fully relaxed $Ni_{107}Al$ fcc-based supercell calculation. Let $E_b\,(Ni_{107}Al)$ be the total energy of the super-cell and let $E_b\,(Ni)$ be the total energy of a single Ni atom in a Ni fcc-crystal.

Determination of J_{2_2}

Let $E\,(D0_{22})$ be the total energy of a surface unit cell of the $D0_{22}$ surface structure that contains two lattice sites in each layer, Fig. E.1, where only the first surface monolayer contains a Ni and an Al atom in each unit cell and all other layers contain only Ni atoms. Let $E\,(L1_2)$ be the total energy of a surface unit cell of the $L1_2$ surface structure that

contains two lattice sites in each layer, Fig. E.1, where only the first surface monolayer contains a Ni and an Al atom in each unit cell and all other layers contain only Ni atoms. The energy difference between these two structures determines J_{2_2},

$$J_{2_2} = \frac{1}{4}\left(E\left(\mathrm{L1_2}\right) - E\left(\mathrm{D0_{22}}\right)\right) . \tag{E.1}$$

Determination of J_{1_2} and H

Let $E\left(\mathrm{Ni/Al}\right)$ be the total energy of a surface unit cell that contains $2N$ atoms in each layer. In the unit cell one Al atom of the otherwise perfect $\mathrm{L1_2}$ surface structure has been replaced by a Ni atom. All atoms but the atoms in the first layer that are shown in Fig. E.1 are assumed to be Ni atoms. Let $E\left(\mathrm{Al/Ni}\right)$ be the total energy of a surface unit cell that contains $2N$ atoms in each layer. In the unit cell one Ni atom of the otherwise perfect $\mathrm{L1_2}$ surface structure has been replaced by an Al atom. All atoms but the atoms in the first layer that are shown in Fig. E.1 are assumed to be Ni atoms.

The energy of the surface structures $E\left(\mathrm{Ni/Al}\right)$ and $E\left(\mathrm{Al/Ni}\right)$ is now compared to the perfect $\mathrm{L1_2}$ ordered surface.

- When one Al atom is replaced by a Ni atom in the surface, two bonds J_{1_2} and two bonds J_{2_2} change their sign. In addition, the energy required to replace an Al atom from the surface with a Ni atom from the bulk material is given by $2H$ (site occupation changes from minus to plus). The total energy change for replacing an Ni atom in an otherwise perfectly ordered $\mathrm{L1_2}$ surface is thus given by:

$$\Delta E\left(\mathrm{Ni/Al}\right) = 2(2J_{1_2} - 2J_{2_2} + H) = E\left(\mathrm{Ni/Al}\right) - NE\left(\mathrm{L1_2}\right) + E_b\left(\mathrm{Ni_{107}Al}\right) - 108E_b\left(\mathrm{Ni}\right) . \tag{E.2}$$

- When one Ni atom is exchanged with an Al atom in the surface, two bonds J_{1_2} and two bondsJ_{2_2} change their sign. In addition, the energy required to replace a Ni atom from the surface with an Al atom from the bulk material is given by $-2H$ (site occupation changes from minus to plus). The total energy change for replacing an Al atom in an otherwise perfectly ordered $\mathrm{L1_2}$ surface is thus given by:

$$\Delta E\left(\mathrm{Al/Ni}\right) = 2(2J_{1_2} - 2J_{2_2} - H) = E\left(\mathrm{Al/Ni}\right) - NE\left(\mathrm{L1_2}\right) + 108E_b\left(\mathrm{Ni}\right) - E_b\left(\mathrm{Ni_{107}Al}\right) . \tag{E.3}$$

This determines J_{1_2} and H:

$$J_{1_2} = \frac{1}{8}\left(\Delta E\left(\mathrm{Ni/Al}\right) + \Delta E\left(\mathrm{Al/Ni}\right)\right) + J_{2_2} , \tag{E.4}$$

$$H = \frac{1}{4}\left(\Delta E\left(\mathrm{Ni/Al}\right) - \Delta E\left(\mathrm{Al/Ni}\right)\right) . \tag{E.5}$$

In the language of the cluster expansion the field H that is applied to the $2d$ Ising model contains the energy of the bonds that are broken in the bulk material and that are formed in the surface if a Ni atom in the bulk is replaced by an Al atom in the surface.

Appendix F

More on surface CVM calculations

F.1 Note on the calculation of surface phase diagrams with the CVM

The surface phase diagram shown in Fig. 10.1 was put together from two independent calculations. First, a phase diagram for a slab that contained $L = 101$ layers with no surface modified interactions was calculated, see Fig. F.1a. This slab does not have a surface phase that can be different from the volume phase (The volume phase is the phase in the center of the slab). In the limit $L \to \infty$ the influence of the surface vanishes and the phase diagram calculated with the slab as described in Sec. 8.2.6 is the same as the bulk phase diagram. For $L = 101$ layers the phase diagram is already close to the phase diagram calculated in the bulk. Second, the surface modified interactions where taken into account in the CVM calculations. The surface (modeled by a 101 layers slab) then displays a surface phase that can can be different from the bulk phase. For example, the surface ordered phase is located in the surface while the bulk material is disordered. The surface order-disorder transition that takes place in the surface was found to be a first order transition. However, as only the few first layers change their concentration when going through the surface order-disorder transition, the overall concentration of the 101 layers slabs stays nearly constant. Therefore the phase boundary lines shown in Fig. F.1b fall together when the underlying bulk is disordered for $c_{\text{bulk}} > 0.8$.

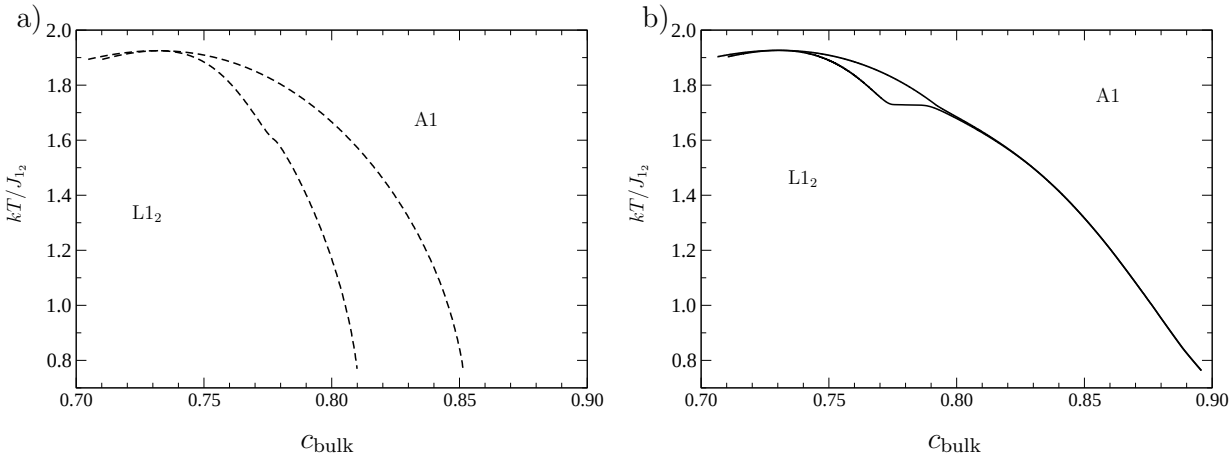

Figure F.1: Phase diagram calculated with no surface modified interactions (a) and phase diagram calculated with surface modified interactions (b) for a 101 layers slab of a fcc (110) surface with nearest-neighbor interactions only.

F.2 Different CVM approximations for the disordered surface

We performed CVM calculations for the disordered surface of NiAl in different approximations for the entropy. For each of the entropy approximations a separate cluster expansion of the surface and the bulk energetics was carried out. The many-body clusters taken into account in the cluster expansion must be contained in the basic clusters of the CVM calculations, hence for this cluster expansions we used three- and four-body clusters contained in the maximum cluster of the entropy. Pair clusters that were not contained in the maximum cluster were modeled within the Bragg-Williams approximation. The cluster expansion for the Tetrahedron approximation reproduces the surface energetics only qualitatively, the cluster expansion for the Octahedron-Tetrahedron approximation gives already a better picture of the energetics. All cluster expansions, for Tetrahedron, Octahedron-Tetrahedron and Double-Tetrahedron-Octahedron approximation display a strong nearest-neighbor interaction and a surface point-cluster that drives the segregation of Al. All calculations also display a similar behavior: Segregation of Al into the first layer and an enhanced pair-correlation in the first layer. The second layer contains less Al than the bulk material. The third layer already displays a behavior more similar to the bulk than to the behavior of the first layer. Figs. F.2 to F.5 summarize the behavior found for the $\mathrm{Ni}_x\mathrm{Al}_{1-x}$ surface with various CVM approximations.

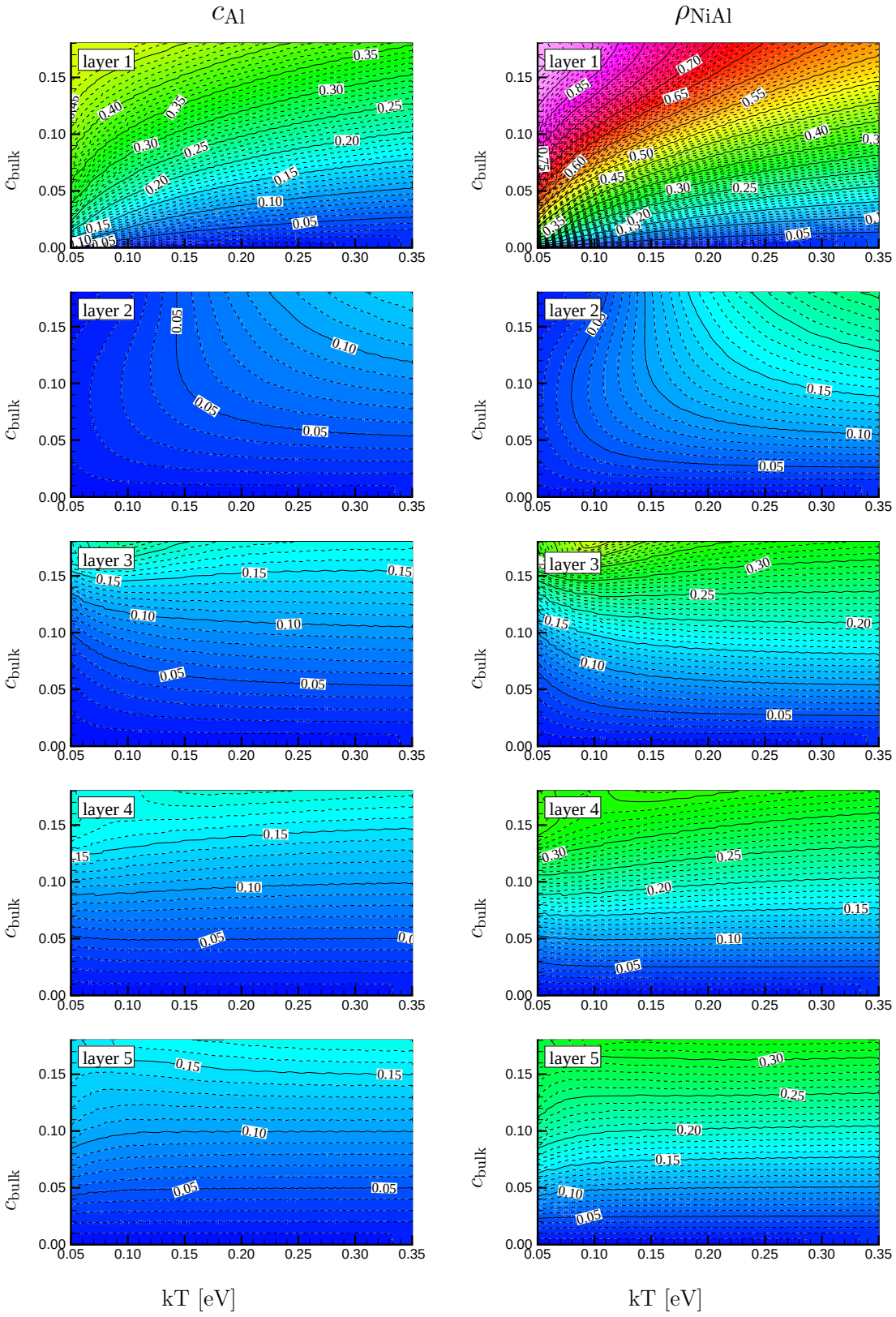

Figure F.2: Al concentration and the probability to find a pair of Ni-Al atoms on nearest-neighbor sites in the first five layers. CVM calculations carried out in Tetrahedron approximation.

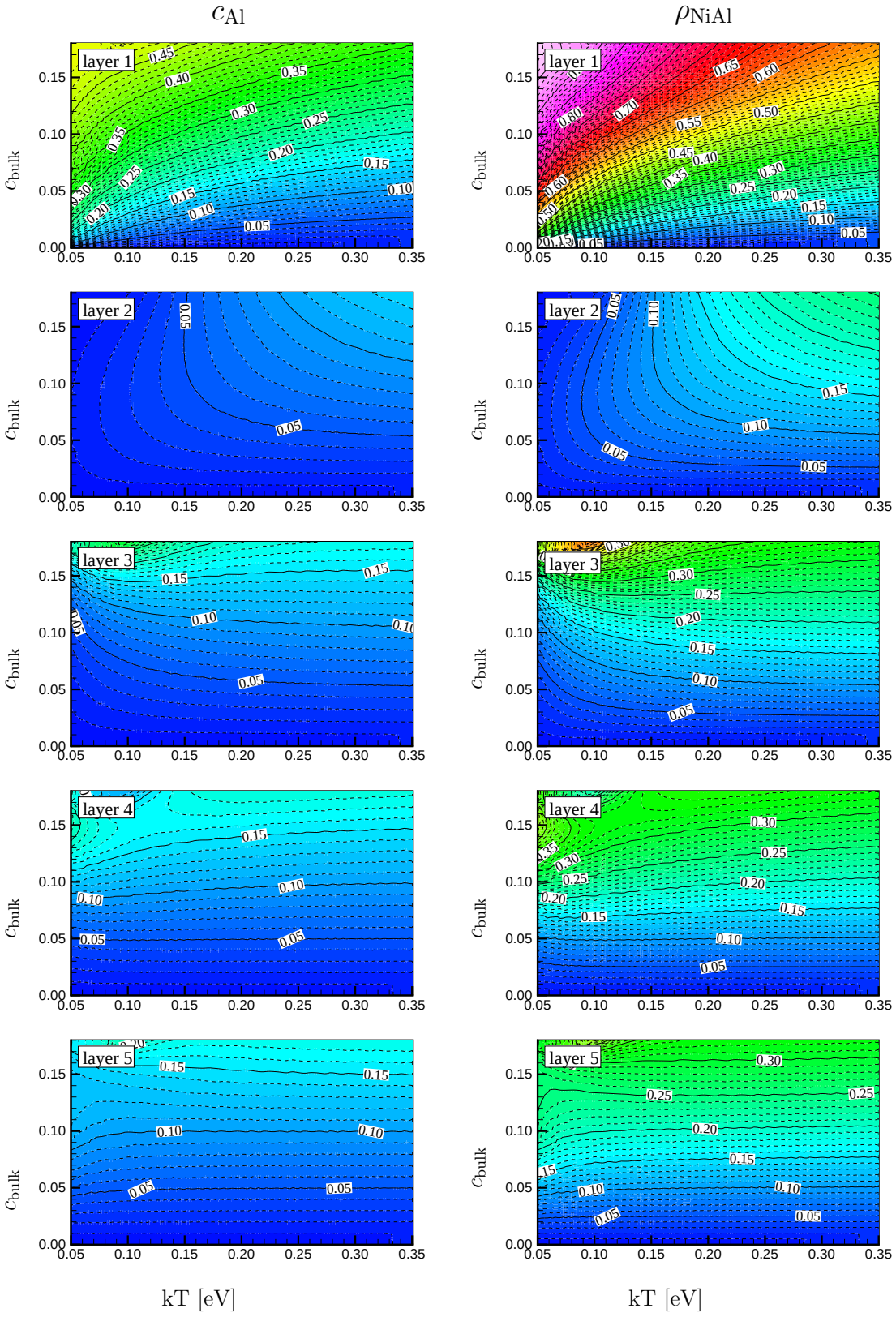

Figure F.3: Al concentration and the probability to find a pair of Ni-Al atoms on nearest-neighbor sites in the first five layers. CVM calculations carried out in Octahedron-Tetrahedron approximation with the cluster expansion of the Tetrahedron approximation.

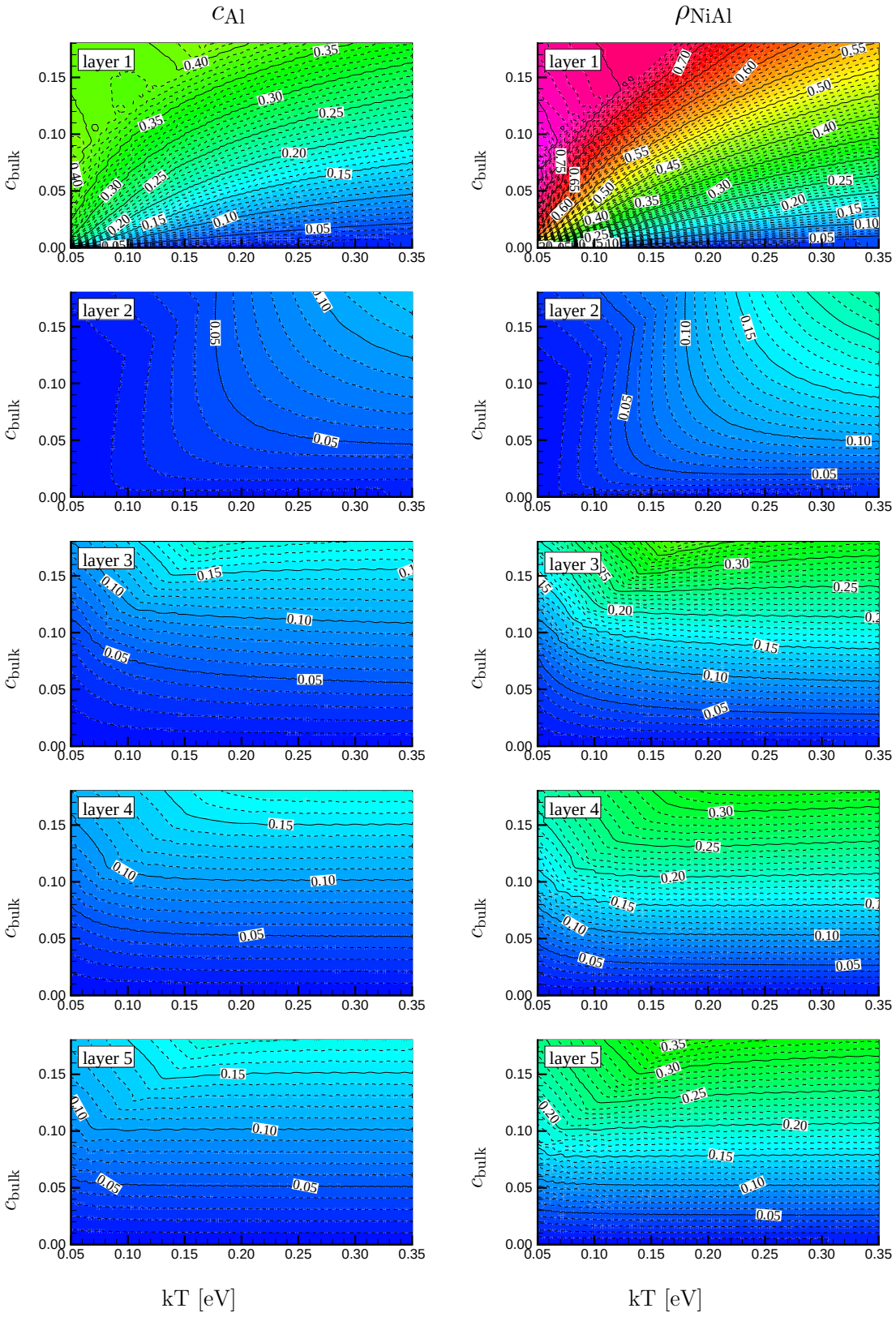

Figure F.4: Al concentration and the probability to find a pair of Ni-Al atoms on nearest-neighbor sites in the first five layers. CVM calculations carried out in Octahedron-Tetrahedron approximation.

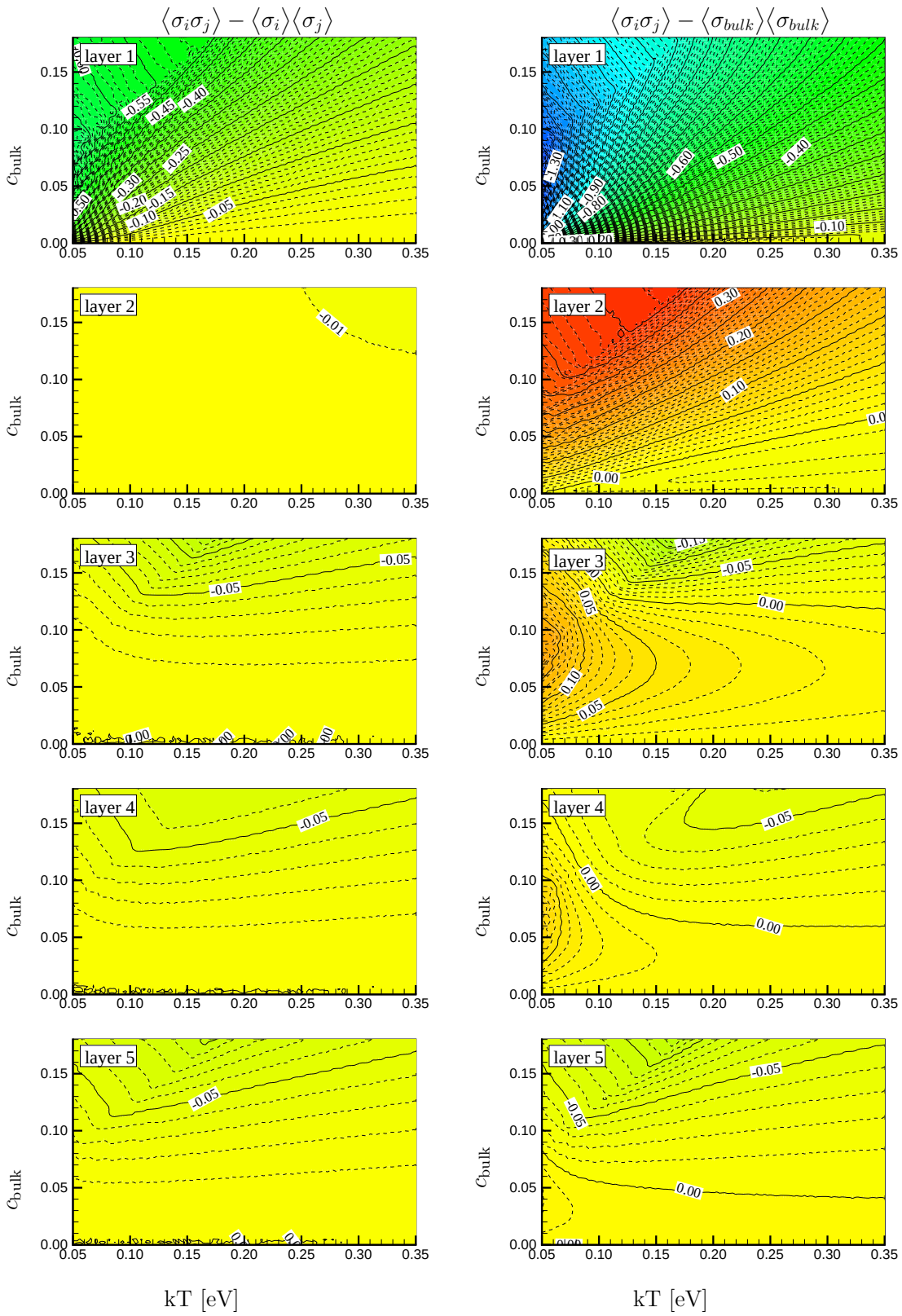

Figure F.5: Pair correlation function $\langle\sigma_i\sigma_j\rangle - \langle\sigma_i\rangle\langle\sigma_j\rangle$ and comparison to the bulk concentration, $\langle\sigma_i\sigma_j\rangle - \langle\sigma_{bulk}\rangle\langle\sigma_{bulk}\rangle$ for nearest-neighbor pairs in the first five layers of the (110) surface. The CVM calculations were carried out in Tetrahedron-Octahedron approximation.

Anhang G

Zusammenfassung

Anders als vor einem Jahrhundert, als die Gesetze der Quantenmechanik und der statistischen Physik gefunden wurden, hat Materialwissenschaft heute nichts mit der Suche nach Naturgesetzen zu tun. Naturgesetze, welche für die Materialwissenschaften von Bedeutung sind, sind bekannt und allgemein akzeptiert. Zu Beginn des 21. Jahrhunderts arbeiten Materialwissenschaftler an einem verbesserten Verständnis der Naturgesetze, um daraus Vorhersagen für Materialeigenschaften zu machen oder das Verhalten von Materialien auf Basis der Naturgesetze zu verstehen und so schlussendlich den Baukasten der Ingenieure um neue Material- und Eigenschaftsklassen zu erweitern.

Die Leistungssteigerung der Computer in den vergangenen Jahren erlaubte die Entwicklung und Umsetzung von Theorien, welche auf "ersten Prinzipien", d.h. direkt auf den Naturgesetzen, beruhen. Diese ab-initio Theorien erlauben die Modellierung makroskopischer Systeme auf der Basis der Naturgesetze. Für die praktische Umsetzung einer ab-initio Theorie ist es von entscheidender Wichtigkeit, geeignete Transformationen, Abzählverfahren und Abschätzungen zu finden, um die physikalisch wichtigsten Zustände eines makroskopischen Systems in der riesigen Anzahl möglicher Systemzustände zu finden, ohne alle möglichen Systemzustände explizit abzuzählen. Die Unmöglichkeit, alle Zustände eines makroskopischen Systems abzuzählen, erfordert aber wiederum die Entwicklung eines "physikalischen Verständnisses" des untersuchten Systems (In diesem Zusammenhang heißt physikalisches Verständnis, dass das generelle Verhalten des Systems mit wenigen Größen beschrieben werden kann). Dies bedeutet, dass eine ab-initio Theorie kompatibel mit phänomenologischen Modellen und deren Terminologie sein muss.

In dieser Arbeit wird die (110) Oberfläche von Ni90%-Al mit einer ab-initio Theorie modelliert. Schon wenige Oberflächenrechnungen zeigen, dass eine phänomenologische Modellierung der Oberfläche mit gebrochenen Bindungen das experimentell beobachtete Verhalten nicht beschreiben kann und sich die Oberfläche in ihrem Verhalten vom Volumenmaterial unterscheidet. Die Tatsache, dass sich das Oberflächenmaterial, gegeben durch einige wenige Atomlagen an der Oberfläche, im Verhalten vom Volumenmaterial unterscheidet und phänomenologische Modelle nicht in der Lage sind das Oberflächenverhalten zu beschreiben, unterstreicht die Wichtigkeit einer ab-initio basierten Theorie für das Verhalten von Oberflächen: Jeder feste Körper wechselwirkt z.B. bei chemischen Reaktionen,

Absorption von Atomen, Wärmeübertrag usw. über seine Oberfläche mit der Umgebung. Eine ab-initio Beschreibung der Oberfläche kann daher wichtige Hinweise und Erkenntnisse bei der Entwicklung und Synthese neuartiger Materialien und Materialeigenschaften liefern.

G.1 Zusammenfassung der einzelnen Kapitel

G.1.1 Kapitel 2

Diese Arbeit wurde initiiert durch Experimente von Dr. H. Reichert aus der Abteilung von Prof. Dosch am Max-Planck-Institut für Metallforschung in Stuttgart. In den Experimenten an der (110) Oberfläche von Ni90%-Al wurde beobachtet, dass Al in die Oberfläche segregiert und sich auf dem ungeordneten Volumenmaterial eine dünne, geordnete Schicht einstellt.

Einführung in die Röntgenstreuung

Soweit es für das Verständnis der Experimente von Bedeutung ist, werden in Kapitel 2 die Grundlagen der Synchrotronstreuung an Oberflächen vorgestellt.

Besprechung verschiedener Arbeiten zu Ni90%-Al(110)

Verschiedene experimentelle und theoretische Arbeiten zur (110) Oberfläche von Ni90%-Al werden kurz besprochen. Weiterhin wird das Experiment von Dr. H. Reichert vorgestellt. Die wichtigsten Ergebnisse und Vermutungen dieses Experiments sind: In der Oberflächen-Monolage von Ni90%-Al(110) liegt Al in einer Konzentration von 50% vor, weiterhin ist die Oberflächen-Monolage in $L1_2$ Struktur geordnet, siehe Fig. 2.11.

G.1.2 Kapitel 3: Dichtefunktionaltheorie

In diesem Kapitel werden die Grundlagen der Dichtefunktionaltheorie und ihre Umsetzung als Kohn-Sham-Gleichungen kurz besprochen. Weiterhin wird sehr kurz auf die verwendeten Näherungen (Lokale Dichte Näherung) und die Implementierung der Kohn-Sham-Gleichungen mit Hilfe von Pseudopotentialen eingegangen. Numerische Details zur verwendeten Methode [36] werden in Anhang B zusammengefasst.

Die Dichtefunktionaltheorie ist der erste Baustein der ab-initio statistischen Mechanik: Mit Hilfe der Dichtefunktionaltheorie ist es möglich, Potentiale zwischen den Atomkernen (als Funktion der Atompositionen) parameterfrei zu bestimmen.

G.1.3 Kapitel 4: Mehrkörper-Potentiale

In diesem Kapitel zeigen wir, dass es möglich ist, jede physikalisch sinnvolle Energie eines Vielteilchensystems, welche gegeben ist als Funktion von Positionen und Typen von

Atomen, eindeutig und exakt in Mehrkörper-Potentiale zu entwickeln. Die Mehrkörper-Potentiale sind dabei unabhängig von Umgebung und Konfiguration der Atome. Wir geben explizite Entwicklungsvorschriften und ein Beispiel für die Entwicklung der Energie in Mehrkörper-Potentiale an.

Dieses Kapitel dient als Grundlage der Clusterentwicklung, welche im nächsten Kapitel abgeleitet wird und welche den nächsten Baustein der ab-initio statistischen Mechanik bildet.

G.1.4 Kapitel 5: Clusterentwicklung

In diesem Kapitel erweitern wir die bekannte Methode der Clusterentwicklung [59]. Die Clusterentwicklung ermöglicht die systematische und im Prinzip exakte Abbildung der konfigurationsabhängigen Systemvariablen eines beliebigen Gittermodells auf ein verallgemeinertes Ising Modell.

In dieser Arbeit heben wir mit Hilfe der Ergebnisse aus Kapitel 4 die Einschränkung der Anwendung der Clusterentwicklung auf Gittermodelle auf. Hierfür leiten wir die Clusterentwicklung aus den Mehrkörper-Potentialen ab und gelangen so zu einer expliziten und allgemeinen Verknüpfung der Entwicklungskoeffizienten der Clusterentwicklung mit den Mehrkörper-Potentialen.

Beispiele für einfache Schlussfolgerungen aus der verallgemeinerten Clusterentwicklung werden vorgestellt, z.B. die Abschirmung der Paarwechselwirkung in NiAl, Einschränkungen bei der Berechnung der Bildungsenergie und die Ankopplung an phänomenologische Modelle (harmonische Entwicklung der Clusterentwicklungskoeffizienten, elastische Wechselwirkungen, Wechselwirkung zwischen Konfiguration und Auslenkung der Atompositionen).

G.1.5 Kapitel 6: Clusterentwicklung in eingeschränkter Geometrie

Die allgemeinen Ergebnisse aus Kapitel 5 erlauben im Gegensatz zur bisher bekannten Clusterentwicklung von Gittermodellen eine direkte Anwendung der Clusterentwicklung auf spezielle Geometrien. Insbesondere wird die Clusterentwicklung an Oberflächen, wie sie für die ab-initio statistische Mechanik von Oberflächen benötigt wird, abgeleitet. Andere mögliche Anwendungen der Clusterentwicklung werden besprochen, z.B. der Fall einer Monolage einer binären Legierung auf einem Substrat oder die Wechselwirkung einzelner Adatome auf einem Substrat. Weiterhin wird abgeschätzt, ob eine reine Paarwechselwirkung in NiAl das experimentell beobachtete Segregationsverhalten von Al erklären kann.

G.1.6 Kapitel 7: Praktische Clusterentwicklung

Die Komplexität und der Aufwand, welche mit ab-initio Rechnungen für Oberflächen einhergehen, zwingen uns, den möglichen Phasenraum der Oberfläche einzuschränken. Dies wird erreicht, indem wir nur Oberflächenkonfigurationen im mechanischen Gleichgewicht

betrachten. Die ab-initio berechneten Energien verschiedener Oberflächenkonfigurationen werden dann wiederum auf ein Gittergasmodell abgebildet. In Kapitel 7 wird beschrieben, mit Hilfe welcher Methoden diese Abbildung durchgeführt wird.

Die durch die Komplexität der ab-initio Rechnungen auferlegte Einschränkung des Phasenraums auf ein effektives Gittergasmodell macht es nun möglich, Betrachtungen zu Segregation und Ordnung in der Oberfläche mit Gittergasmethoden der statistischen Physik durchzuführen. Die von uns verwendete Methode, die Cluster-Variations-Methode, wird im nächsten Kapitel vorgestellt.

G.1.7 Kapitel 8: Modellierung des Einflußes der Temperatur

In diesem Kapitel wird das Konzept von langreichender und kurzreichender Ordnung vorgestellt. Ausführlich wird auf die Gleichungen der Cluster-Variations-Methode eingegangen. Die Monte-Carlo Methode wird, da sie in der weiteren Arbeit nicht verwendet wird, nur kurz vorgestellt. Weiterhin wird die Verknüpfung des Röntgenstreusignals mit der kurzreichenden Ordnung hergeleitet.

Mit Kapitel 8 steht uns eine ab-initio statistische Mechanik für Oberflächen zur Verfügung, welche es uns erlaubt, Segregation und Ordnung an der Oberfläche von Ni90%-Al parameterfrei zu untersuchen.

G.1.8 Kapitel 9: Die (110) Oberfläche von Ni90%-Al

In diesem Kapitel untersuchen wir, basierend auf einer Vielzahl von ab-initio Rechnungen für die Oberfläche als auch für das Volumenmaterial, die Energetik der Oberfläche von Ni-Al im Bereich von $3/4 \leq c_{\mathrm{Ni}} \leq 1$. Wir finden zunächst, dass die Segregation von Al mit einem einfachen Modell gebrochener Bindungen an der Oberfläche nicht beschrieben werden kann. Weiterhin finden wir, dass die Segregation von Al auch nicht durch Relaxation oder einen einfachen Größeneffekt verursacht wird, sondern durch kompliziertere, allgemeine Modifikationen der elektronischen Struktur an der Oberfläche. Die Modifikationen der elektronischen Struktur an der Oberfläche versuchen wir in den beiden letzten Abschnitten von Kapitel 9 zu erfassen.

Basierend auf den ab-initio Rechnungen finden wir:

- Al segregiert spontan in die Oberfläche.
- Die Segregation von Al stoppt bei einer Konzentration von 50% in der ersten Lage. Dies rührt von der stark abstoßenden nächsten-Nachbar Wechselwirkung zwischen Al Atomen her, welche eine Besetzung von nächsten-Nachbar Plätzen mit Al Atomen energetisch ungünstig macht.

$\Rightarrow$ Aufgrund der Struktur der fcc (110) Oberfläche ergeben sich in der Oberfläche geordnete nächste-Nachbar Ketten, welche alternierend mit Ni und Al besetzt sind. Die Oberfläche ist also geordnet.

- Die Wechselwirkung zwischen den geordneten NiAl Ketten im Abstand von zweit-nächsten-Nachbarn ist schwach.

- Für eine Konzentration von $c_{\mathrm{Ni}} \to 1$ erwarten wir eine $\mathrm{D0}_{22}$ geordnete Oberflächen-Monolage.

- Erhöhung der Volumen Al Konzentration führt zu einer Destabilisierung der $\mathrm{D0}_{22}$ Monolage zugunsten einer $\mathrm{L1}_2$ geordneten Monolage ab $c_{\mathrm{Ni}} \approx 0.1$. Die Energieunterschiede zwischen der $\mathrm{D0}_{22}$ Monolage und der $\mathrm{L1}_2$ Monolage sind aber so klein, dass aufgrund der gemachten Näherungen (Lokale Dichte Näherung,...) die Größe des Energieunterschieds als ungefähr null angenommen werden muß.

- Al Atome in der zweiten Lage werden von Al Atomen in der ersten Lage stark abgestoßen.

Mit ab-initio Rechnungen können wir somit die experimentell gefundene Oberflächenkonzentration von 50% Al und die Ordnung in der Oberfläche verstehen.

Eine Clusterentwicklung der Energetik der Oberfläche ist in der Lage die Energien der ab-initio berechneten Oberflächenkonfigurationen zu reproduzieren und zeigt, dass die Entwicklungskoeffizienten innerhalb von drei Lagen von der Oberfläche in sehr guter Näherung ihren Volumenwert annehmen.

G.1.9 Kapitel 10: Die (110) Oberfläche von Ni90%-Al bei endlicher Temperatur

In diesem Kapitel führen wir zunächst Modellrechnungen zum besseren Verständnis der (110) Oberfläche von Ni90%-Al durch. Aufgrund der dominanten nächsten-Nachbar Wechselwirkung im Ni-Al System beginnen wir mit einem Modell, welches nur nächste-Nachbar Kopplungen in Betracht zieht. Durch Vergleich mit dem $1d$ Ising Modell finden wir, dass eine geordnete Oberflächenphase nur stabil sein kann, wenn ihr Ordnungsparameter nur allmählich in das Volumen zerfällt.

Durch Hinzunahme der schwachen zweit-nächsten-Nachbar Wechselwirkung und Vergleich mit dem $2d$ Ising Modell stellen wir fest, dass die schwache zweit-nächste-Nachbar Wechselwirkung eine geordnete Phase, welche ausschließlich auf die erste Lage beschränkt ist, ermöglicht. Da die Größe der zweit-nächsten-Nachbar Wechselwirkung direkt von der Energiedifferenz zwischen $\mathrm{D0}_{22}$ und $\mathrm{L1}_2$ geordneter Oberflächen-Monolage bestimmt wird, welche ihrerseits zu klein ist, als dass wir mit der lokalen Dichte Näherung zuverlässige Werte angeben könnten, können wir kein Phasendiagramm berechnen.

Aufgrund der starken nächsten-Nachbar Wechselwirkung bleibt die Ordnung entlang der nächsten-Nachbar Ketten als starke, kurzreichende Ordnung auch in der nicht langreichend geordneten Oberflächenphase erhalten. Für die nicht langreichend geordnete Oberfläche führen wir Cluster-Variations Rechnungen für Ni-Al(110) durch. Wir finden, dass sich das System ab der dritten Lage von der Oberfläche nahezu wie Volumenmaterial verhält.

G.2 Ab-initio statistische Mechanik für Ni90%-Al(110)

In den Kapiteln 3 bis 8 wurden die Grundlagen einer ab-initio statistischen Mechanik vorgestellt. Das komplexe Verhalten von Vielteilchensystemen erfordert eine Hierarchie von Näherungen und Annahmen auf verschiedenen Ebenen:

- Das quantenmechanische Vielteilchenproblem wird in der Dichtefunktionaltheorie auf effektive Einteilchengleichungen abgebildet. In den Rechnungen wurde die lokale Dichte Näherung verwendet, da das exakte Austausch-Korrelations-Funktional unbekannt ist.

- Der Phasenraum der Oberfläche wurde drastisch eingeschränkt, indem nur Atompositionen im mechanischen Gleichgewicht betrachtet wurden. Anregungen wie z.B. Phononen oder Anregungen der elektronischen Struktur wurden vernachlässigt. Die Energie verschiedener Konfigurationen der Oberfläche, d.h. verschiedener Besetzungen der Atompositionen mit Ni und Al Atomen, wurde auf eine Clusterentwicklung der Oberfläche abgebildet.

- Die Berechnung der Entropie wurde durch die Einführungen eines maximalen Clusters in der Cluster-Variations-Methode vereinfacht. Durch diese Näherung umgeht man das Problem, alle möglichen Systemzustände explizit berechnen zu müssen.

Alle diese Näherungen und Annahmen können, zumindest im Prinzip, überprüft werden. Weiterhin kann die Theorie erweitert werden, um die Auswirkungen von Phononen, Anregungen der elektronischen Struktur oder Korrelationen beliebiger Reichweite zu erfassen. Bei der Ableitung der ab-initio Theorie wurden keine freien Parameter eingeführt, jeder Parameter kann systematisch aus den Naturgesetzen abgeleitet oder genähert werden.

Segregation und Ordnung an Ni90%-Al(110)

Basierend auf ab-initio Rechnungen und einer Modellierung der Oberfläche bei endlichen Temperaturen in den Kapiteln 9 und 10 wurde gefunden, dass Al spontan in die Oberfläche segregiert. Die Segregation von Al wird dabei verursacht von allgemeinen Modifikationen der elektronischen Struktur der Oberfläche und nicht von einfachen Relaxations- oder Größeneffekten. Die starke nächste-Nachbar Wechselwirkung in der Oberfläche stoppt die Segregation von Al bei einer Konzentration von 50% in der Oberflächen-Monolage. Weiterhin erzeugt die starke nächste-Nachbar Wechselwirkung geordnete Ni-Al-Ni-Al-Ni- Ketten auf nächsten-Nachbar Plätzen in der Oberfläche. Die kleine Energiedifferenz die für verschiedene Anordnungen der geordneten Ni-Al Ketten in der Oberfläche berechnet wurde, führte zur Schlussfolgerung, dass im Grenzfall $c_{\mathrm{Ni}} \to 1$ die Oberfläche als schwach gekoppelte $1d$ anitferromagnetische Ising Ketten in Kontakt mit einen Teilchenreservoir beschrieben werden kann. Obwohl die Energiedifferenzen zwischen den verschiedenen Anordnungen der geordneten $1d$ Ni-Al Ketten in der Oberläche klein sind, sind diese Energiedifferenzen entscheidend für die Entordnungstemperatur der Oberfläche. Aufgrund der in den ab-initio Rechnungen gemachten lokalen Dichte Näherung, können diese kleinen Energiedifferenzen

nicht exakt bestimmt werden und das Phasendiagramm der Oberfläche kann nur skizziert werden. Aufgrund der starken nächsten-Nachbar Wechselwirkung in der Oberfläche existieren jedoch starke Korrelationen entlang der nächsten-Nachbar Bindungen weit über der abgeschätzten Entordnungstemperatur.

Anhand der ab-initio Rechnungen wurde weiterhin festgestellt, dass die Oberflächenmodifikationen der Energetik innerhalb weniger Lagen von der Oberfläche in das Volumenmaterial zerfallen. Ebenso verhält es sich mit der Al Segregation in die Oberfläche: Die Segregation von Al in die Oberfläche und die Ordnung der Oberfläche beschränken sich im wesentlichen auf die Oberflächenlage.

Vergleich zwischen Theorie und Experiment

Eine erhöhte Oberflächenkonzentration von Al wurde experimentell für verschiedene Oberflächen von Ni90%-Al gefunden. Für die (110) Oberfläche wurde dieses Verhalten durch Rechnungen bestätigt. Weiterhin konnte die Konzentration von 50% Al in der Oberfläche, wie sie von Reichert gefunden wurde (Sec. 2.3.2), verstanden werden. In Übereinstimmung mit den Experimenten von Reichert konnte die Abnahme der Al Konzentration mit abnehmender Temperatur, wie sie von Polak et al. [14,15] beobachtet wurde, nicht bestätigt werden.

Aufgrund der endlichen Genauigkeit der ab-initio Rechnungen in lokaler Dichte Näherung kann über die experimentell gefundene $L1_2$ geordnete Oberfläche nur spekuliert werden. Anhand unserer Rechnungen können wir nicht entscheiden, ob die Oberfläche bei den experimentellen Bedingungen von 1050 K und einer Ni Volumenkonzentration von 90% in $L1_2$ Struktur ordnet, oder in $D0_{22}$ Struktur, oder ob die Oberfläche keine langreichende Ordnung aufweist sondern nur starke Korrelationen entlang der nächsten-Nachbar Bindungen.

Für ein besseres Verständnis des temperaturabhängigen Verhaltens der Oberfläche sollte das System von experimenteller als auch theoretischer Seite angegangen werden:

- Weitere Experimente bei verschiedenen Temperaturen und Konzentrationen würden wichtige Informationen über den Zerfall des Ordnungsparameters in das Volumenmaterial hinein liefern und damit klären helfen, ob die Ordnung in der Oberfläche grundsätzlich auf die erste Lage beschränkt ist oder ob die geordnete Oberfläche ein Precursor des $L1_2$-A1 zwei-Phasengebietes ist und damit tiefer in das Volumen eindringt wenn die Ni-Volumenkonzentration erniedrigt wird. Auch könnte die Existenz der in dieser Arbeit theoretisch gefundenen geordneten Oberfläche mit $D0_{22}$ Terminierung bei einer Ni-Volumenkonzentration nahe $c_{\mathrm{Ni}} = 1$ überprüft werden.

- Weitere Rechnungen mit höherer Genauigkeit für die Energiedifferenz zwischen der $D0_{22}$ und der $L1_2$ Oberflächen Monolage würden wichtige Informationen für das Oberflächenphasendiagramm liefern. Methoden mit höherer Genauigkeit zur quantenmechanischen Simulation von Oberflächen werden aufgrund ihres Aufwands jedoch in den nächsten Jahren noch nicht zur Verfügung stehen.

References

[1] I.K. Robinson and D.J. Tweet, Rep. Prog. Phys. **55**, 599 (1992).

[2] H. Dosch, *Critical phenomena at surfaces and interfaces: evanescent x-ray and neutron scattering* (Springer, Berlin, Heidelberg, 1992).

[3] S. Dietrich and A. Haase, Physics Reports **260**, 1 (1995).

[4] B.E. Warren, *X-ray diffraction* (Addison-Wesley, Reading, MA, 1969).

[5] J.D. Jackson, *Classical electrodynamics* (Wiley, New York, 1975).

[6] F. Chassagne, M. Bessiere, Y. Calvayrac, P. Cedenese, and S. Lefebvre, Acta. metall. **37**, 2329 (1989).

[7] B. Schönfeld, L. Reinhard, and W. Bührer, Acta mater. **45**, 5187 (1997).

[8] *Binary alloy phase diagrams*, edited by T.B. Massalski (American Society for Metals - ASM International, Metals Park, Ohio, 1996).

[9] F. Lechermann and M. Fähnle, Phys. Rev. B **63**, 012104 (2001).

[10] T.C. Schulthess, E. Wetli, and M. Erbudak, Surf. Sci. Lett. **320**, L95 (1994).

[11] T.C. Schulthess, R. Monnier, and S. Crampin, Phys. Rev. B **50**, 18564 (1994).

[12] R. Monnier, Phil. Mag. B **75**, 67 (1997).

[13] T.C. Schulthess and R. Monnier, in *Current problems in condensed matter*, edited by J.L. Moran-Lopez (Plenum Press, New York, 1998), p. 247.

[14] M. Polak, J. Deng, and L. Rubinovich, Phys. Rev. Lett. **78**, 1058 (1997).

[15] M. Polak and L. Rubinovich, Surf. Sci. Rep. **38**, 127 (2000).

[16] L. Hammer, W. Meier, V. Blum, and K. Heinz, J. Phys.: Condens. Matter **14**, 4145 (2002).

[17] J.M. Roussel, A. Saul, L. Rubinovich, and M. Polak, J. Phys.: Condens. Matter **11**, 9901 (1999).

[18] K.W. Evans-Lutterodt and M.-T. Tang, J. Appl. Crystallogr. **28**, 318 (1995).

[19] H. Reichert, private communication, 2001.

[20] M. Born and J.R. Oppenheimer, Ann. Physik **84**, 457 (1927).

[21] B. Meyer, V. Schott, and M. Fähnle, Phys. Rev. B **58**, R140673 (1998).

[22] R. Heid and K.P. Bohnen, Phys. Rev. B **60**, R3709 (1999).

[23] K.M. Ho and K.P. Bohnen, Phys. Rev. B **38**, 12897 (1988).

[24] B. Meyer, Ph.D. thesis, Universität Stuttgart, 1998.

[25] V. Schott, Ph.D. thesis, Universität Stuttgart, 1998.

[26] W. Kohn, Rev. Mod. Phys. **71**, 1253 (1999).

[27] P. Hohenberg and W. Kohn, Phys. Rev. **136**, B864 (1964).

[28] M. Levy, Phys. Rev. A **26**, 1200 (1982).

[29] W. Kohn and L.J. Sham, Phys. Rev. **140**, A1133 (1965).

[30] *Strong Coulomb correlations in electronic structure calculations: beyond the local density approximation*, edited by V.I. Anisimov (Gordon & Breach, Amsterdam, 2000).

[31] O. Gunnarsson and B.I. Lundqvist, Phys. Rev. B **13**, 4274 (1976).

[32] U. von Barth and L. Hedin, J. Phys. C: Solid State Phys. **5**, 2977 (1972).

[33] L. Hedin and B.I. Lundqvist, J. Phys. C: Solid State Phys. **4**, 2064 (1971).

[34] D.M. Ceperly and B.J. Adler, Phys. Rev. Lett. **45**, 566 (1980).

[35] J.P. Perdew and A. Zunger, Phys. Rev. B **23**, 5048 (1981).

[36] B. Meyer, C. Elsässer, and M. Fähnle, *Fortran90 Program for Mixed-Basis Pseudopotential Calculations*, 1998.

[37] S.G. Louie, K.M. Ho, and M.L. Cohen, Phys. Rev. B **19**, 1774 (1979).

[38] C. Elsässer, N. Takeuchi, K.M. Ho, C.T. Chan, P. Braun, and M. Fähnle, J. Phys.: Condens. Matter **2**, 4371 (1990).

[39] J. C. Phillip and L. Kleinmann, Phys. Rev. **116**, 287 (1959).

[40] W.C. Topp and J.J. Hopfield, Phys. Rev. B **7**, 1295 (1973).

[41] D.R. Hamann, M. Schlüter, and L. Chiang, Phys. Rev. Lett. **43**, 1494 (1979).

[42] G.P. Kerker, J. Phys. C: Solid State Phys. **13**, L189 (1980).

[43] L. Kleinmann and D.M. Bylander, Phys. Rev. Lett. **48**, 1425 (1982).

[44] M.T. Yin and M.L. Cohen, Phys. Rev. B **26**, 3259 (1982).

[45] G.B. Bachelet, D.R. Hamann, and M. Schlüter, Phys. Rev. B **26**, 4199 (1982).

[46] C.L. Fu and K.M. Ho, Phys. Rev. B **28**, 5480 (1983).

[47] D. Vanderbilt, Phys. Rev. B **32**, 8412 (1985).

[48] E.L. Shirley, D.C. Allan, R.M. Martin, and J.D. Joannopoulos, Phys. Rev. B **40**, 3652 (1989).

[49] X. Gonze, J.P. Vigneron, and J.-P. Michenaud, J. Phys.: Condens. Matter **1**, 525 (1989).

[50] I. Stich, R. Car, M. Parrinello, and S. Baroni, Phys. Rev. B **39**, 4997 (1989).

[51] N. Troullier and J.L. Martins, Solid State Comm. **74**, 613 (1990).

[52] D. Vanderbilt, Phys. Rev. B **41**, 7882 (1990).

[53] P.E. Blöchl, Phys. Rev. B **41**, 5414 (1990).

[54] S. Goedecker and K. Maschke, Phys. Rev. B **42**, 8858 (1990).

[55] R.D. King-Smith, M.C. Payne, and J.S. Lin, Phys. Rev. B **44**, 13063 (1991).

[56] N. Troullier and J.L. Martins, Phys. Rev. B **43**, 8861 (1991).

[57] C. Wolverton and A. Zunger, Phys. Rev. B **52**, 8813 (1995).

[58] O. Grotheer and M. Fähnle, Phys. Rev. B **58**, 13459 (1998).

[59] J.M. Sanchez, F. Ducastelle, and D. Gratias, Physica **128A**, 334 (1984).

[60] J. Tersoff, Phys. Rev. Lett. **56**, 632 (1986).

[61] J.M. Sanchez and D. de Fontaine, Phys. Rev. B **17**, 2926 (1978).

[62] H. Kanzaki, J. Phys. Chem. Solids **2**, 24 (1957).

[63] V.N. Bugaev, H. Reichert, O. Shchyglo, A. Udyanski, Y. Sikula, and H. Dosch, Phys. Rev. B **65**, R180203 (2002).

[64] Z.W. Lu, B.M. Klein, and A. Zunger, Superlattices and Microstructures **18**, 161 (1995).

[65] D. de Fontaine, *Solid state physics*, edited by H. Ehrenreich, F. Seitz, and D. Turnbull (Academic, New York, 1979), Vol. 34, p. 73.

[66] A.G. Khachaturyan, *Theory of structural transformations in solids* (Wiley, New York, 1983).

[67] H. Reichert, V.N. Bugaev, O. Shchyglo, A. Schöps, Y. Sikula, and H. Dosch, Phys. Rev. Lett. **87**, 236105 (2001).

[68] V. Ozolins, M. Asta, and J.J. Hoyt, Phys. Rev. Lett. **88**, 096101 (2002).

[69] B.D. Krack, V. Ozolins, M. Asta, and I. Daruka, Phys. Rev. Lett. **88**, 186101 (2002).

[70] A.R. Miedema, Z. Metallkde. **69**, 455 (1978).

[71] J.R. Chelikowsky, Surf. Sci. Lett. **139**, L197 (1984).

[72] J.W.D. Connolly and A.R. Williams, Phys. Rev. B **27**, 5169 (1983).

[73] D.B. Laks, L.G. Ferreira, S. Froyen, and A. Zunger, Phys. Rev. B **46**, 12587 (1992).

[74] G.D. Garbulsky and G. Ceder, Phys. Rev. B **51**, 67 (1995).

[75] M.H.F. Sluiter, Y. Watanabe, D. de Fontaine, and Y. Kawazoe, Phys. Rev. B **53**, 6137 (1996).

[76] C. Wolverton and A. Zunger, Phys. Rev. Lett. **75**, 3162 (1995).

[77] C. Wolverton, V. Ozolins, and A. Zunger, J. Phys.: Condens. Matter **12**, 2749 (2000).

[78] C. Wolverton, V. Ozolins, and A. Zunger, Phys. Rev. B **57**, 4332 (1998).

[79] A. van der Walle and G. Ceder, J. Phase Equilibria **23**, 348 (2002).

[80] R. Kikuchi, Phys. Rev. **81**, 988 (1951).

[81] A. Finel, Ph.D. thesis, Universite Pierre at Marie Curie, Paris, 1997.

[82] F. Ducastelle, *Order and phase stability in alloys* (North Holland, Amsterdam, 1991).

[83] D. de Fontaine, Sol. Stat. Phys. **47**, 33 (1994).

[84] T. Morita, J. Math. Phys. **13**, 115 (1972).

[85] W.L. Bragg and E.J. Williams, Proc. Roy. Soc. **A145**, 699 (1934).

[86] R. Kikuchi, J. Chem. Phys. **60**, 1071 (1977).

[87] R. Kikuchi, J. Chem. Phys. **65**, 4545 (1976).

[88] H.B. Callen, *Thermodynamics and an introduction to thermostatistics* (Wiley, New York, 1985).

[89] R. Kikuchi and K. Masuda-Jindo, Comp. Mat. Sci. **8**, 1 (1997).

[90] R. Kikuchi, J. Phase Equilibria **19**, 412 (1998).

[91] K. Masuda-Jindo and R. Kikuchi, Surf. Sci. **399**, 160 (1998).

[92] R. Kikuchi, J. Stat. Phys. **95**, 1323 (1999).

[93] R. Kikuchi and K. Masuda-Jindo, Comp. Mat. Sci. **14**, 295 (1999).

[94] A. Finel, Prog. Theo. Phys. Supp. **115**, 59 (1994).

[95] M.E.J. Newman and G.T. Barkema, *Monte Carlo methods in statistical physics* (Clarendon press, Oxford, 1999).

[96] G.T. Barkema and M.E.J. Newman, in *Monte Carlo methods in chemical physics*, Vol. 105 of *Advances in chemical physics*, edited by D.M. Ferguson, J.I. Siepmann, and D.G. Truhlar (John Wiley & Sons, New York, 1999), p. 483.

[97] K. Binder and D.W. Heermann, *Monte Carlo simulation in statistical physics: an introduction*, Vol. 80 of *Springer series in solid state sciences* (Springer, Berlin, 2002).

[98] J.M. Sanchez, J.R. Barefoot, R.N. Jarrett, and J.K. Tien, Acta. metall. **32**, 1519 (1984).

[99] J.M. Sanchez, J.P. Stark, and V.L. Moruzzi, Phys. Rev. B **44**, 5411 (1991).

[100] P.J. Craievich, J.M. Sanchez, R.E. Watson, and M. Weinert, Phys. Rev. B **55**, 787 (1997).

[101] P.J. Craievich and J.M. Sanchez, Comp. Mat. Sci. **8**, 92 (1997).

[102] A. van der Walle, G. Ceder, and U.V. Waghmare, Phys. Rev. Lett. **80**, 4911 (1998).

[103] V. Ozolins, C. Wolverton, and A. Zunger, Phys. Rev. B **58**, R5897 (1998).

[104] V. Ozolins and M. Asta, Phys. Rev. Lett. **86**, 448 (2001).

[105] A. van der Walle and G. Ceder, Rev. Mod. Phys. **74**, 11 (2002).

[106] J.M. Sanchez, Physica **111A**, 200 (1982).

[107] J.M. Sanchez, V. Pierron-Bohnes, and F. Mejia-Lira, Phys. Rev. B **51**, 3429 (1995).

[108] D. Le Bolloc'h, A. Finel, and R. Caudron, Phys. Rev. B **62**, 12082 (2000).

[109] R. Brout, *Phase transitions* (Benjamin, New York, 1965).

[110] R.V. Chepulskii and V.N. Bugaev, J. Phys.: Condens. Matter **10**, 8771 (1998).

[111] V. Gerold and J. Kern, Acta. metall. **35**, 393 (1987).

[112] C. Wolverton, A. Zunger, and B. Schönfeld, Sol. Stat. Comm. **101**, 519 (1997).

[113] M.A. Krivoglaz and A.A. Smirnov, *The theory of order and disorder in alloys* (McDonald, London, 1964).

[114] P.C. Clapp and S.C. Moss, Phys. Rev. **142**, 418 (1966).

[115] J.M. Sanchez, private communication.

[116] Z.W. Lu, S.-H. Wei, A. Zunger, S. Frota-Pessoa, and L.G. Ferreira, Phys. Rev. B **44**, 512 (1991).

[117] S. Müller, L.-W. Wang, and A. Zunger, Phys. Rev. B **60**, 16448 (1999).

[118] A. Pasturel, C. Colinet, A.T. Paxton, and M. van Schilfgaarde, J. Phys.: Condens. Matter **4**, 945 (1992).

[119] M. Sluiter, P.E.A. Turchi, F.J. Pinski, and G.M. Stocks, Mat. Sci. Eng. **A152**, 1 (1992).

[120] C. Wolverton and A. Zunger, Phys. Rev. B **59**, 12165 (1999).

[121] D. Sondericker and F. Jona, Phys. Rev. B **34**, 6775 (1986).

[122] R. Drautz, H. Reichert, M. Fähnle, H. Dosch, and J.M. Sanchez, Phys. Rev. Lett. **87**, 236102 (2001).

[123] G. Bester, private communication, 2001.

[124] G. Bester, Ph.D. thesis, Universität Stuttgart, 2001.

[125] A. Diaz-Ortiz, J.M. Sanchez, and J.L. Moran-Lopez, Phys. Rev. Lett. **81**, 1146 (1998).

[126] W. Schweika, K. Binder, and D.P. Landau, Phys. Rev. Lett. **65**, 3321 (1990).

[127] W. Schweika, D.P. Landau, and K. Binder, Phys. Rev. B **53**, 8937 (1996).

[128] L. Onsager, Phys. Rev. **65**, 117 (1944).

[129] E. Müller-Hartmann and J. Zittartz, Z. Physik B **27**, 261 (1977).

[130] X.-Z. Wang and J.S. Kim, Phys. Rev. E **56**, 2793 (1997).

[131] R.J. Baxter, *Exactly solved models in statistical mechanics* (Academic Press, London, 1982).

[132] J. Moreno and J.M. Soler, Phys. Rev. B **45**, 13991 (1992).

[133] R. Haydock, *Solid state physics*, edited by H. Ehrenreich, F. Seitz, and D. Turnball (Academic, New York, 1980), Vol. 35, p. 215.

[134] A. P. Horsfield, Mat. Sci. Eng. **B37**, 219 (1996).

[135] A. P. Horsfield, A.M. Bratkovsky, M. Fearn, D.G. Pettifor, and M. Aoki, Phys. Rev. B **53**, 12694 (1996).

[136] M. Aoki, Phys. Rev. Lett. **71**, 3842 (1993).

[137] D.G. Pettifor and I.I. Oleinik, Phys. Rev. B **59**, 8487 (1999).

[138] D.G. Pettifor and I.I. Oleinik, Phys. Rev. Lett. **84**, 4124 (2000).

[139] T. Ozaki, M. Aoki, and D.G. Pettifor, Phys. Rev. B **61**, 7972 (2000).

[140] D. Nguyen-Manh, D.G. Pettifor, and V. Vitek, Phys. Rev. Lett. **85**, 4136 (2000).

[141] A.P. Sutton, M.W. Finnis, D.G. Pettifor, and Y. Ohta, J. Phys. C: Solid State Phys. **21**, 25 (1988).

[142] L.E. Ballentine and M. Kolar, J. Phys. C: Solid State Phys. **19**, 981 (1986).

[143] N. Börnsen, B. Meyer, O. Grotheer, and M. Fähnle, Intermetallics **5**, 597 (1997).

[144] G. Bester and M. Fähnle, J. Phys.: Condens. Matter **13**, 11541 (2001).

[145] J.M. Sanchez and D. de Fontaine, Phys. Rev. B **25**, 1759 (1982).

[146] A. Finel and F. Ducastelle, Europhys. Lett. **1**, 135 (1986).

[147] A. Finel and F. Ducastelle, Europhys. Lett. **1**, 543(E) (1986).

[148] S. Kämmerer, B. Dünweg, K. Binder, and M. d'Onorio de Meo, Phys. Rev. B **53**, 2345 (1996).

[149] J.M. Sanchez, *Cluster Variation Code for Phase Diagram Calculations of Binary Alloys and Surfaces*, 2001.

[150] A.F. Kohan, P.D. Tepesch, G. Ceder, and C. Wolverton, Comp. Mat. Sci. **9**, 389 (1998).

[151] P.D. Tepesch, M. Asta, and G. Ceder, Model. Simul. Mater. Sci. Eng. **6**, 787 (1998).

[152] L. Ferreira, C. Wolverton, and A. Zunger, J. Chem. Phys. **108**, 2912 (1998).

Danksagung

Die vorliegende Arbeit entstand am Max-Planck-Institut für Metallforschung in Stuttgart und am Texas Materials Institute der University of Texas at Austin, USA. Mein Dank gilt allen, die mich bei der Entstehung dieser Arbeit unterstützt haben.

- Mein besonderer Dank gilt meinem Doktorvater Prof. Dr. M. Fähnle. Durch sein Engagement, seine Diskussionsbereitschaft, seine Hilfestellungen, seine kritischen und hinterfragenden Bemerkungen und sein Interesse am Fortgang meiner Arbeit hat er wesentlich zum Erfolg meiner Dissertation beigetragen.

- Prof. Dr. H. Dosch und Dr. H. Reichert danke ich für die enge Zusammenarbeit, für die Einführungen in den Themenkreis der Synchrotron-Streuung an Oberflächen, für die Daten zum experimentellen Verhalten der Ni90%-Al (110) Oberfläche und für ihr Interesse an meiner Dissertation und die Unterstützung meiner Arbeit.

- Prof. Dr. G. Schütz und Prof. Dr. S. Dietrich danke ich für die Möglichkeit am Max-Planck-Institut für Metallforschung in Stuttgart meine Doktorarbeit anfertigen zu können.

- Bei Prof. Dr. J.M. Sanchez bedanke ich mich für seine Gastfreundschaft und seine Ratschläge während meines Aufenthaltes in seiner Arbeitsgruppe von Oktober 1999 bis September 2000, und weiterhin für sein Interesse an meiner Arbeit auch nach dem Ende meines Aufenthaltes in Austin.

- Prof. Dr. J.L. Morán-López danke ich für seine Gastfreundschaft während meines Aufenthaltes am IPICYT in San Luis Potosi, Mexiko, von Oktober bis Dezember 2001.

- Prof. Dr. A. Díaz-Ortíz danke ich für seine Freundschaft während meines Aufenthaltes am IPICYT in San Luis Potosi, Mexiko, von Oktober bis Dezember 2001, und für die gute Zusammenarbeit im Anschluß an diesen Aufenthalt.

- Prof. Dr. G. Wunner danke ich für die Übernahme des Mitberichts zu meiner Dissertation. Prof. Dr. D. Schweitzer danke ich für die Übernahme des Prüfungsvorsitzes.

- Dem Deutschen Akademischen Austauschdienst danke ich für die Verleihung von zwei Auslandsstipendien, welche meine Forschungsaufenthalte an der University of Texas at Austin, USA und am IPICYT, Mexiko erst möglich gemacht haben.